THE UNIVERSITY OF CALGARY

ANALYSIS AND CONSTRUCTION OF MULTISPAN CABLE-STAYED BRIDGES

BY

Alaa G. Sherif

A THESIS

SUBMITTED TO THE FACULTY OF GRADUATE STUDIES

IN PARTIAL FULFILLMENT OF THE REQUIREMENTS FOR THE

DEGREE OF MASTER OF SCIENCE

DEPARTMENT OF CIVIL ENGINEERING

CALGARY, ALBERTA

August, 1991

ISBN 0-315-71163-9

THE UNIVERSITY OF CALGARY

FACULTY OF GRADUATE STUDIES

The undersigned certify that they have read, and recommend to the Faculty of Graduate Studies for acceptance, a thesis entitled, "Analysis and Construction of Multispan Cable-Stayed Bridges," submitted by Alaa G. Sherif in partial fulfillment of the requirements for the degree of Master of Science.

Dr. Walter H. Dilger (Supervisor)
Department of Civil Engineering

Gamil Tadros

Dr. Gamil S. Tadros
President, Speco Engineering

Dr. Arthur E. McMullen
Department of Civil Engineering

K. L. Chowdhury

Dr. K. L. Chowdhury
Department of Mechanical Engineering

Date September 5, 1991

Abstract

Although cable-stayed bridges have proved to be an efficient bridge system, aesthetically appealing and economical for medium and long-span bridges, the majority of cable-stayed bridges that have been constructed are of the two-span asymmetrical or three-span symmetrical types.

In this study an efficient statical system and a fast construction method for continuous multi-span cable-stayed bridges are described. Also the highway live loads for long-span bridges according to the Canadian, American and European codes are compared. The proposed statical system consists of stiff, diamond-shaped pylons and a slender solid concrete deck of 250 m span suspended from the pylons by a multi-cable system.

To study the static behaviour of such a system, a conventional linear analysis and a geometrical nonlinear analysis , taking into consideration the actual behaviour of the cables (sagging), the effect of large deflections and the effect of axial forces are carried out. For both types of analysis the computer program ANSYS is used and the results are compared.

The effect of the deck-pylon connections on the maximum straining actions in the different bridge components (deck, pylon and cables) and on the buckling of the slender deck is studied by examining five different types of deck-pylon connections. In addition, the influence of the cable areas on the maximum bending moments in the deck is investigated.

Since the stability of the chosen system is achieved by the stiff pylons, a parametric study is carried out to find the optimum pylon dimensions for such a system.

Concerning the construction of multispan cable-stayed bridges, a fast and economical method is described and analysed by the computer program ANSYS. In the proposed construction method, the 250 m long concrete deck is poured in one operation on a steel truss in an elevated position, and then lowered after hardening to its final position, in which it will be suspended from the cables. The truss is then launched to pour the next concrete deck. The lowering process of the truss is simulated in the computer analysis by using interface elements. This construction procedure will shorten the construction time of multi-span cable-stayed bridges significantly. It is estimated that the construction of one span (250 m) will take only four to five weeks.

Acknowledgements

I would like to express my deepest gratitude to my supervisor Professor Dr. W. Dilger for his caring guidance, untiring advice, encouragement and support throughout all stages of the research program.

I also wish to express my sincere gratitude to Dr. G.S. Tadros for his generous donation of time, constructive criticism and valuable discussions.

The financial support received from the Natural Science and Engineering Research Council of Canada and the Department of Civil Engineering at the University of Calgary is deeply appreciated.

Last, but certainly not least, I am grateful to my dear parents and sister, for their unlimited love and support during my whole life. They have always been there for me, especially whenever I needed them most.

Contents

List of Tables

List of Figures

List of Symbols

All symbols are defined where they first appear. SI units are used throughout the study presented herein. The following list contains the most frequently used symbols.

A	= cross-section area
A_{av}	= average cross-section area for a tapered beam
A_i	= cross-section area for cable number i
A_p	= projected area of an immersed body, perpendicular to the flow direction of the fluid
A_r	= effective area in resisting shear deformations (reduced area)
A_1, A_2	= cross-section areas for ends 1 and 2 for a tapered beam
b_i	= spacing between the anchor points of the cables in the deck
b_t	= width of the pylon at the level of the deck (distance between the pylon legs)
C_d	= coefficient of drag for an immersed body
d_t	= height of the inclined pylon legs below the deck
D_{o-j}	= vertical deflection of deck node connected to cable j, due to dead load and zero initial prestressing force in the cables
D_{req-j}	= required final deflection of the deck node connected to cable j, due to dead load
E	= modulus of elasticity
E_{eq}	= equivalent modulus of elasticity (for cables)
f	= cable sag

f_{pu} = rupture stress of the cable material (steel)

F = concentrated force

F_D = drag force on an immersed body

g = dead load intensity of the deck

G = shear modulus

h_t = height of the pylon obove the deck

H = horizontal component of the end reaction of a hanging cable

I = moment of inertia of a cross-section about its center of gravity

I_{av} = average moment of inertia for a tapered beam

$I_1,\ I_2$ = moments of inertia for ends 1 and 2 for a tapered beam

k = spring constant

k_n = stiffness of the interface element normal to its surfaces

k^{tg} = slope of the active force-deflection segment of a nonlinear spring element

l = bridge span

l_l = loaded span length of a bridge

L = element length

= chord length in case of a cable

L_o = strain-free length of a cable

M = bending moment on a section

N = normal force on a section

P = axial force acting on a beam element

$P_{Bending}$ = point load to be applied on a bridge for calculating bending moments

P_{Shear} = point load to be applied on a bridge for calculating shearing forces

q = live load intensity on the deck

q_c = critical live load intensity causing buckling of the deck

R_i = reaction of the idealized continuous beam at cable number i

t_b = depth of beam

ΔT = temperature loading

T_c = tension force in the cable assumed to act along its chord

$T_{g,i}$ = tension force in cable number i due to self-weight and permanent loads

T_{in-j} = initial prestressing force in cable j to obtain the required deflections of the deck nodes due to dead load

T_{max} = maximum tension in a cable acting along the cable axis

u = axial deformation

= displacement in x-direction

v = vertical deformation

= displacement in y-direction

V = fluid velocity

w = intensity of transverse loading on a beam

w_c = weight of cable per unit length of its axis (catenary configuration)

w_{cable} = cable weight

w_p = equivalent weight of cable per unit length of its span (parabola configuration)

W = standard truck weight

y = distance measured from the center of gravity of a member

= deflection of a beam element

Δy_i = difference between the vertical displacement obtained from step i, and the final required vertical displacement of the deck node

α = coefficient of thermal expansion

γ = specific weight (weight per unit volume)

$\delta_{i,j}$ = vertical displacement of deck node connected to cable i due to a unit initial force in cable j

ϵ_x = axial strain in a layer at a distance y from the centroid of a section

ε = initial strain in a cable

ε_{i+1} = initial strain in a cable for iteration step $(i+1)$

θ = angle of inclination to the horizontal of the cable chord

θ_i = angle of inclination to the horizontal of the cable chord for iteration step i

ν = Poisson's ratio

ρ = fluid density

σ = tensile stress in the cable

σ_g = allowed stress in the cable due to self-weight and permanent loads

σ_{per} = permissible tensile stress in the cable

$\Delta\sigma_{per}$ = permissible stress variation in the cable due to live load

 = roller support

 = hinge support

List of Matrices

All matrices are defined where they first appear. [ ]-Brackets stand for a matrix, while { }-brackets stand for a vector or array. The following list contains the most frequently used matrices.

$\{D\}$	= vector of joint displacements
$\{D_n\}$	= vector of joint displacements for iteration step n
$\{F\}$	= total load vector
$\{F_m\}$	= vector of total applied loads at load step m
$\{F_{m,n}^{nr}\}$	= vector of restoring loads for load step m and iteration n
$\{F_n^{nr}\}$	= vector of restoring loads for iteration n
$[k]$	= member stiffness matrix in the local member coordinates
$[k_p]$	= stiffness matrix for a beam taking into account the $(P-\delta)$ effect
$[k_s]$	= stiffness matrix expressing the $(P-\delta)$ effect on the element stiffness matrix (sometimes called stress stiffening matrix)
$[K]$	= structure stiffness matrix in the global structure coordinates
$[K_{m,n}]$	= tangent structure stiffness matrix for load step m and iteration n
$[K_n]$	= tangent structure stiffness matrix for iteration n
$[T_n]$	= coordinate transformation matrix

Chapter 1

INTRODUCTION

1.1 GENERAL

The cable-stayed bridge is an innovative structure that is both old and new in concept. It is old in the sense that the idea of supporting a beam by inclined ropes or chains hanging from a mast or tower has been applied by the ancient Egyptians for their sailing ships (Figure 1.1) several thousands years ago, and it is new in that its modern-day implementation began in the 1950s in Germany and started to seriously attract the attention of bridge engineers in North America only as recently as 1970. The importance of cable-stayed bridges increased rapidly with the enormous progress made in computational facilities and material technology.

Nowadays cable-stayed bridges have become so successful that they have taken their rightful place among classical bridge systems. A large number of cable-stayed bridges has been build around the world, most of them are of the two-span asymmetrical or three-span symmetrical types (see Figure 1.2).

Only a very few of them are of the multispan type, as for example the Maracaibo bridge in Venezuela, which has a continuous system as shown in Figure 1.3(a).

For the crossing of the Great Belt in Denmark, a system as shown in Figure 1.3(b) is suggested by Finsterwalder. This system consists of very stiff pylons and expansion joints at the centre of each span to reduce the effect of temperature and time dependent-effects.

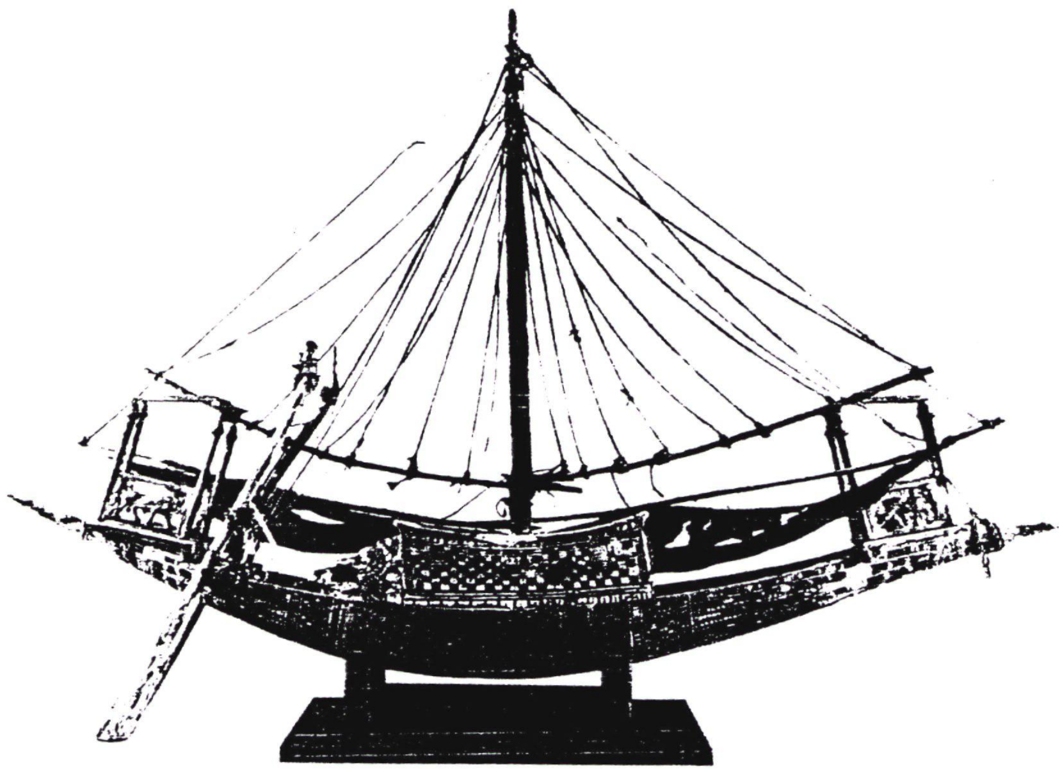

Figure 1.1: Model of an ancient Egyptian Pharaoh boat

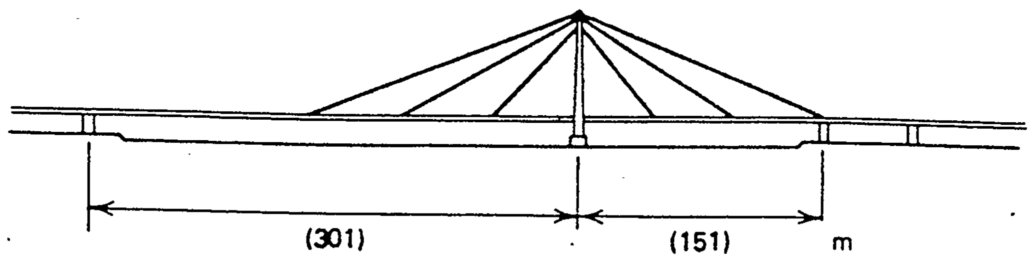

(a) Two-span asymmetrical
(Severin Bridge at Cologne, Germany)

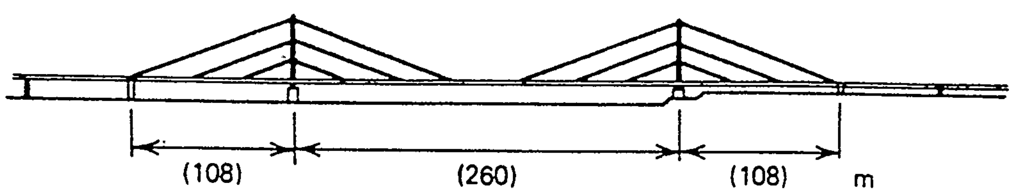

(b) Three-span symmetrical
(North Bridge at Düsseldorf, Germany)

Figure 1.2: Typical span arrangements for cable-stayed bridges

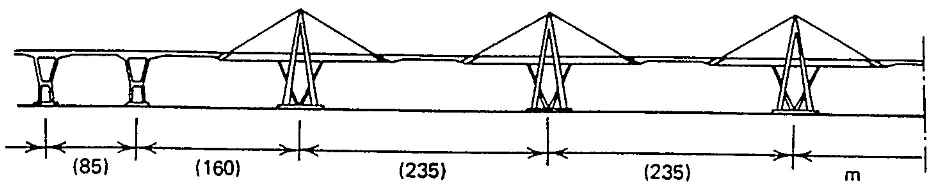

(a) Statical system of the Maracaibo bridge in Venezuela

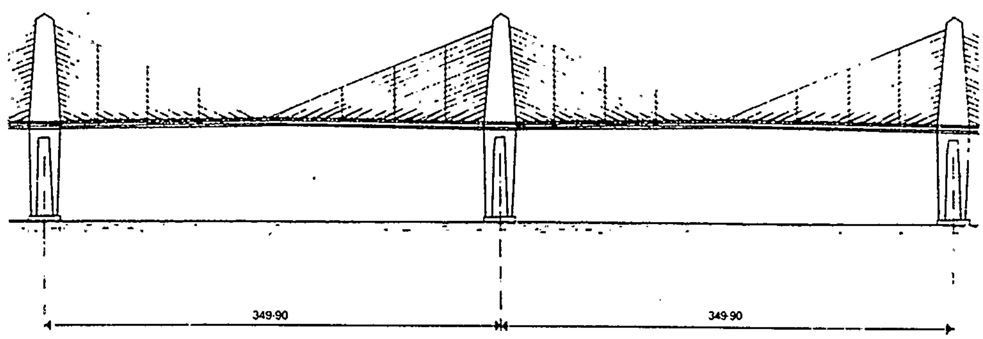

(b) Proposal by Finsterwalder for the Great Belt bridge in Denmark

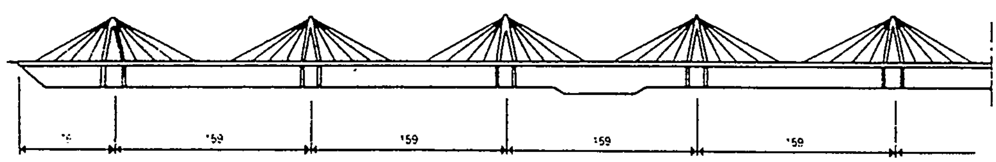

(c) Proposal by Leonhardt for crossing the Ganges in India

Figure 1.3: Different statical systems for multispan cable-stayed bridges

A similar solution was proposed by Leonhardt for crossing the Ganges in India as shown in Figure 1.3(c).

In this study the proposal call for a fixed link across Northumberland Strait between New Brunswick and Prince Edward Island in Canada (see Figure 1.4) is adopted. The total length of the proposed bridge is about 13 km. The structure investigated is a multispan cable-stayed bridge with an idealized 12.0x0.60 m solid concrete slab and 250 m long spans. Diamond-shaped pylons have been chosen to provide the stiffness required for the resistance of unbalanced live loads.

Since more than 40 identical spans are to be constructed, conventional construction methods such as precast or cast-in-place segmental construction are not suitable for such a project, because they would take excessively long to construct such a long bridge, especially under the harsh environmental conditions existing in the region. The method discussed in this study is a cast-in-place concrete deck on a steel truss extending over two spans, leading to the construction of one span (250 m) in only four to five weeks.

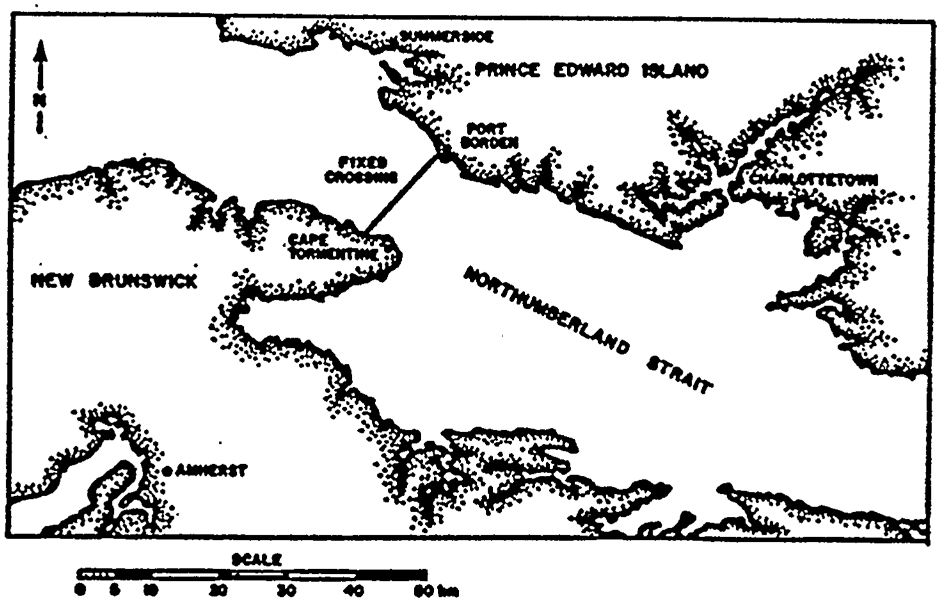

Figure 1.4: Location of the proposed bridge

1.2 OBJECTIVES

The objectives of the research project presented in this thesis are:

1. To compare the highway live loads for long-span bridges according to the Canadian, American and European codes.

2. To review the basic informations needed for the understanding of the behaviour and analysis of cable-stayed bridges.

3. To compare between a conventional linear analysis and a geometrical nonlinear analysis of cable-stayed bridges taking into consideration the actual behaviour of the cables,the effect of large deflections and the effect of axial forces.

4. To propose an efficient statical system for continuous cable-stayed bridges.

5. To discuss an economical and fast construction method for long continuous cable-stayed bridges and to simulate the proposed method using the computer program ANSYS.

1.3 SCOPE

In this study the static behaviour and the construction of continuous cable-stayed bridges are discussed.

In Chapter 2 the highway live loads on long bridges according to the Canadian, American and European codes are compared.

In Chapter 3 different structural systems for multispan cable-stayed bridges are presented. The various pylon configurations, cable arrangements and deck types are discussed.

Chapter 4 presents a literature review needed for the understanding of the behaviour and analysis of a cable-stayed bridge, including the characteristical behaviour of a cable, the effect of axial forces on the beam stiffness and the effect of large deflections in the analysis. The different techniques for the solution of nonlinear problems, which are available in the used computer program ANSYS are also reviewed.

In Chapter 5 the analysis of the proposed bridge due to dead load, highway live load and temperature is carried out. The results of a conventional linear and a geometric nonlinear analysis are compared.

In Chapter 6 a parametric study is carried out to investigate the effect of the deck-pylon connection type, pylon configuration and cable areas on the behaviour of a continuous cable-stayed bridge.

The construction method is described and the different construction steps are analysed in Chapter 7.

Chapter 8 contains a summary of the most important results, conclusions and recommendations for further research.

Appendix A includes the description of the different element types used in the computer analysis.

Chapter 2

LOADS ON LONG BRIDGES

2.1 INTRODUCTION

A bridge must be designed to resist all loads and load effects that may be expected during its intended life. Besides the own weight and highway live load other loads which have to be considered are:

- Dynamic load effects
- Temperature, creep and shrinkage effects
- Wind on structure and on traffic
- Longitudinal loads due to braking
- Collision
- Differential foundation settlement
- Earthquake loading
- Ice pressure and stream flow

In this study only the effects of the own weight, highway live load and temperature on the proposed bridge are investigated.

2.2 THE OWN WEIGHT

For the serviceability limit state, the permanent loads are taken as the actual (unfactored) loads. The densities of the different materials are input data for the computer program for the analysis of the structure due to its own weight. The concrete density is taken as 2400 kg/m^3 and that of the steel as 7850 kg/m^3.

For the 12.0$\times$0.60 m solid concrete slab, this gives a dead load intensity of 170 kN/m. In addition a superimposed dead load of 30 kN/m is applied on the deck to accommodate the weight of the wearing surface, side rails, curbs ...etc. This means that the total dead load intensity of the deck for the proposed bridge is $g = 200$kN/m.

2.3 THE HIGHWAY LIVE LOADS

2.3.1 Introduction

There are wide disparities throughout the world concerning highway live loads on bridges. But a comparison of numerous codes (Canadian, American and European codes) shows that, whereas their make-up may differ widely, their overall effects on the forces on the structure do so to a much lesser degree.

In general, the highway live load consists of a standard truck and/or a uniformly distributed lane load. Numerous traffic surveys and associated probabilistic studies have shown that the actual highway live loads decrease as the area over which they are moving increases.

The highway live load for the proposed bridge of 250 m span and a two-lane deck is calculated according to the Canadian Code and compared with the American and

European (FIP) Codes.

2.3.2 Highway live load according to the Canadian Code

According to the National Standard of Canada (CAN/CSA-S6-88) specifications, the highway live load on a bridge consists of a standard truck (W = 600 kN) or of a lane load as shown in Figure 2.1, whichever produces the maximum load effect. The lane load consists of a uniformly distributed load of $0.02W$=12.0 kN/m on a 3 m width, plus concentrated loads representing a reduced truck load of $0.6W$=360 kN. For continuous spans, the lane load shall be continuous or discontinuous, as may be necessary to produce maximum load effects, and the dynamic load allowance for the uniformly distributed portion of the lane load is 0.10.

Since the objective of this study is to investigate the overall behaviour of continuous cable-stayed bridges, not to design sections or study local effects such as punching in the deck, only the distributed portion of the lane load will be considered.

It has to be noted that the Canadian Code is not applicable for long-span bridges with spans exceeding 150 m. A reduction of the standard truck load needs special discussions with the authorities. According to the proposal call of Public Works Canada for the investigated Northumberland Strait Crossing project, the weight of the design truck is given by the following equation:

$$\left.\begin{array}{llrcl} W = 630 + 1.2 \cdot l_l & for & l_l = 0 & to & 100\ m \\ W = 750 - 0.4 \cdot (l_l - 100) & for & l_l = 100 & to & 500\ m \end{array}\right\} \qquad (2.1)$$

where: W = weight of design truck (kN)

l_l = loaded length of the bridge (m)

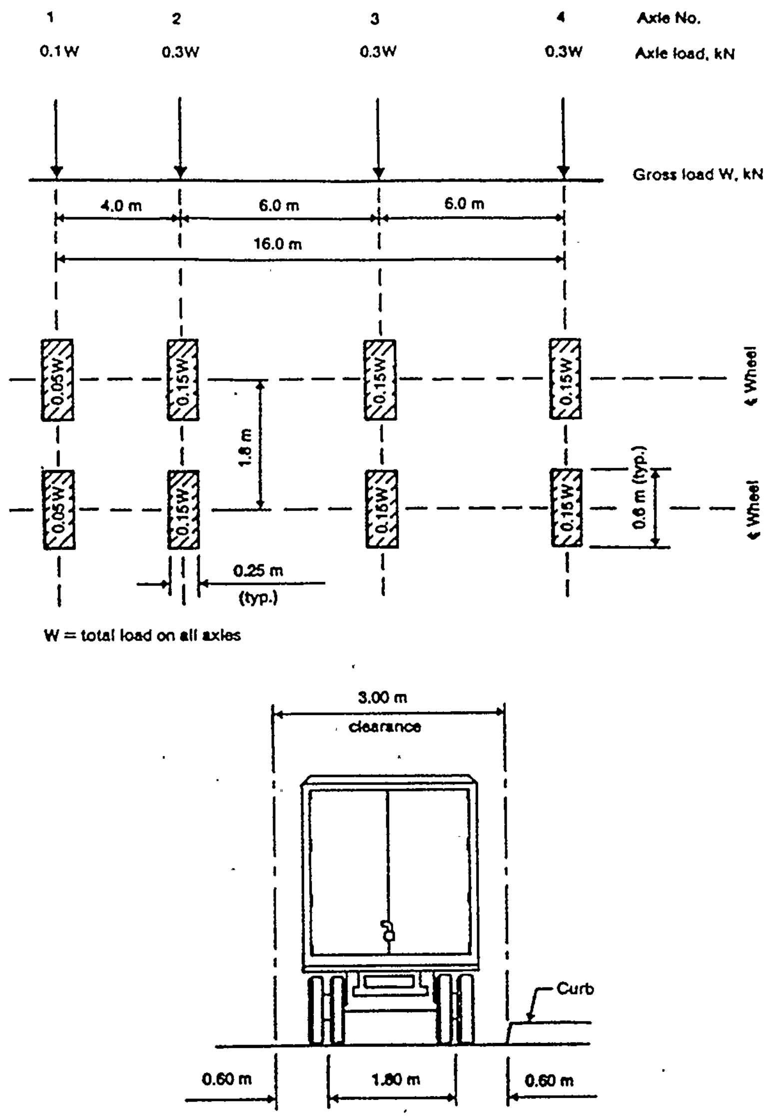

Standard CS-W Truck

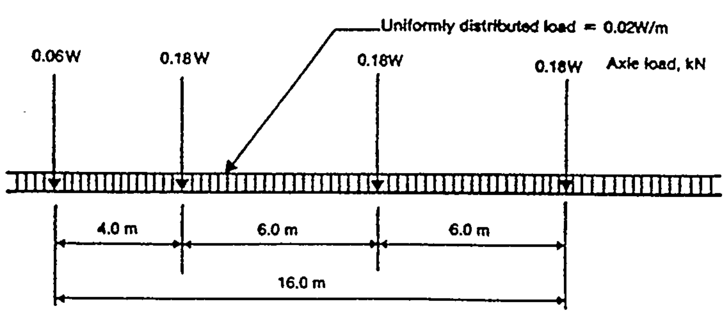

Lane Load

Figure 2.1: Highway live load according to the Canadian Code

Using these values of W, and a dynamic load allowance of 0.10, the distributed portion of the highway live load as a function of the loaded length of a bridge is shown in Figure 2.2. Loading two lanes and using a reduction factor of 0.9 for multiple lane loading (see Table 2.1), the live load intensity obtained from Figure 2.2 for a loaded length of 250 m is q=27.3 kN/m (corresponding to a truck load W of 690 kN).

If the standard truck load W=600 kN of the Canadian Code is used, the distributed lane load is reduced to 23.8 kN/m. As the trend of the different codes (as will be shown next) is to reduce the loading with an increase of the loaded length, the load intensity of 23.8 kN/m obtained from the Canadian Code is adopted in this study.

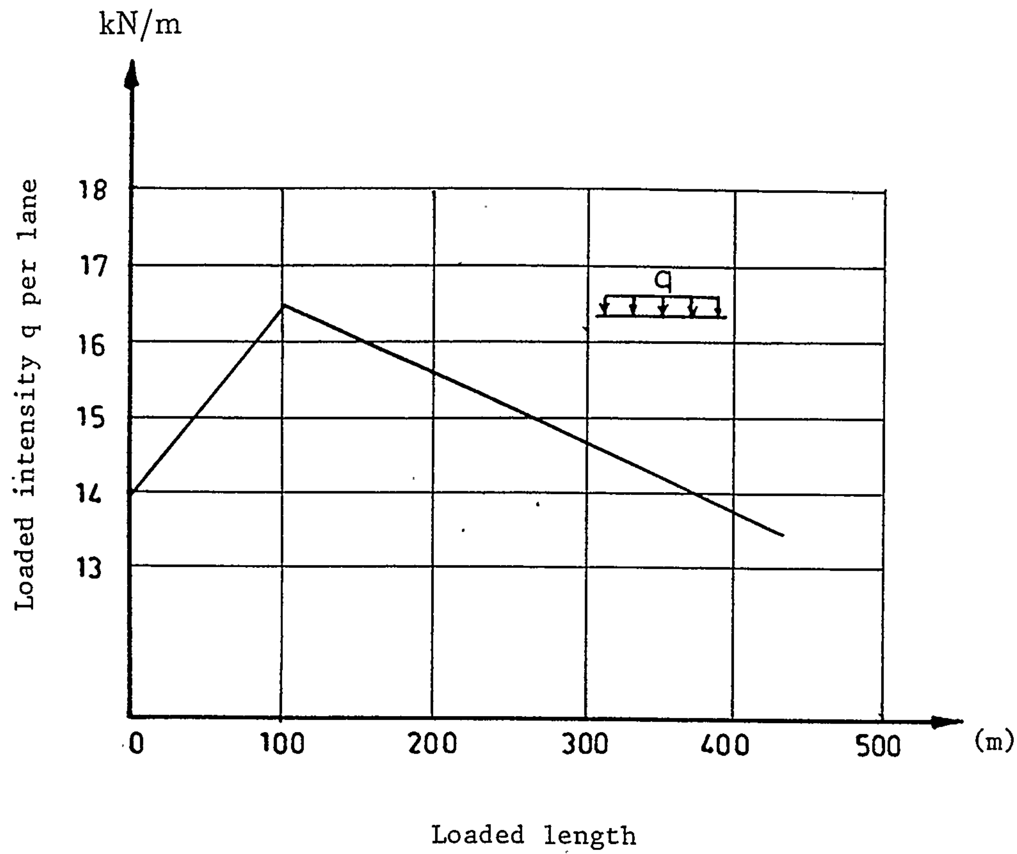

Figure 2.2: Distributed portion of highway live load including the dynamic effect, calculated from the truck loading proposed by PWC for the Northumberland Strait Crossing project

Table 2.1: Reduction factors for multi-lane loading according to the Canadian Code

Number of loaded lanes	Reduction factor
1	1.00
2	0.90
3	0.80
4	0.70
5	0.60
6 or more	0.55

2.3.3 Highway live load according to the European Code

The European standard truck of 60 tons corresponds to the Canadian 600 kN truck. In the FIP recommendations for practical design, an attempt has been made to combine all the effects of live loads in a single, uniformly distributed load (see Figure 2.3). These values include the dynamic effects.

For multi-lane loadings, a reduction in load is assumed as shown in Figure 2.4. In order to study local effects (for example punching of the deck), a single point load has to be considered. The value of this load is 200, 300 or 400 kN for light, normal or heavy traffic respectively.

For the proposed two-lane bridge with a loaded length of 250 m, the highway live load would be 20 kN/m for light traffic, 30 kN/m for normal traffic and 40 kN/m for heavy traffic (compare with the Canadian Code which gives 23.8 kN/m).

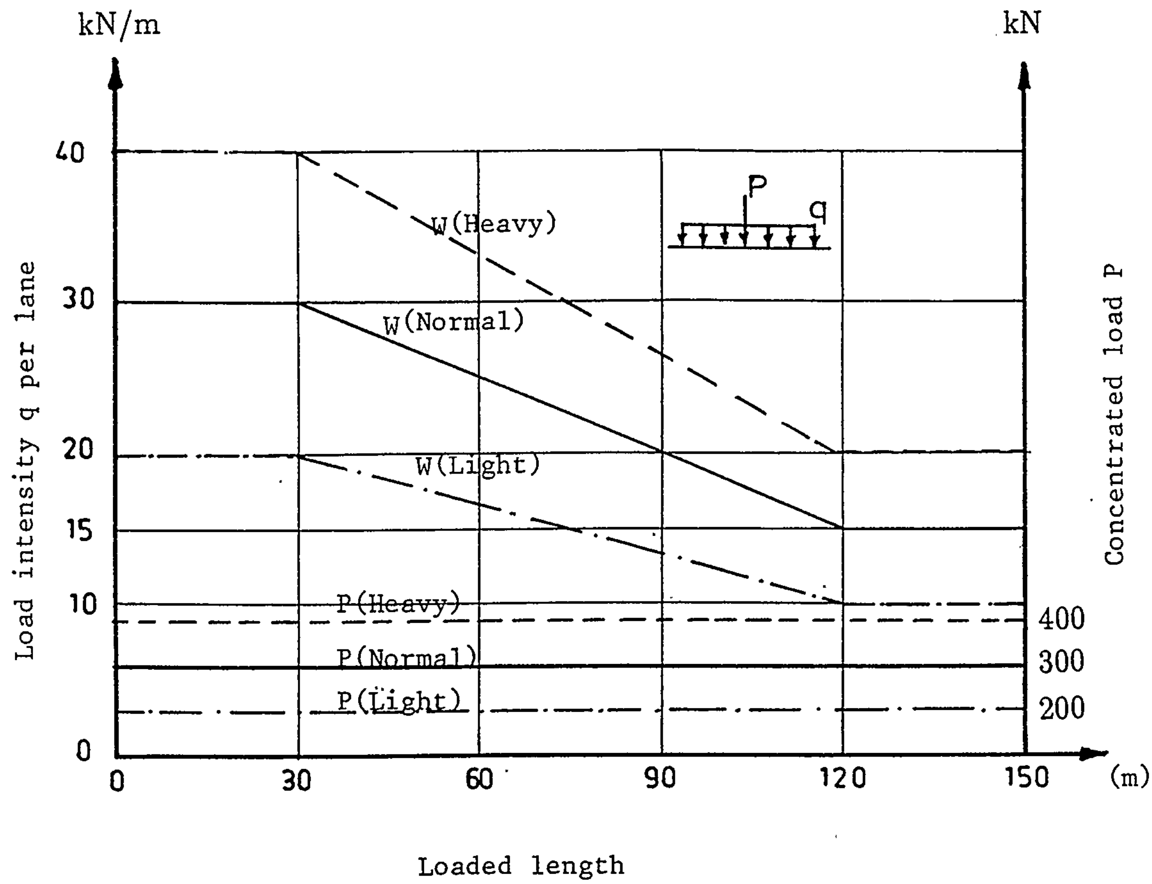

Figure 2.3: Highway live loads including dynamic effect according to the European Code (FIP)

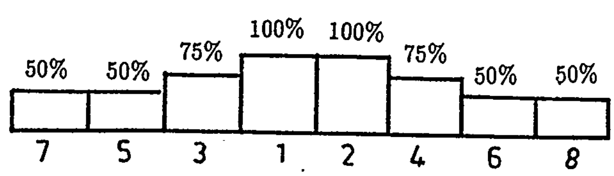

Figure 2.4: Reduction factors for multi-lane loading according to the European Code (FIP)

2.3.4 Highway live load according to the American Code

The present American AASHTO Code (1983 edition) specifies the standard HS 20-44 truck with a total load of only 72,000 lbs which is about 320 kN (compare with the Canadian 600 kN truck).

The lane load consists of a uniformly distributed load of 640 lb/ft which is about 9.5 kN/m (compare with 12 kN/m according to the Canadian Code). The magnitude of the single point load used in studying local effects (such as shear in punching problems) is about 26,000 lbs (115 kN). Adding the dynamic effect, this value would correspond to the 200 kN point load used in the European Code for light traffic. It should be noted that the AASHTO specifications are only applicable to spans up to 500 ft (152 m), and therefore do not include the long-span bridges.

For spans in excess of 152 m, reductions recommended by Ivy et al (1954) as shown in Figure 2.5, are generally accepted criteria. The reduction in the lane load starts for loaded spans exceeding 300 m, whereas in the European Code the reduction starts for spans exceeding 150 m.

To include the effect of the loaded span length on the highway live loads, and to distinguish between light, medium and heavy traffic, the ASCE Committee on Loads and Forces on Bridges (1981) recommends a highway live load as shown in Figure 2.6. The values 7.5%, 30%, and 100% H.V. (Heavy Vehicles) correspond to the European light, medium and heavy traffic. Using the curves of Figure 2.6 and the reduction factors for multi-lane loading shown in Figure 2.7, the highway live load for the proposed two-lane bridge with a loaded span length of 250 m is 13.6, 20.4 and 23.8 kN/m for light, medium and heavy traffic respectively.

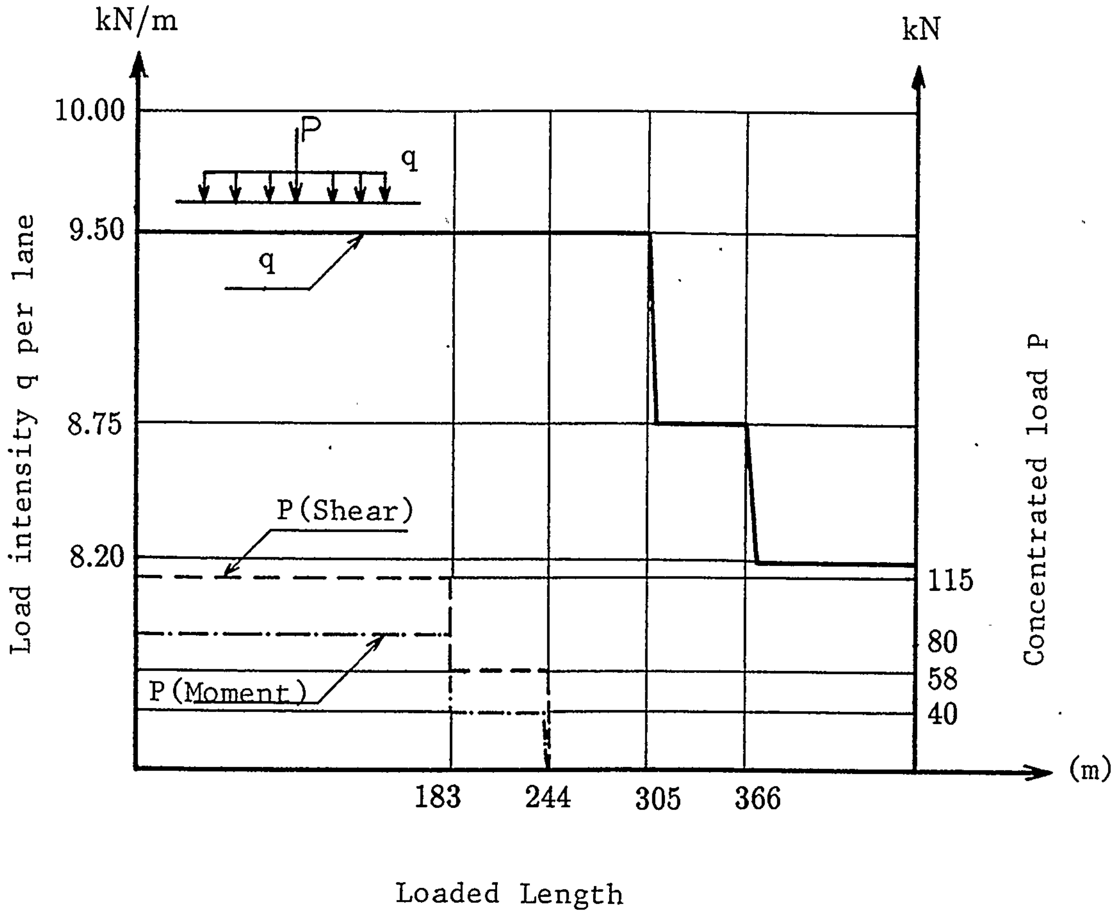

Figure 2.5: Highway live loads as recommended by Ivy et al (1954) for the American Code (converted to SI units).

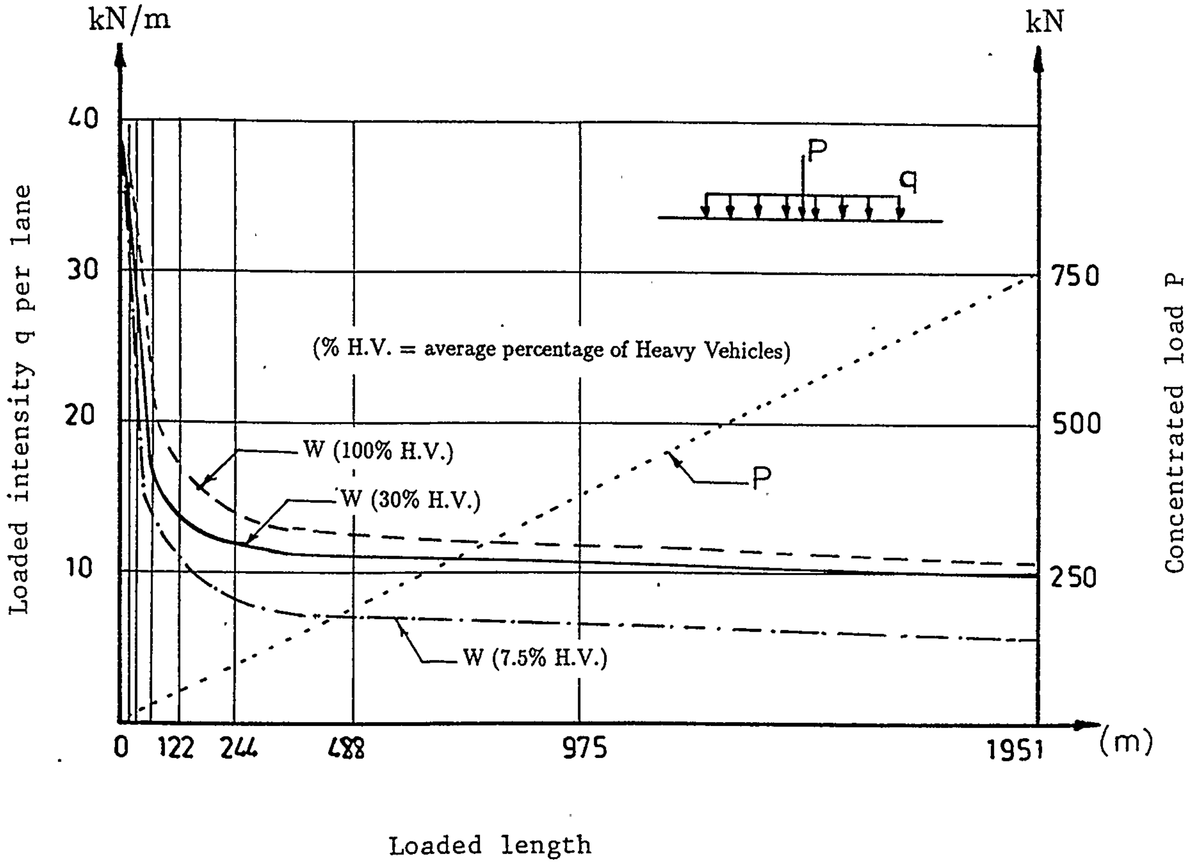

Figure 2.6: Highway live loads including dynamic effect according to the American Committee on Loads and Forces on Bridges (1981)

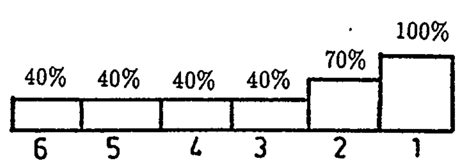

Figure 2.7: Reduction factors for multi-lane loading according to the American Committee on Loads and Forces on Bridges (1981)

2.3.5 Comparison between the three codes

A comparison between the highway live loads for the proposed bridge according to the different codes is shown in Table 2.2. The Canadian and American Codes are giving the same live load intensity of 23.8 kN/m for a heavy traffic. This load corresponds approximately to the light traffic value (20 kN/m) of the European Code, which in general is recommending higher live loads. Using the loading recommended by Public Works Canada in the project proposal, which is about 27.3 kN/m, would correspond to the European medium traffic value of 30 kN/m.

2.4 TEMPERATURE LOADING

The temperature in a bridge affects the structure in two ways. First there is an axial deformation due to minimum and maximum temperature, the second design parameter is the thermal gradient, which shall be considered in the design of continuous structures according to the Canadian Code. In order to study these two effects, three cases of temperature distributions are analysed.

- Temperature Distribution No.1

  All the elements of the bridge (deck, pylons and cables) are subjected to a uniform temperature drop of $\Delta T = -40°C$.

- Temperature Distribution No.2

  - $\Delta T = -40°C$ for the concrete components (deck and pylons)
  - $\Delta T = -20°C$ for the steel components (cables)

Table 2.2: Comparison between the highway live loads for the proposed bridge according to the different codes

	Canadian Code		American Code		European Code
	Public Works Canada	CAN/CSA S6-88	Ivy et al	ASCE Committee	
q (kN/m)	27.3	23.8	17.8	Light 13.6 Medium 20.4 Heavy 23.8	20 30 40
$P_{Bending}$ (kN)	–	–	0	Light 100 Medium 100 Heavy 100	200 300 400
P_{Shear} (kN)	–	–	0	Light 100 Medium 100 Heavy 100	200 300 400

Note: For the Canadian Code the remaining truck load of 0.6 W = 414 kN is to be added as concentrated axle loads

- Temperature Distribution No.3

  In this case a more realistic temperature distribution is applied. It is assumed that the bridge components near the water will cool down more than the other components. This leads to a temperature distribution as follows:

  - Pylon:

    $\Delta T = -40°C$ for lower part of the pylons (below the deck level)

    $\Delta T = -20°C$ for upper inclined legs of the pylons (above the deck level)

  - Deck:

    $\Delta T = -40°C$ for the bottom of the deck

    $\Delta T = -20°C$ for the top of the deck

  - Cables:

    $\Delta T = -20°C$ for the cables

These temperature distributions are constant throughout the length of the bridge. The thermal expansion coefficient of the concrete is taken as $10 \times 10^{-6}/°C$ and for the steel cables $11.7 \times 10^{-6}/°C$.

2.5 SUMMARY

The highway live loads according to the Canadian, American and European Codes are compared. The conclusion is that the Canadian and American Codes are giving about the same live load intensity, whereas the European Code specifies in general higher live loads. In addition, the three temperature distributions used to examine the behaviour of continuous cable-stayed bridges are presented in this chapter.

Chapter 3

DIMENSIONS AND STRUCTURAL SYSTEMS FOR MULTI-SPAN CABLE-STAYED BRIDGES

3.1 INTRODUCTION

In this chapter the different structural systems for continuous cable-stayed bridges are reviewed and compared. Based on this comparison an efficient system is chosen for the proposed bridge. In addition, the different cable arrangements are discussed and a preliminary design of the cables is made.

3.2 STRUCTURAL SYSTEMS FOR MULTI-SPAN CABLE-STAYED BRIDGES

The majority of cable-stayed bridges that have been constructed are of the two-span asymmetrical or three-span symmetrical types. In such types of cable-stayed bridges the back-stay cables, which are anchored at the fixed end support, stabilize the pylons and help the forestays to support the main span in an efficient manner as shown in Figure 3.1(a). In a continuous (multi-span) cable-stayed bridge those back-stays are not available, and an efficient horizontal fixing of the pylon tops is consequently not obtained. Under unbalanced live loads this leads to a rotation of the inner cable systems, causing unacceptable vertical deflections of the deck (Figure 3.1(b)).

The stability of multi-span cable-stayed bridges can be achieved according to Gimsing (1983) by the following structural systems (see Figure 3.2):

1. Stiff superstructure (girder depth $\approx l/60$) as shown in Figure 3.2(b).

   This system gives a heavy deck for long span bridges, increasing the cable forces due to the own weight of the structure.

2. Stiff pylons as shown in Figure 3.2(c),(d).

   The inertia of the pylons can be increased in two ways, by using a wall-like pylon (Fig. 3.2(c)) or by using twin pylons with inclined legs (Fig. 3.2(d)). Since the horizontal forces are resisted in this system by the pylons, which are fixed at their bases, fairly strong soil conditions are needed for the foundations of the pylons.

3. Stabilizing the pylon tops by using different cable configurations as shown in Fig. 3.2 (e), (f) and (g). The major disadvantage of such systems is the sort of chain reaction created in case of failure of one cable.

Gimsing (1976) also presented a comparison of the deflections of different multi-span systems (see Figure 3.3). The deflection diagrams are for the central span under a uniformly distributed load. Similar results are found for uniform load and deflections in a side span.

(a) Three-span (stabilizing back-stays available)

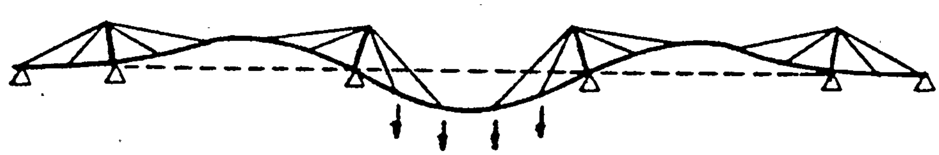

(b) Multi-span (stabilizing back-stays not available)

Figure 3.1: Deflections of cable-stayed bridges

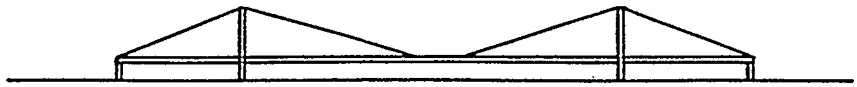

(a) Conventional system

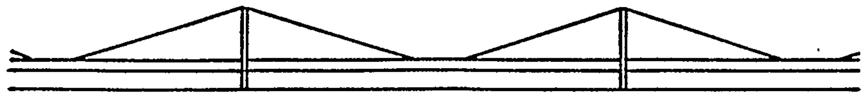

(b) Flexible pylons, stiff deck

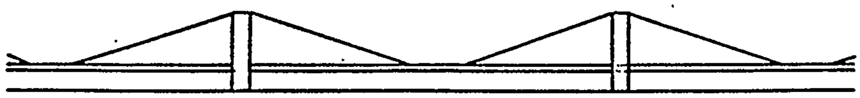

(c) Stiff wall-like pylons, flexible deck

(d) Stiff twin pylons, flexible deck

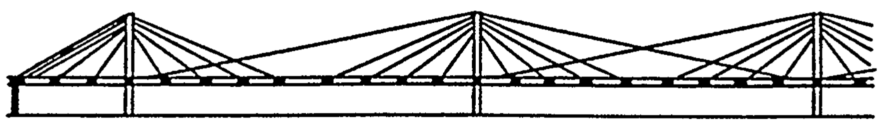

(e) Back-stays anchored to adjacent pylons

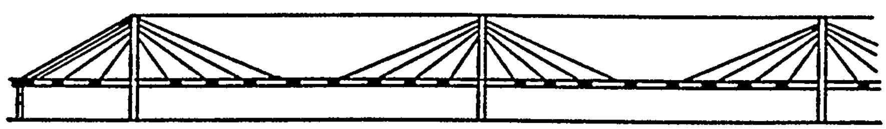

(f) Continuous cable connecting top of pylons

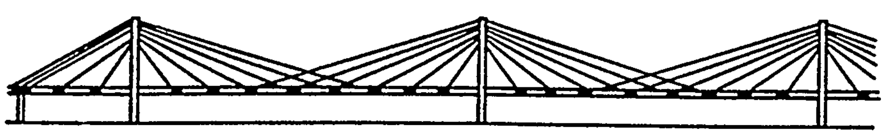

(g) Cables overlapping in midspan regions

Figure 3.2: Structural systems for multi-span cable-stayed bridges

Conclusions to be drawn from the study of Gimsing are as follows:

1. The fixing of the pylons with common flexural stiffness has a minor influence on the deflections. Compare System B (hinged pylons) with System C (fixed pylons).

2. Fixing the pylons and increasing their flexural stiffness by a factor of 10 do not reduce the deflections significantly. Compare System B with System D.

3. A cable connecting the pylon tops (System E) reduces the deflections of the bridge significantly.

4. A triangular pylon structure supported on proper bearings (System F) is the most efficient way to reduce the deflections in a multi-span cable-stayed bridge.

Based on the above discussion, a system composed of stiff triangular pylons and a relatively flexible deck seems to be the optimum solution for the proposed multi-span cable-stayed bridge.

The dimensions of the pylons, deck and cables will be discussed next.

3.3 DIMENSIONS OF THE PYLONS

Stiff twin pylons with dimensions as shown in Figure 3.4 are chosen. They consist of inclined upper legs connected by a horizontal tie-beam at the level of the deck, and sloped lower legs. In the transverse direction, the pylon legs are not sloped as shown in Figure 3.5. Inclination of the pylon legs in both directions, the longitudinal and transversal ones, would complicate the erection of the pylons.

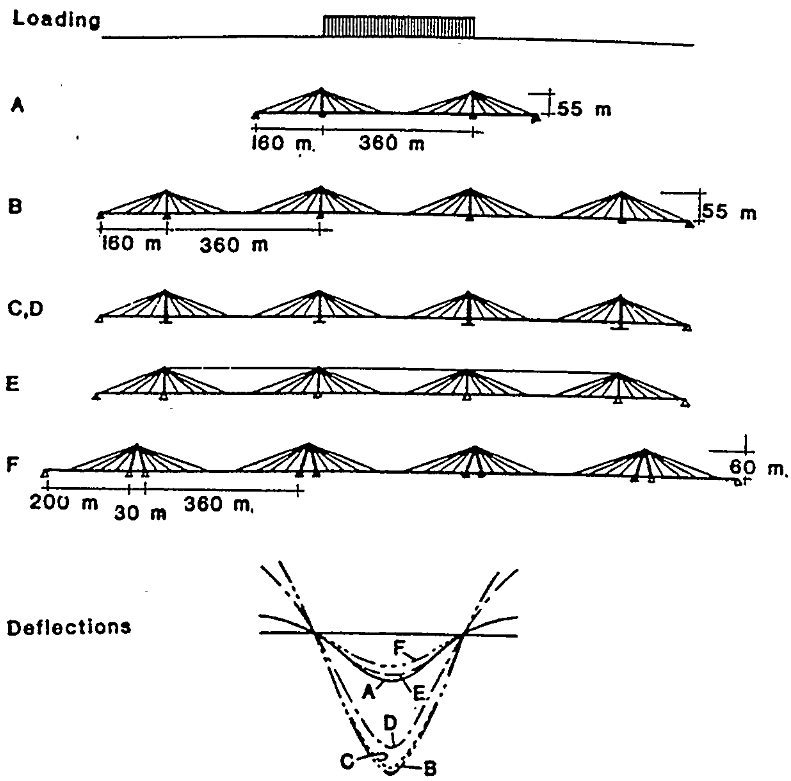

A: Conventional system with hinged connections between the superstructure and the substructure

B: Multi-span system with the same member dimensions as System A

C: Fixed connection between pylons and substructure, same member dimensions as in System A

D: Fixed connection between pylons and substructure, moment of inertia of the pylons is increased by an order of magnitude 10

E: Same as B, except for the addition of the horizontal cable between the pylons

F: Triangular pylon structures supported on rollers

Figure 3.3: Deflections of different systems for multi-span cable-stayed bridges (Adapted from Gimsing, 1976)

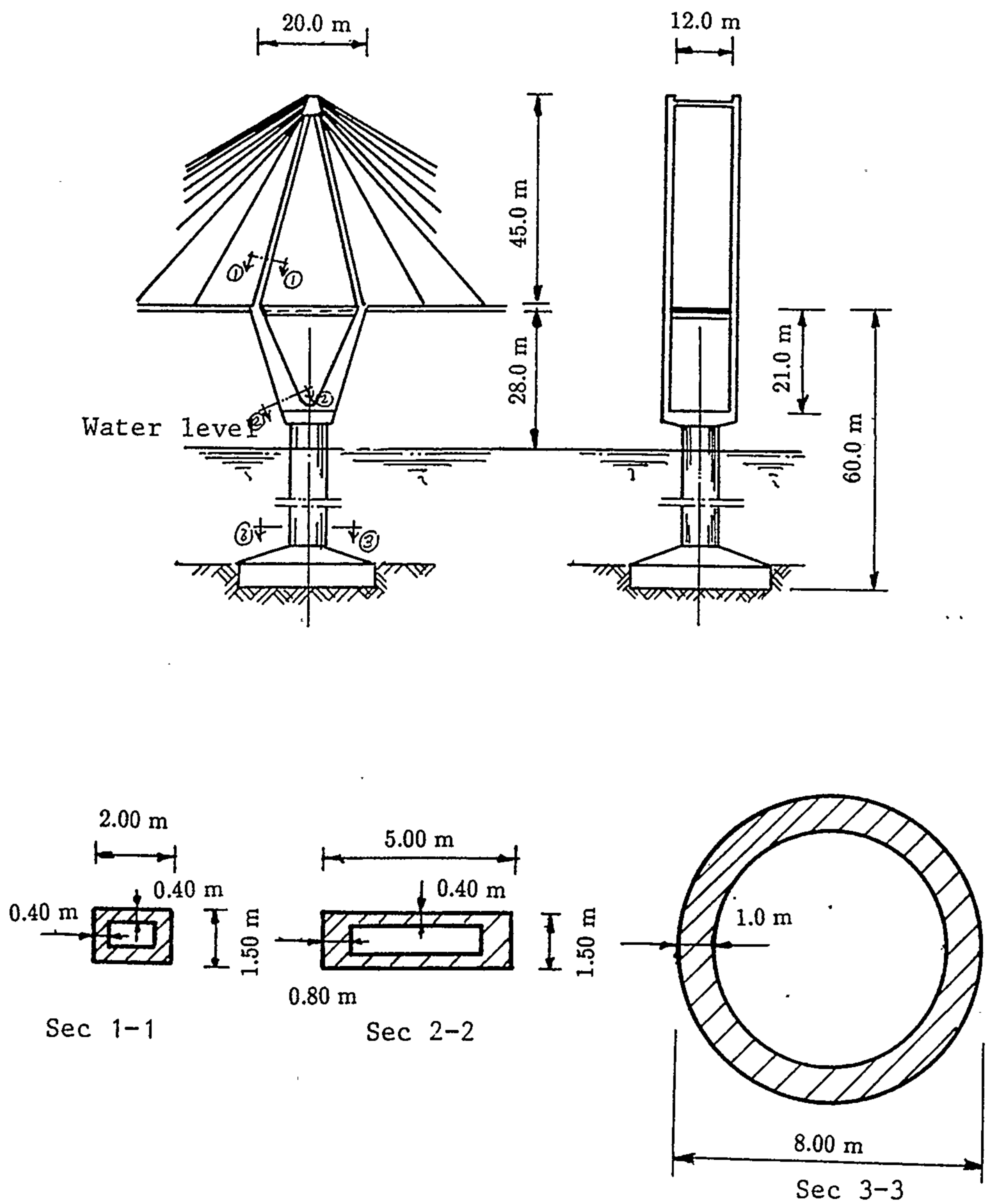

Figure 3.4: Pylon configuration and dimensions for the proposed bridge

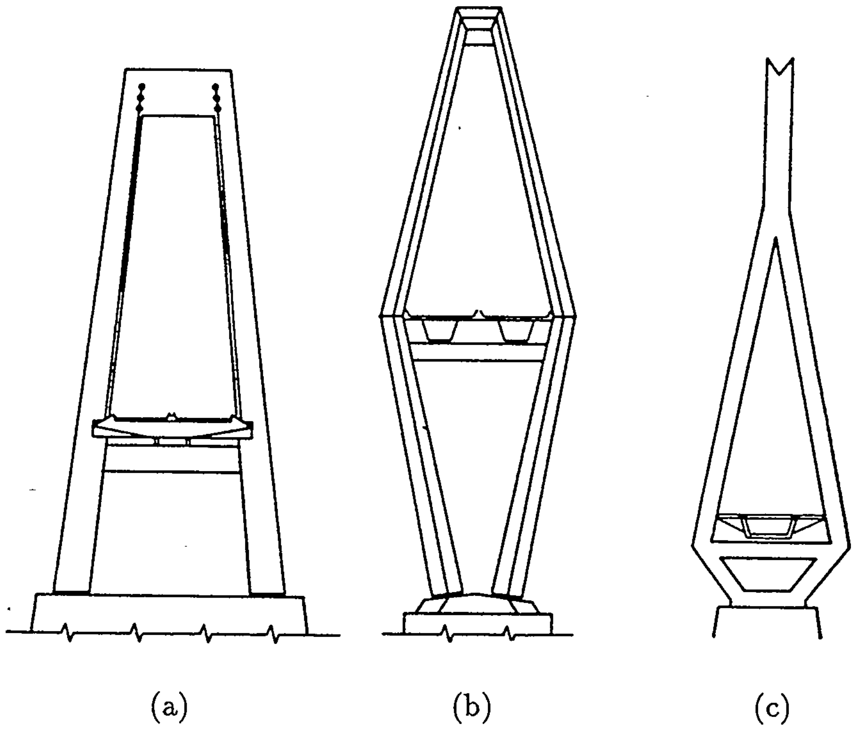

(a) modified A-frame

(b) diamond

(c) modified diamond

Figure 3.5: Alternate pylon configurations in the transversal direction

The inclination of the upper legs is chosen such that no tension develops in those members under the maximum unbalanced live load conditions. A hollow cross-section with a constant depth of 2.0 m (Figure 3.4) is sufficient for those legs, since they are primarily subjected to axial forces as will be shown later in the analysis.

The cable forces and the required quantity of cable steel decreases with the height of the pylon above the deck level. This is shown by Leonhardt (1987) in Figure 3.6. An optimum range for the pylon height above the deck level is between $0.2l$ and $0.25l$ (where l is the length of the midspan). For the proposed bridge a height of 45 m ($0.18l$) for the upper legs is believed to be reasonable.

The height of the sloped lower legs is taken as 21 m to accommodate the truss used for the construction of the deck, as will be described later. The depth of the hollow cross-section of those lower legs is increasing from 2.0 m at the deck level to 5.0 m at the vertical pier shaft (Figure 3.4), to resist the bending moments created by unbalanced live loads as will be shown later in the analysis.

To reduce the ice loads, a hollow circular pier shaft (with 8.0 m outside diameter and 1.0 m wall thickness) is selected instead of the parallel vertical pier legs shown in Figure 3.2(d).

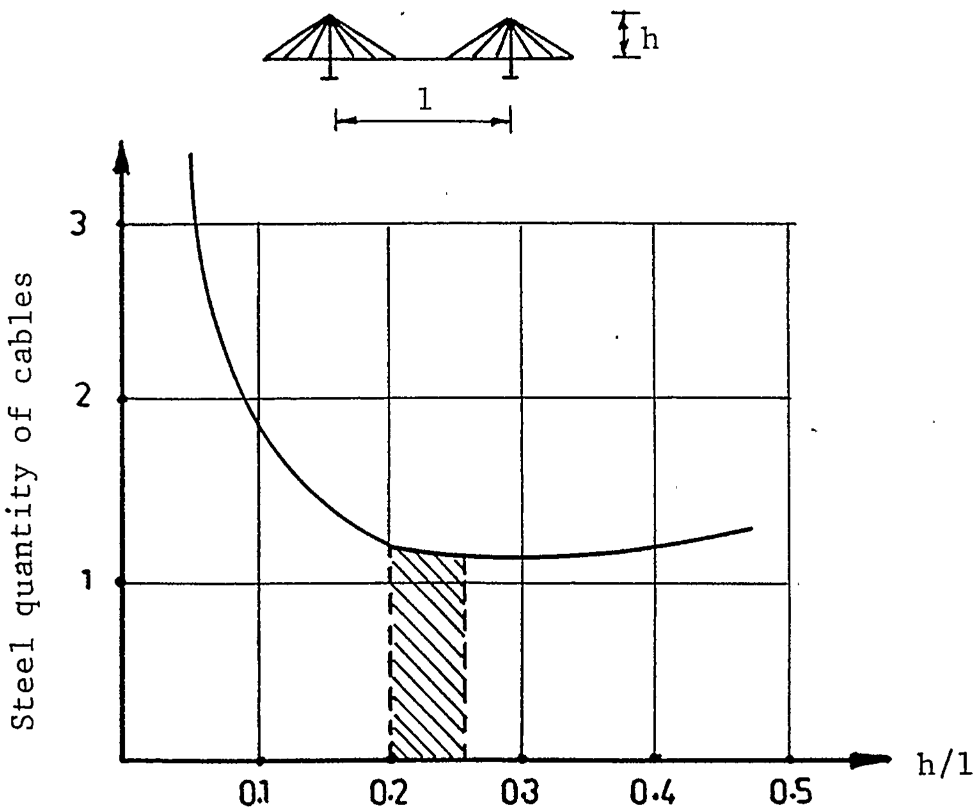

Figure 3.6: Quantity of cable steel as a function of the relative height of the pylons (Adapted from F. Leonhardt, 1987)

3.4 THE CABLES

In this section the different cable arrangements for cable-stayed bridges are discussed, followed by the preliminary design of the cables.

3.4.1 The different longitudinal cable arrangements

A tabular summary of the various cable arrangements is presented in Figure 3.7. Basically, there are four different cable configurations. These basic systems are referred to as fan, harp, semi-harp and star systems.

- The fan system

  The stays are at a maximum angle of inclination to the deck, which means that the cables are nearly in an optimum position to support the dead and live loads and simultaneously produce a minimum axial force component acting on the deck. In addition the bending moments in the deck are less, if compared to the harp system. In a parametric study done by Walther et al (1988), it is shown that for the same bridge, using a fan cable configuration instead of a harp type, decreases the normal forces in the deck by up to 40 percent and the maximum bending moments in the deck are reduced by up to 25 percent.

- The harp system

  The cable connections are distributed throughout the height of the pylon, resulting in an efficient pylon design compared to the fan system, which has all the cables at the top of the pylon. The concentrated load at the top of the pylon (due to unbalanced live loads) produces large shearing forces and bending moments along the entire height of the pylon. In addition, high

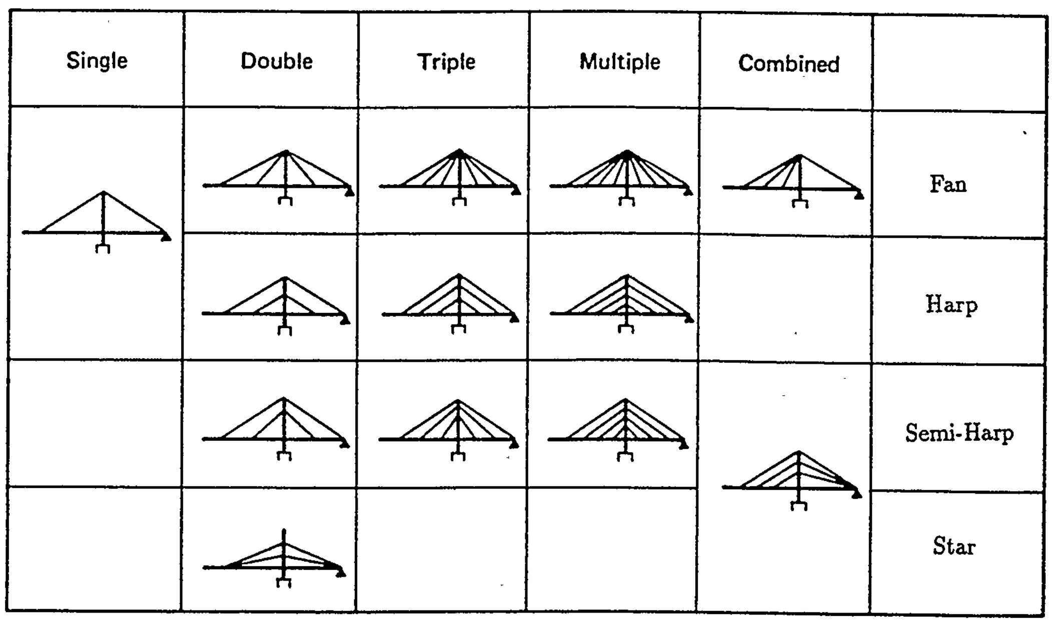

Figure 3.7: Different systems of longitudinal cable arrangements

cable forces may cause problems in anchoring the cables to the pylon in the fan configuration. The harp system may also be preferred over the radiating system for aesthetic reasons, because it minimizes the visual intersection of cables when viewed from an oblique angle.

- The semi-harp system

  This system represents a compromise between the extremes of the harp and fan systems, and is useful when it becomes difficult to accommodate all the cables at the top of the pylon.

- The star system

  The star system is only used for its unique aesthetic appearance. There are no major structural advantages of using this system.

The conclusion of the above discussion is that the harp system is beneficial in designing the pylon (reducing the bending moments), whereas the fan system is beneficial in designing the deck. So if a triangular pylon configuration in which the inclined legs are primarily subjected to axial forces is used, then the advantage of the harp system is reduced. The optimum cable configuration will be the fan type.

The number of cables depends on the length of span, type of loading, height of pylons, economy and aesthetics. Using only a few cable stays results in large cable forces, which require complicated anchorage systems. In addition, deep girders are required to span the long distance between the cable anchor points.

A large number of cables provides a continuous support for the deck, thus permitting the use of a shallow depth girder and increasing the stability of the bridge against dynamic wind forces (Leonhardt, 1980).

3.4.2 Preliminary design of the cables

The following simple equation can be used for the preliminary design of the cables (Walther et al, 1988):

$$A_i = \frac{T_{g,i}}{\sigma_g} \tag{3.1}$$

where:

A_i = cross-section area of cable number (i)

$T_{g,i}$ = tension force in cable number (i) due to self-weight and permanent loads

σ_g = allowable stress in the cables due to self-weight and permanent loads

The calculation of $T_{g,i}$ and σ_g is discussed next.

- Calculation of the tension in the cables $T_{g,i}$

  If the deformations in the deck and pylons are neglected, it is possible to regard the deck as a continuous structure, rigidly supported by the cables as shown in Figure 3.8.

  The reactions R_i of the idealized continuous beam represent the vertical components of the forces in the cables due to dead load. From those reactions the cable forces $T_{g,i}$ are obtained using the simple expression:

$$T_{g,i} = \frac{R_i}{\sin \theta_i} \tag{3.2}$$

where:

R_i = reaction of the idealized continuous beam at cable number (i)

θ_i = inclination of cable number (i) to the horizontal

Usually the reaction R_i can be calculated with acceptable accuracy for the preliminary design (see Figure 3.8) as:

$$R_i = g \cdot b_i \tag{3.3}$$

where:

g = dead load intensity of the deck

b_i = the spacing between the anchor points of the cables in the deck

- Calculation of the allowable cable stress σ_g

  The allowed stress σ_g in the cables due to self-weight and permanent loads is governed either by the strength or the fatigue criterion (Walther et al, 1988). This depends on the ratio $\eta = q/g$ (live load/dead load intensities). If the value of η is small, the stress variation due to live load $(\Delta\sigma_q)$ is less than the value of the permissible limit $(\Delta\sigma_{per})$, which enables the use of the full load-carrying capacity of the cables (strength criterion). For high values of η, the stress variation $(\Delta\sigma_q)$ becomes decisive and the fatigue criterion becomes governing in the design of the cables.

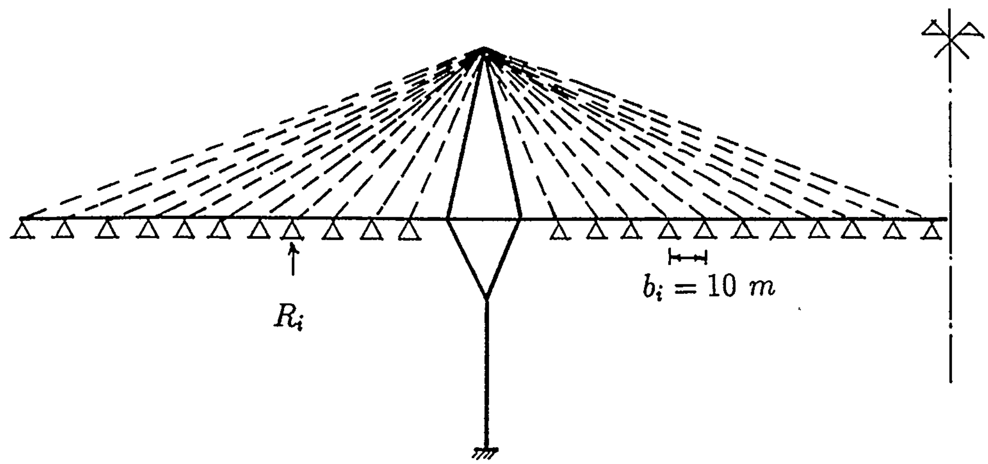

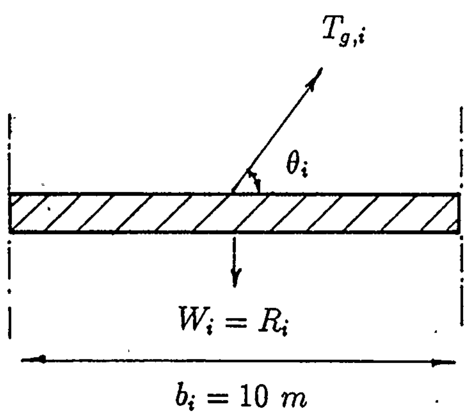

Figure 3.8: Deck idealized as a continuous beam

According to Walther et al (1988), equations giving σ_g as a function of the ratio η for those two criteria can be established.

1. The strength criterion:

$$\sigma_g = \frac{g}{g+q} \cdot \sigma_{per} \tag{3.4}$$

where:

g	$=$ dead load intensity
q	$=$ live load intensity
σ_{per}	$=$ permissible stress in the cables
	$= 0.45 f_{pu}$ in case of using a global safety factor of 2.2 against the rupture strength of the steel
f_{pu}	$=$ rupture stress of the steel

2. The fatigue criterion:

$$\Delta\sigma_{per} = \frac{T_q}{A} = \frac{T_q}{A} \cdot \frac{T_g}{T_g} = \frac{T_q}{T_g} \cdot \sigma_g$$

Hence,

$$\sigma_g = \left(\frac{q}{g}\right)^{-1} \cdot \Delta\sigma_{per} \tag{3.5}$$

where:

$\Delta\sigma_{per}$ $=$ permissible stress variation due to live load

Using $\phi 15.2$ ASTM A 416-74 Grade 250 strands (rupture stress $f_{pu} = 1700 N/mm^2$, $\Delta\sigma_{per} = 200 N/mm^2$ and area of one strand $= 140 mm^2$), curves giving σ_g as a function of the ratio η can be plotted for the two criteria of strength and fatigue as shown in Figure 3.9. The conclusion is that for values of η less than 0.4,

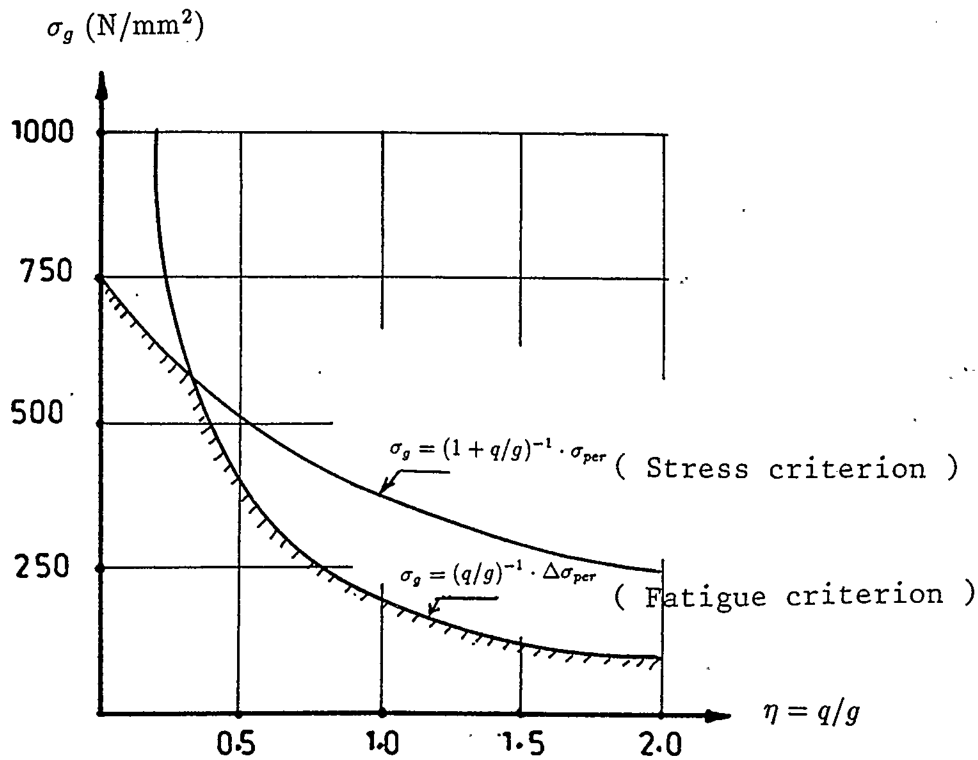

Figure 3.9: Permissible cable stress σ_g due to dead load as a function of the (live load/dead load) ratio η

the strength criterion is governing the design, whereas for values greater than 0.4, the fatigue criterion is more critical.

In the case of the proposed bridge $\eta = q/g = 0.12$, which means that the strength criterion (Equation 3.3) is to be used for the design of the cables.

Except for the cables close to the pylons, no later adjustments of the areas calculated by this preliminary method were necessary. The cable areas are listed in Table 3.1.

3.5 THE DECK

In this section steel and concrete decks are briefly compared, followed by a discussion about different concrete cross-section types.

3.5.1 Steel decks versus concrete decks

Although steel decks have been extensively used for the first modern cable-stayed bridges (see Figure 3.10), a number of cable-stayed bridges in the last two decades have been constructed using a reinforced or prestressed concrete deck system. Prestressed concrete proved to be a strongly competitive construction material compared to steel for the deck systems of cable-stayed bridges.

A metal deck provides the optimum answer to the demand for economy in the use of materials. It is, in fact, possible to limit its self-weight to a value which is about one fifth of that of a concrete deck (Walther et al, 1988). On the other hand, the use of a steel cross-section is today two to four times as expensive as its equivalent in concrete. Thus, the reduced self-weight of the deck must result in appreciable savings

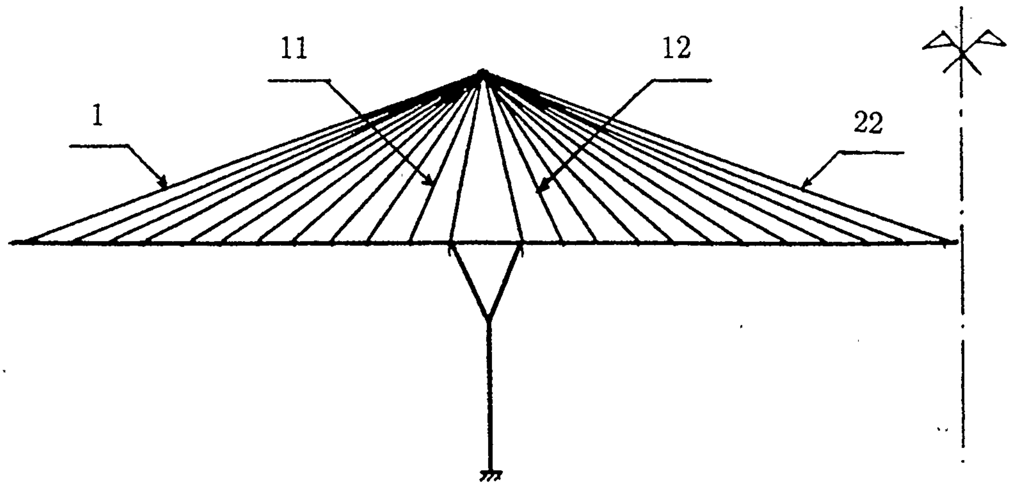

Table 3.1: Cable Areas

Cable Number	Cross-section Area (mm^2)
1	32 x 140 = 4480
2	32 x 140 = 4480
3	26 x 140 = 3640
4	26 x 140 = 3640
5	22 x 140 = 3080
6	22 x 140 = 3080
7	18 x 140 = 2520
8	18 x 140 = 2520
9	16 x 140 = 2240
10	16 x 140 = 2240
11	10 x 140 = 1400

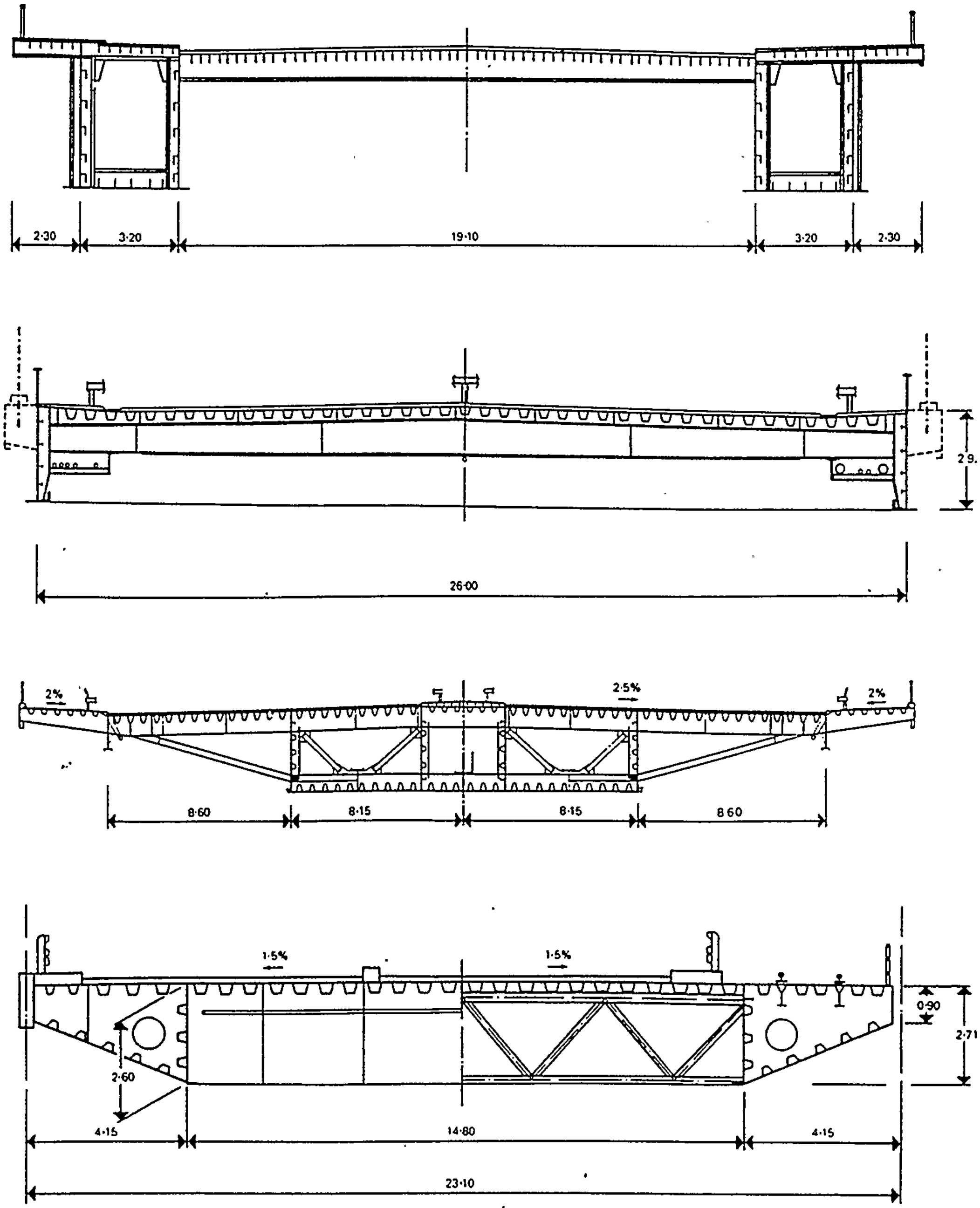

Figure 3.10: Examples of steel decks (Adapted from Walther et al, 1988)

in the other load-bearing elements (cables, pylons and foundations), if a steel deck is to be more economical than a concrete deck.

For the proposed bridge a concrete deck is believed therefore to be the optimum solution. Different concrete cross-section types are discussed next.

3.5.2 Concrete cross-section types for the deck

Several types of concrete cross-sections are shown in Figure 3.11. The major factors affecting the choice of the deck cross-section type are:

- Suspending system (double or single plane of cables)
- Longitudinal spacing of the cables
- Deck width
- Deck span
- Live load to be carried

If the deck is suspended along its edges, a very simple cross-section for the deck can be used. No torsional rigidity is necessary because the cables give a stiff support along each edge and the transverse deflections due to unsymmetrical loading are small. According to Leonhardt (1980), for a deck width up to 15 m, a simple solid or hollow concrete slab width edge beams is sufficient. The edge beams are beneficial in anchoring the cables and securing the buckling safety.

A parametric study performed by Walther et al (1988) shows that increasing the deck inertia in the longitudinal direction is not basically favourable. A deck with a high inertia attracts considerable bending moments accompanied by an extension of

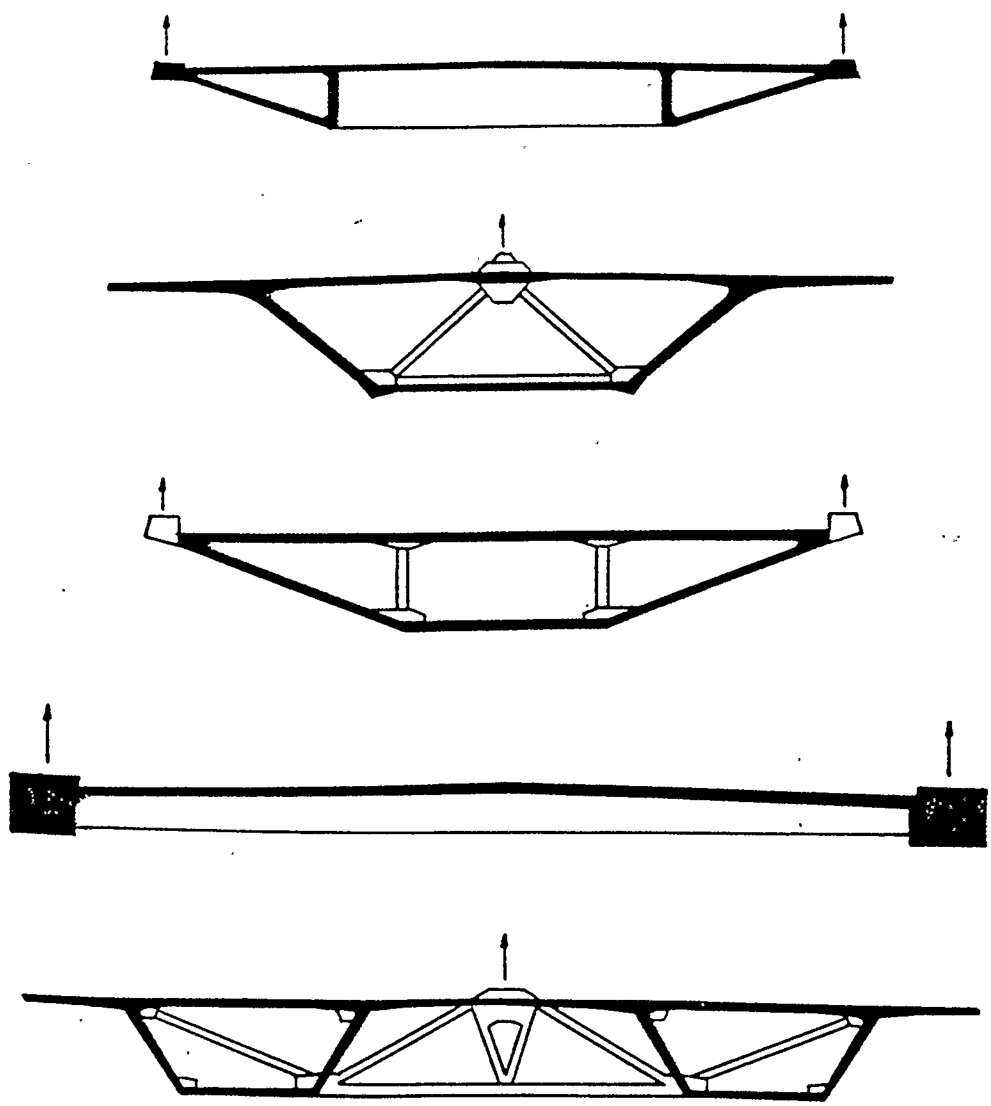

Figure 3.11: Examples of concrete decks (Adapted from Podolny et al, 1986)

the highly stressed zones of the deck, without appreciably reducing the forces in the pylons and the cables.

Based on the above discussion, an idealized solid concrete slab with dimensions 12.0x0.60 m (see Figure 3.12) is chosen for the proposed bridge. The slab is resting on two roller supports and one hinge support on each pylon. At both ends of the 500 m long continuous slab, expansion joints which are capable of transferring only vertical (shear) forces will provide the continuity of the bridge, allowing expansion and contraction of the deck due to temperature.

3.6 SUMMARY

Based on the comparison of different systems an efficient system for a multi-span cable-stayed bridge is chosen. This system consists of:

- Stiff diamond-shaped pylons
- A simple solid cross-section of 0.60 m thickness
- Fan-type cable configuration

In addition a preliminary design method for the cables is presented in this chapter.

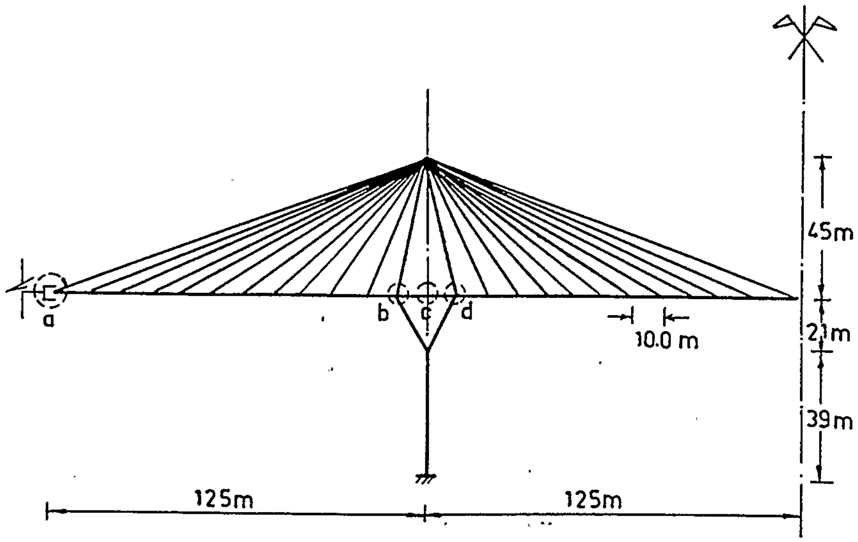

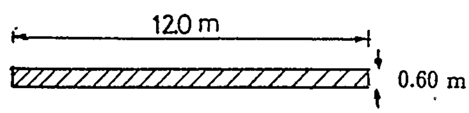

Deck cross-section

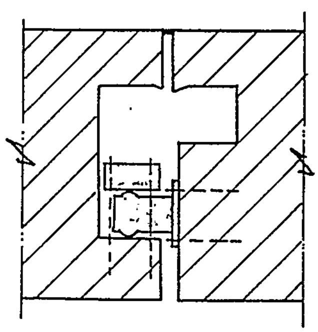

(a)

Hinge for the transfer of vertical upward and downward reactions

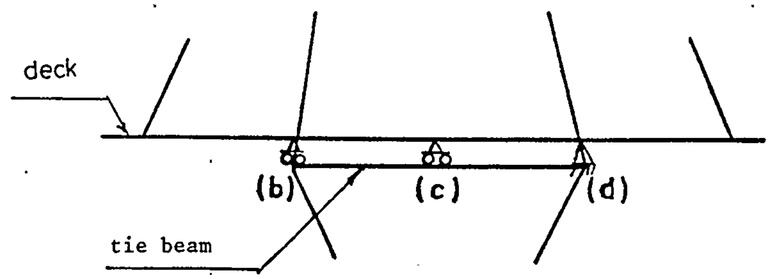

Deck-pylon connection

Figure 3.12: Statical system and dimensions of the deck for the proposed bridge

Chapter 4

THE ANALYSIS OF CABLE-STAYED BRIDGES

4.1 INTRODUCTION

In this chapter the different methods of analysing cable-stayed bridges are briefly reviewed, followed by a general description of the model used in the computer analysis done in this study.

For the geometrical nonlinear analysis, the behaviour of a cable element, effect of axial forces on the beam stiffness and the effect of large deflections are discussed. Also the several solution techniques for nonlinear problems available in the used computer program ANSYS are presented.

At the end of this chapter, the approximations inherent in a linear analysis are discussed.

4.2 THE DIFFERENT METHODS OF ANALYSIS

The analysis of a cable-stayed bridge requires an appropriate idealization, or modeling of the structure. The restraints, if any, present at each joint in the structure should be determined in order to mathematically model the bridge. Connections between the cables, deck and pylons are idealized at their points of intersection.

For a single-plane system the structure may be idealized as a two-dimensional plane frame. The effect of torsion on the deck would have to be superimposed on the deck. A two-plane system may be idealized as a three-dimensional space frame with torsional forces included in the analysis.

Several methods have been employed in the analysis of cable-stayed bridges. Perhaps the most important methods are:

- The reduction method introduced by Falk in 1956

  This method is ideally suited to systems consisting of a number of elements linked together end to end in the form of a chain, because only successive matrix multiplications are necessary to fit the elements together.

- The simulation method proposed by Protte and Tross in 1966

  The main system is chosen as a continuous main girder with independent pylons having fixed supports, and the cables were introduced as redundants.

- The force-displacement method developed by Smith in 1967

  In this method the unknowns in the matrix formulation include displacements and forces.

- The flexibility method used by Troitsky and Lazar in 1971

  In this method the unknowns (redundants) are the forces in the structure.

- The stiffness method used by Podolny in 1971

  In the stiffness method the unknowns are the displacements and rotations at the joints of the structure.

Detailed description of the previously mentioned methods can be found in Troitsky (1977). In the present study the computer program ANSYS, which adopts the stiffness approach, is used for the analysis. Detailed information about the stiffness method are available in numerous textbooks (e.g. Ghali and Neville, 1989).

The following steps describe the outline of the solution procedure (Seif, 1986):

1. The structure is idealized as a set of elements connected together at the joints (nodes).

2. The global structure coordinates are arbitrarily chosen together with a set of local coordinates for each member.

3. For each member, the stiffness matrix $[k]$ is generated in the local member axes, and then rotated into the global structure axes.

4. The structure stiffness matrix $[K]$ is assembled from the member stiffness matrices obtained in step 3.

5. The load vector $\{F\}$ contains loads which are applied directly to the nodes in the global axes, and equivalent node forces calculated from member loads after rotated into the global structure axes.

6. $[K]$ and $\{F\}$ are corrected for known boundary conditions (support restraints).

7. The joint displacements $\{D\}$ are found by solving the equilibrium equation:

$$[K] \cdot \{D\} = \{F\} \tag{4.1}$$

8. The final member end forces are calculated by multiplying the member stiffness matrix $[k]$ in the global axes by its end joint displacements, and then adding the resulting vector to the member fixed end forces.

4.3 MODEL USED IN THE COMPUTER ANALYSIS

Two types of analysis are performed, a geometrical nonlinear analysis and a conventional linear analysis. A two dimensional model as shown in Figure 4.1 (for the linear analysis) and Figure 4.2 (for the nonlinear analysis) is used. Since the value of the live load intensity applied on the deck is only 12 percent of the own weight of the deck, the torsional effects of unsymmetrical transverse live load cases are not of major influence. It is believed that there is no need for a three-dimensional model.

In both types of analysis, the deck and the parts of the pylons with constant cross-sections are represented by a conventional beam element, whereas the lower sloped legs of the pylons ,which have variable cross-sections, are modeled using tapered beam elements.

For the cables, truss elements are used in the linear analysis, and cable elements are used in the geometrical nonlinear analysis.

The expansion joints at the ends of the 500 m long deck, transferring only vertical reactions, are represented by springs. The stiffness of those springs are calculated by applying a vertical concentrated force F at one end of the deck, and calculating the corresponding vertical deflection of this end.

The deck-pylon connection is simulated by coupling the vertical displacements of the deck node and the corresponding pylon node to create a roller between them,

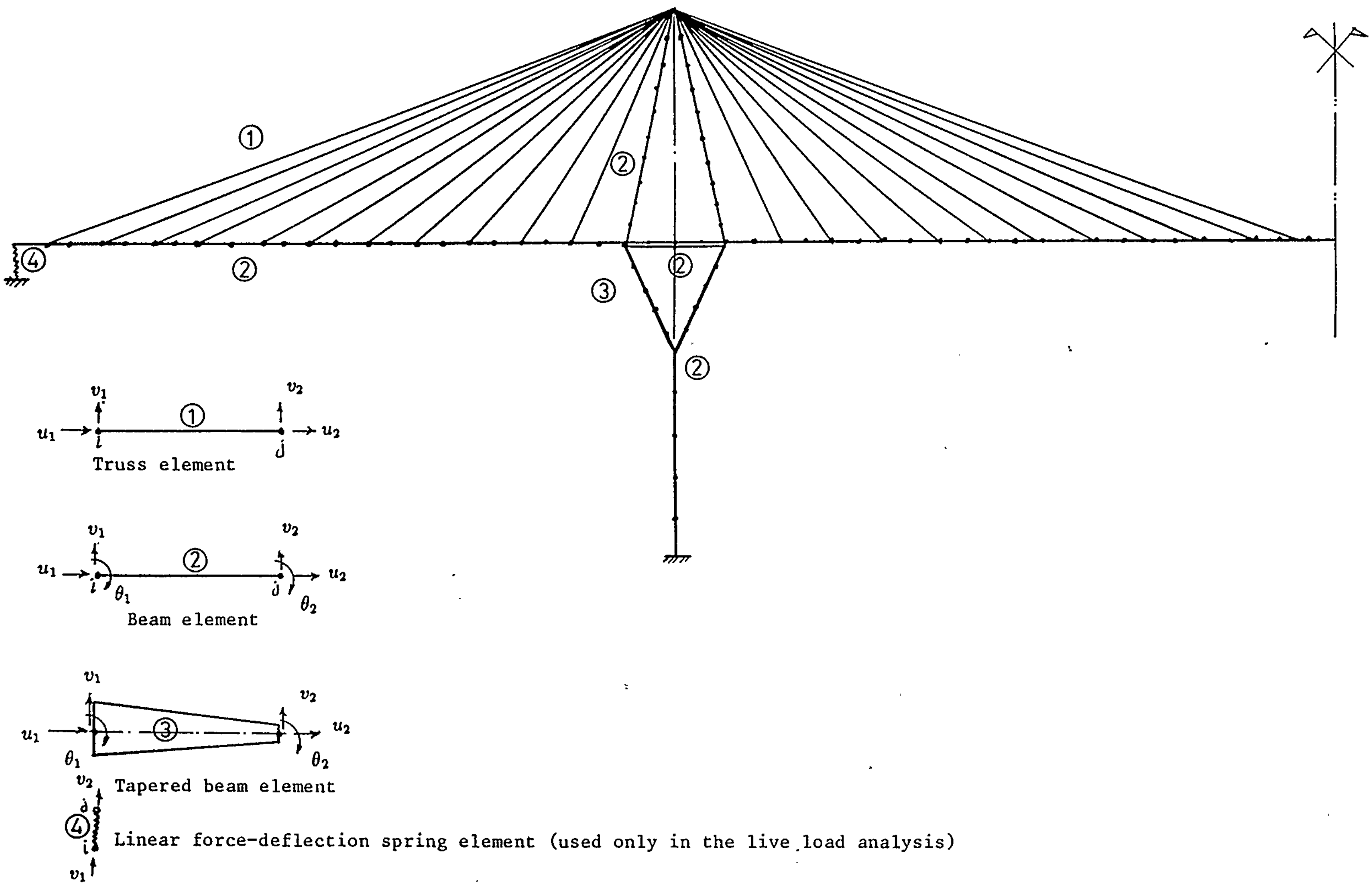

Figure 4.1: Nodes and elements for the linear analysis

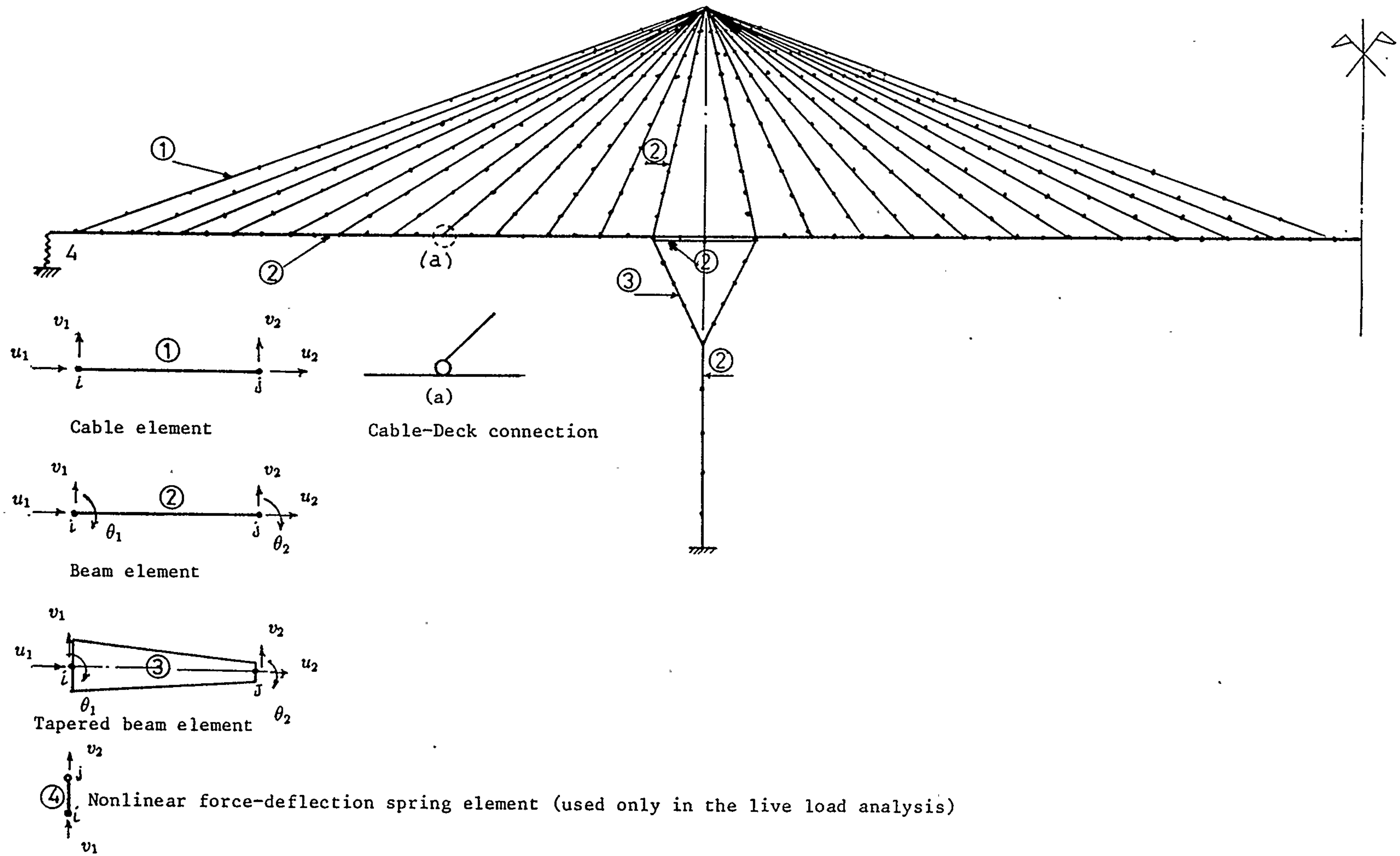

Figure 4.2: Nodes and elements for the geometric nonlinear analysis

and coupling the vertical and horizontal displacements to create a hinged support. Coupling of the displacements of two nodes means that the two nodes have the same displacements.

Shear deformations are taken into account in both types of analysis. A detailed description of the geometric nonlinear and conventional linear analysis is presented next.

4.4 THE GEOMETRIC NONLINEAR ANALYSIS

4.4.1 Introduction

The sources of the nonlinear behaviour of cable-stayed bridges (excluding the material nonlinearity) are the cables, the high axial forces in the deck and pylon, and the large deflections of the system associated with unbalanced live loads. These sources will be discussed next without detailed technical derivations, because they are available from many textbooks about the theory and analysis of structures. Therefore, only those equations considered to be basic for the understanding of the analysis of cable-stayed bridges are presented.

4.4.2 The behaviour of a cable

1. The catenary curve

   Because of its virtually zero stiffness in bending, a cable can only balance its own weight by taking the form of a hanging chain, which is the well known catenary curve shown in Figure 4.3(a).

Considering the equilibrium of a segment of the cable, the equation for the catenary elastic curve with respect to the coordinates shown in Figure 4.3 is:

$$y = a \cdot \cosh \frac{x}{a} \tag{4.2}$$

where:

a	$= H/w_c$
H	= horizontal component of the end reaction
w_c	= weight of the cable per unit length along the cable axis

The cable sag f may be expressed as:

$$f = a \cdot (\cosh \frac{l}{2a} - 1) \tag{4.3}$$

where:

l	= horizontal projected length of the cable chord (cable span)

Introducing the parameters $n = f/l$ and $m = 2a/l$, Equation 4.3 can be rewritten as:

$$n = \frac{m}{2} \cdot (\cosh \frac{1}{m} - 1) \tag{4.4}$$

which is an expression for the catenary curve in non-dimensional terms of n and m. This expression will be used later in comparing the catenary profile with the parabolic one.

2. The parabolic curve

   The equilibrium configuration of the cable, if it is assumed to be weightless, under a uniformly distributed load along its span, is a parabolic curve (Figure 4.3(b)). Using the same coordinate system as for the catenary, the basic equation for a parabolic cable supporting a uniformly distributed load along its span is:

$$y = a + \frac{x^2}{2a} \tag{4.5}$$

   where:

   $a \quad = H/w_p$

   $H \quad$ = horizontal component of the end reaction

   $w_p \quad$ = equivalent weight of the cable per unit length of its span

   In this case the cable sag f can be expressed as:

$$f = \frac{l^2}{8a} \tag{4.6}$$

   Substituting the terms n and m as previously defined to convert to a non-dimensional equation, the following expression for the parabolic curve is obtained:

$$n = \frac{1}{4m} \tag{4.7}$$

3. Catenary versus parabola

   Since the mathematical expression for a parabolic curve is simple when compared with the equation for a catenary curve, it is sometimes preferred to use the parabolic equation. So did Ernst (1965) for example, in deriving his

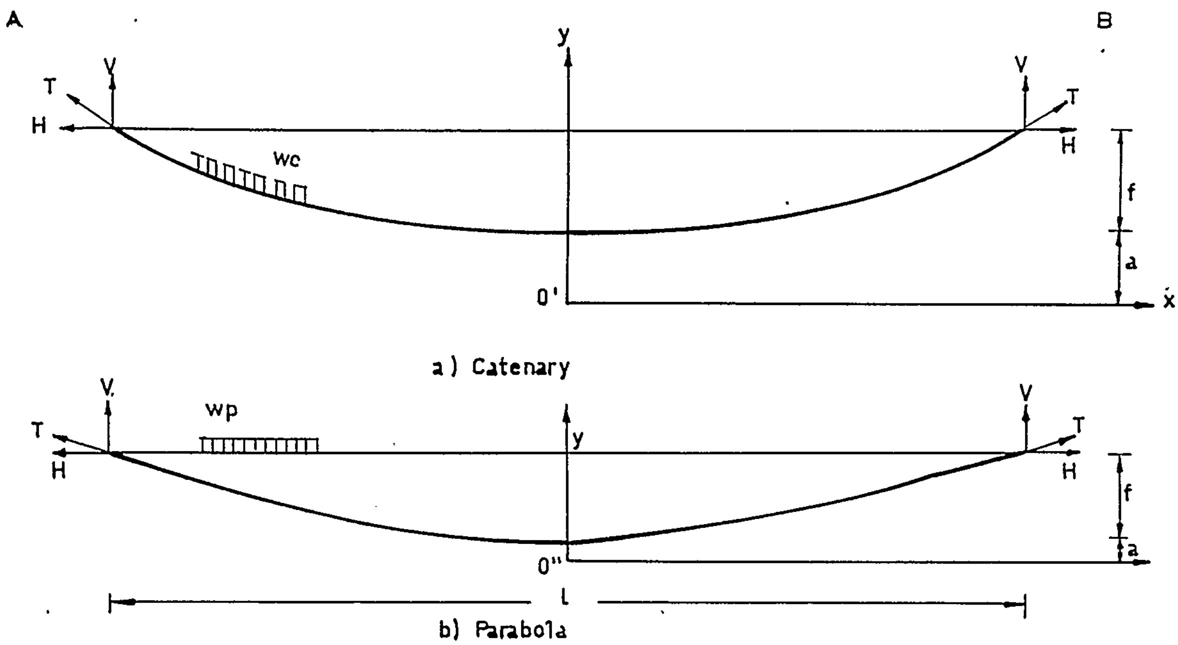

Figure 4.3: Sagging cable configurations

equivalent modulus of elasticity for cables (which will be used later in the linear analysis). Therefore, it is advantageous to compare the two expressions to determine the range for which a parabolic curve may be substituted for a catenary curve. This was done by Odenhausen (1965). He introduced a logarithmic plot, as shown in Figure 4.4, of Equations 4.4 and 4.7 with $n = f/l$ as abscissa and $m = 2a/l$ as the ordinate. The plot indicates that the two curves begin to diverge at a sag ratio $n = f/l$ of approximately 0.20. For typical cables used in cable-stayed bridges, the ratio $n = f/l$ is by far less than 0.20 (in the range of 0.015 in this study), which means that there is no difference between the catenary curve and the parabolic curve. The foregoing comparison applies to cables with a horizontal chord, while the cables of cable-stayed bridges have inclined chords (see Figure 4.5). Francis (1965) showed that a parabolic curve may be used instead of catenary curve without introducing any significant errors, if the ratio of the horizontal component of the cable tension H, to the cable weight w_{cable}, is greater than unity and the chord inclination does not exceed 70 degrees. These conditions are usually met in cable-stayed bridges.

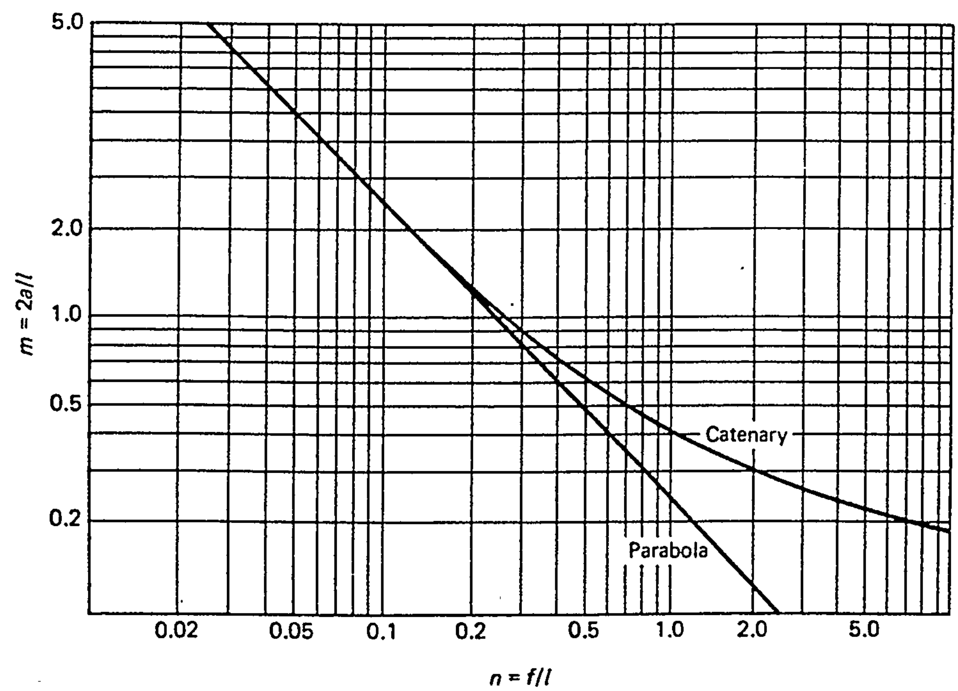

Figure 4.4: Comparison between catenary and parabola cable configurations (Adapted from Odenhausen, 1965)

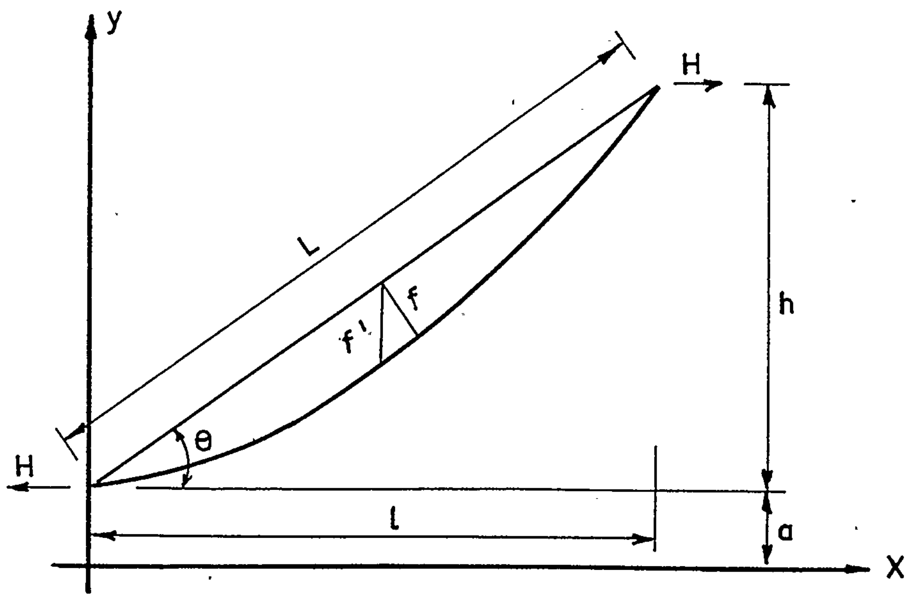

Figure 4.5: Cable with inclined chord

4. Cable element used in the computer nonlinear analysis

The sagging of a cable is a major cause of the nonlinear behaviour of cable-stayed bridge systems. Consider the cable between points A and B of Figure 4.6. The force needed to move point B to B̀ along the chord AB

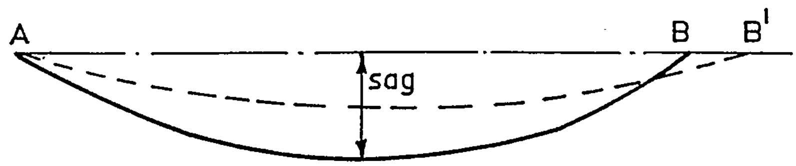

Figure 4.6: Sagging cable

depends not only on the cross-sectional area and the modulus of elasticity of the cable, but also on the cable sag. For a sagging cable, this force is less than for a straight cable, and as the tension in the sagging cable increases, its sag decreases. This means that even if the stress in the cables is within the linear elastic limit of the steel, the relationship between the force and the deformation is not linear.

In the analysis performed by the computer program ANSYS, a nonlinear cable element, which has the capability of sagging due to its own weight forming a catenary curve, is used. This cable element can resist only a tension force, if for any reason an absolute compressive force is applied, the stiffness of this element is removed. This feature simulates a slacked cable. Ten elements are used to model one cable stay, to obtain an accurate sagging profile of a cable. For more information about this cable element refer to Appendix A.

4.4.3 The effect of axial forces on the beam stiffness

4.4.3.1 Introduction

The main structural characteristic of the cable-stayed system is the integral action between the pylons, deck and cables. Horizontal compressive forces due to the cable action are taken directly by the deck, while the vertical compressive forces are transmitted by the cables to the pylon. This means that deck and pylon are subjected to high compressive axial forces.

By modeling the deck and pylon by a beam element in the stiffness method analysis, the effect of axial forces on the stiffness of a beam element (sometimes called $P - \delta$ effect) has to be considered. As the beam deflects, the moment due to axial loads changes and with it the deflections. The equilibrium position is obtained by using an iterative procedure.

Two methods are available to account for the axial force effect through adjusting the member stiffness matrix. The general solution approach and the Przemieniecki approach. These methods are briefly discussed next.

4.4.3.2 The general solution approach

The differential equation governing the deflection y of a prismatic beam element (see Figure 4.7(a)) subjected to an axial compressive force P with any boundary conditions is (Ghali and Neville, 1989):

$$\frac{d^4y}{dx^4} + \frac{P}{EI} \cdot \frac{d^2y}{dx^2} = w \tag{4.8}$$

where:

w = intensity of transverse loading

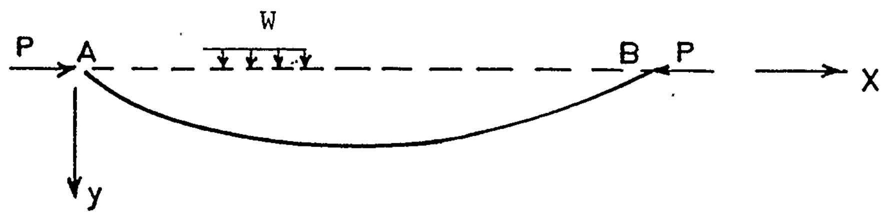

(a) Deflection

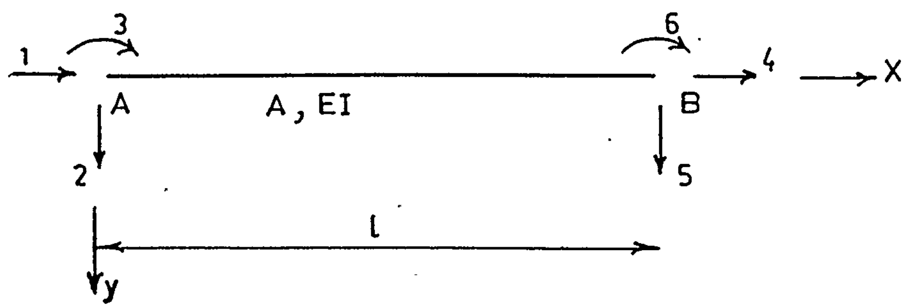

(b) Degrees of freedom

Figure 4.7: Beam element subjected to an axial compressive force P and a transverse loading w

Using this equation in deriving the stiffness matrix of the beam element according to the degrees of freedom 1 to 6 as shown in Figure 4.7(b) leads to the following member stiffness matrix if the beam is subjected to an axial compressive force (Ghali and Neville, 1989):

$$[k_p] = \begin{bmatrix} \frac{EA}{L} & & & & & \\ 0 & \frac{2(s_c+t_c)}{L^2} - \frac{P}{L} & & & & \\ 0 & \frac{s_c+t_c}{L} & s_c & & & \\ -\frac{EA}{L} & 0 & 0 & \frac{EA}{L} & & \\ 0 & -\frac{2(s_c+t_c)}{L^2} + \frac{P}{L} & -\frac{s_c+t_c}{L} & 0 & \frac{2(s_c+t_c)}{L^2} - \frac{P}{L} & \\ 0 & \frac{s_c+t_c}{L} & t_c & 0 & -\frac{s_c+t_c}{L} & s_c \end{bmatrix} \quad (4.9)$$

where:

$$s_c = \frac{\overline{u} \cdot (\sin \overline{u} - \overline{u} \cos \overline{u})}{(2 - 2\cos \overline{u} - \overline{u} \sin \overline{u})} \cdot \frac{EI}{L}$$

$$t_c = \frac{\overline{u} \cdot (\overline{u} - \sin \overline{u})}{(2 - 2\cos \overline{u} - \overline{u} \sin \overline{u})} \cdot \frac{EI}{L}$$

$$\overline{u} = L \cdot \sqrt{\frac{P}{EI}}$$

P = absolute value of the compressive force

E = modulus of elasticity

A = cross-section area of the beam element

I = moment of inertia of the beam element

L = length of beam element

For an axial tensile force, the beam stiffness matrix becomes:

$$[k_p] = \begin{bmatrix} \frac{EA}{L} & & & & & \\ 0 & \frac{2(s_t+t_t)}{L^2} + \frac{P}{L} & & & & \\ 0 & \frac{s_t+t_t}{L} & s_t & & & \\ -\frac{EA}{L} & 0 & 0 & \frac{EA}{L} & & \\ 0 & -\frac{2(s_t+t_t)}{L^2} - \frac{P}{L} & -\frac{s_t+t_t}{L} & 0 & \frac{2(s_t+t_t)}{L^2} + \frac{P}{L} & \\ 0 & \frac{s_t+t_t}{L} & t_t & 0 & -\frac{s_t+t_t}{L} & s_t \end{bmatrix} \tag{4.10}$$

where:

$$s_t = \frac{\overline{u} \cdot (\overline{u} \cosh \overline{u} - \sinh \overline{u})}{(2 - 2\cosh \overline{u} + \overline{u} \sinh \overline{u})} \cdot \frac{EI}{L}$$

$$t_t = \frac{\overline{u} \cdot (\sinh \overline{u} - \overline{u})}{(2 - 2\cosh \overline{u} + \overline{u} \sinh \overline{u})} \cdot \frac{EI}{L}$$

$$\overline{u} = L \cdot \sqrt{\frac{P}{EI}}$$

P = tensile force

E = modulus of elasticity

A = cross-section area of the beam element

I = moment of inertia of the beam element

L = length of beam element

4.4.3.3 The Przemieniecki approach

In this method the axial strain used in developing the element stiffness matrix is expressed by (Przemieniecki, 1968):

$$\epsilon_x = \frac{\partial u}{\partial x} - \left(\frac{\partial^2 v}{\partial x^2}\right) \cdot y + \frac{1}{2} \cdot \left(\frac{\partial v}{\partial x}\right)^2 \tag{4.11}$$

where:

ϵ_x	= axial strain in a layer at a distance y from the centroid
u	= axial deformation (in x-direction)
v	= vertical deformation (in y-direction)
y	= distance measured from the center of gravity of the member

By using the third term of Equation 4.11, the effect of the moment due to axial load is included in the solution. The obtained beam matrix can be put in the following form:

$$[k_p] = [k] + [k_s] \tag{4.12}$$

where:

$[k_p]$	= stiffness matrix for a beam element subjected to an axial force P
$[k]$	= traditional stiffness matrix for a beam element, would be obtained if the first two terms only of Equation 4.11 are used
$[k_s]$	= stiffness matrix expressing the effect of the axial force on the element stiffness matrix (sometimes called stress stiffening matrix)

$[k]$ and $[k_s]$ are given next.

$$[k] = \begin{bmatrix} \frac{EA}{L} & & & & & \\ 0 & \frac{12EI}{L^3} & & & & \\ 0 & \frac{6EI}{L^2} & \frac{4EI}{L} & & & \\ -\frac{EA}{L} & 0 & 0 & \frac{EA}{L} & & \\ 0 & -\frac{12EI}{L^3} & -\frac{6EI}{L^2} & 0 & \frac{12EI}{L^3} & \\ 0 & \frac{6EI}{L^2} & \frac{2EI}{L} & 0 & -\frac{6EI}{L^2} & \frac{4EI}{L} \end{bmatrix} \tag{4.13}$$

$$[k_s] = \begin{bmatrix} 0 & & & & & \\ 0 & \frac{6P}{5L} & & & & \\ 0 & \frac{P}{10} & \frac{2PL}{15} & & & \\ 0 & 0 & 0 & 0 & & \\ 0 & -\frac{6P}{5L} & -\frac{P}{15} & 0 & \frac{6P}{5L} & \\ 0 & \frac{P}{10} & -\frac{PL}{30} & 0 & -\frac{P}{10} & \frac{2PL}{15} \end{bmatrix} \tag{4.14}$$

where:

P = axial force acting on the beam

4.4.3.4 The general solution versus the Przemieniecki approach

A comparison between the stiffness matrices obtained by the two methods shows that a difference does exist. According to Seif (1986), this may be because Przemieniecki used a group of shape functions to describe the deflected shape of the beam element, that do not account for the presence of the axial force, while the general solution is based on the elastic shape of the beam that accounts for the presence of the axial force. Figure 4.8 illustrates the difference by using the end-rotational stiffness value k_{33} to compare between the two methods. For low values of $\overline{u} = L \cdot \sqrt{\frac{P}{EI}}$ $(\overline{u} < 2)$ the difference is negligible.

Since the computer program ANSYS which is used in the present study, adopts the Przemieniecki approach, the lengths of the beam elements in the model are chosen to give low values of $\overline{u}$. By increasing the number of elements, the value of $\overline{u}$ decreases, resulting in obtaining the same solutions whether the general solution approach is used or the Przemieniecki approach (refer to Appendix A for program verification).

Since the final axial force (which affects the member stiffness) is not known in advance, an iterative procedure has to be used in such a type of analysis.

4.4.3.5 Stability study of structures using the effect of axial forces

If the compressive axial force exceeds the buckling load of a member during any of the iterations of the analysis, an element on the main diagonal of the stiffness matrix becomes negative, resulting in a singular stiffness matrix and the analysis is stopped. So the stability or buckling phenomena can be studied using such a type of analysis.

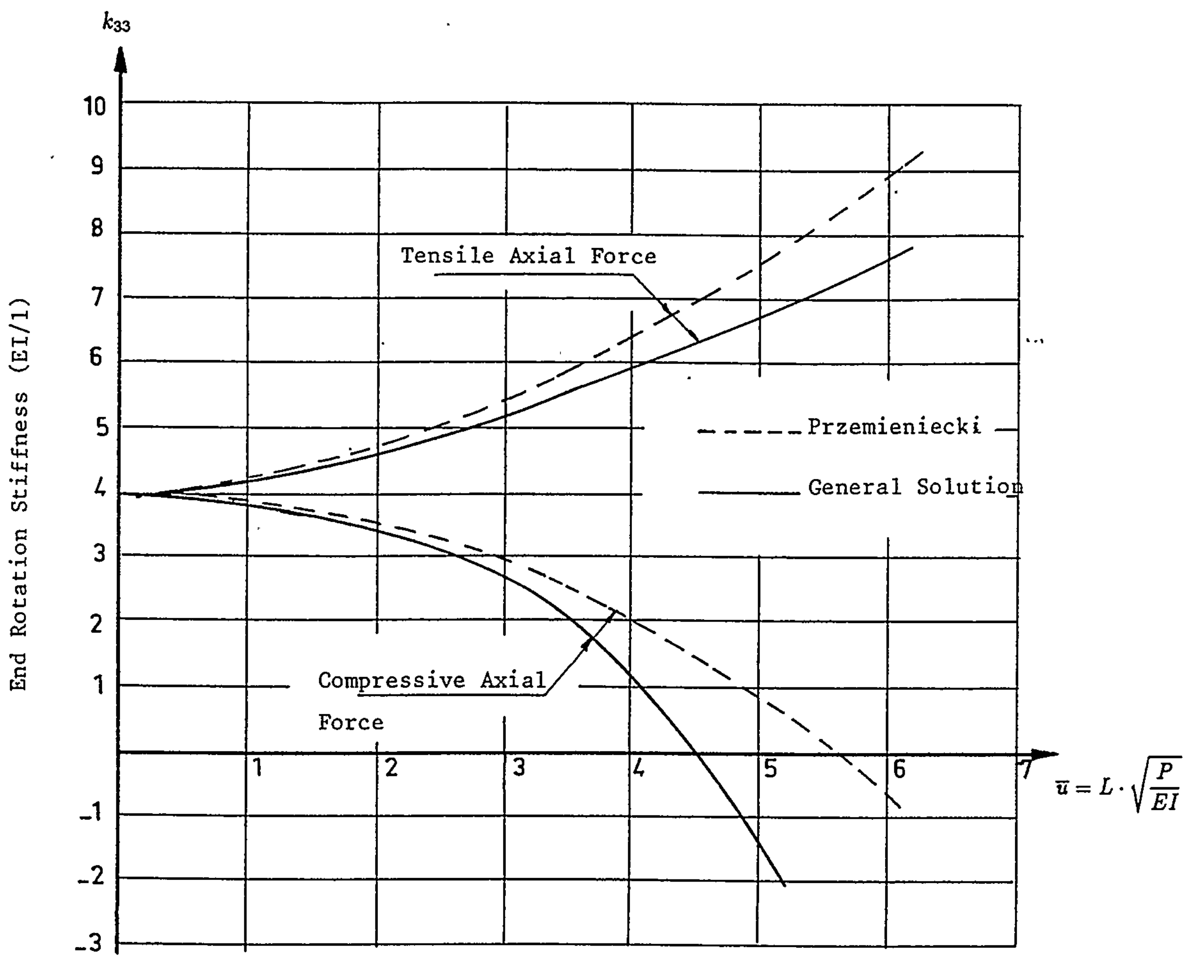

Figure 4.8: Comparison of end-rotational stiffness k_{33} for a prismatic beam subjected to an axial force P

4.4.4 The effect of large deflections

4.4.4.1 Introduction

Some types of structures (especially those including cables like cable-stayed bridges) undergo large deflections under certain load cases. The deflections can be large enough such that the structure stiffness matrix based on the initial geometry does not characterize the deformed structure. The equilibrium equation of the stiffness method $[K]\cdot\{D\} = \{F\}$ (Equation 4.1) must be written with respect to the deformed geometry. But this deformed geometry is not known in advance, so an iterative procedure has to be used in the analysis.

Two methods are available for solving large deflection problems, the Lagrangian method and the Eulerian methods. These methods are introduced next.

4.4.4.2 The Lagrangian Method

In the Lagrangian method the equilibrium equations are written with reference to a structure that remains stationary throughout the analysis. The large deformation effect is encountered in this method by including more terms in the strain Equation 4.11 which is used in the development of the element stiffness matrix, obtaining the following equation for a beam element in bending:

$$\epsilon_x = \frac{\partial u}{\partial x} + \frac{1}{2}\cdot\left(\frac{\partial u}{\partial x}\right)^2 + \frac{1}{2}\cdot\left(\frac{\partial v}{\partial x}\right)^2 - \left(\frac{\partial^2 v}{\partial x^2}\right)\cdot y + \left(\frac{\partial^2 u}{\partial x^2}\cdot\frac{\partial v}{\partial x}\right)\cdot y + \ldots \qquad (4.15)$$

4.4.4.3 The Eulerian Method

In the Eulerian method (known also as updated Lagrangian), which is used by the computer program ANSYS, the equilibrium equation $[K]\cdot\{D\} = \{F\}$ is written with respect to the updated geometry of the structure. This is done by ANSYS by applying the load in increments, for each load step the large deflection process can be summarized as a three step process for each element:

1. Determination of the updated transformation matrix $[T_n]$ for the element. This matrix relates the current element coordinate system to the global Cartesian coordinate system (see Figure 4.9).

2. The displacement field can be decomposed into a rigid body translation, a rigid body rotation and a component which causes strains. In this step the deformational displacement is extracted from the total element displacement for computing the stresses

3. After the rotational increments are computed, the node rotations are updated appropriately.

During a large deflection analysis performed by ANSYS, the loads applied through the nodal coordinates do not rotate with the node. But pressure loads (distributed loads on the member) remain normal to the member and follow the rotation (as shown in Figure 4.10). This may not represent the reality, where gravity loads on members are acting always downwards, despite the member direction.

For more detailed information about this procedure please refer to ANSYS 4.4 Theoretical Manual.

4.4.4.4 Stability study of structures using a large deflection analysis

Buckling (a stability phenomenon) can be analysed with the large deflection process. By observing the rate of change in deflection (per iteration), an estimate of the stability of the structure can be made. If the change of displacement at any node is

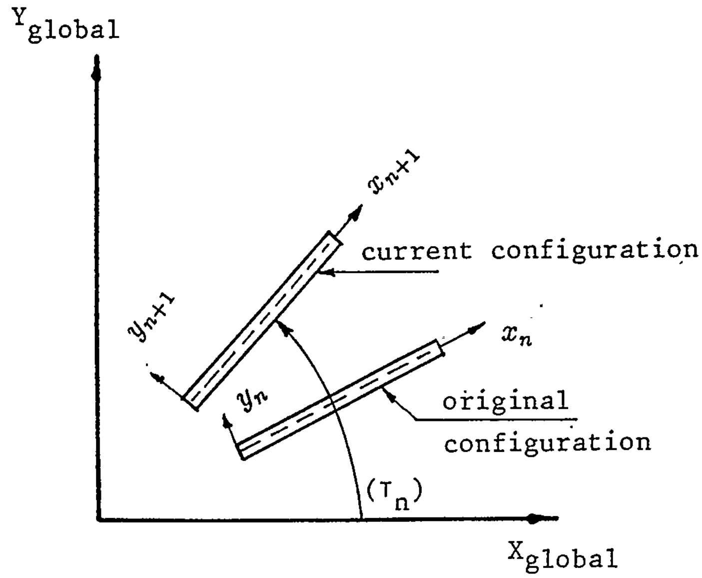

Figure 4.9: Transformation matrix $[T_n]$ in a large deflection analysis

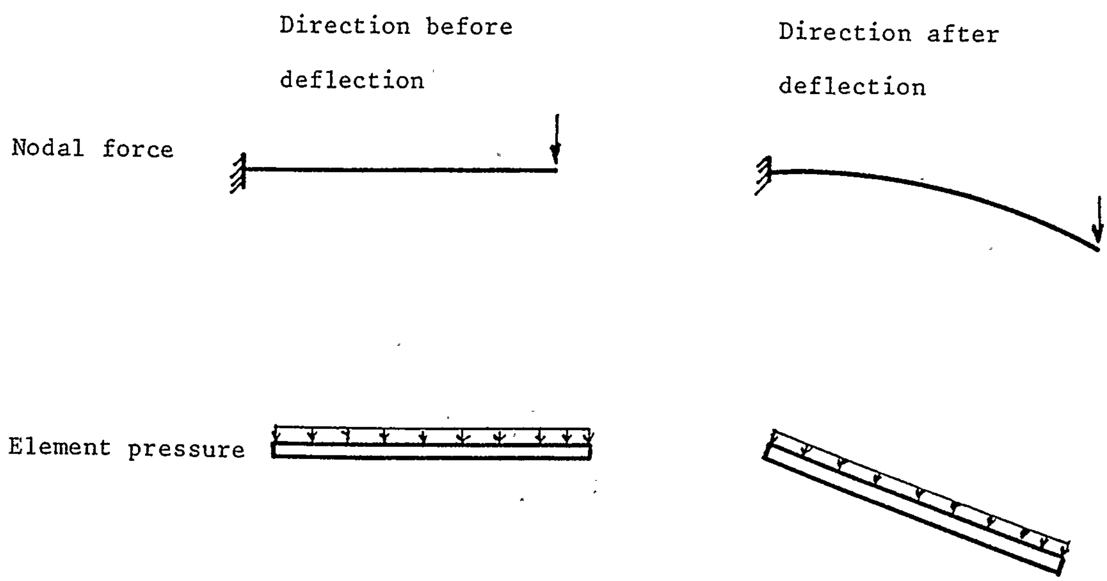

Figure 4.10: Load directions during a large deflection analysis performed by the computer program ANSYS

increasing, the loading is above critical and the structure will eventually buckle. If the displacement change is constant or decreasing, the structure is at or below the critical buckling load.

4.4.5 Iterative procedures for the solution of nonlinear problems

4.4.5.1 Introduction

The stiffness method yields to a set of simultaneous equations (Equation 4.1):

$$[K] \cdot \{D\} = \{F\}$$

If the stiffness matrix $[K]$ of the structure contains only constant elements, then the displacements $\{D\}$ are proportional to the loads $\{F\}$, as shown in Figure 4.11(a). But if the stiffness matrix $[K]$ is itself a function of the unknown displacements (or their derivatives), as is the case for the geometric nonlinearities discussed before, then the equilibrium equation (Equation 4.1) is a nonlinear equation. In this case the force-deflection relationship of the structure is nonlinear, resulting in a stiffening structure like cables, or in a softening structure like most conventional structures (Figure 4.11(b),(c)).

Several iterative techniques are available for the solution of such problems (see Cook, 1989). The Newton-Raphson procedure is an efficient technique used by the program ANSYS, therefore this method and its modifications are discussed next.

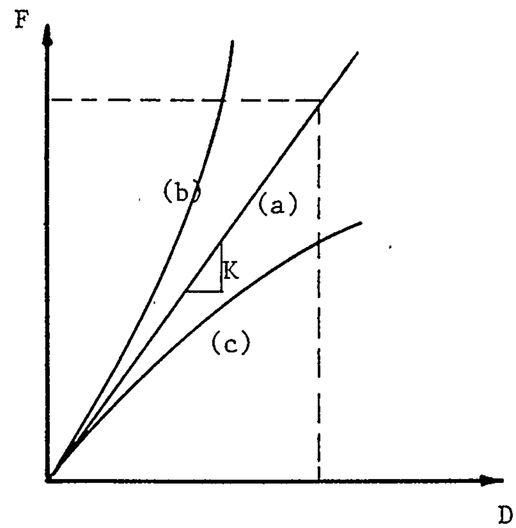

a- linear behaviour

b- nonlinear behaviour (stiffening)

c- nonlinear behaviour (softening)

Figure 4.11: Force-deflection relationships for different types of structures

4.4.5.2 The Full Newton-Raphson procedure

In this method the nonlinear equilibrium equation (Equation 4.1) is written in the form of (Bathe, 1982):

$$[K_n] \cdot \{\Delta D_n\} = \{F\} - \{F_n^{nr}\} \tag{4.16}$$

$$\{D_{n+1}\} = \{D_n\} + \{\Delta D_n\} \tag{4.17}$$

where:

$[K_n]$ = tangent stiffness matrix for the structure for iteration n

$\{F\}$ = vector of applied loads

$\{F_n^{nr}\}$ = vector of restoring loads for iteration n

$\{D_n\}$ = vector of displacements for iteration n

$\{\Delta D_n\}$ = displacement difference between step $n+1$ and step n

The right-hand side of Equation 4.16 is the out-of-balance load vector, or in other words the amount the structural system is out of equilibrium.

Figure 4.12(a) shows the solution procedure for a one degree of freedom model. The general algorithm proceeds as follows:

1. Assume $\{D_n\}$, which is usually the converged solution from the previous step. For the first step $(n = 0)$ $\{D_n\} = \{0\}$.

2. Compute the updated tangent matrix $[K_n]$ and the restoring force $\{F_n^{nr}\}$ from the configuration $\{D_n\}$.

3. Calculate $\{\Delta D_n\}$ using Equation 4.16.

4. Calculate $\{D_{n+1}\}$ using Equation 4.17.

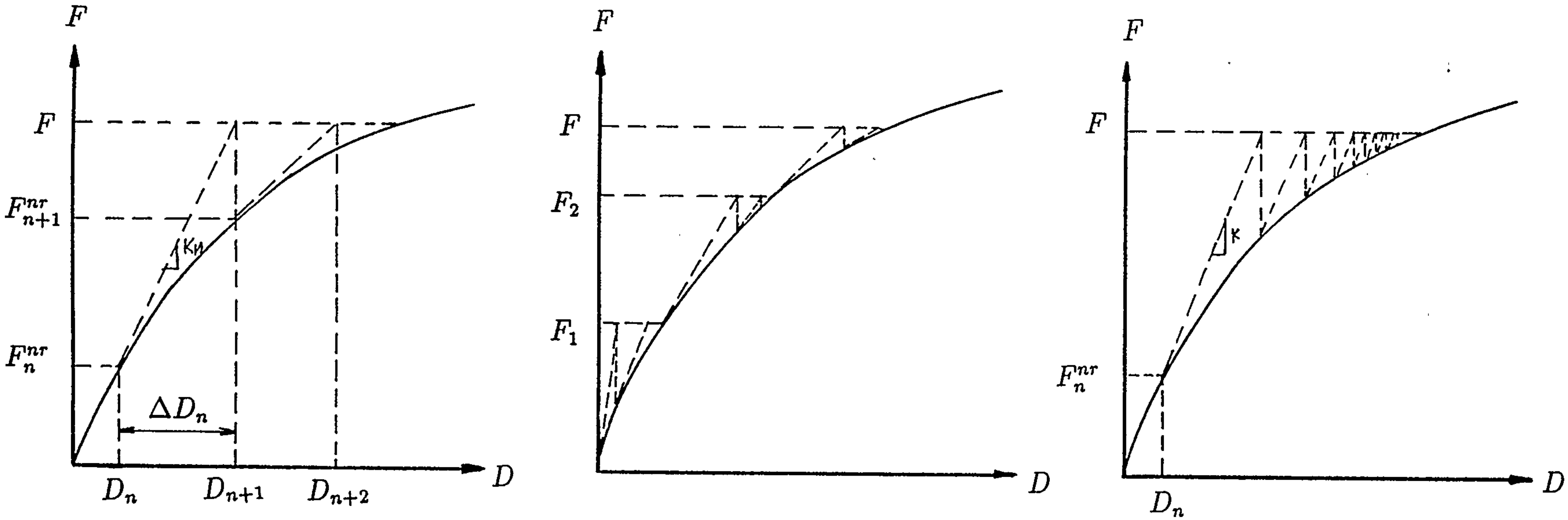

(a) Full Newton-Raphson

(b) Incremental Newton-Raphson

(c) Initial-Stiffness Newton-Raphson

Figure 4.12: Newton-Raphson techniques for the solution of nonlinear problems

The solution obtained at the end of the iteration process would correspond to load level $\{F\}$. So the final converged solution would be in equilibrium, that is, the restoring force $\{F_n^{nr}\}$, which is computed from the current stress state, would equal the applied loads $\{F\}$. None of the intermediate steps are in equilibrium. This method has two limitations. The first one is that if the analysis includes path-dependent nonlinearities (such as plasticity), then the solution process requires that some intermediate steps be in equilibrium in order to correctly follow the load path. The second limitation is that this method guarantees convergence only if the solution at any iteration $\{D_n\}$ is near the exact solution. To overcome these two limitations, the following modified methods may be used.

4.4.5.3 The Incremental Newton-Raphson procedure

In this method the final load $\{F\}$ is reached by stepping the load in increments and performing the Newton-Raphson iterations at each step (see Figure 4.12(b)). Equation 4.16 is then written in form:

$$[K_{m,n}] \cdot \{\Delta D_n\} = \{F_m\} - \{F_{m,n}^{nr}\} \tag{4.18}$$

where:

$[K_{m,n}]$	= tangent stiffness matrix for load step m and iteration n
$\{F_m\}$	= vector of total applied loads at load step m
$\{F_{m,n}^{nr}\}$	= vector of restoring loads for load step m and iteration n

4.4.5.4 The Initial-Stiffness Newton-Raphson procedure

In the previous two procedures, the stiffness matrix is updated in every iteration. Alternatively, the stiffness matrix could be formulated only once at the beginning of the analysis and then used throughout the analysis (see Figure 4.12(c)). This method converges more slowly, but requires fewer matrix reformulations and inversions.

Since the program ANSYS has the option of choosing which Newton-Raphson procedure is to be used in the analysis, the incremental Newton-Raphson procedure has been chosen for its accuracy. A load step is said to be converged if the change of deflection at all degrees of freedom is less than 0.001. This accuracy is reached in the present analysis after three iterations. For a comparison, the Initial-Stiffness Newton-Raphson procedure (no updating of the stiffness matrix) is used in the analysis. A converged solution is not reached even after fifty iterations. It is therefore recommended to update the stiffness matrix every iteration in a large deflection analysis with a large number of degrees of freedom.

4.5 THE LINEAR ANALYSIS

4.5.1 Introduction

Since most of the computer programs available for the analysis of cable-stayed bridges assume linearity, a linear analysis is performed using the computer program ANSYS. By comparing the linear analysis with the nonlinear analysis, an estimate of the error introduced by neglecting the sources of the geometric nonlinearity in cable-stayed bridges can be achieved.

The structure components which distinguish a cable-stayed bridge from any other conventional structure type, and which need special attention in a linear analysis, are the cables. As a cable represents a flexible member with virtually no resistance to applied moments, one traditional truss element may be used for the representation of each cable stay (see Figure 4.2). The difference between a truss element and a cable element is the sag of the cable element. This sag causes the nonlinear force-deflection relationship of a cable. By using a traditional truss element and neglecting the sag, two errors are introduced. The first error is the linear force-deflection relationship which is now assumed for the cable stay. The second error comes from the assumption that the cable force is acting along the inclined chord of the cable stay even though in reality the force acts along the axis of the sagging cable. The effects of these two errors are discussed next.

4.5.2 The equivalent modulus of elasticity

As a result of the flexibility of the cable and the changes in its length and sag, it is necessary to adopt a corrective technique to account for this nonelastic feature. Several investigators (Ernst, 1965, Tung and Kudder, 1968) have studied this problem. In this study the fundamental approach provided by Ernst (1965) is adopted. The solution is based on the idea of assuming a straight member with a varying modulus of elasticity that depends on the magnitude of the tension force, so that the behaviour of this substitute member with an equivalent modulus of elasticity is identical to that of a sagging cable.

Ernst (1965) developed the following expression for the equivalent modulus of elasticity:

$$E_{eq} = \frac{E}{1 + \frac{(\gamma l)^2}{12\sigma^3} \cdot E} \tag{4.19}$$

where:

E_{eq}	= equivalent modulus of elasticity
E	= tangent modulus of elasticity
γ	= specific weight of the cable material, weight per unit volume
σ	= tensile stress in the cable
l	= horizontal projected length of the cable chord

Figure 4.13 shows the ratio (E_{eq}/E) calculated from Equation 4.19 for the illustrated specific values of E, f_{pu} and different stress levels in the cable. The equivalent modulus of elasticity E_{eq} defined in Equation 4.19 is valid only for a single value of the stress σ. But during the analysis, the stress level in the cables changes with the applied live load from a lower limit to an upper limit. This means that the equivalent modulus E_{eq} is also changing during the analysis. To take this effect into consideration, the following modified equation of Ernst (1965) can be used:

$$E_{eq} = \frac{E}{1 + \frac{(\gamma l)^2}{12\sigma_m^3} \cdot \frac{(1+\mu)^4}{16\mu^2} \cdot E} \tag{4.20}$$

where:

$$\mu = \frac{lower\ limit\ stress}{upper\ limit\ stress} = \frac{\sigma_{low}}{\sigma_{up}}$$

$$\sigma_m = \frac{\sigma_{low} + \sigma_{up}}{2}$$

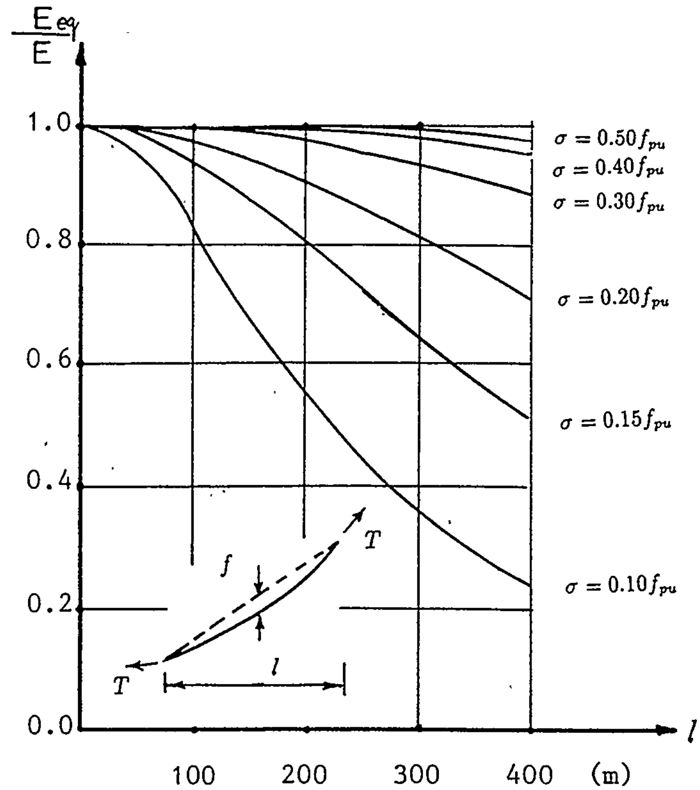

$$E = 190,000 N/mm^2$$
$$f_{pu} = 1,700 N/mm^2$$
$$\gamma = 78.5 kN/m^3$$
$$\sigma = T/A$$

$$E_{eq} = \frac{E}{1 + \frac{(\gamma l)^2}{12\sigma^3} \cdot E}$$

Figure 4.13: Ratio E_{eq}/E showing the influence of the cable sag on its stiffness

By comparing Equations 4.19 and 4.20, an equivalent stress σ can be derived as a function of σ_m and μ (Walther et al, 1988):

$$\sigma = \sigma_m \cdot \left(\frac{16\mu^2}{(1+\mu)^4} \right)^{\frac{1}{3}} \tag{4.21}$$

This equivalent stress makes it possible to use Equation 4.19 and Figure 4.13 directly. This is the first error introduced by using a truss element in modeling a cable stay, the second error is discussed next.

4.5.3 Cable tension versus component along inclined chord

By using a truss member in the analysis, the inclined cable in a cable-stayed bridge is assumed to be a straight line between the cable anchors at the pylon and the deck. Although the cable is not actually following the chord line, because of the sag due to its own weight, the tension force calculated in the truss member is assumed to be the tension in the cable.

The accuracy of this assumption was investigated by Podolny (1971). He compared the maximum tension in the cable T_{max} with the tension along the chord T_c (see Figure 4.14). The results of his study are plotted in Figure 4.15 as percentage error versus the sag ratio $n = f/l$ for various angles of inclination of the chord.

As indicated by Figure 4.15, for sag ratios n between 1/200 to 1/600, which is normally the case in cable-stayed bridges, the error is negligible. This can also be concluded by comparing the results of the nonlinear analysis with the results of the linear analysis in the next chapter.

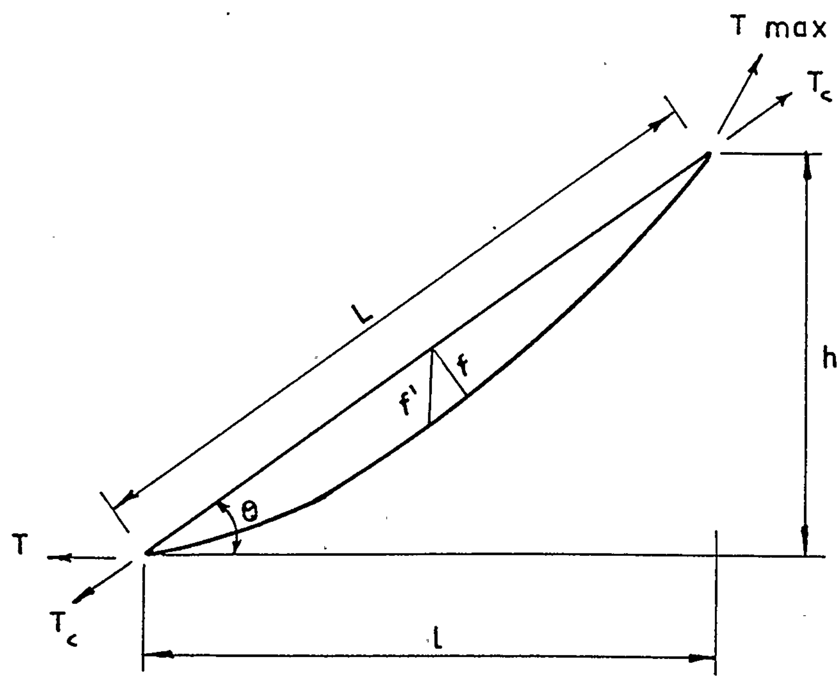

Figure 4.14: Maximum tension T_{max} and tension T_c along the cable chord

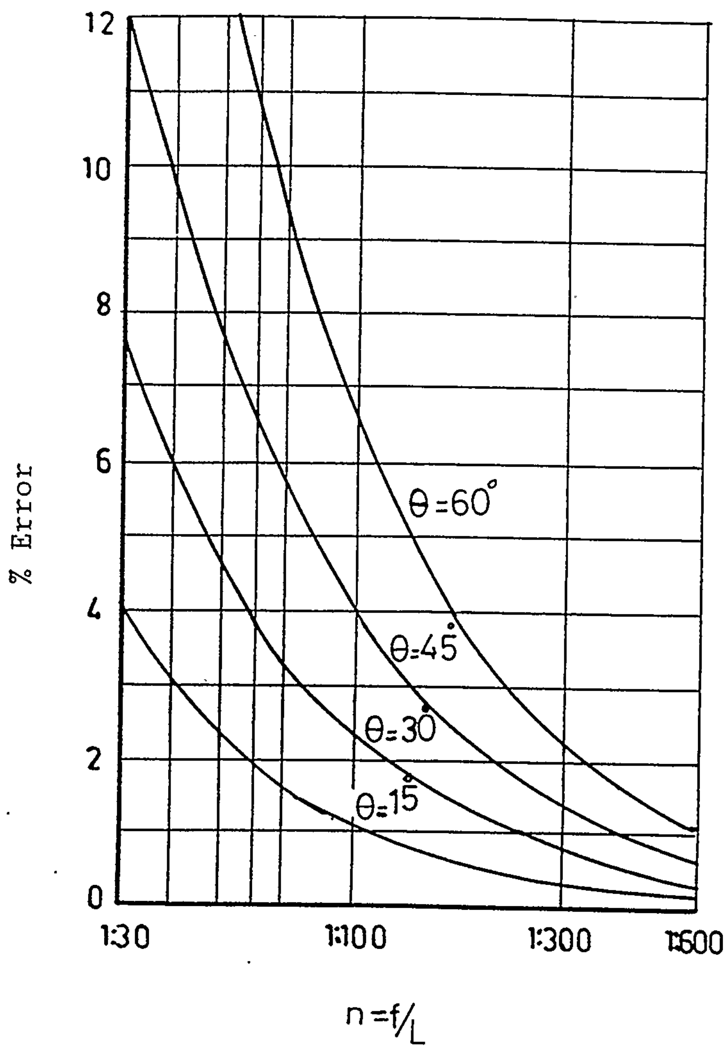

Figure 4.15: Percentage error of maximum cable tension versus component along the inclined cable chord (Adapted from Podolny, 1971)

4.6 SUMMARY

In this chapter the different methods of analysing cable-stayed bridges are briefly reviewed, with an emphasis on the stiffness method which is used in this study. The models used in the conventional linear and geometric nonlinear analyses are introduced. In addition, the sources of the geometric nonlinear behaviour of cable-stayed bridges, which are the behaviour of the cables (catenary and parabolic configurations), the effect of axial forces (general solution approach and Przemieniecki approach) and the effect of large deflections (Lagrangian and Eulerian methods), are discussed and compared.

Since a difference between the general solution approach and the Przemieniecki approach does exist in a certain range of element lengths, and since the program ANSYS uses the Przemieniecki approach, the element lengths of the model are chosen small enough that both methods are identical.

Also the different techniques for solving nonlinear problems, which are available options in the computer program ANSYS, are reviewed. At the end of the chapter the errors introduced by using a truss member in modeling the cable stays in the linear analysis are discussed and the equivalent modulus of elasticity for cables is introduced.

Chapter 5

ANALYSIS OF THE PROPOSED BRIDGE

5.1 INTRODUCTION

In this chapter the proposed bridge is analysed under its own weight, highway live loads and temperature. In the dead load analysis the prestressing forces in the cables are adjusted to result in a horizontal deck alignment. For the highway live load analysis, the maximum force and moment envelopes for the different bridge components are calculated by investing several load cases.

The results of the conventional linear and of the geometric nonlinear analyses are compared. In addition the effect of shear deformations is investigated.

5.2 THE DEAD LOAD ANALYSIS

5.2.1 General

In each construction cycle one pylon with a deck of 250 m length is constructed in one stage, and this deck will be connected to the previously completed span after the deformations due to its dead load have occurred. Therefore, the dead load analysis is performed for a model consisting of one pylon with a 250 m long double cantilever deck without springs at its ends, as shown in Figure 5.1. The dead load intensity as mentioned before is $g = 200kN/m$. A horizontal deck level due to the own weight is reached by different methods in the linear analysis and in the geometric nonlinear

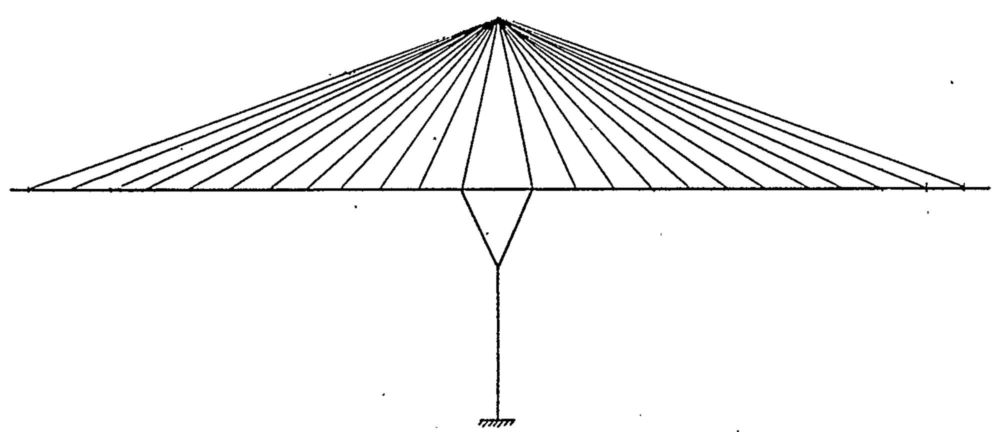

Figure 5.1: Model used in the dead load analysis

(For dimensions see Figure 3.12)

analysis. A uniform deflection of 8 mm is chosen for the deck alignment, because the vertical deflection of the pylon at the deck level turned out to be 8 mm.

5.2.1.1 Horizontal deck in the linear analysis

A horizontal deck level (uniform 8 mm downward deflection of the deck nodes) is reached by adjusting the initial forces (initial strains) in the cables. For the calculation of these forces, the principle of superposition, which is applicable in a linear analysis, is used. This leads to the following system of equilibrium equations:

$$
\begin{array}{ccccc}
\delta_{1,1} \cdot T_{in-1} + \delta_{1,2} \cdot T_{in-2} + \cdots + \delta_{1,n} \cdot T_{in-n} + D_{o-1} = D_{req-1} \\
\vdots \quad \vdots \quad \vdots \quad \vdots \quad \vdots \\
\delta_{n,1} \cdot T_{in-1} + \delta_{n,2} \cdot T_{in-2} + \cdots + \delta_{n,n} \cdot T_{in-n} + D_{o-n} = D_{req-n}
\end{array}
$$

or in matrix form:

$$[\delta]_{n\times n} \cdot \{T_{in}\}_n + \{D_o\}_n = \{D_{req}\}_n \tag{5.1}$$

where:

$\delta_{i,j}$ = vertical deflection of deck node connected to cable i due to a unit initial force in cable j, calculated in a separate analysis

T_{in-j} = required (unknown) initial prestressing force in cable j to obtain the required deflections of the deck nodes

D_{o-j} = vertical deflection of deck node connected to cable j due to dead load and zero initial prestressing forces in the cables, calculated in a separate analysis

D_{req-j} = required final deflection of the deck node connected to cable j

n = number of cables (22 for this study)

The coefficients of the matrix $[\delta]_{n\times n}$ are calculated by introducing an initial unit force (in form of an initial strain) in cable i, and computing the vertical deflections of the deck nodes. Figure 5.2 shows the case for the first cable ($i = 1$). Solving Equation 5.1 gives the required initial cable forces to give a horizontal deck of 8 mm uniform downward deflection. These forces are listed in Table 5.1.

5.2.1.2 Horizontal deck in the geometric nonlinear analysis

As in the linear analysis, the initial strains (prestressing forces) in the cables required to obtain a horizontal deck of 8 mm uniform downward deflection are calculated. Since in a nonlinear analysis the principle of superposition (used in the linear analysis) is in general not applicable, an iterative procedure is used. The initial strains (prestressing forces) in all cables are adjusted simultaneously according to the following equation for each cable (see Figure 5.3):

$$\varepsilon_{i+1} = \frac{\Delta y_i \cdot \sin\theta_i}{L_i} \tag{5.2}$$

where:

ε_{i+1} = initial cable strain for step $(i+1)$

Δy_i = difference between the vertical displacement obtained from step i and the final required vertical displacement of the deck node

L_i = cable chord length in step i

θ_i = angle of inclination of cable chord in step i

This procedure is repeated until a satisfying horizontal deck level is reached, as shown in Figure 5.4 for the deck node connected to cable number 1. The prestressing forces (= initial strain x EA) obtained by this method are given in Table 5.1.

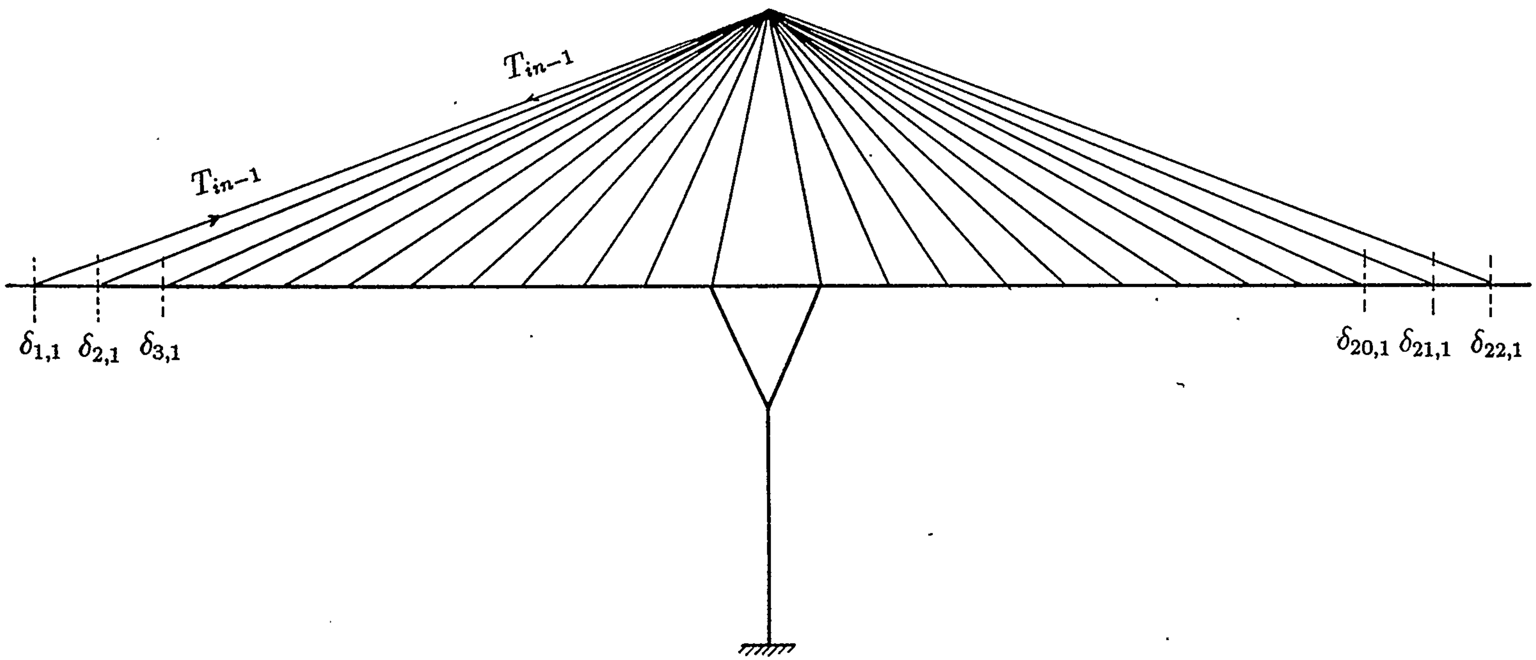

Figure 5.2: Calculation of the deflections $\delta_{1,1}$ to $\delta_{22,1}$

Table 5.1: Forces in the cables and stress-free lengths L_o

Cable No.	Linear Analysis					Nonlinear Analysis				
	Init. (kN)	D.L. (kN)	L.L. (kN)		L_o (m)	Init. (kN)	D.L. (kN)	L.L. (kN)		L_o (m)
			Tens.	Comp.				Tens.	Comp.	
1	3061	2954	306	-29	127.697	3055	2962	313	-32	127.700
2	2878	2757	308	-16	118.445	2871	2763	313	-17	118.448
3	2405	2305	253	-4	109.276	2399	2309	255	-4	109.278
4	2444	2338	262	-4	100.266	2442	2346	274	-11	100.268
5	2088	1993	235	-11	91.460	2085	1996	244	-17	91.461
6	2051	1948	234	-10	82.924	2047	1950	239	-15	82.925
7	1702	1617	186	-5	74.733	1703	1623	186	-7	74.733
8	1615	1527	178	-2	67.041	1617	1534	176	-2	67.041
9	1363	1277	148	-	60.015	1356	1275	149	-	60.016
10	1447	1355	128	-2	53.899	1444	1355.	128	-2	53.899
11	930	885	47	-3	49.072	937	894	47	-3	49.071
12	919	886	44	-2	49.074	927	896	45	-2	49.073
13	1422	1354	126	-1	53.902	1420	1354	129	-2	53.903
14	1337	1277	148	-	60.019	1331	1275	150	-1	60.020
15	1586	1527	178	-4	67.045	1589	1534	175	-3	67.045
16	1674	1617	188	-10	74.738	1676	1623	189	-13	74.738
17	2018	1948	241	-20	82.929	2016	1951	249	-30	82.930
18	2057	1993	244	-19	91.465	2055	1997	260	-33	91.465
19	2410	2338	270	-3	100.271	2410	2346	291	-18	100.272
20	2373	2305	285	-32	109.281	2368	2309	284	-31	109.283
21	2842	2757	396	-116	118.450	2836	2763	405	-119	118.453
22	3026	2954	446	-212	127.702	3022	2962	464	-218	127.705

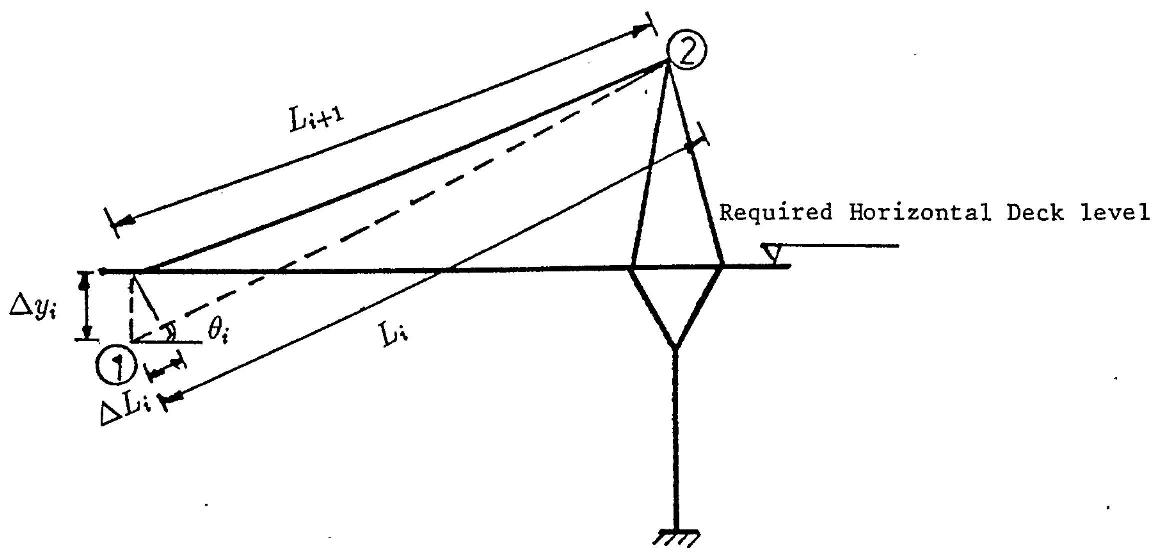

Figure 5.3: Iterative procedure for one cable to obtain the required deck alignment

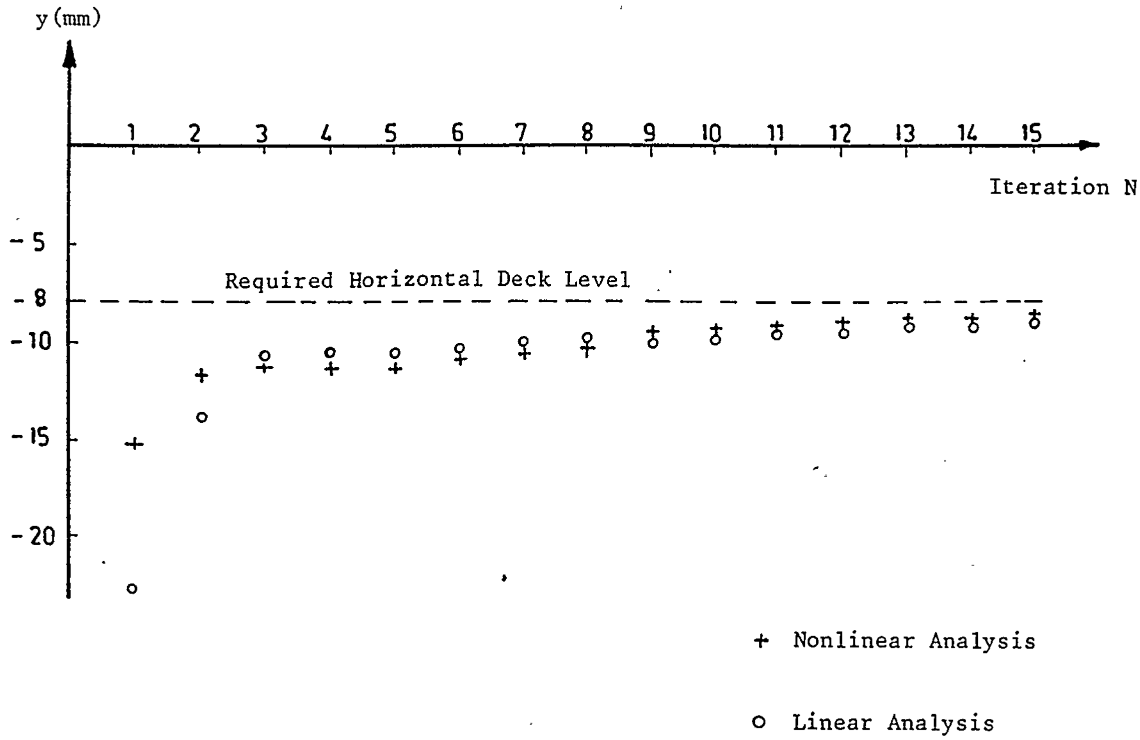

Figure 5.4: Iteration number versus horizontal level of the deck node connected to cable number 1

To compare between the linear and geometric nonlinear behaviour of the bridge, the same iterative technique is used in a linear analysis. The results for the linear analysis are also shown in Figure 5.4.

Knowing the initial strains ε in the cables, and the distance L between their two ends (before any deformations occur), the strain-free length L_o of each cable can be calculated as follows:

$$L_o = \frac{L}{1+\varepsilon} \tag{5.3}$$

The strain-free lengths of the cables (listed in Table 5.1) are needed later when discussing the construction steps of the bridge.

5.2.2 Results and conclusions

1. Effect of shear deformations

   The effect of shear deformations on the cable forces and moments in the pylons and deck is negligible, since including shear deformations in the analysis did not change the results by more than 2%.

2. Forces in the cables (Table 5.1)

   For the assumed cross-sections of the cables, the average tensile stress due to the dead load of the bridge is about $\sigma = 0.375 f_{pu}$, where f_{pu} is the rupture strength of the cable material. With a maximum horizontal projected cable length of $l = 120\ m$, it can be concluded from Figure 4.13 of the previous chapter that the ratio (E_{eq}/E) for these values of σ and l is about unity. This means that the cables react like bars which are not influenced by their sags, or in other words the stress-strain relationships of the cables are more or less linear.

Furthermore, the sag ratio ($n = f/l$) for the cables varies from 1/600 for cable number 1 ($\theta = 21°$) to the value 1/1000 for cable number 11 ($\theta = 66°$). Using Figure 4.15 (Chapter 4) it can be seen that the error introduced by calculating the tension force along the cable chord (by using a straight member) instead of the maximum tension in the curved cable is absolutely negligible. This is also shown by comparing the cable forces obtained from the linear solution with those obtained from the geometric nonlinear solution (Table 5.1). The use of ten nonlinear cable elements for the modeling of one cable stay in the nonlinear analysis, did not change the cable forces obtained from the linear analysis, in which one simple truss element represented one stay cable, by more than 0.5 percent. This difference is negligible, especially if compared with the enormous increase in the computational effort and time associated with the use of the nonlinear cable elements instead of the simple truss elements.

3. Deck alignment

   Both methods used in obtaining a horizontal deck level, the principle of superposition for the linear analysis and the iterative technique for the nonlinear analysis, give almost identical initial cable strains (prestressing forces) as shown in Table 5.1.

4. Bending moments and normal forces in the deck (Fig. 5.5 and 5.6)

   The bending moments under the effect of dead load are relatively small. This is due on one hand to the relatively close spacing of the cables, and on the other to the fact that these cables are tensioned so as to act as point supports. Further, the deck, instead of being primarily a flexural member, now acts

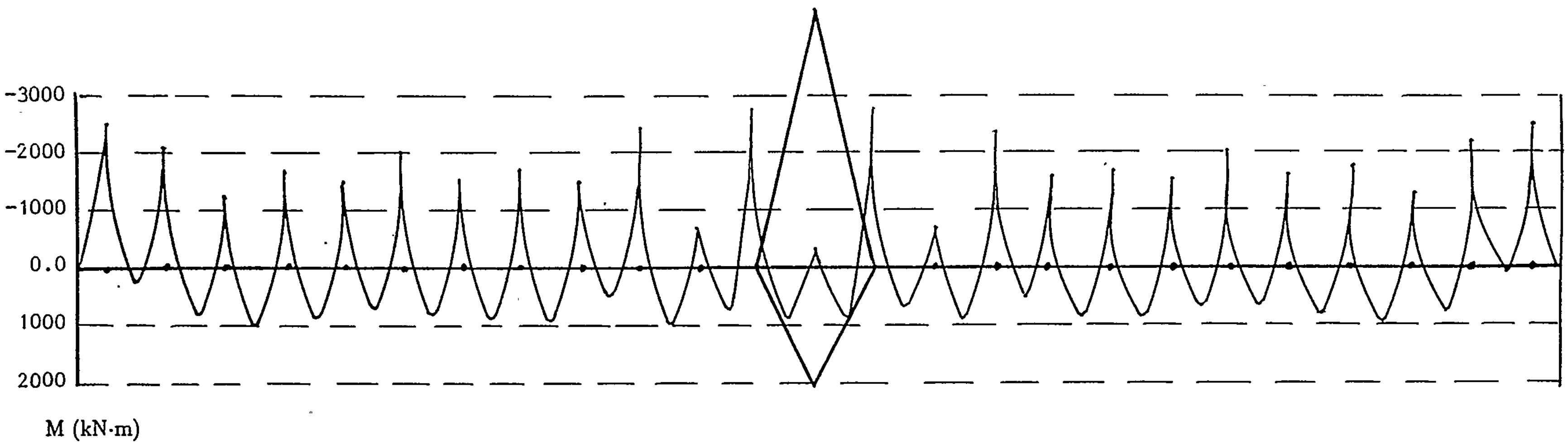

Figure 5.5: Deck bending moment diagram due to dead load

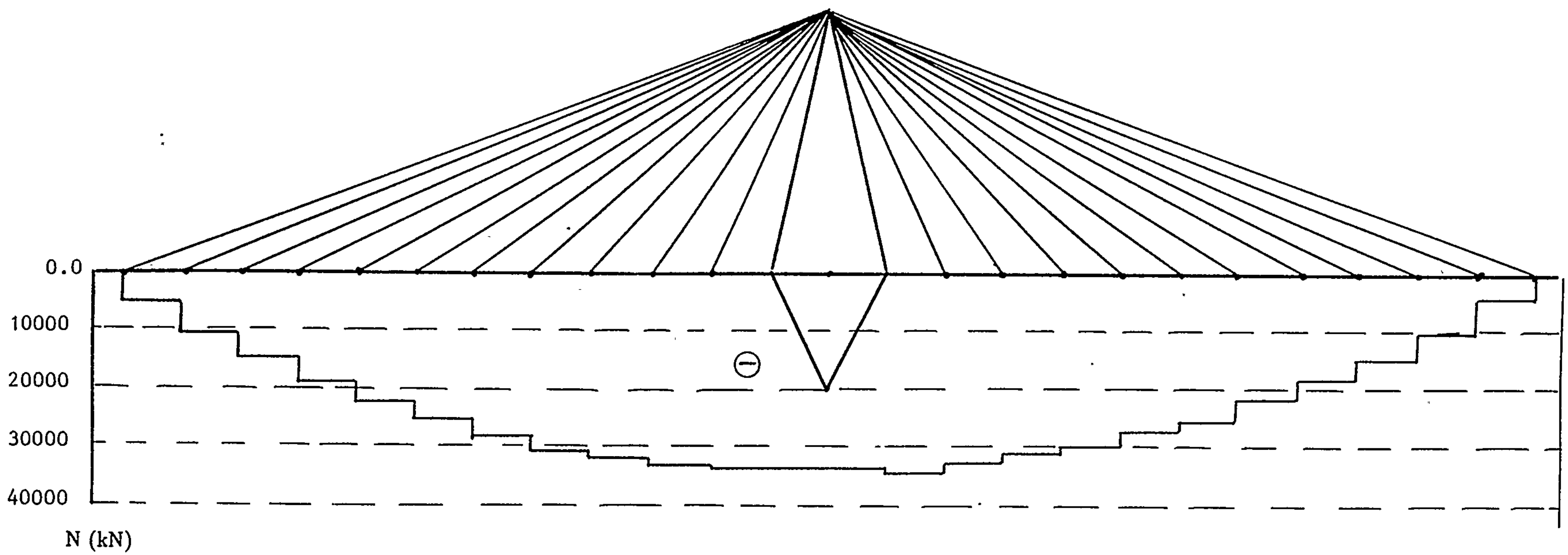

Figure 5.6: Deck normal force diagram due to dead load

primarily as a compressive member of a cantilever structure suspended from the pylon by the inclined stays. Therefore, the deck in multicable-stay systems does not require a large bending stiffness in order to resist bending moments. Longitudinal bending stiffness is governed in such systems by:

- Deflections due to live loads
- Buckling due to large compressive forces induced by the inclined stays

If the deck system is considered as a continuous beam, supported on rigid supports instead of the flexible cables, the negative moments over the supports can be estimated by the simple equation:

$$M = \frac{g \cdot b_i^2}{12} \tag{5.4}$$

where:

g = dead load intensity of the deck (= 200 kN/m)

b_i = the spacing between the anchor points of the cables in the deck = 10 m in this case

Equation 5.4 gives a moment of 1667 kN·m. Except for the cables near the pylon and at both ends of the deck, this moment is fairly close to those obtained by the computer analysis. Concerning the difference between linear and nonlinear analyses, a maximum difference of 2 percent in the bending moments and 0.5 percent in the normal forces are obtained. For design purposes these differences are of course negligible.

5. Bending moments and normal forces in the pylon (Fig. 5.7 and 5.8)

   While the upper inclined legs of the pylon are primarily subjected to axial compressive forces, for the lower legs the bending moments are increasing with the increase of the width of those legs. Since the structure is almost symmetrical about the pylon axis (except the deck-pylon connection consisting of the unsymmetrical configuration of two rollers and one hinge), the bending moments in the vertical shaft are almost zero. Again, the maximum difference in the bending moments between the linear and nonlinear analyses is about 2 percent. The normal forces obtained from both analyses are almost identical.

6. Conclusions

   The conclusion from the previous results is that designing the cables for a high stress, and keeping the differential deflections of the deck and rotation of the pylon as low as possible, will lead to a linear behaviour of the structure. This is the case for the dead load analysis, where the cable stresses are about $0.375 f_{pu}$, the deck is horizontal and the structure is almost symmetrical about the pylon axis. Thus the use of a simple linear analysis instead of a more complicated geometric nonlinear analysis due to dead load is justified.

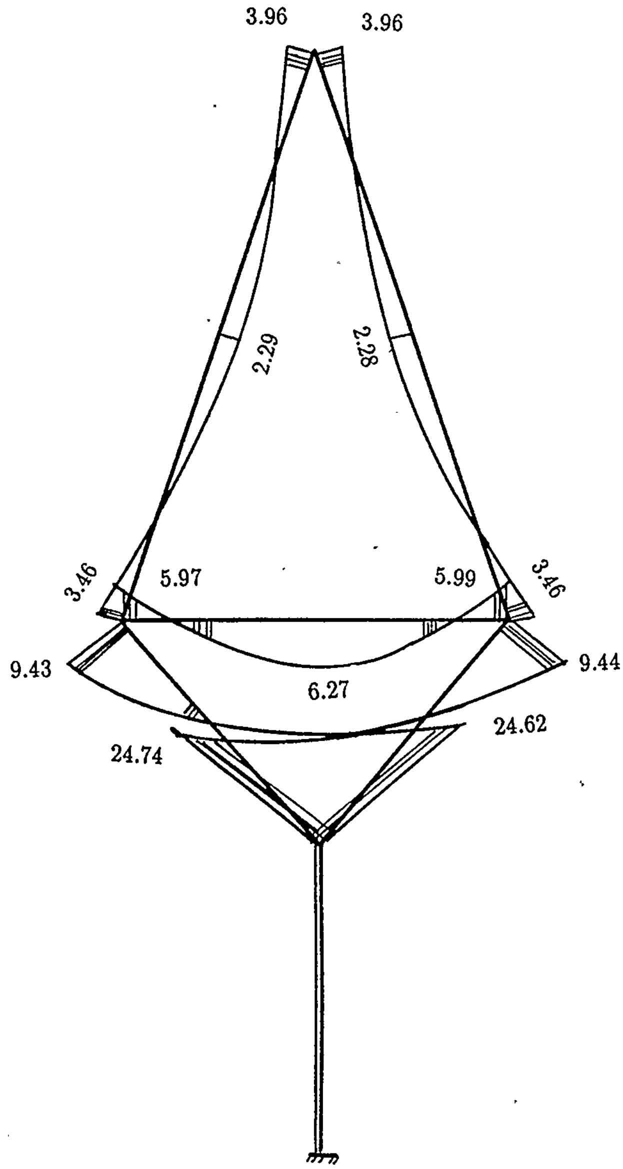

Figure 5.7: Bending moment diagram (MN·m) in left pylon due to dead load

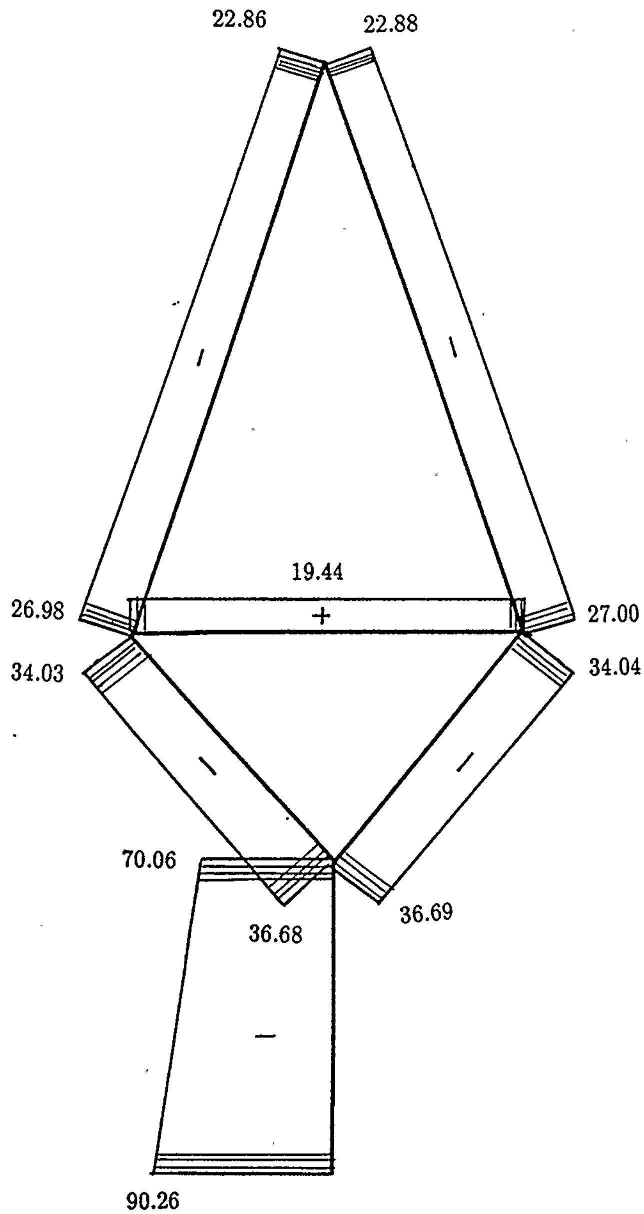

Figure 5.8: Normal force diagram (MN) in left pylon due to dead load

5.3 THE HIGHWAY LIVE LOAD ANALYSIS

5.3.1 General

The highway live loads will act on the complete, continuous bridge. Therefore, the analysis is performed using a model consisting of two pylons connected by a 500 m long deck (see Figure 5.9). The load cases used to obtain the maximum bending moments and normal forces in the bridge are shown in Figure 5.10. The springs at the ends of the deck are used if only the 500 m long bridge is loaded. They are removed in other load cases to simulate the loading on the whole continuous bridge. By removing the spring at one end, the shearing force at this end becomes zero, and a case of symmetry for the whole bridge about this end is achieved.

Since in reality the live loads are superimposed loads on the dead loads, the effect of the live loads alone in this analysis is achieved by using the following algorithm: (Effect of live loads) = (Effect of live loads + dead loads) - (Effect of dead loads)

5.3.2 Results and conclusions

1. Effect of shear deformations

   The effect of shear deformations on the cable forces and straining actions in the pylons and deck is less than 3 percent, which is negligible for design purposes.

2. Behaviour of the springs at the ends of the deck

   In calculating the force-deflection relationship (see Figure 5.11) of the spring simulating the shear joint at one end of the 500 m long deck, the boundary condition (free or hinged) of the far end of the deck has an effect of less than 0.5 percent on the deflection of the deck end under the applied concentrated

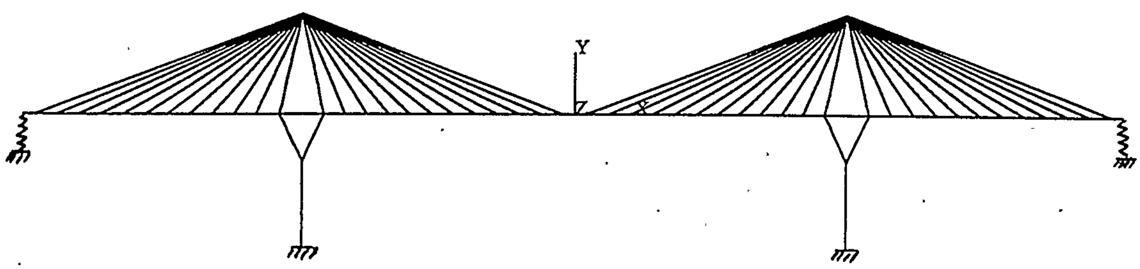

Figure 5.9: Model used in the live load analysis

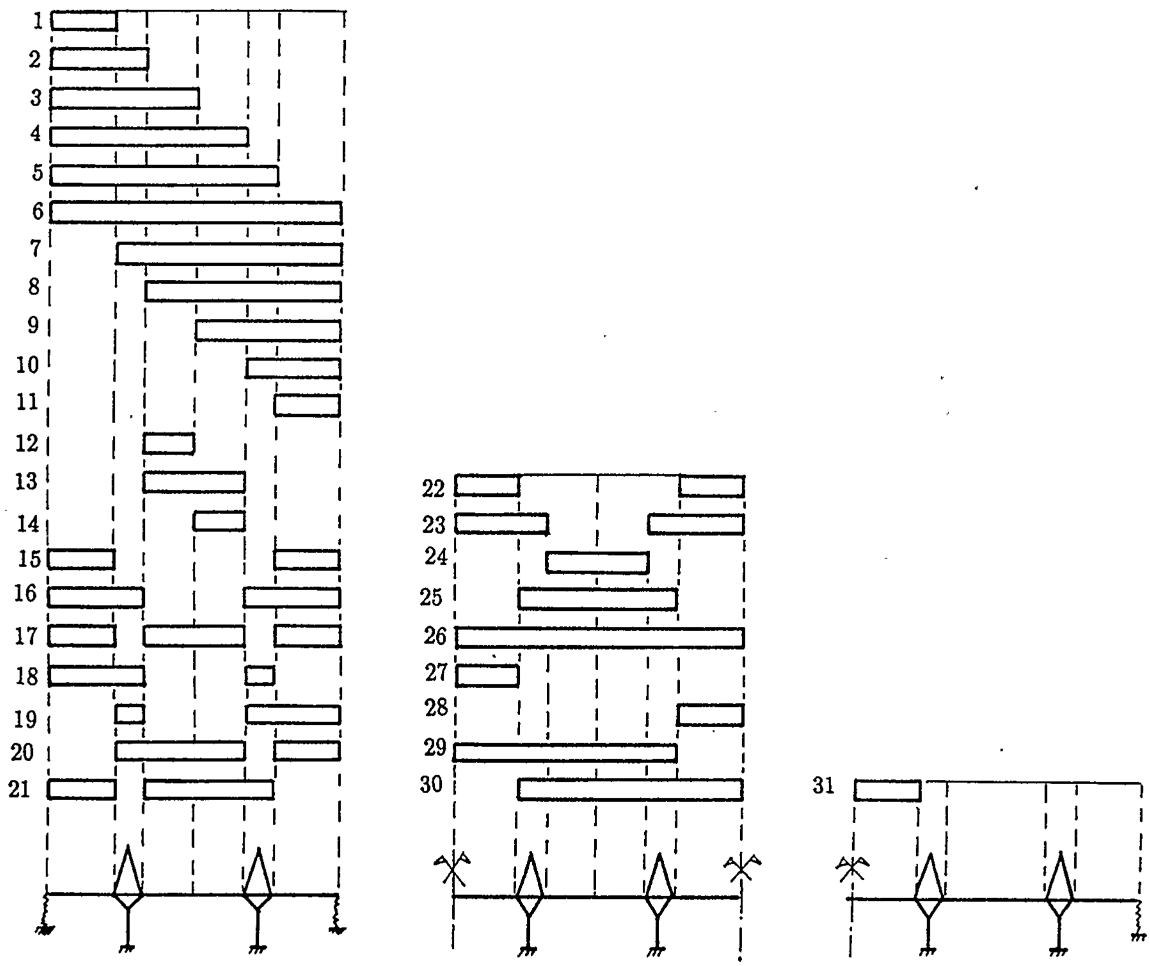

Figure 5.10: Investigated highway live load cases

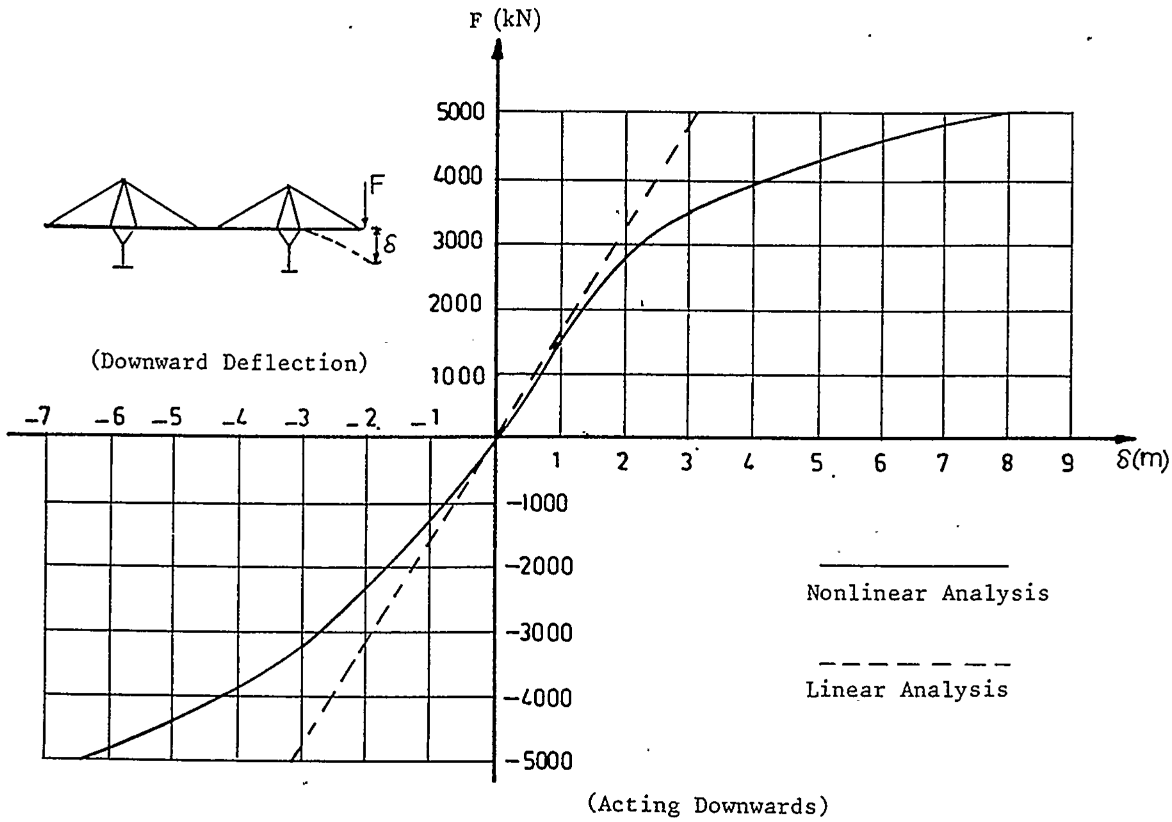

Figure 5.11: Force-deflection relationship of the springs simulating shear joints at the ends of the deck

load. In the geometric nonlinear analysis the force in the springs varies between 203 kN compression and 118 kN tension due to the different live load cases. This range is between 219 kN compression and 122 kN tension in the linear analysis. Referring to Figure 5.11, these ranges are in the linear part of the force-deflection relationship of the springs, so the use of the nonlinear spring element instead of a linear one is not necessary for the used value of live loads. For the justification of the use of springs for the simulation of the continuity of the bridge, a model consisting of six pylons is analysed for different load cases. The results are compared with the two-pylon model in Table 5.2. The results are identical, which justifies the use of the two-pylon model with springs in analysing the continuous bridge.

3. Behaviour of the cables

   For the linear analysis the equivalent modulus of elasticity E_{eq} for each cable is calculated using Equation 4.20 with the equivalent stress obtained from Equation 4.21 (Chapter 4). For the outer cable ($l = 120\ m$), this gives the following values (calculated from Table 5.1):

$$
\begin{aligned}
\sigma_{low} &= \text{tensile stress due to D.L.} + \text{maximum compressive stress due to L.L.} \\
&= 653 N/mm^2 = 0.384 f_{pu} \\
\sigma_{up} &= \text{tensile stress due to D.L.} + \text{maximum tensile stress due to L.L.} \\
&= 728 N/mm^2 = 0.428 f_{pu} \\
\mu &= \frac{\sigma_{low}}{\sigma_{up}} = 0.897 \\
\sigma_m &= \frac{\sigma_{low} + \sigma_{up}}{2} = 691 N/mm^2 = 0.406 f_{pu}
\end{aligned}
$$

Table 5.2: Comparison of reaction forces (kN, kN·m) of different systems

Statical system / Load case		
Statical system	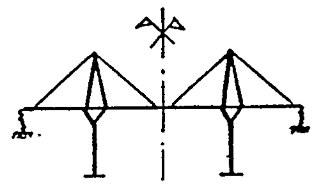	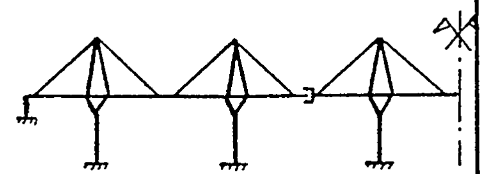
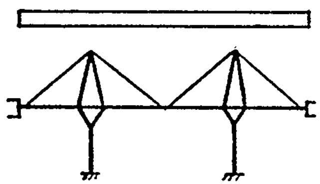	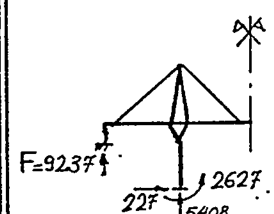	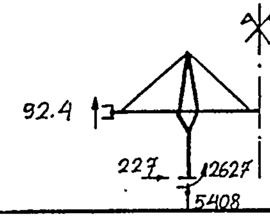
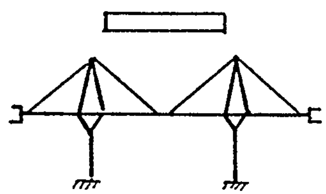	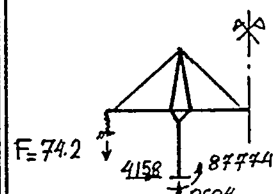	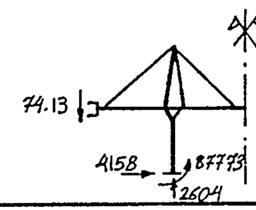
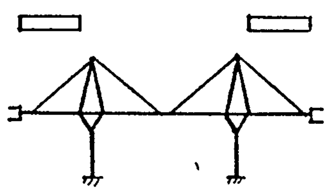	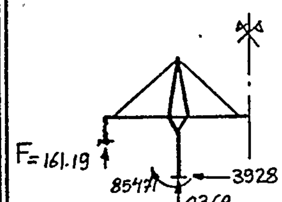	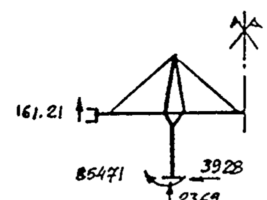

Load case

thus:

$$\sigma = \sigma_m \cdot \left(\frac{16\mu^2}{(1+\mu)^4}\right)^{\frac{1}{3}} = 689N/mm^2 = 0.405 f_{pu}$$

Using Figure 4.13 of Chapter 4 with these values, the ratio (E_{eq}/E) approaches unity. This again means that the cables act as bars not influenced by their sag.

4. Forces in the cables (Table 5.1)

   The maximum tensile forces in the cables due to live load is about 14 percent of the forces due to dead load. For a live load intensity of 12 percent of the dead load, this means that the effect of loading cases in a multicable system is minor on the maximum cable forces. A comparison between the geometric nonlinear analysis, and the linear analysis gives a maximum difference in the cable tension forces of about 8 percent. Since the cables act as linear bars, the difference must be caused by the difference in the deflection of the deck (as will be discussed later), not by the behaviour of the cables.

5. Bending moments and normal forces in the deck (Fig. 5.12 and 5.13)

   The moment envelope under live load has three distinct zones, where the maximum positive and negative moments appear (see Figure 5.12). These zones are near the joint providing the continuity of the deck (side span), in the vicinity of the pylons, and around the center of the main span. To understand this bending moment envelope, the beam-on-elastic-supports analogy (Figure 5.14) may be useful.

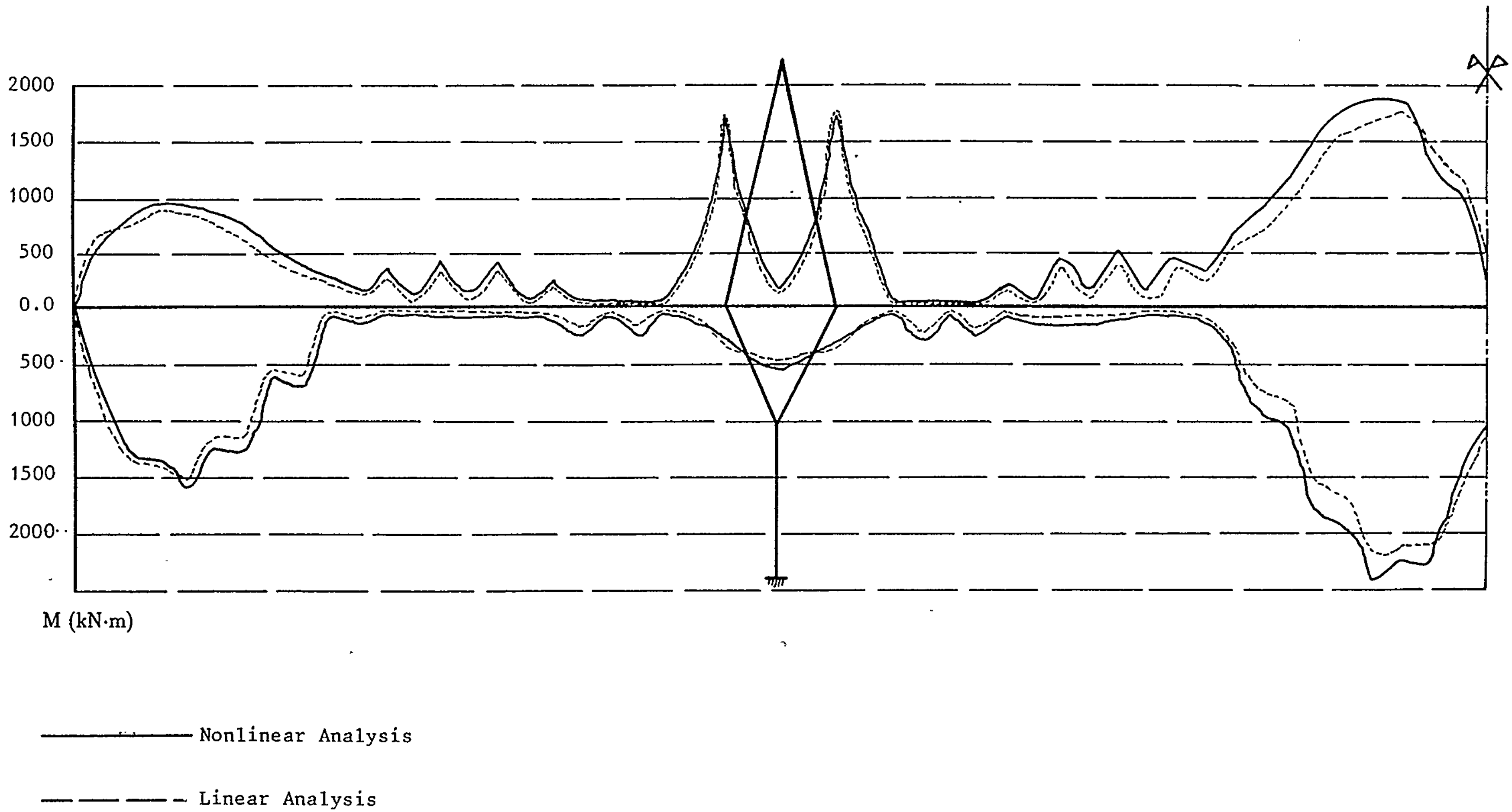

Figure 5.12: Deck bending moment envelope due to highway live load

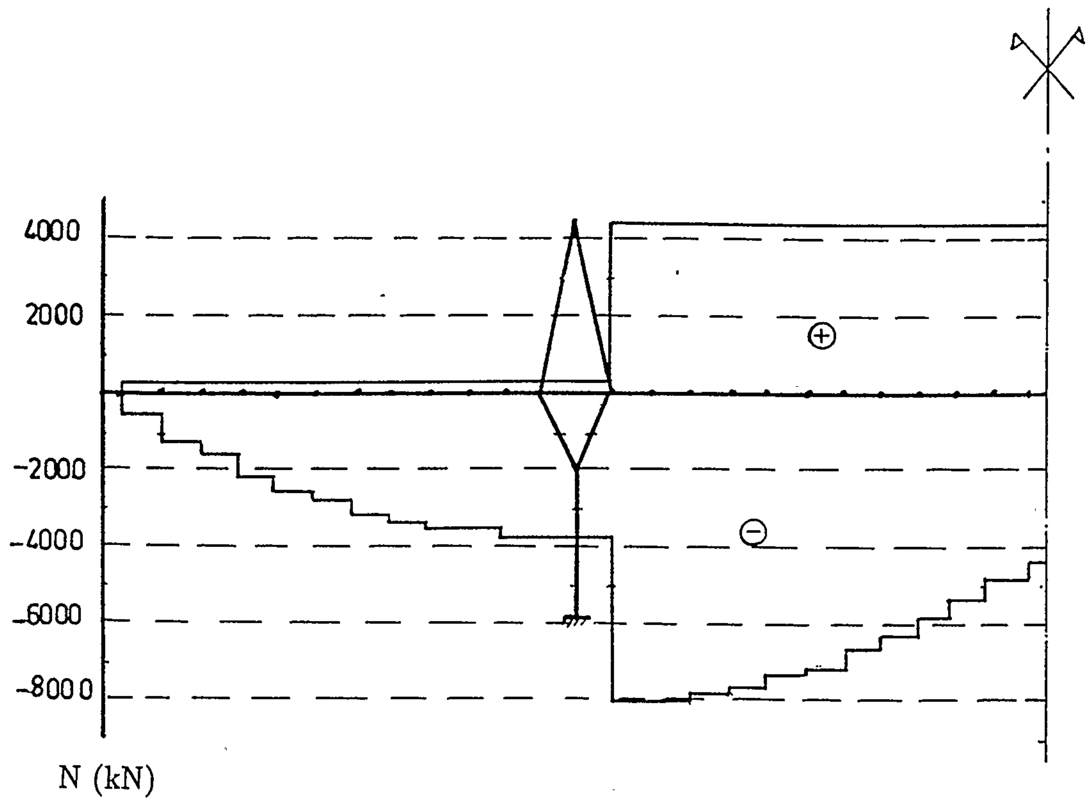

Figure 5.13: Deck normal force envelope due to highway live load

In this approach the cables are substituted by springs, if the shortening of the pylon is neglected, the elastic support spring constant k, which is the vertical force needed to develop a unit displacement (see Figure 5.15), can be calculated as follows (Troitsky, 1977):

$$\Delta L = 1 \cdot \sin\theta = \frac{T \cdot L}{E \cdot A}$$

where T = tension force in the cables

or

$$T = \frac{E \cdot A}{L} \cdot \sin\theta \tag{5.5}$$

$$k = T \cdot \sin\theta \tag{5.6}$$

From Equations 5.5 and 5.6

$$k = \frac{E \cdot A}{L} \cdot \sin^2\theta \tag{5.7}$$

From Equation 5.7 it can be concluded that the spring constants are increasing rapidly by moving towards the pylon (angle θ is increasing while the ratio (A/L) remains approximately constant). High positive bending moments are achieved by loading the zones with low spring constants (far away from the pylon), as shown in Table 5.3. This is comparable with high positive field bending moments for a beam resting on soft soil (low spring constants).

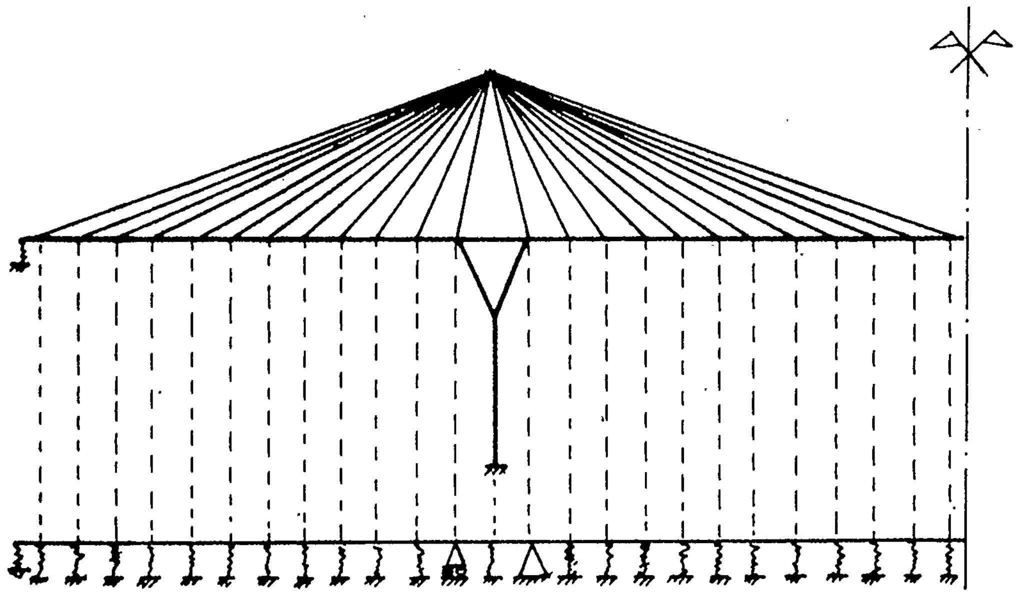

Figure 5.14: Beam-on-elastic-supports analogy

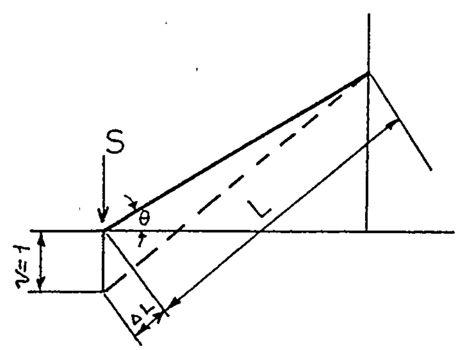

Figure 5.15: Elastic support spring constant

The high negative bending moments in the same regions (far away from the pylon) are mainly achieved by unbalanced live loads, resulting in large rotations of the system. For example, load case number 20 causes the maximum negative bending moments in the side span (see Table 5.3). The deck is connected to the pylon at three points (Figure 5.14). At two points of them, the deck is supported directly on the pylon. Due to the infinite stiffness of the pylon, compared to the deck, these two points may be considered as rigid supports, causing the high negative bending moments. At the third point, the deck is supported on the tie-beam, which provides a much more flexible support than the two other points, resulting in a lower negative bending moment. Although the live load intensity is only 12 percent of the dead load intensity, the maximum positive bending moment due to live load reaches a value of 2500 kN·m, which is 2.5 times the value of the maximum bending moment due dead load (about 1000 kN·m). For the negative bending moments, the live load gives a maximum value of about 1800 kN·m, which is about 65 percent of the value due to dead load (2800 kN·m). Comparing the bending moment envelopes of the linear and the geometric nonlinear analyses, a maximum difference of 25 percent in the regions of relatively high bending moments is obtained. This percentage increases to 100 percent in the regions of low (insignificant) bending moments. These differences are far less for the normal forces. The maximum difference is less than 1 percent. Maximum tension due to live load is achieved by load cases 14 and 22, while maximum compression is achieved by load cases 26 and 24 in the side and main spans of the deck respectively (see Table 5.3). A sudden increase in the normal force envelope (Figure 5.13) is caused by the hinged

Table 5.3: Critical load cases for deck bending moments and and normal forces

Load cases for maximum bending moments	Load cases for maximum normal forces
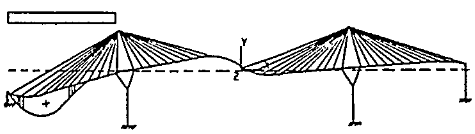 1	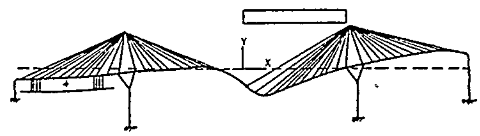 14
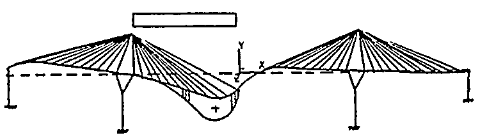 12	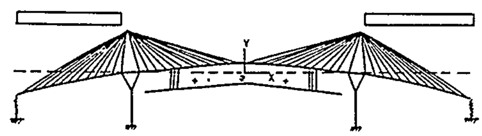 22
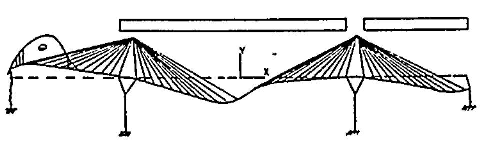 20	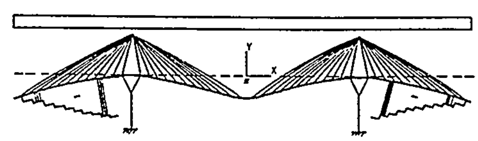 26
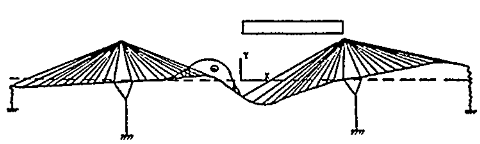 14	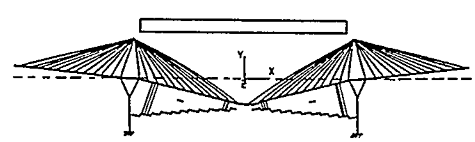 24

connection between deck and pylon at this point. The normal forces in the deck are transferred to the pylon by this hinge.

6. Deck deflections (Figure 5.16)

   The maximum downward deflection (330 mm) occurs at the expansion joint, this gives a deflection/span ratio of about 1/760. This ratio is 1/1100 for the maximum deflection of the midspan. Because of the hinged connection between deck and pylon, the maximum horizontal displacement of the deck is less than 30 mm. Such a displacement can be easily accommodated by the expansion joints. The maximum difference in the deflections between the linear and nonlinear analyses is about 7 percent.

7. Bending moments and normal forces in the pylons (Fig. 5.17 and 5.18)

   As in the dead load analysis, the upper inclined legs of the pylons are subjected primarily to axial forces (in this case tension or compression). For the lower legs, the bending moments increase rapidly towards the vertical shaft, due to unbalanced live load cases. And since horizontal forces in the deck are transferred to the pylon through the hinge at the deck level, very high bending moments are created in the vertical pylon shaft. The maximum difference in the bending moments between the two analyses (linear and nonlinear) is about 2 percent. The normal forces obtained from both analyses are almost identical.

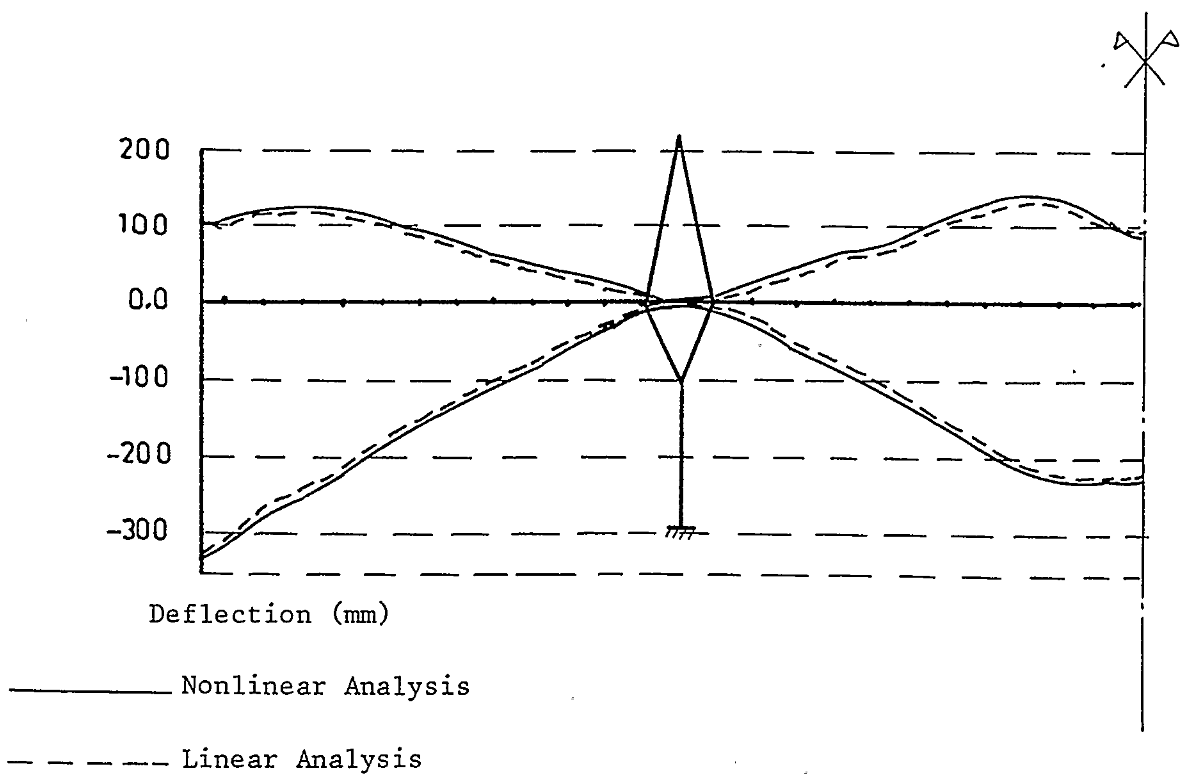

Figure 5.16: Deck deflection envelope due to highway live load

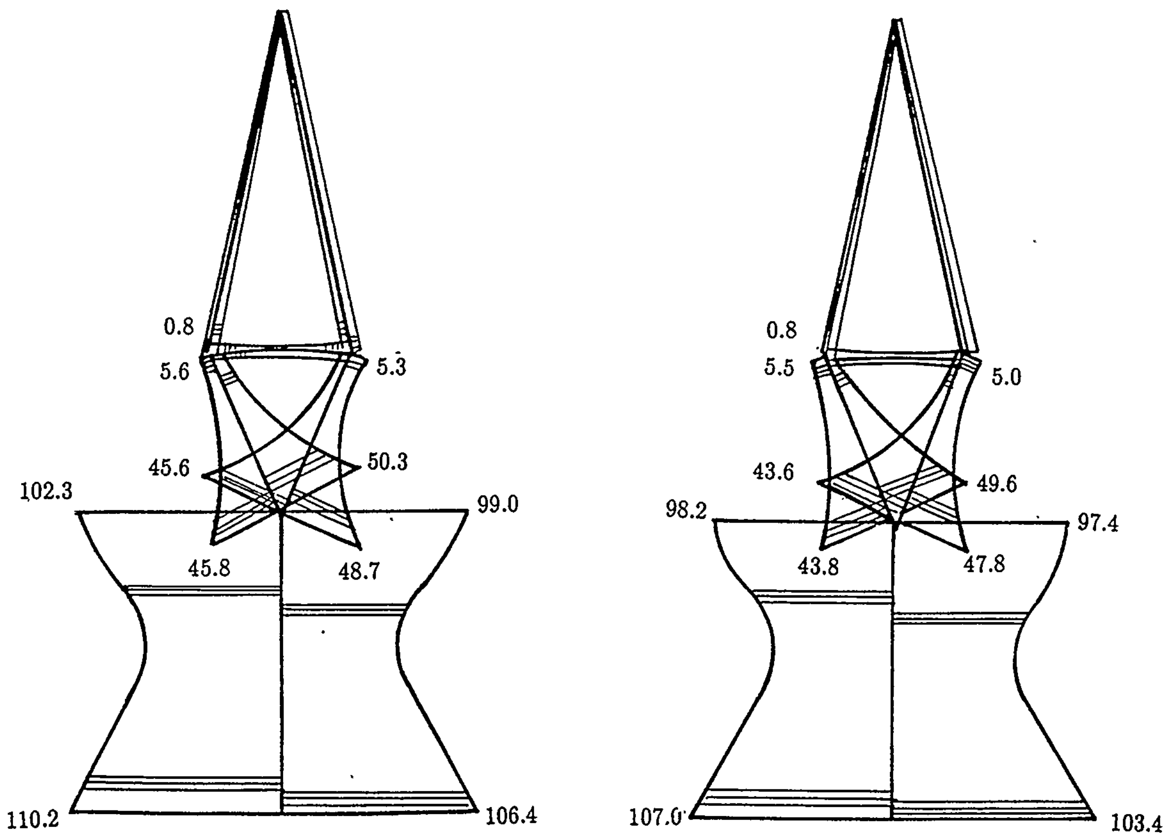

a- Nonlinear Analysis

b- Linear Analysis

Figure 5.17: Bending moment envelope (MN·m) in left pylon due to live load

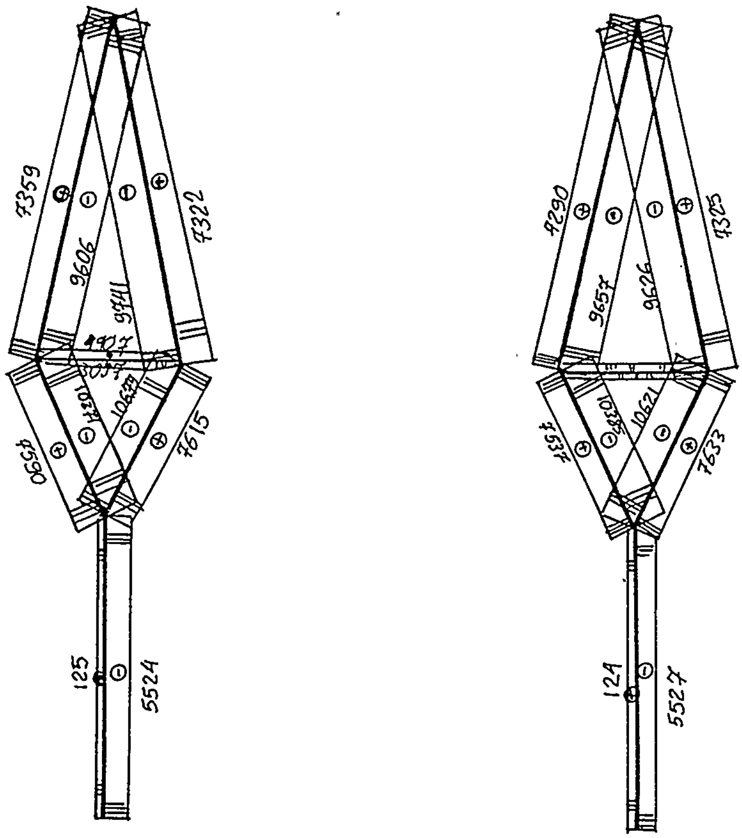

a- Nonlinear Analysis   b- Linear Analysis

Figure 5.18: Normal force envelope (kN) in left pylon due to live load

8. Conclusions

   From this discussion, it is concluded that the bending moments in the deck due to live load are significantly larger when the geometric nonlinear effects are included in the analysis. This is mainly caused by the effect of high axial forces and large deflections of the flexible deck. Bending moments in the stiff pylon are much less affected. The normal forces in the deck and pylons are almost identical in both types of analyses. Another conclusion is that for a multicable system the maximum forces in the cables are almost proportional to the load intensity applied on the deck, whereas the maximum bending moments in the deck are greatly affected by cases of loading.

5.4 THE TEMPERATURE ANALYSIS

5.4.1 General

Three types of temperature distributions (as indicated in Figure 5.19) are investigated. It is assumed that these temperature distributions are constant throughout the whole length of the bridge. Therefore the temperature analysis is performed using the same model used in the highway live load analysis. Since symmetry exists at both ends of the 500 m long deck, no springs are used at the ends of the deck (see Figure 5.19).

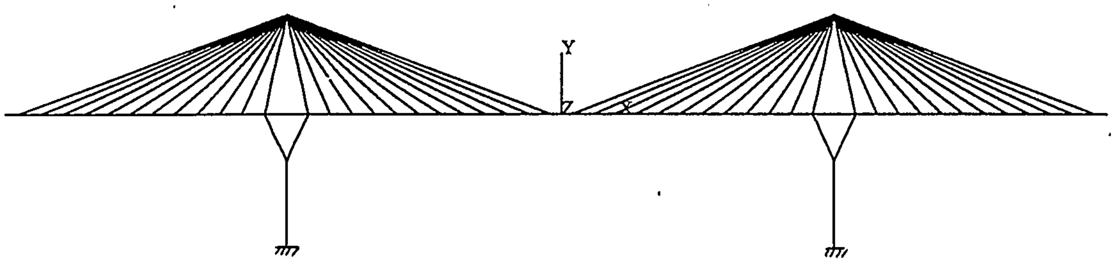

Temperature 1

Cables	$\Delta T = -40°C$
Deck	$\Delta T = -40°C$
Pylon	$\Delta T = -40°C$

Temperature 2

Cables	$\Delta T = -20°C$
Deck	$\Delta T = -40°C$
Pylon	$\Delta T = -40°C$

Temperature 3

Cables		$\Delta T = -20°C$
Deck	Top	$\Delta T = -20°C$
	Bottom	$\Delta T = -40°C$
Pylon	Upper legs	$\Delta T = -20°C$
	Lower legs	$\Delta T = -40°C$
	Shaft	$\Delta T = -40°C$

Figure 5.19: Model used in the temperature analysis

5.4.2 Results and conclusions

1. Forces in the cables

   Except for the cables next to the pylons, the forces in the cables due to the three temperature distributions are negligible. A maximum tensile force of 10 kN, which is about 20 percent of the maximum tensile force due to the highway live load, is reached in the cable next to the pylon. This force is due to temperature distribution 1 (the whole structure is exposed to $\Delta T = -40°C$).

2. Bending moments and normal forces in the deck (Fig. 5.20, 5.21 and 5.22)

   For temperature distributions 1 and 2 (constant temperature throughout the deck thickness), the high bending moments occur in the vicinity of the pylon and at the centre of the main span (Fig. 5.20 and 5.21). The moments in the side span, which is connected to the expansion joint capable of transferring only shear forces, are almost zero. It should be noted, that due to symmetry of the temperature loadings for the whole continuous bridge about axes through the expansion joints, the shear forces are zero at these joints. Therefore no springs are used at the ends of the deck, or in other words the side spans of the two-pylon model are free and acting as a suspended cantilever, resulting in those zero bending moments. For temperature distributions 1 and 2, the maximum difference between the linear and geometric nonlinear analyses in the regions of relatively high bending moments is about 8 percent. This difference increases to 22 percent in regions of relatively low bending moments. The temperature distribution 3 (linear temperature gradient through the deck thickness) causes high bending moments reaching the maximum values of the highway live load analysis of about 3000 kN·m at the centre of the main span.

The average bending moment along the deck is about 2600 kN·m, which is reached after a certain transition length (0.45 of the side span length) as shown in Figure 5.22. Comparing this moment with the fixed end moment of a beam, with the same cross-section and material properties of the deck, and exposed to the same linear temperature distribution, the later case can be calculated using the following equation (Ghali and Neville, 1989):

$$M = \frac{EI \cdot \alpha}{t_b} \cdot \Delta T \tag{5.8}$$

where:

M	= fixed end moment
t_b	= depth of the beam
α	= coefficient of thermal expansion of the material
ΔT	= temperature difference between the top and bottom fibres of the beam

Not surprisingly, Equation 5.8 gives a moment of 2567 kN·m, which is almost identical with the moment obtained from the complicated nonlinear computer analysis. This means that after a certain transition zone, the deck may be considered as a fixed beam, and Equation 5.8 may be used in calculating the moment in the deck due to a linear temperature distribution through its depth. Since the forces in the cables are negligible, the normal forces in the deck, which are a result of the cable forces are also negligible.

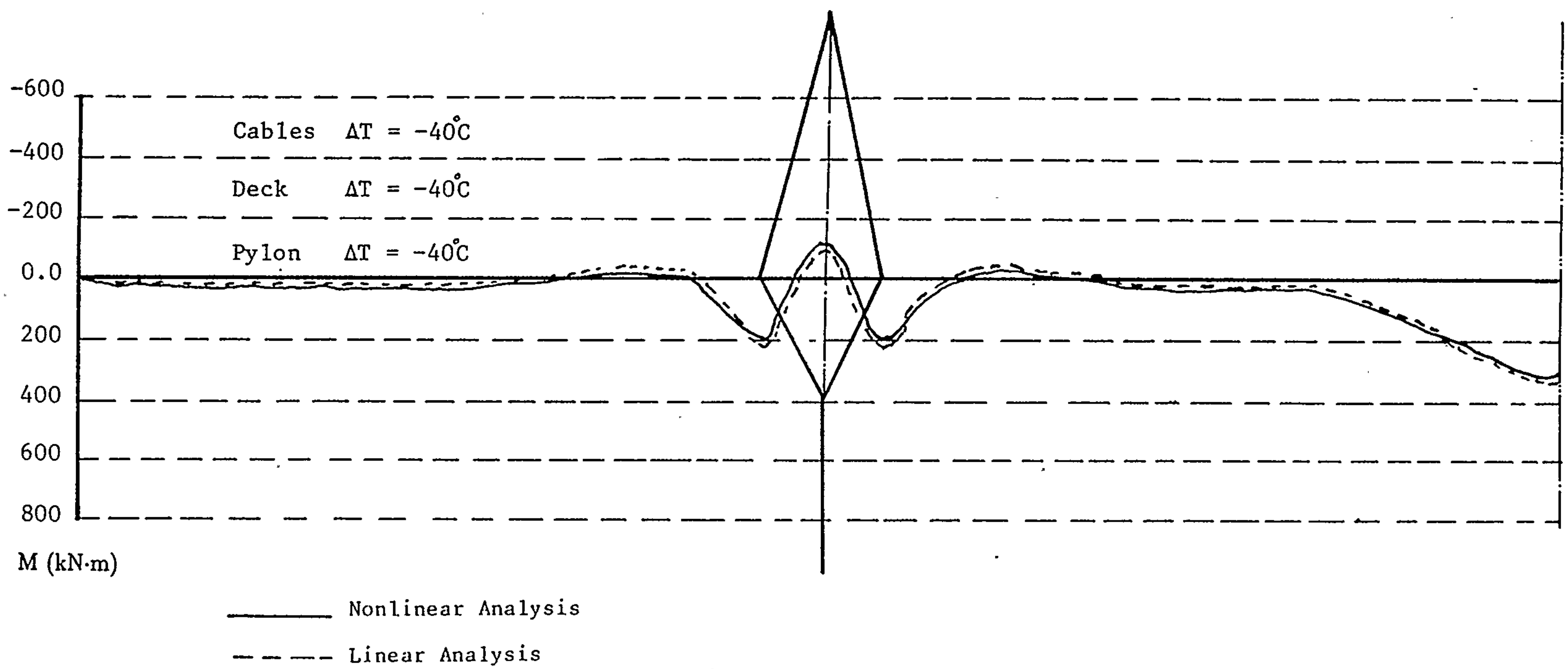

Figure 5.20: Deck bending moment diagram due to temperature distribution 1

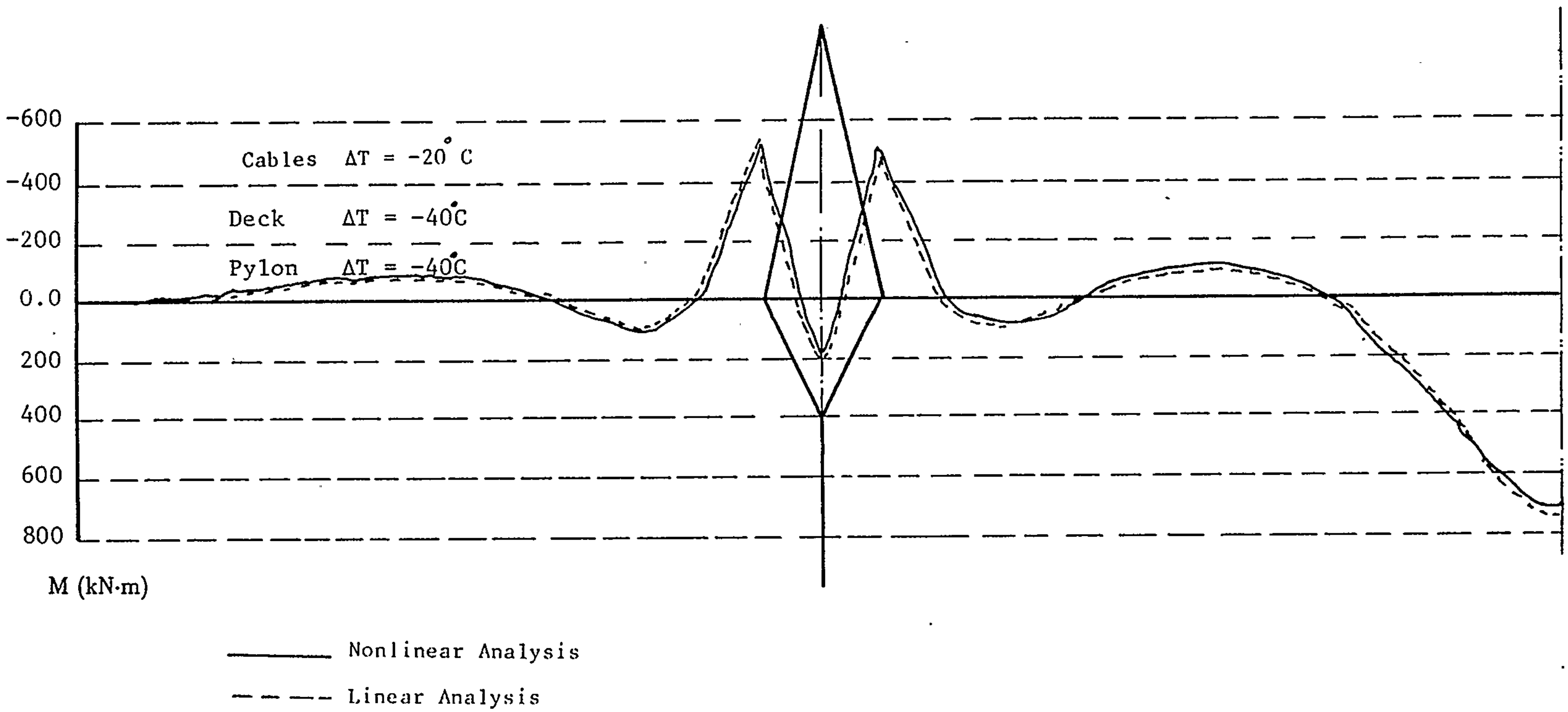

Figure 5.21: Deck bending moment diagram due to temperature distribution 2

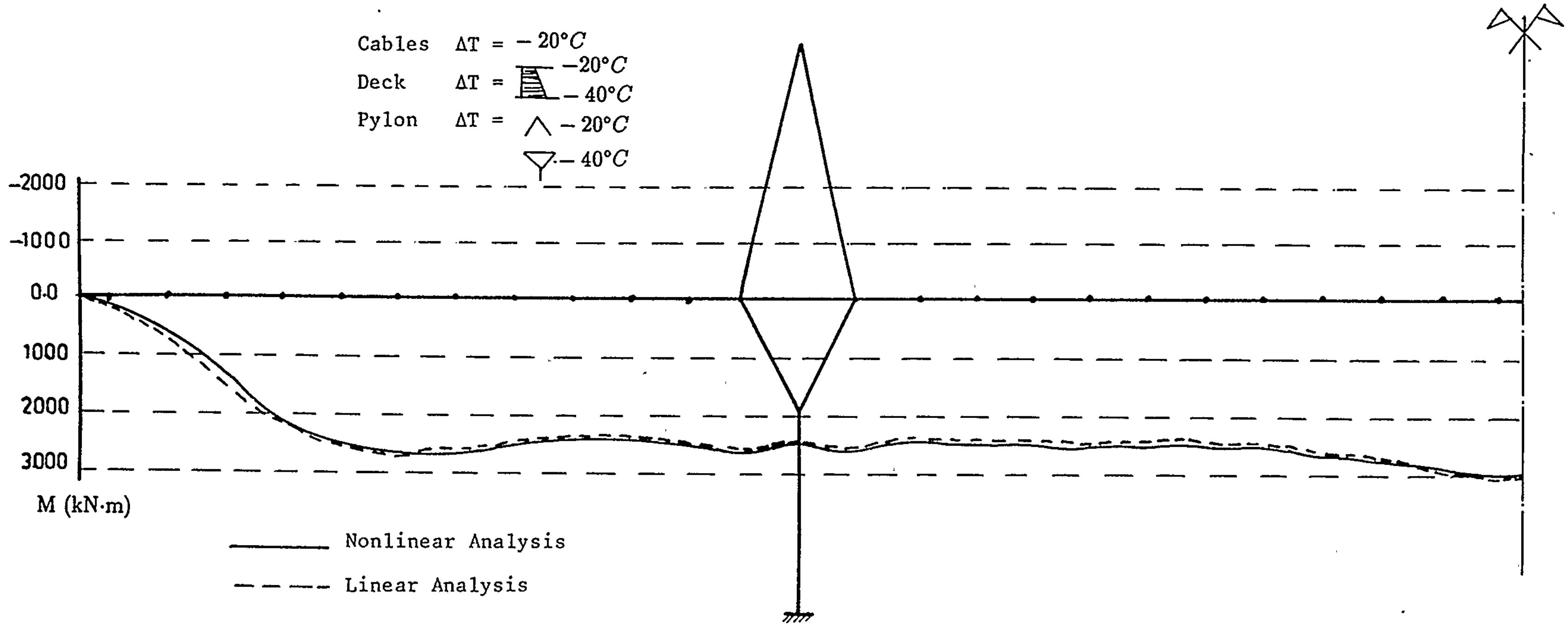

Figure 5.22: Deck bending moment diagram due to temperature distribution 3

3. Deck deflections (Figure 5.23)

   The maximum vertical deflection (about 230 mm) is caused by temperature distribution number 2 . This value is the same as the maximum vertical deflection at the centre of the main span induced by the highway live loads. The maximum horizontal displacement of the 500 m long continuous deck at the expansion joint is about 100 mm. This results in a gap of 200 mm, which can be accommodated by traditional expansion joints.

4. Bending moments in the pylons (Figure 5.24)

   In the chosen structural system consisting of stiff pylons and a flexible deck, the horizontal force created by the contraction (or expansion) of the deck is resisted by the stiff pylons via the hinged connection between the deck and the pylon. This leads to very high bending moments in the vertical pylon shaft. The moments are reaching the values obtained in the highway live load analysis. The maximum difference in the bending moments between the linear analysis and the geometric nonlinear analysis is about 18 percent for the upper legs (low bending moments) and less than 1 percent for the vertical shaft (high bending moments).

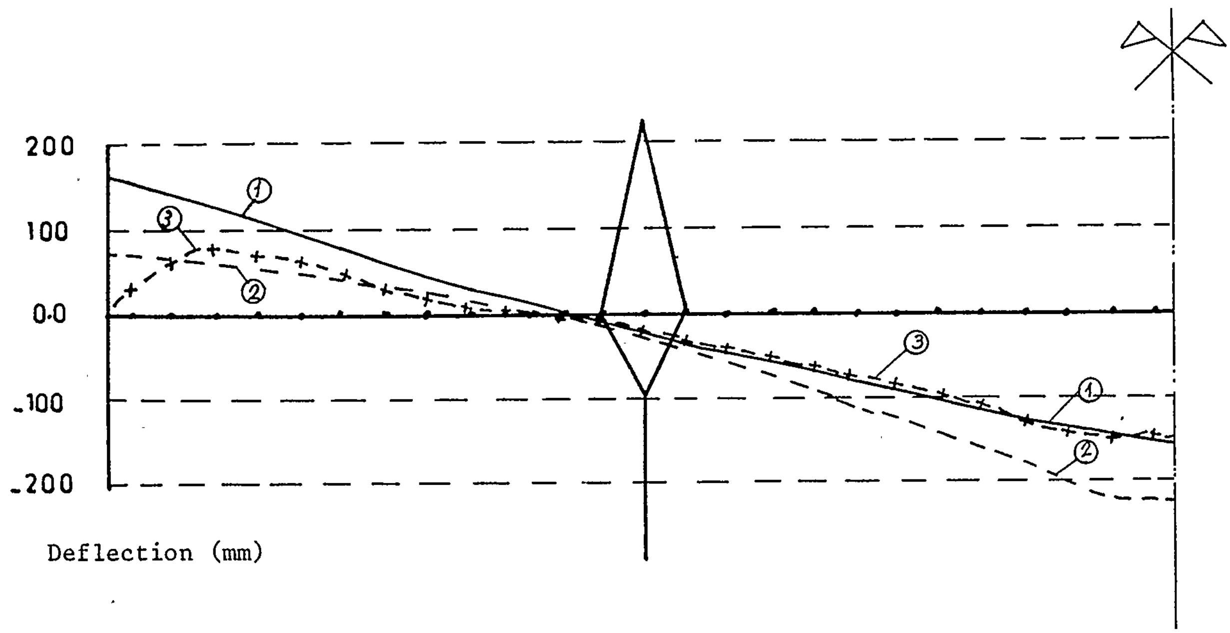

Figure 5.23: Deck deflections due to temperature distributions 1, 2 and 3

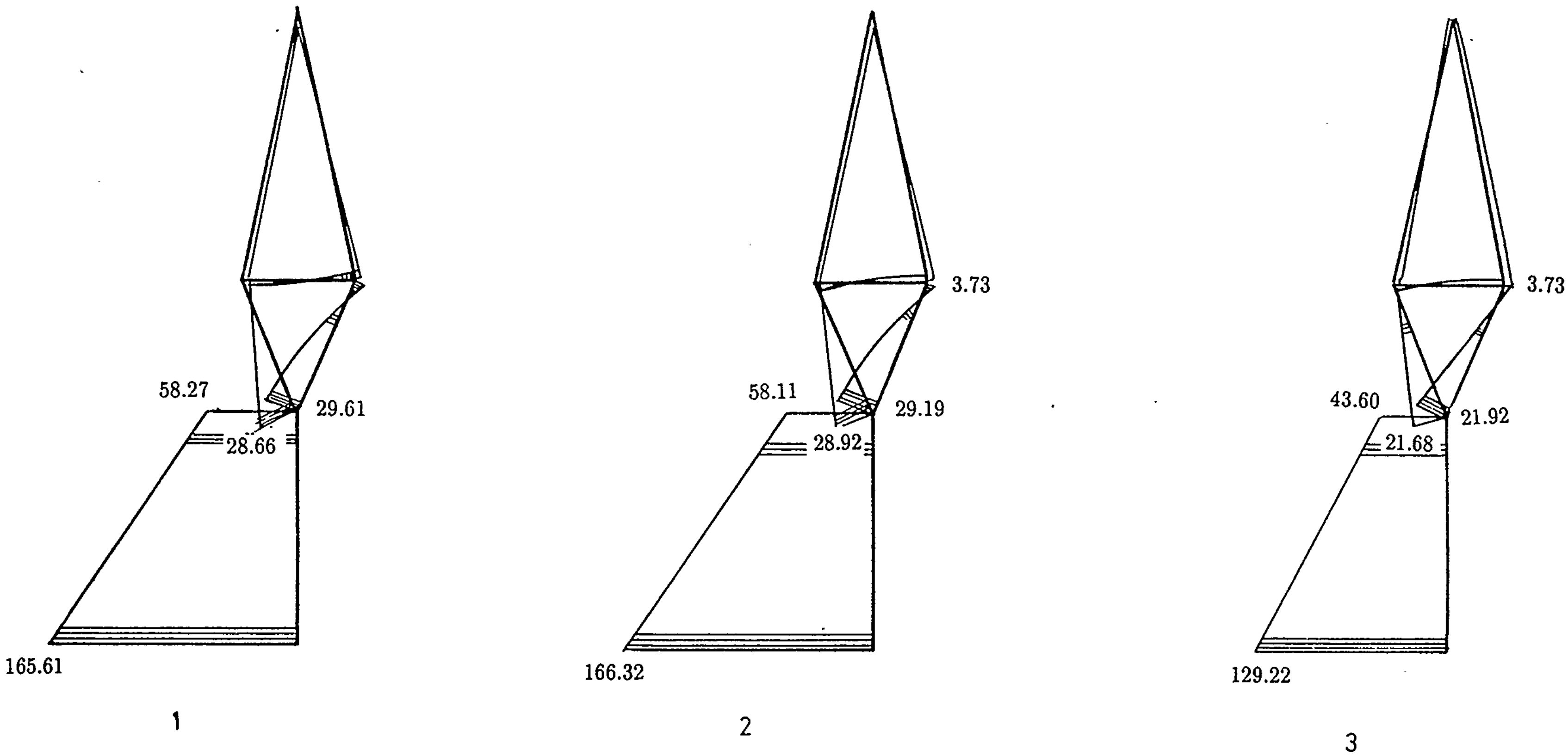

Figure 5.24: Bending moment diagrams (MN·m) in the left pylon due to temperature distributions 1, 2 and 3

5.5 SUMMARY

A conventional linear and a geometric nonlinear analysis are performed for the proposed bridge to study its behaviour under its own weight, highway live loads and temperature.

In the dead load analysis two methods are used to calculate the required initial strains (forces) in the cables to obtain a horizontal deck due to dead load. A superposition technique for the linear and an iterative procedure for the nonlinear analysis. Both methods gave same results.

In the live load analysis different load cases are investigated to obtain the envelopes for the maximum straining actions in the different components of the bridge. The beam-on-elastic-support analogy is used in trying to explain the moment envelope of the deck.

In the temperature analysis three cases of temperature distributions are investigated. For the bending moments in the deck, the linear varying temperature through the deck thickness is the critical case. The resulting moment is compared with the fixed end moment of a beam subjected to the same temperature distribution. Almost identical moment values are obtained after a certain transition length in the deck.

Chapter 6

PARAMETRIC STUDY

6.1 INTRODUCTION

The static behaviour of a cable-stayed bridge is the result of the complex interaction between its three structural components which are the deck, the pylons and the cables.

Based on the system chosen for the proposed bridge which consists of a flexible deck and stiff pylons, the influence of the following parameters on the characteristics of continuous cable-stayed bridges are examined in this chapter:

1. The different connection types between deck and pylon.

2. The dimensions of the pylon.

3. The areas of the cables.

6.2 THE DECK-PYLON CONNECTIONS

6.2.1 Introduction

In the proposed bridge the deck is resting at three points on each pylon (including the tie-beam). To study the effect of the connection type between deck and pylons on the behaviour of a continuous cable-stayed bridge, five different connection types (see Figure 6.1) are investigated.

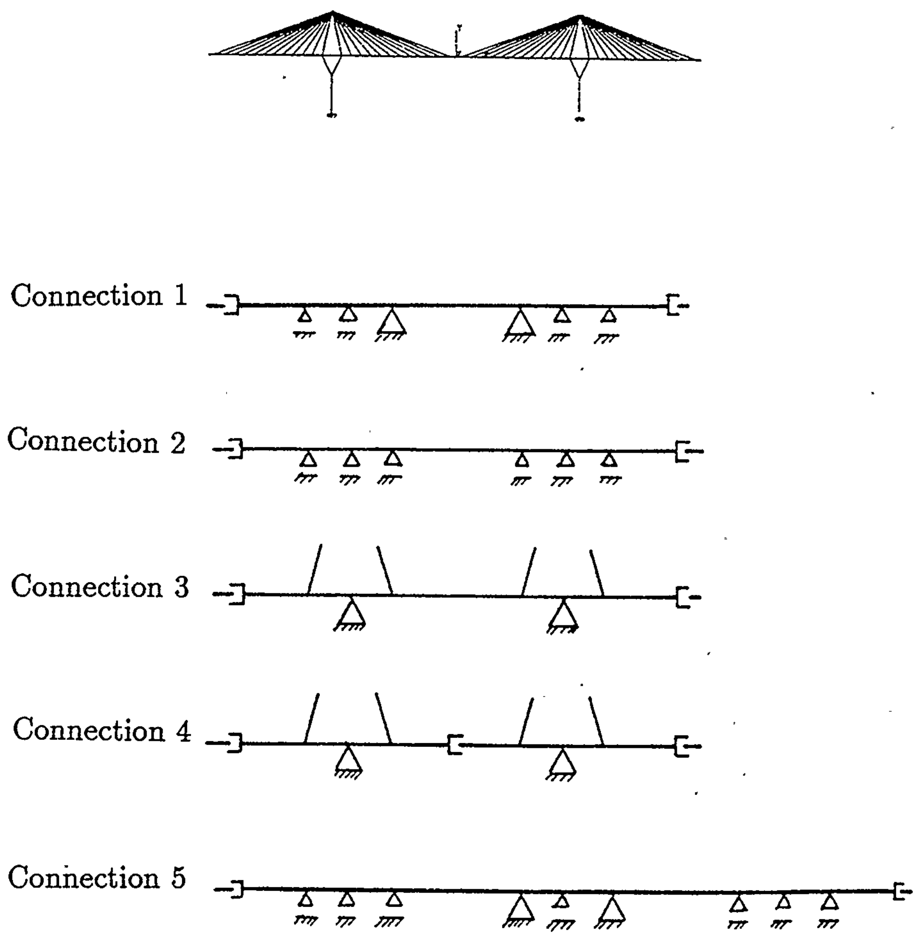

Figure 6.1: Different deck-pylon connections

- **Connection 1**

  In this connection type the bridge system consists of a 500 m long continuous slab resting on two pylons. At both ends of the slab shear joints (expansion joints), capable of transferring only a shear force, provide the continuity of the about 13 km long bridge. Each deck-pylon connection consists of two rollers, which allow a horizontal movement of the deck on the pylon, and one hinge preventing such a type of movement.

- **Connection 2**

  For this type of connection the bridge has the same structural system as in Connection 1, except that each deck-pylon connection consists of three rollers allowing a free horizontal movement of the deck against the pylon.

- **Connection 3**

  In this connection the bridge system consists of a 500 m long continuous slab resting on two pylons (as in Connection 1). Each deck-pylon connection consists of one hinge, while the other two points of the deck are suspended by cables instead of being supported directly on the pylon.

- **Connection 4**

  For this connection the bridge consists of the same structural system as in Connection 3, except that a shear joint (expansion joint) is introduced at the midspan of the system.

- **Connection 5**

  In this type of connection the bridge system consists of a 750 m long continuous slab resting on three pylons. Each of the deck-pylon connections for the two outer pylons consists of three rollers. Whereas for the pylon in the middle, the deck is connected to the pylon by two hinges and one roller.

The effect of these different connections on the behaviour of the deck, pylons and cables are discussed next.

6.2.2 Effect of the deck-pylon connection type on the deck

6.2.2.1 Deck deflections

From Figure 6.2 and Figure 6.3 it can be seen that the minimum deflections are obtained by connection types 1 and 3, which consist of a 500 m long deck connected to each pylon with at least one hinge preventing the horizontal movement of the deck against the pylons. Deck and pylons form a sort of frame action resulting in decreasing the deflections to a deflection/span ratio of 1/1000.

Introducing an expansion joint at the midspan (Connection 4) is increasing the deck deflections to reach a maximum deflection/span ratio of 1/500, which is double the value obtained in connection types 1 and 3. Deck and pylons are acting almost as a double cantilever system, but still the ratio 1/500 may be accepted.

Using a floating deck resting on the pylons via rollers only (Connection 2), or even permitting a horizontal movement of the deck against one pylon, and preventing such a movement at the other pylon (Connection 5) leads to unacceptable deck deflections with a maximum deflection/span ratio of over 1/200 (see Figure 6.3).

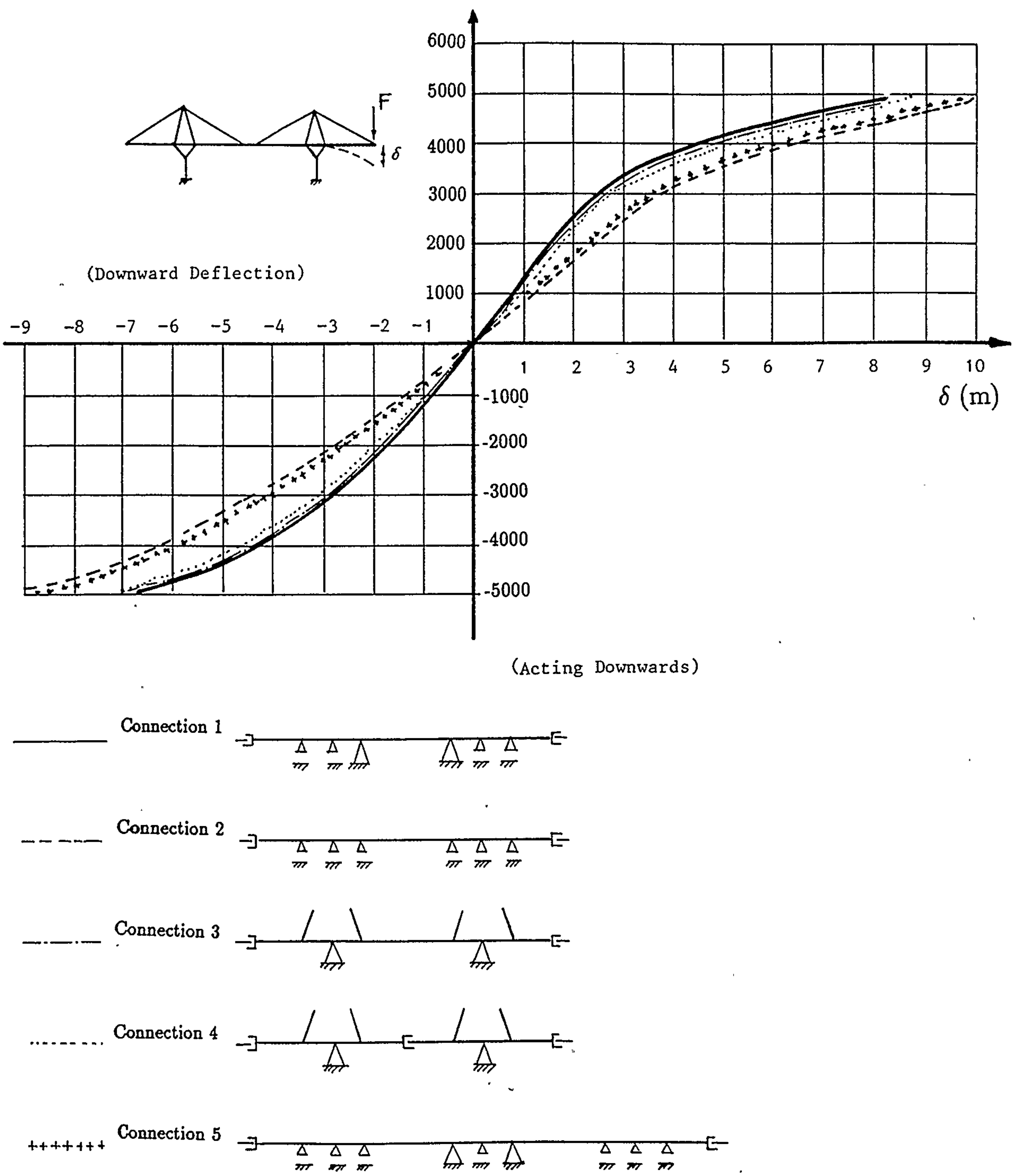

Figure 6.2: Force-deflection relationships for different deck-pylon connections

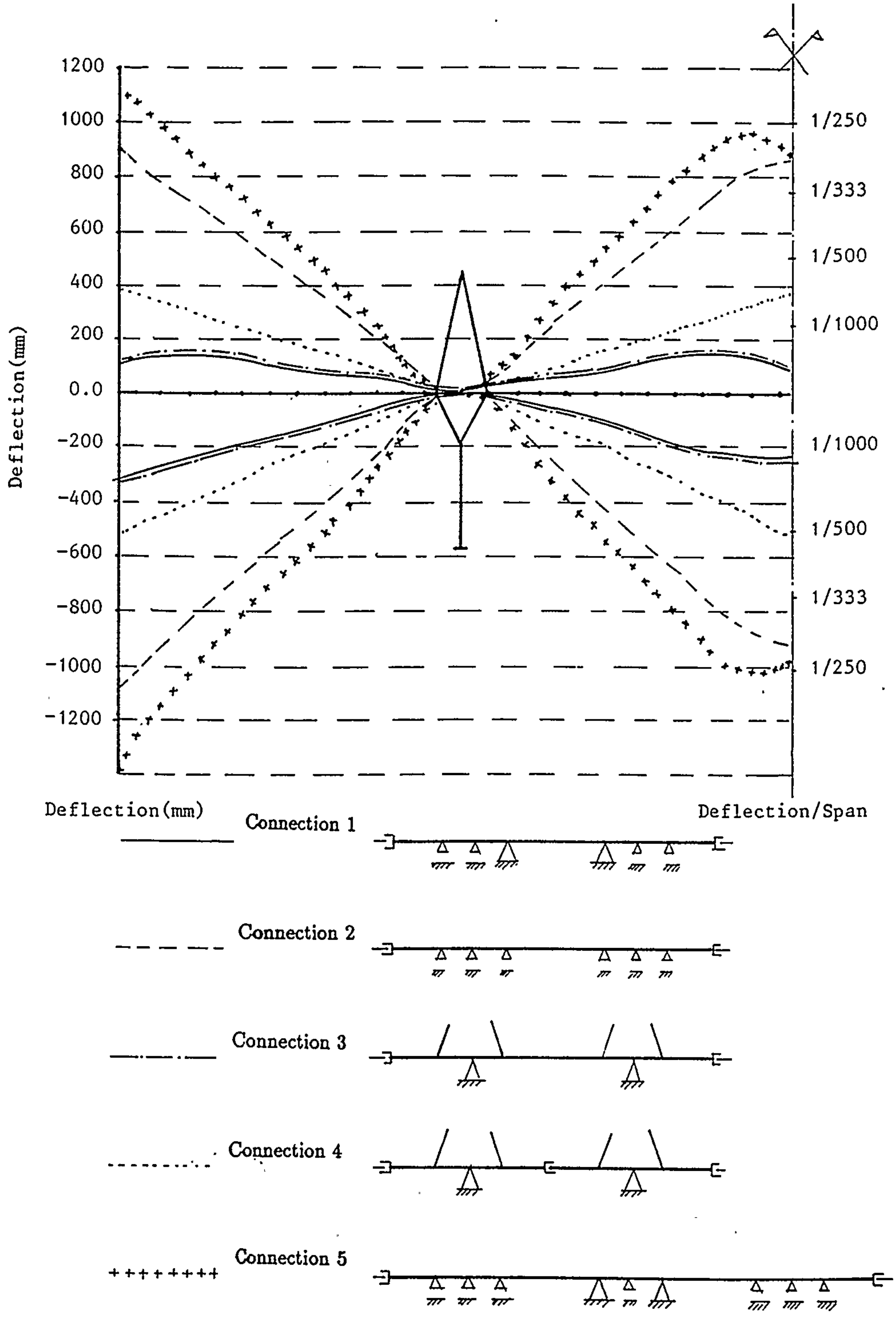

Figure 6.3: Deck deflection envelopes due to highway live loads for different deck-pylon connections

In such a system the horizontal movement of the deck is resisted by the cables which provide a much more flexible support against the horizontal movement compared to a rigid hinge between deck and pylon. In addition the horizontal forces in the deck are transferred to the top of the pylon via the cables, causing large bending of the pylon leading to excessive deck deflections.

6.2.2.2 Deck bending moment envelopes due to highway live loads

A comparison between the bending moment envelopes for the first three deck-pylon connections as shown in Figure 6.4 shows that having only rollers between the deck and the pylons results in increasing the maximum moments in the deck significantly. In the mid- and side-spans the maximum negative moments in the deck are caused by unbalanced live loads leading to large rotations of the system. Using rollers only (Connection 2) increases the deck deflections and rotations significantly. In the side-span for example, this leads to an increase in the spring force at the end of the deck from 118 kN (Connection 1) to 318 kN (Connection 2) for the critical load cases. The maximum negative moments are increasing with the same ratio of the spring forces from 1000 kN·m (Connection 1) to 2670 kN·m (Connection 2).

The increase in the positive moments in the side-span is also caused by large deflections of the deck leading to an increase in the spring force due to critical load cases from 203 kN (Connection 1) to 384 kN (Connection 2). The maximum positive moment is increasing again by the same ratio of the spring forces from 1602 kN·m (Connection 1) to 3232 kN·m (Connection 2).

The large deflections of the deck cause a high curvature of the deck at the points over the roller supports producing very high positive and negative bending moments at these points (see Figure 6.4).

The conclusion is that allowing a horizontal movement of the deck against the pylons by using only rollers to connect the deck with the pylon (Connection 2) increases the bending moments in the deck to unacceptable values. Even if this horizontal movement is allowed at one pylon and prevented at another one (as in Connection 5), these unacceptable high moments would not be reduced, since the deflections are not significantly reduced in Connection 5.

To decrease the high negative moments over the supports in Connection 1, it is useful to suspend the deck from cables instead of the rigid supports. This is achieved in Connection 3. The cables provide a much more flexible support for the deck than the rigid rollers, so the negative moments at the two additional cables are decreased significantly, but the negative moment at the hinge support also increases to a high value (see Figure 6.4).

This means that from an economical point of view it is not advantageous to introduce additional cables (which are the most expensive elements in a cable-stayed bridge) for the deck-pylon connection to decrease the bending moments in the deck, instead of supporting the deck directly on the pylon.

Introducing an expansion joint at the midspan (Connection 4) reduces the moments at this point to zero, but at the same time increases the moments in the side-span (see Figure 6.5), since the deflections of the deck are increased in this system which acts almost as a double cantilever.

From the previous discussion Connection 1 seems more efficient than the other connection types regarding the decrease of the maximum bending moments produced in the deck.

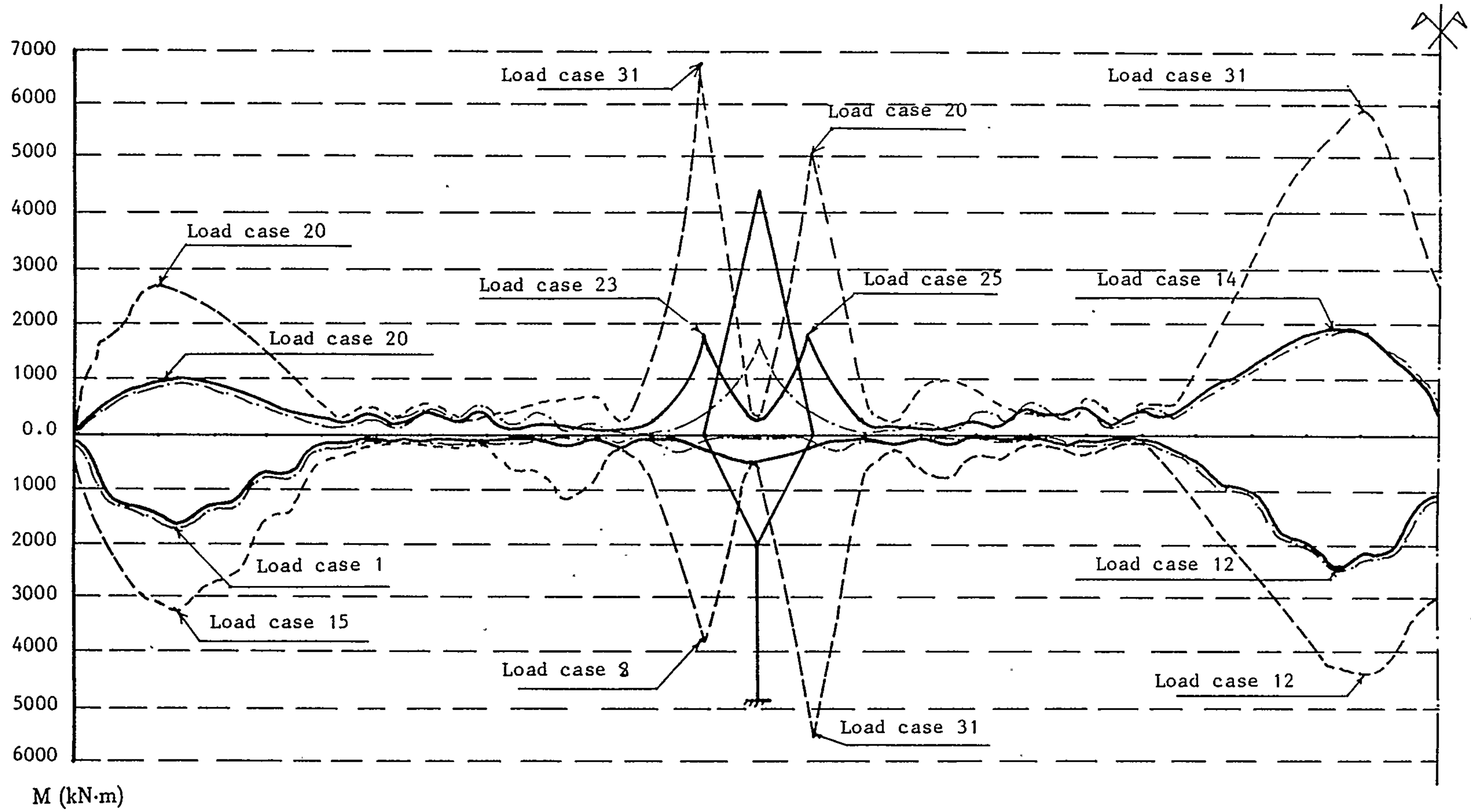

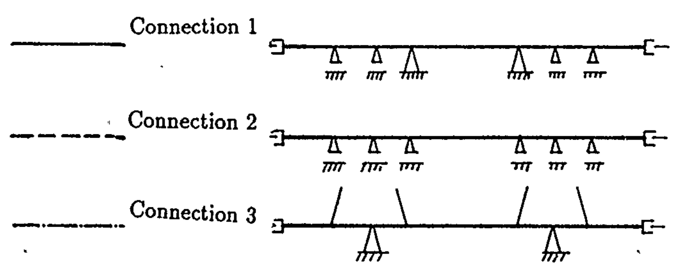

Figure 6.4: Deck bending moment envelopes due to highway live loads for deck-pylon connections 1,2 and 3

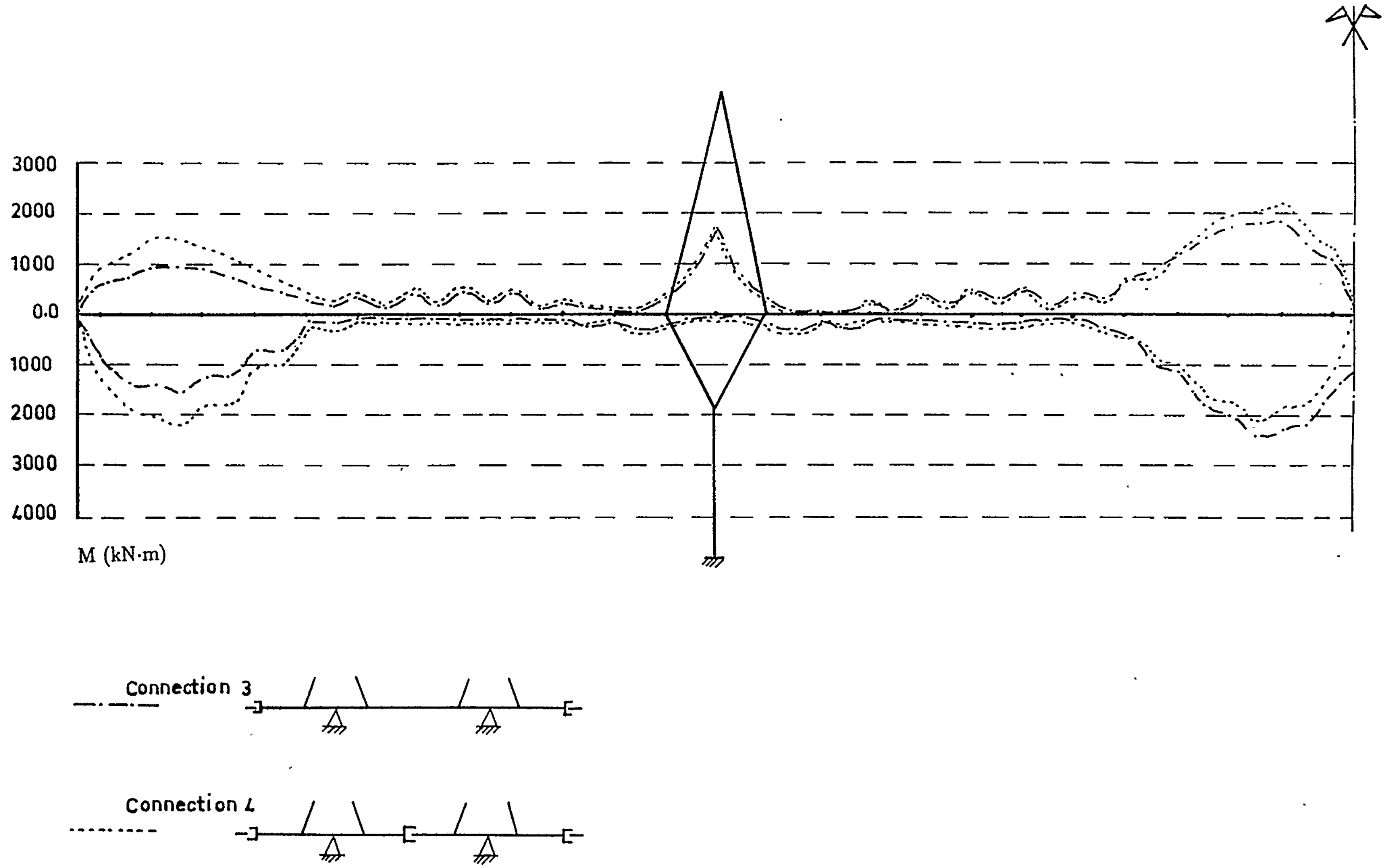

Figure 6.5: Deck bending moment envelopes due to highway live loads
for deck-pylon connections 3 and 4

6.2.2.3 Deck normal force envelopes due to highway live loads

A comparison between the normal force envelopes of different deck-pylon connection systems (see Figure 6.6) shows that the main difference between using a hinge and not using a hinge, is the sudden jump in the normal force at the location of the hinge, representing the amount of horizontal force transferred to the pylon at the deck level. This is true except for Connection 4, where the system is symmetrical about each pylon axis, so that the maximum normal forces in the deck are also symmetrical about those axes. For the side-span the different deck-pylon connections give almost the same normal force envelopes. The difference appears in the main span as shown in Figure 6.6. Connections 1 and 3 (continuous deck and using a hinge between deck and pylon) cause high compressive forces (load case 24) and relatively high tension forces (load case 22), this may cause fatigue problems, especially if the live load is a high percentage of the dead load.

In general, a compression force in the deck is advantageous, since it reduces the amount of prestressing required. To reduce the maximum tension forces in the deck significantly, an expansion joint at the midspan is useful, which is the case of Connection 4. This joint decreases the maximum compression forces too as shown in Figure 6.6. Such a system may be efficient regarding fatigue problems in the deck. Connection 2 (only rollers) gives a more or less constant maximum compression force and an increasing tension force in the main span.

The conclusion from the above discussion is that Connection 4 is to be considered should fatigue due to high compression and tension forces is a problem in the systems consisting of connection types 1 and 3.

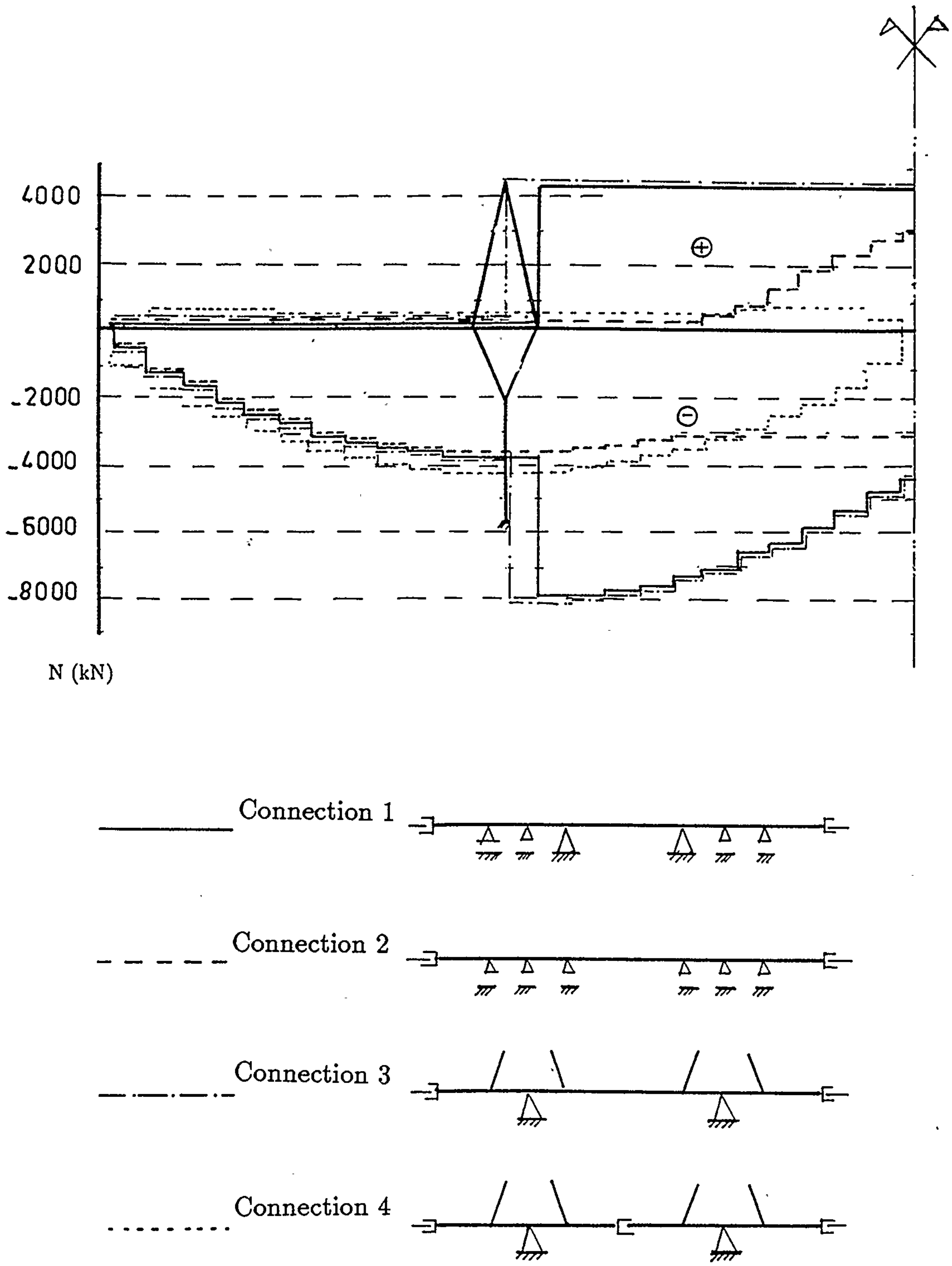

Figure 6.6: Deck normal force envelopes due to highway live loads for different deck-pylon connections

6.2.2.4 Buckling of the deck

Since the slender deck in the chosen multicable-stay system is acting primarily as compression chord member of a cantilever structure suspended from the pylon by inclined stays, buckling due to large compressive forces induced by the inclined stays may be a problem.

To study the buckling phenomenon of such a system, and the effect of the type of deck-pylon connection on the critical buckling load of the deck, the live load on the deck is increased gradually in a geometric nonlinear analysis until a negative pivot on the main diagonal of the structure stiffness matrix is reached. This indicates buckling. The analysis is carried out for live load cases 24 and 26 superimposed on the dead load, and the normal force diagrams due to the critical buckling loads for the different deck-pylon connections are shown in Figure 6.7 and Figure 6.8.

For load case 24, Connection 1 gives the minimum critical buckling load q_c of 199 kN/m, while the system of Connection 2 gives the maximum critical buckling load, the deck starts to buckle at q_c equal to 2563 kN/m, which is over 12 times the critical load of Connection 1. For load case 26 the critical buckling load ($q_c \approx$ 660 kN/m) is almost the same for all the different deck-pylon connections.

At this point it should be mentioned, that even the smallest buckling load q_c of 199 kN/m for Connection 1 is over eight times the highway live load intensity q of 23.8 kN/m for which the bridge is designed. This means that the previously mentioned critical buckling loads are only theoretical values, indicating the behaviour and resistance of the different deck-pylon connection systems against the buckling phenomena of the deck. Actually the various structural components of the bridge (for example the cables) will fail before reaching the critical buckling loads mentioned

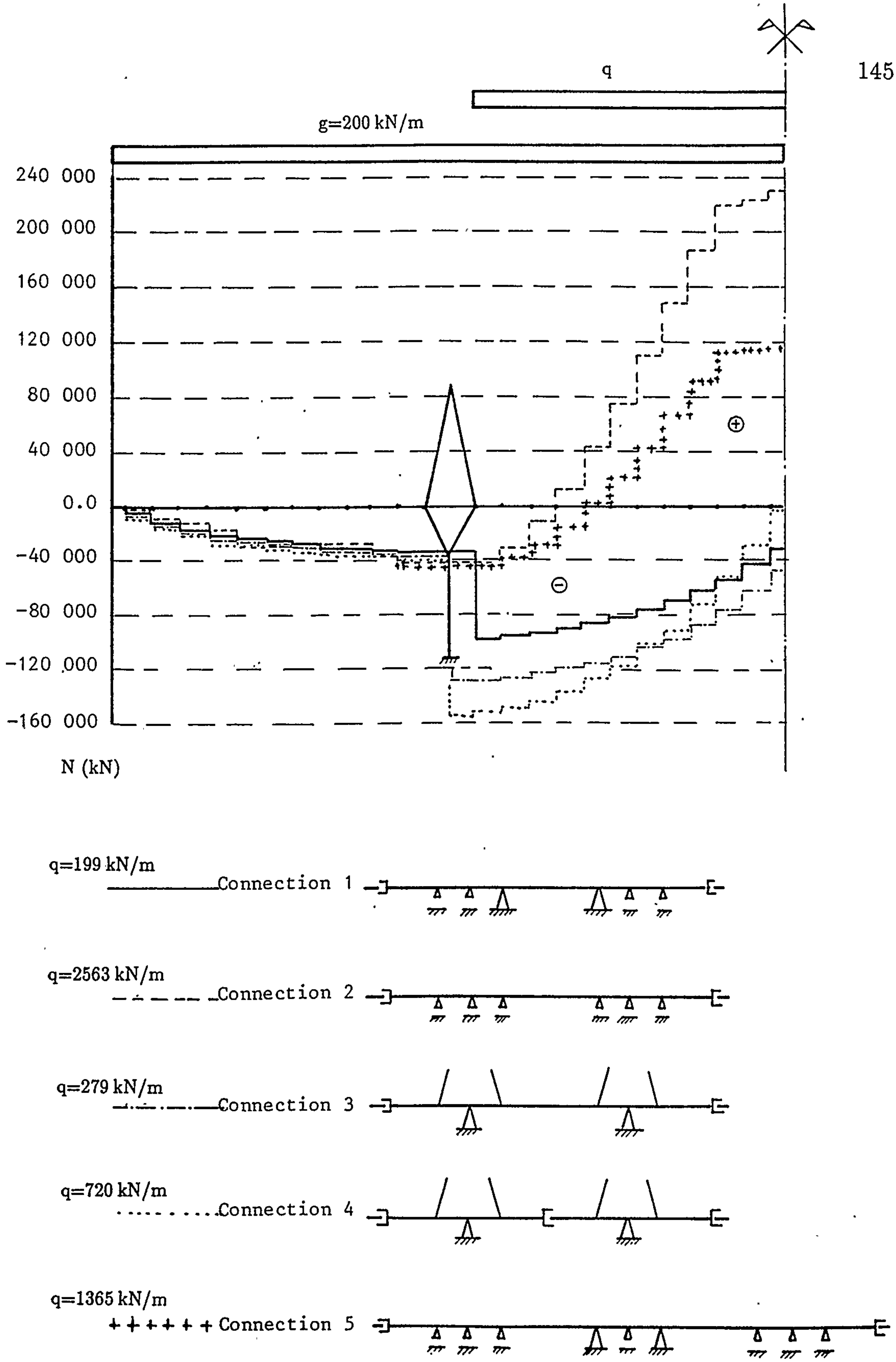

Figure 6.7: Deck normal force diagrams at buckling due to live load case 24 for different deck-pylon connections

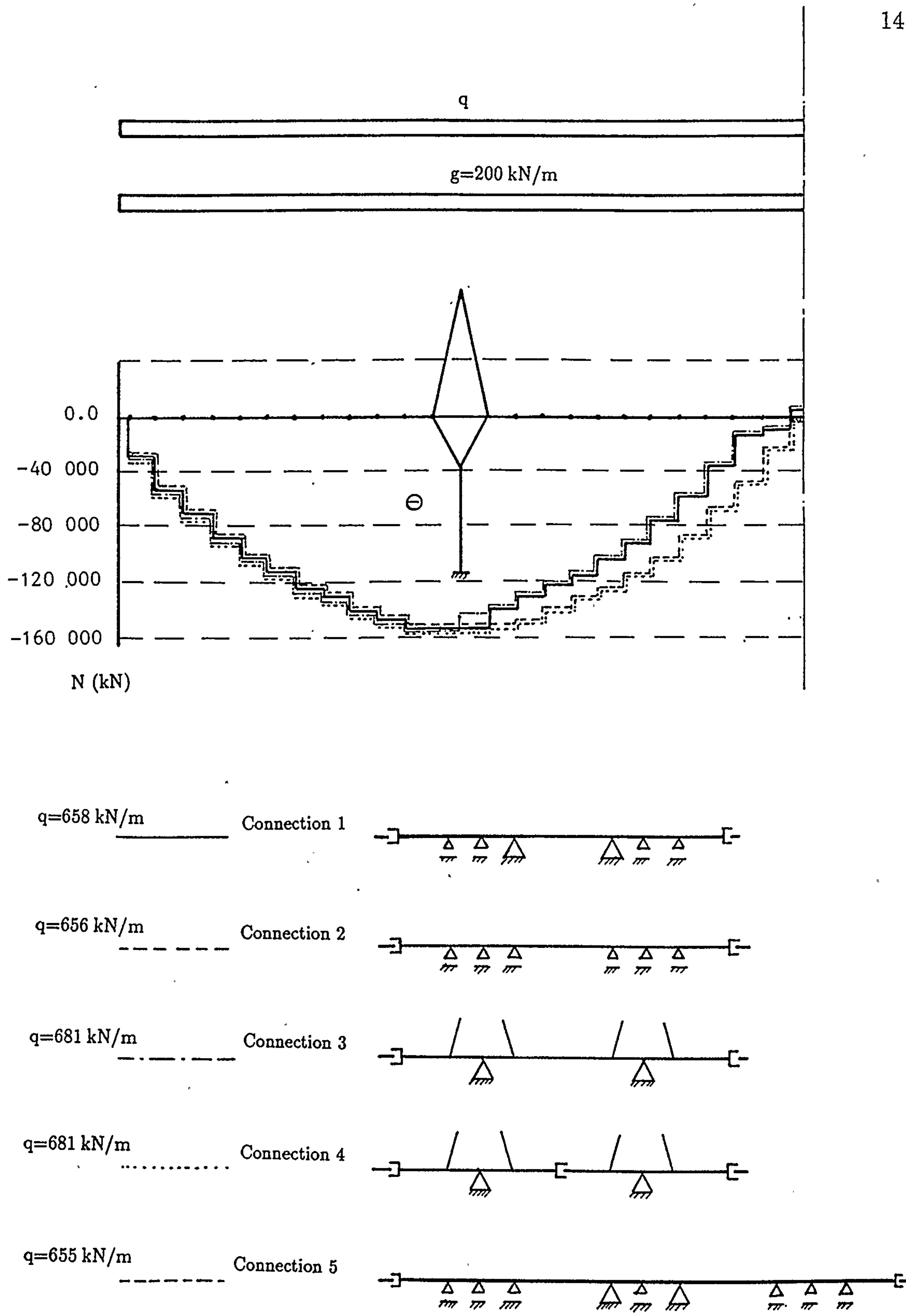

Figure 6.8: Deck normal force diagrams at buckling due to live load case 26 for different deck-pylon connections

before.

This means that the chosen system of a multicable-stayed bridge with a slender deck is effective in preventing instability of the deck.

6.2.3 Effect of the type of deck-pylon connection on the pylons

6.2.3.1 Pylon bending moment envelopes due to highway live loads

A comparison between the bending moment envelopes in the vertical shaft of the pylon (see Figure 6.9) shows that the highest bending moment values are reached in Connection 2 (only rollers). In this connection type the horizontal forces in the deck due to unbalanced live loads are transferred to the top of the pylon via the cables, thus increasing the moment arm and producing very high bending moments (a maximum of 361 MN·m) in the vertical shaft of the pylon.

Transferring the horizontal forces in the deck to the pylons by using a hinge at every second pylon (Connection 5) decreases the maximum moment by 33 percent from 361 MN·m to 241 MN·m.

Transferring the horizontal forces in the deck to the pylons directly by a hinge at each pylon (connection types 1 and 3) creates a much more efficient system decreasing the maximum moments to 110 MN·m.

Using an expansion joint in the midspan (Connection 4) produces a constant maximum bending moment of 175 MN·m in the pylon shaft. This system is acting as a double cantilever.

The conclusion is that the best systems regarding the bending moments in the vertical pylon shaft due to highway live loads are connection types 1 and 3 (using a hinge at each pylon). An expansion joint in the midspan increases the moments by

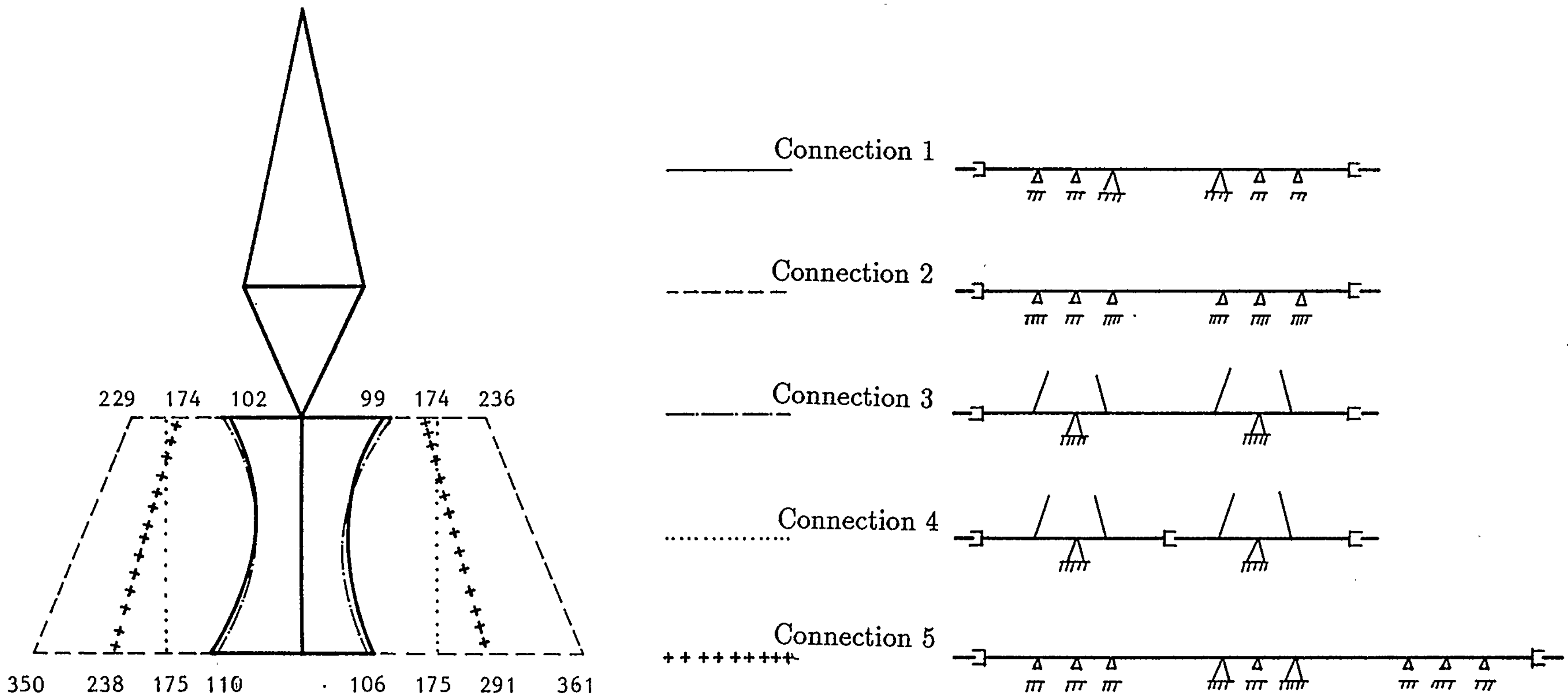

Figure 6.9: Bending moment envelopes (MN·m) in left pylon shaft due to highway live loads for different deck-pylon connections

60 percent, and the other connection types cause unacceptably high moments.

6.2.3.2 Bending moments in the pylons due to temperature

The most efficient system is Connection 4 as shown in Figure 6.10. An expansion joint at the midspan allows a free contraction (or expansion) of the deck due to temperature without being resisted by the pylons, so almost zero bending moments are created in the vertical pylon shaft due to temperature. A continuous deck and a hinge between the deck and each pylon (as in connection types 1 and 3) causes the highest bending moments (see Figure 6.10). In such a system a free contraction (or expansion) of the deck due to temperature is resisted by the pylons via the hinges.

Comparing between those two systems with regard to the maximum total moments (highway live load and temperature combined) and using a temperature load factor of 0.8 for the serviceability limit state according to the Canadian Code, the maximum total moments are listed in Table 6.1. For Connection 1 the maximum total bending moment is 213.2 MN·m. If an expansion joint is used (Connection 4), this value is reduced to 175 MN·m. This means that the expansion joint at the midspan reduces the maximum total moment in the pylon shaft by only 18 percent, although the maximum moment due to highway live loads alone was reduced by 60 percent. The total maximum moments reached in Connection 2 (only rollers) is 354 MN·m, and it is 266 MN·m for Connection 5 (hinge at every second pylon). These values are by far higher than the values of the previous systems.

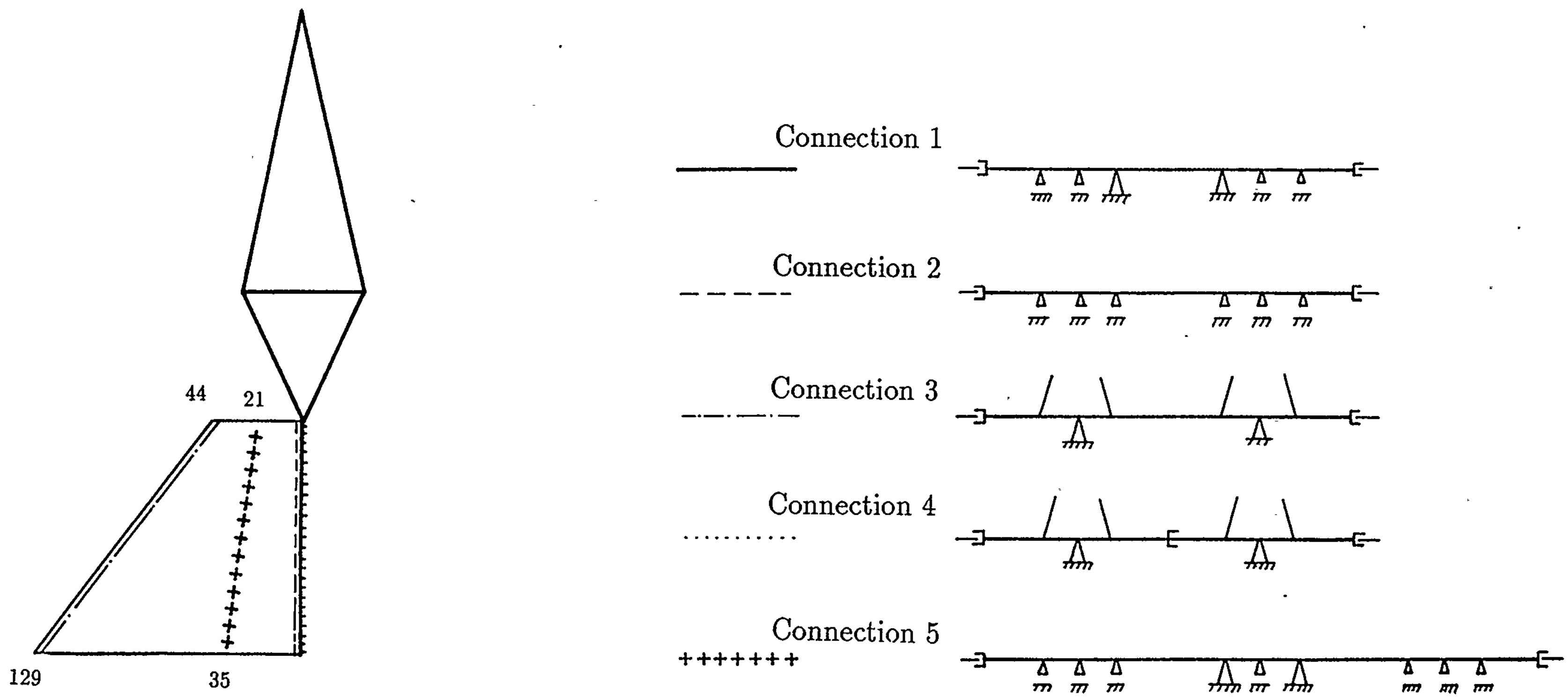

Figure 6.10: Bending moment diagrams (MN·m) in left pylon shaft due to temperature distribution number 1 for different deck-pylon connections

Table 6.1: Maximum total bending moments (MN·m) in pylon for different types of deck-pylon connections

Connection Type	L.L.	Temp.	L.L. + 0.8 Temp.
1	110	129	213.2
2	350	.5	354.0
3	110	128	212.4
4	175	0	175.0
5	238	35	266.0

6.2.3.3 Pylon normal force envelopes due to highway live loads

The maximum compression and tension force envelopes in the pylons for the different deck-pylon connections are shown in Figure 6.11. As expected, the maximum normal forces in the pylon are not significantly influenced by the type of deck-pylon connection, except for the tension forces in the vertical shaft. The values vary from 125 kN for Connection 1 to 602 kN for Connection 3. But it should be noticed that these values are negligible compared with the values of the compression force due to dead load (between 70,063 and 90,256 kN).

6.2.4 Effect of the deck-pylon connection type on the maximum cable forces

Table 6.2 contains the maximum tensile forces in selected cables for different deck-pylon connections. Except for connections allowing a horizontal movement between deck and pylon, the type of the deck-pylon connection does not significantly influence the maximum cable forces. For example, in case of Connection 2 an increase of about 17 percent in the maximum force in cable number 1 (most outside one) is caused by transferring the horizontal forces in the deck due to unbalanced live loads via the cables to the pylon, instead of transferring these forces directly to the pylon by using a hinge.

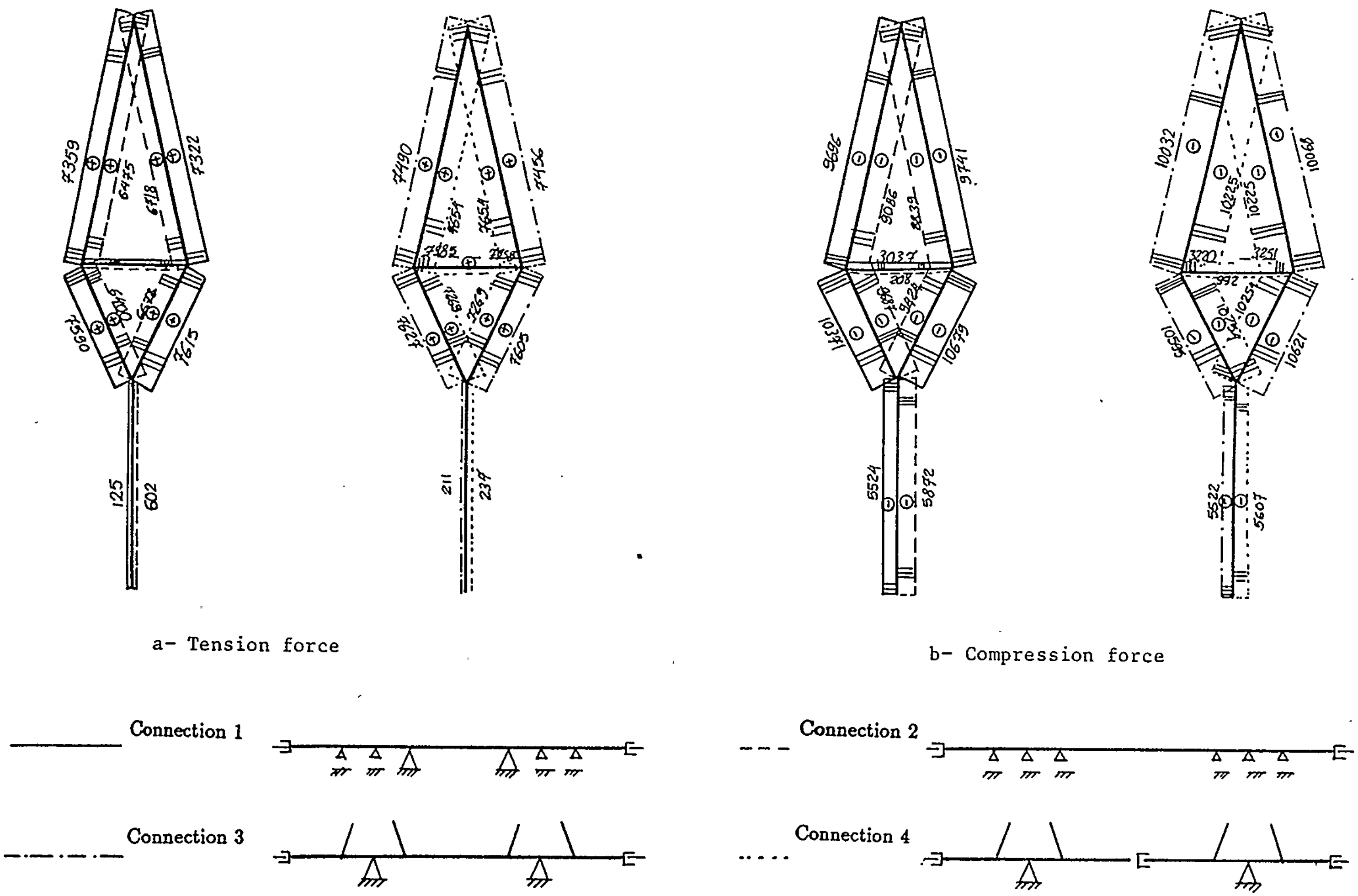

Figure 6.11: Normal force envelopes (kN) in left pylon due to highway live loads for different deck-pylon connections

Table 6.2: Max tension force (kN) in selected cables due to live load for different deck-pylon connections

Cable Number	Connection				
	1	2	3	4	5
1	313	365	313	313	365
10	128	127	147	148	127

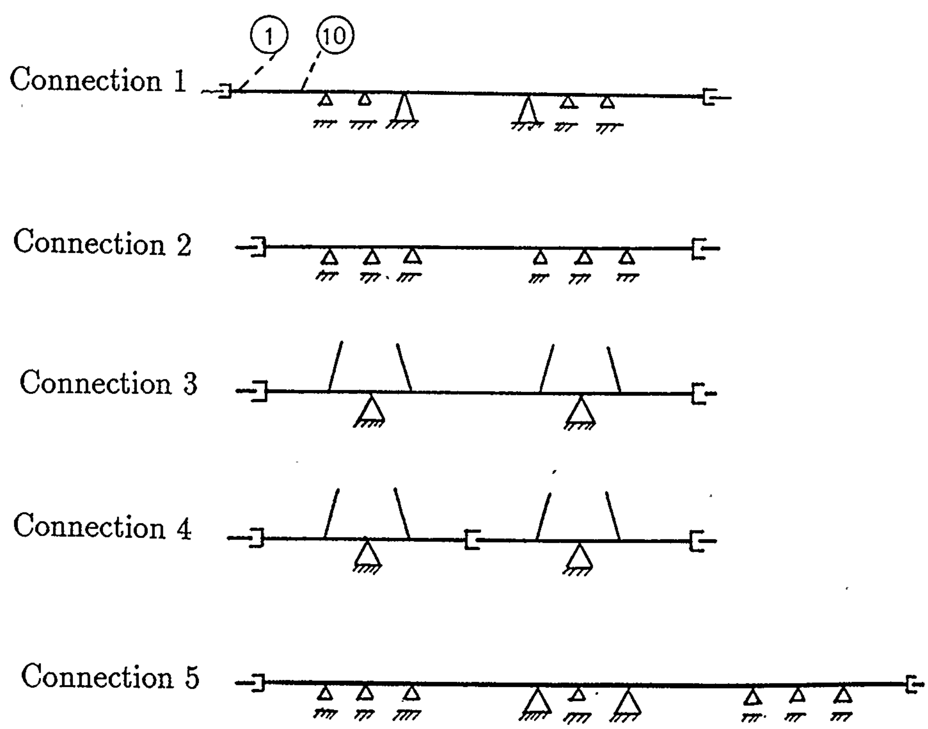

6.2.5 Summary and conclusions

The effects of different deck-pylon connection types on the behaviour of the structural components (deck, pylons and cables) of cable-stayed bridges have been discussed. The conclusion is that the most efficient deck-pylon connection type is Connection 1 with the continuous deck prevented from the horizontal movement against the pylon. Connection 3 decreases the moments in the deck at the points suspended by additional cables instead of resting directly on the pylons, but still may be not economical since the cables are the most expensive components of a cable-stayed bridge. Connection 2 (only rollers) gives unacceptable deck deflections, which are not significantly decreased by using a hinge at every second pylon as in Connection 5.

6.3 THE DIMENSIONS OF THE PYLON

6.3.1 Introduction

The longitudinal stiffness of the proposed bridge, which is required for the resistance of unbalanced live loads, is provided by the stiff pylons. The diamond shape is therefore believed to be an efficient configuration for the pylons. Using deck-pylon connection type 1 (two rollers and one hinge), the effect of three dimensions on the behaviour of the proposed bridge are examined next. These dimensions are:

1. The width of the pylon diamond (see Figure 6.12) at the level of the deck (b_t).
2. The height of the pylon above the deck (h_t).
3. The height of the inclined pylon legs below the deck (d_t).

The effects of these parameters on the maximum deck deflections and on the maximum bending moments in the pylons are investigated.

6.3.2 The width of the pylon at the level of the deck

6.3.2.1 The maximum deck deflections

Figure 6.13 shows the maximum upward and downward deck deflections as a function of the pylon width (b_t). It is obvious that an increase in the width (b_t) leads to a decrease in the maximum deck deflections. This decrease is significant until a ratio (b_t/l), where l is the span, of 0.06 is reached. At this point the curves are almost asymptotic, or in other words the maximum deck deflections are almost constant despite the increase in the pylon width (b_t). Trying to understand this behaviour the following concept may be useful.

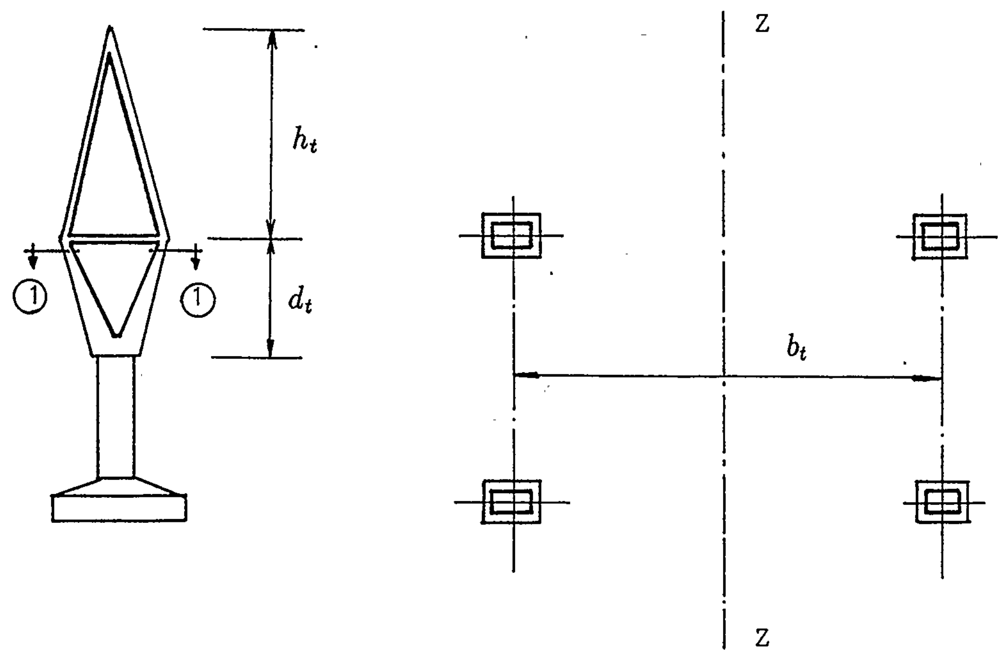

Section 1 - 1

Figure 6.12: Cross-section in the pylon at the level of the deck

By increasing the width (b_t), two factors influencing the deck deflections are affected. The first factor leads to a decrease in the deck deflections, while the second factor leads to an increase in the these deflections. The first factor is dominant until a ratio (b_t/l) of about 0.06. After that, both factors are balancing each other, resulting in an almost constant value of the maximum deck deflections.

The first factor is that increasing the width (b_t) is increasing the moment of inertia of the pylon cross-section at the deck level about the axis $z - z$ (see Figure 6.12). This rapid increase in the moment of inertia increases the pylon stiffness leading to a decrease in the deck deflections.

At the same time the increase of the pylon width (b_t) increases the inclination to the vertical of the lower legs of the pylon, decreasing their resistance to vertical loads and increasing the bending moments in those legs, causing an increase in the deck deflections. This may be the second factor affected by changing the parameter (b_t).

6.3.2.2 The maximum bending moments in the pylon shaft

As shown in Figure 6.14, the maximum bending moments in the pylon shaft are not caused by the same case of loading for all (b_t/l) values. For example, the maximum positive bending moment envelope for the top point of the pylon shaft (point 3 in Figure 6.14) is formed by load cases 24 and 30.

For (b_t/l) values less than 0.015 load case 24 is the critical case, whereas for values greater than 0.015 load case 30 causes the maximum positive bending moments. This means that the smallest maximum positive bending moment at the top point of the vertical pylon shaft is obtained at a (b_t/l) ratio of about 0.015, this ratio is about 0.027 for the smallest maximum positive and negative bending moments at the bottom point of the pylon shaft (point 4 in Figure 6.14).

At this point it should be mentioned, that decreasing the pylon width reduces the stiffness of the pylon significantly, and so the deflections are increased. The importance of a geometric nonlinear analysis which includes the effect of large deflections, becomes obvious if Figure 6.15 and Figure 6.16 are studied. This figure illustrates the bending moment at the fixation of the pylon (point 4) due to load case 24 for different b_t values. A linear analysis is compared with a geometric nonlinear analysis. The curves start to deviate significantly for a pylon width less than 4 m which corresponds to a (b_t/l) value of 0.016.

This difference is mainly due to the effect of large deflections, not due to the $(P - \delta)$ effect. Since excluding the $(P - \delta)$ effect from the analysis, did not change the results of the geometric nonlinear analysis.

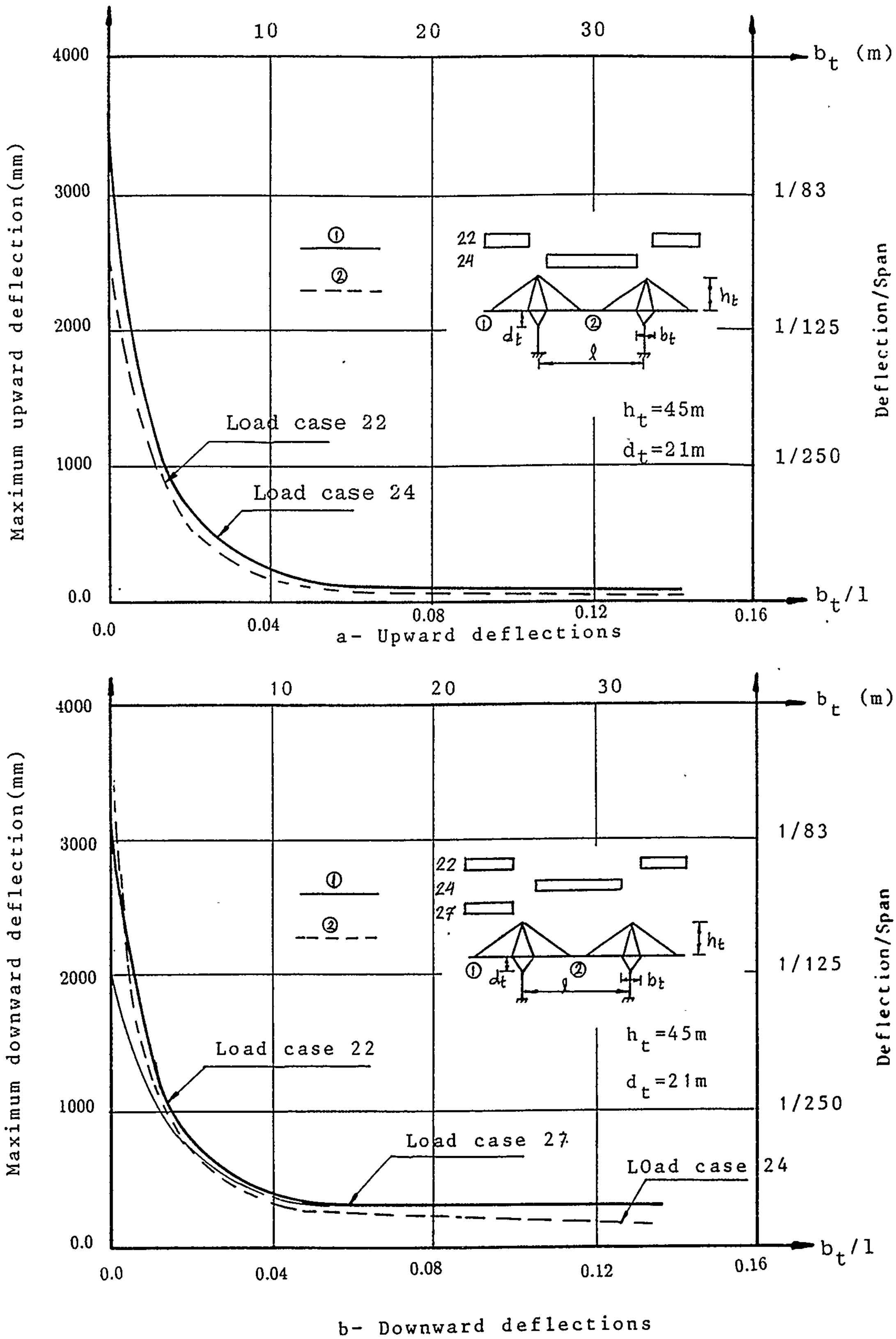

Figure 6.13: Effect of the pylon width (b_t) on the maximum deck deflections

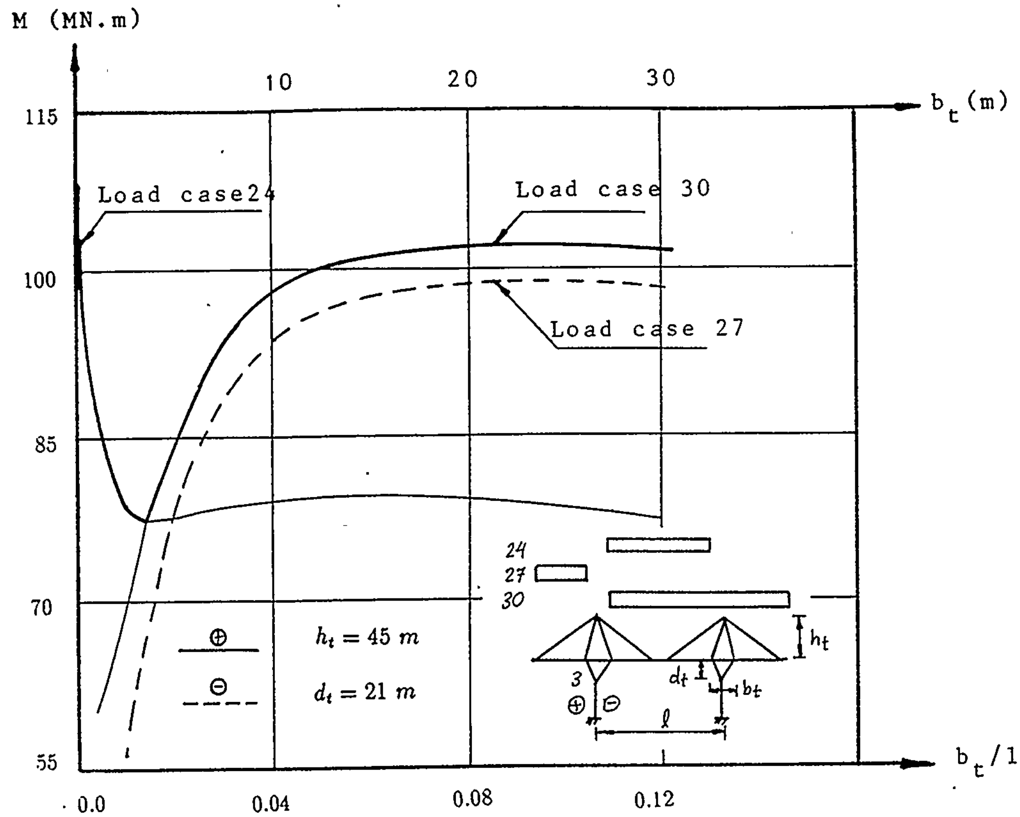

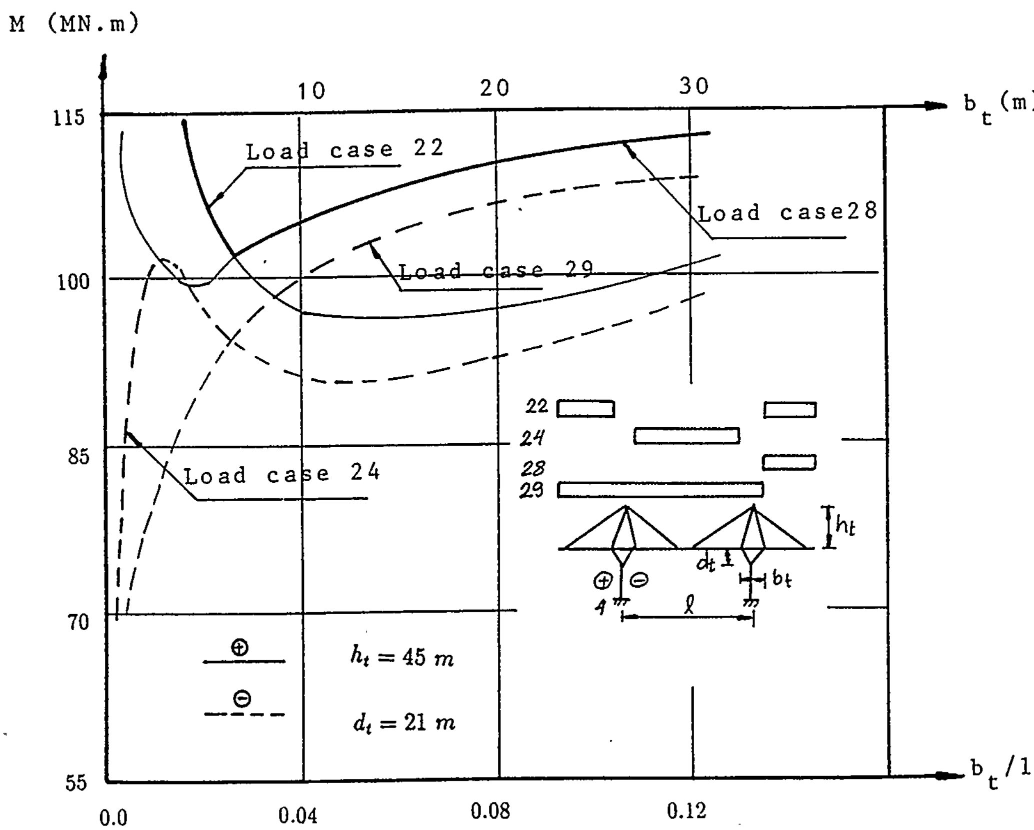

Figure 6.14: Effect of the pylon width (b_t) on the maximum bending moments in the pylon shaft (3: upper point, 4: lower point)

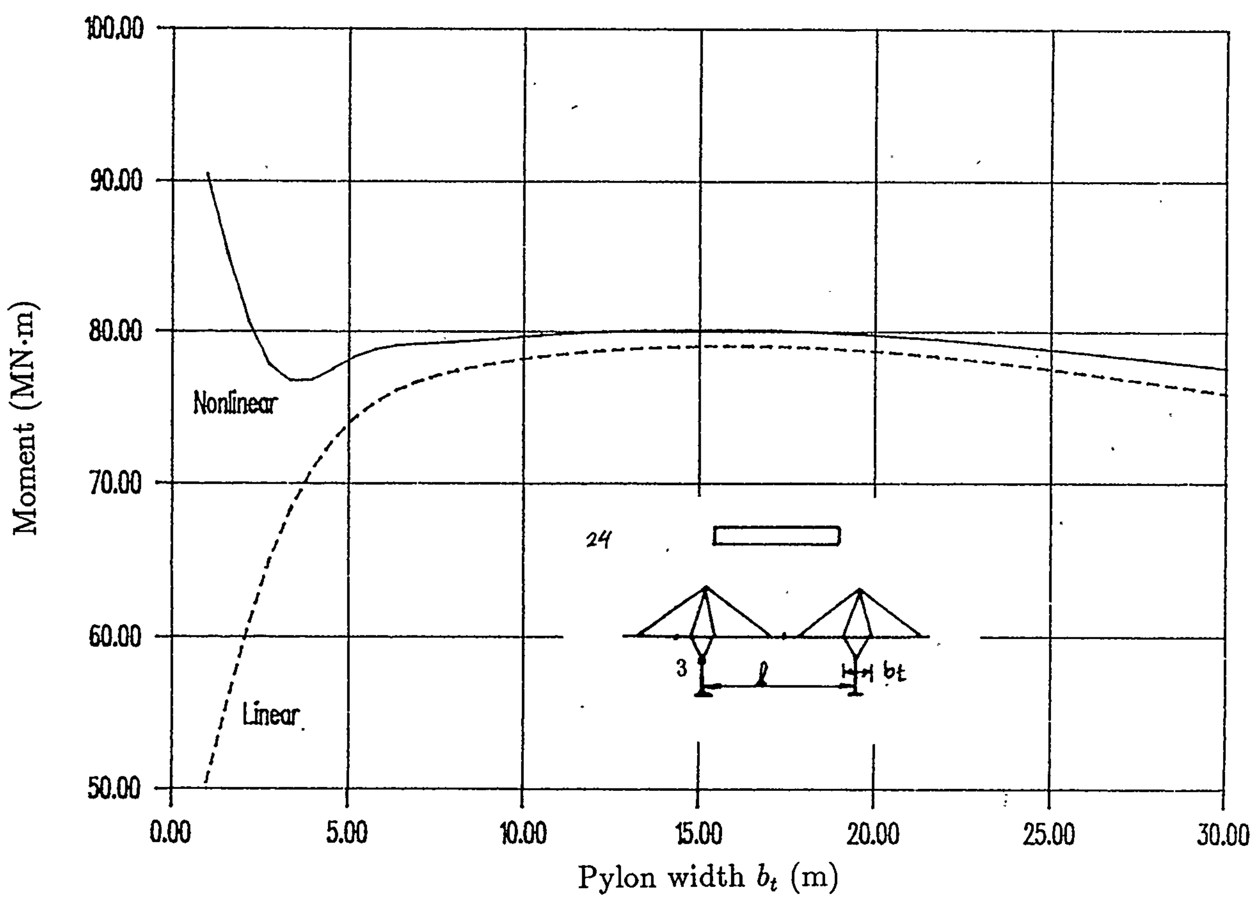

Figure 6.15: Effect of the geometric nonlinearities on the bending moment at the upper point of the pylon shaft (point 3)

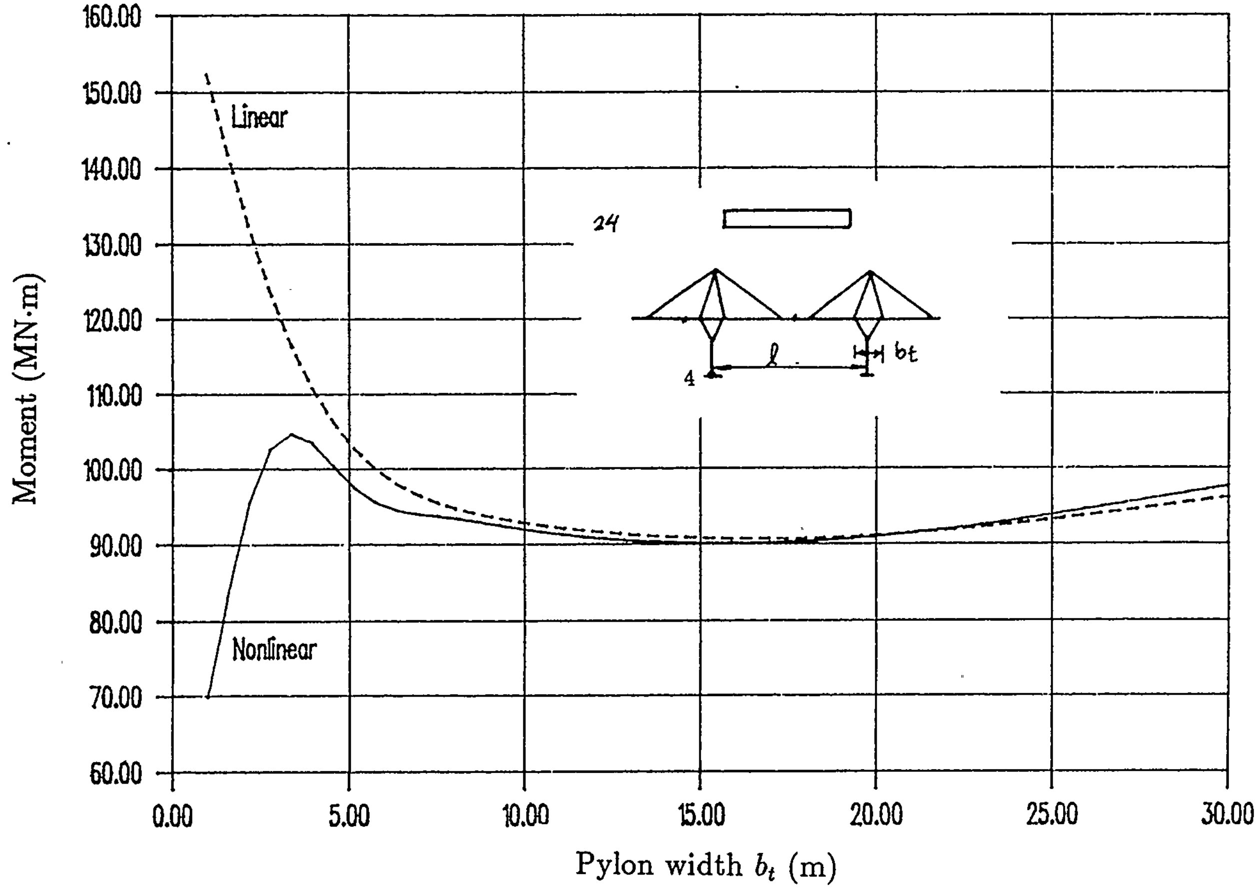

Figure 6.16: Effect of the geometric nonlinearities on the bending moment at the fixation of the pylon shaft (point 4)

6.3.3 The height of the pylon above the deck

6.3.3.1 The maximum deck deflections

Figure 6.17 shows the maximum upward and downward deck deflections as a function of the height of the pylon above the deck (h_t). An increase in (h_t) decreases the maximum downward deflections of the deck. This is because an increase in (h_t) leads to an increase in the cable inclination to the horizontal (θ), causing an increase in the equivalent elastic support spring constant (k) of the cables, which was given by Equation 5.7 in Chapter 5 as $k = EA/L \cdot \sin^2 \theta$.

A feasible range for the ratio (h_t/l) is between 0.18 and 0.24 (see Figure 6.17). It should be noted that for values greater than 0.16 for the ratio (h_t/l) a slight increase in the maximum upward deck deflection is obtained.

6.3.3.2 The maximum bending moments in the pylon shaft

As shown in Figure 6.18, an increase in the pylon height above the deck level decreases the maximum bending moments in the pylon. However, it may be not economical to increase the pylon height, because increasing the pylon height (h_t) say by 50 percent from 40 to 60 m, decreases the maximum positive bending moments at the top of the pylon shaft from 106 MN·m to only 94.5 MN·m i.e. by 12 percent.

As in the case of the deck deflections, a feasible range for the ratio (h_t/l) lies between 0.18 and 0.24.

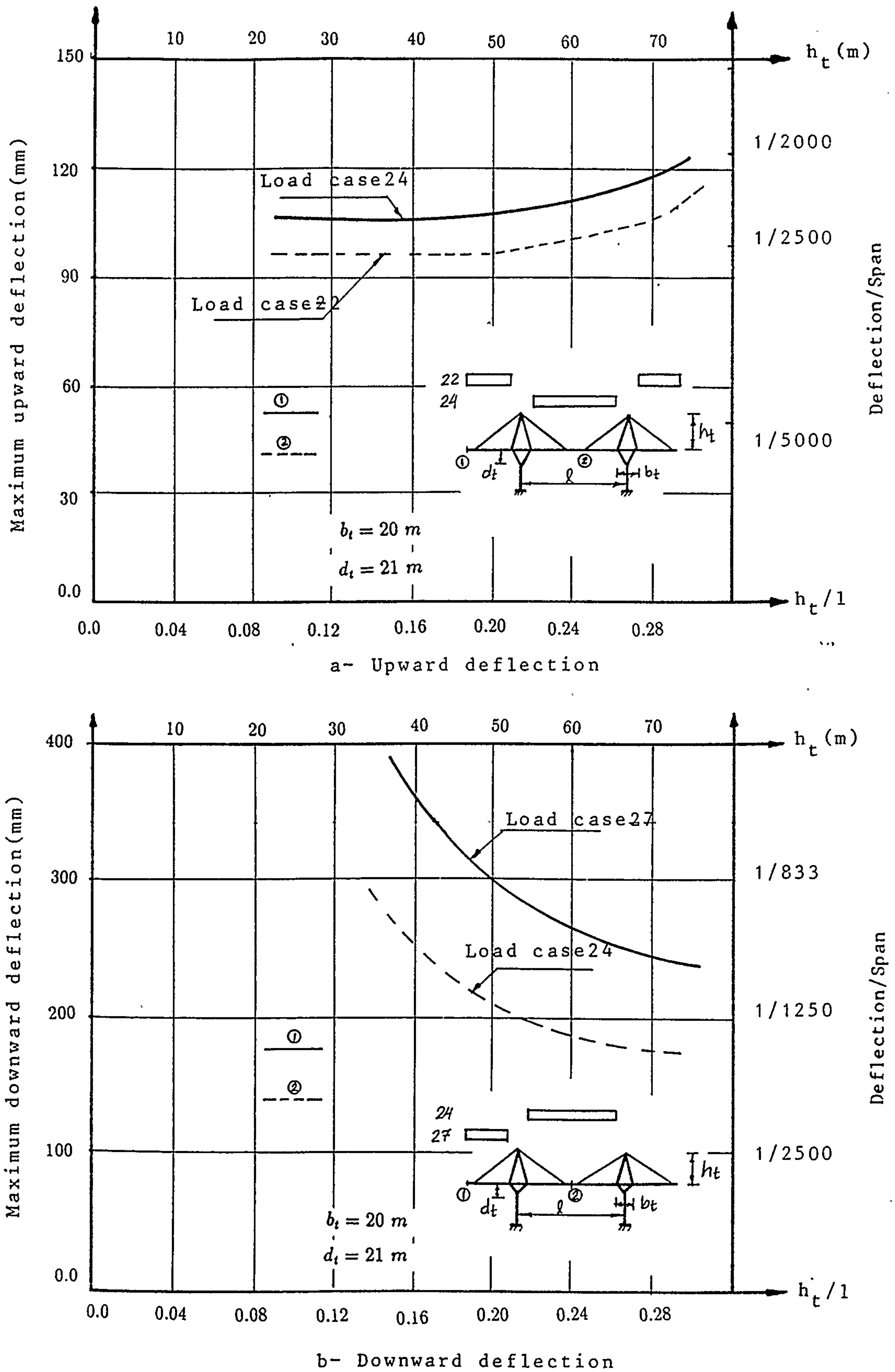

Figure 6.17: Effect of the pylon height (h_t) on the maximum deck deflections

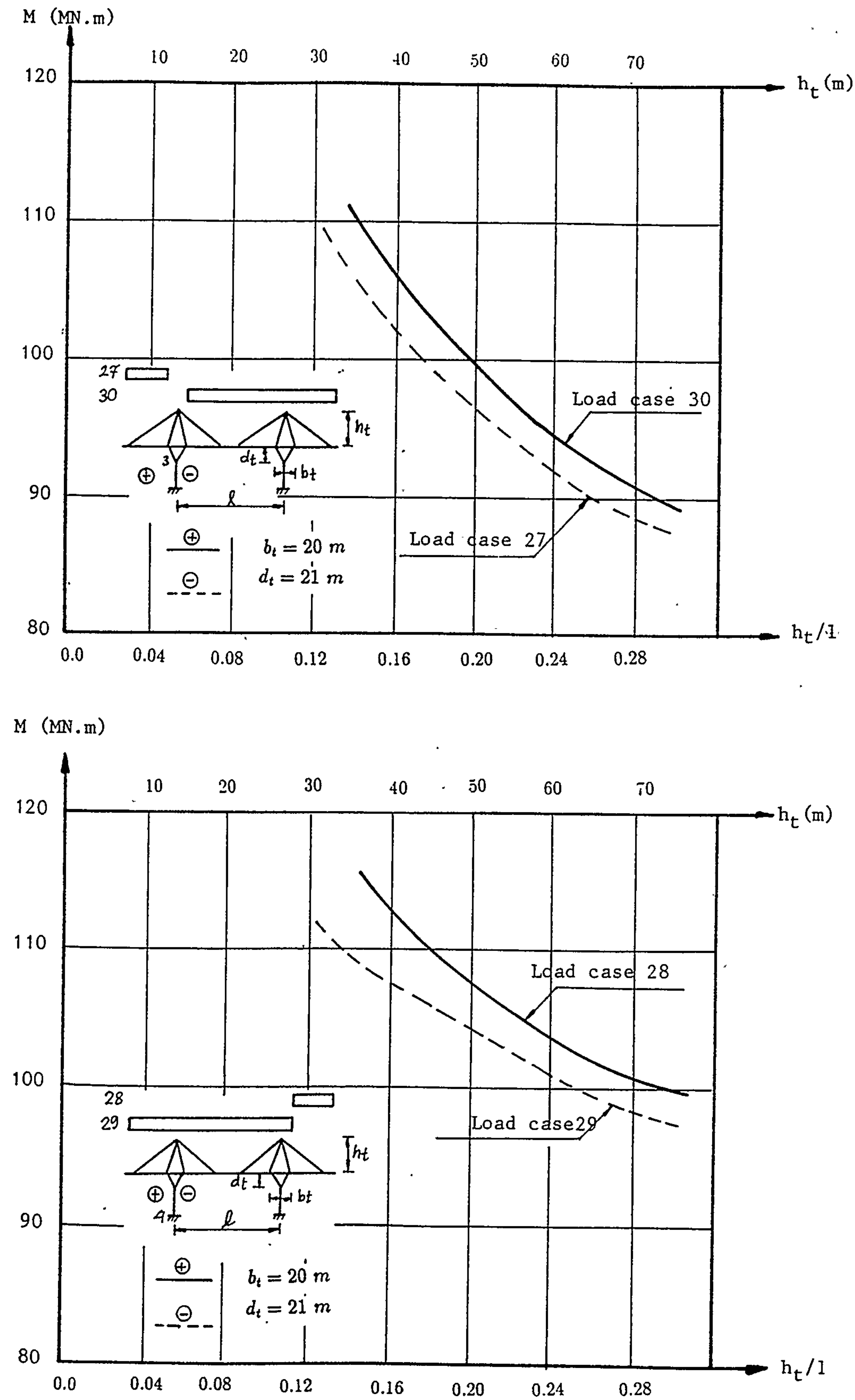

Figure 6.18: Effect of the pylon height (h_t) on the maximum bending moments in the pylon shaft (3: upper point, 4: lower point)

6.3.4 The height of the inclined pylon legs below the deck

6.3.4.1 The maximum deck deflections

Figure 6.19 illustrates the effect of the height of the pylon legs below the deck (d_t) on the maximum upward and downward deck deflections. The figure shows that the trend is a decrease in the deck deflections if (d_t) is increased. The upward deflections are much more affected than the downward deflections.

A feasible range of the ratio (d_t/l) is between 0.06 and 0.10. At this point it should be mentioned that for construction purposes, the depth (d_t) is restricted for the proposed bridge to 21 m (d_t/l=0.08) to accommodate the truss used in the construction of the deck. This will be described later in Chapter 7 discussing the construction method.

6.3.4.2 The maximum bending moments in the pylon shaft

As illustrated in Figure 6.20, an increase in the height of the lower pylon legs (d_t) leads to continuous decrease in the moments at the top of the vertical pylon shaft. This result may however not be taken without care, since by increasing (d_t) the position of the top point of the pylon shaft is changing (total pylon height is constant), so that a comparison of moments is not totally justified.

For the bottom point of the vertical pylon shaft the maximum moment is increasing slightly reaching a maximum at a (d_t/l) ratio of 0.09, and starts to decrease after this value. But in general, for the bottom point of the pylon shaft, the maximum moments are not significantly affected by the parameter (d_t).

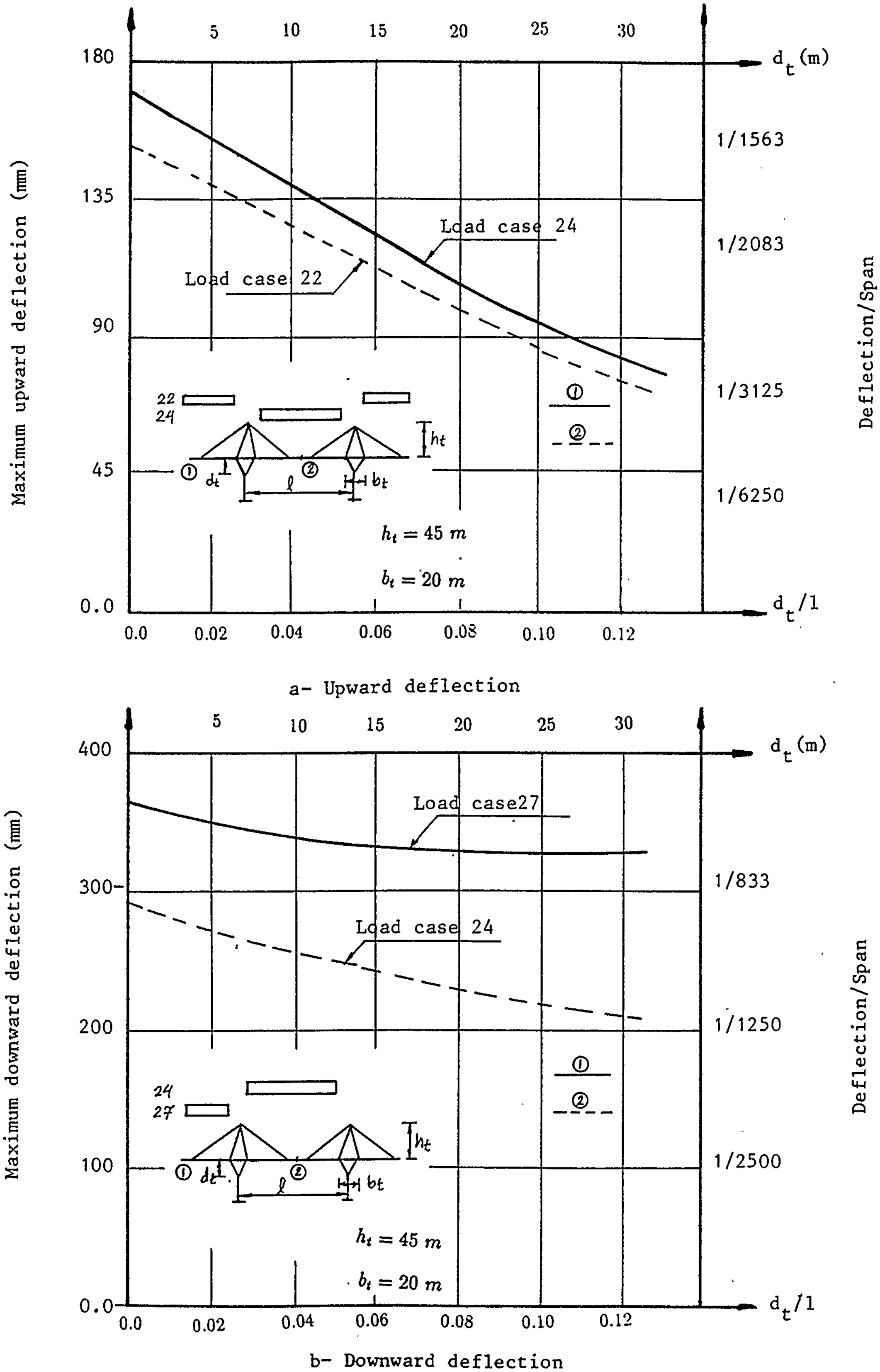

Figure 6.19: Effect of the height of the inclined lower pylon legs (d_t) on the maximum deck deflections

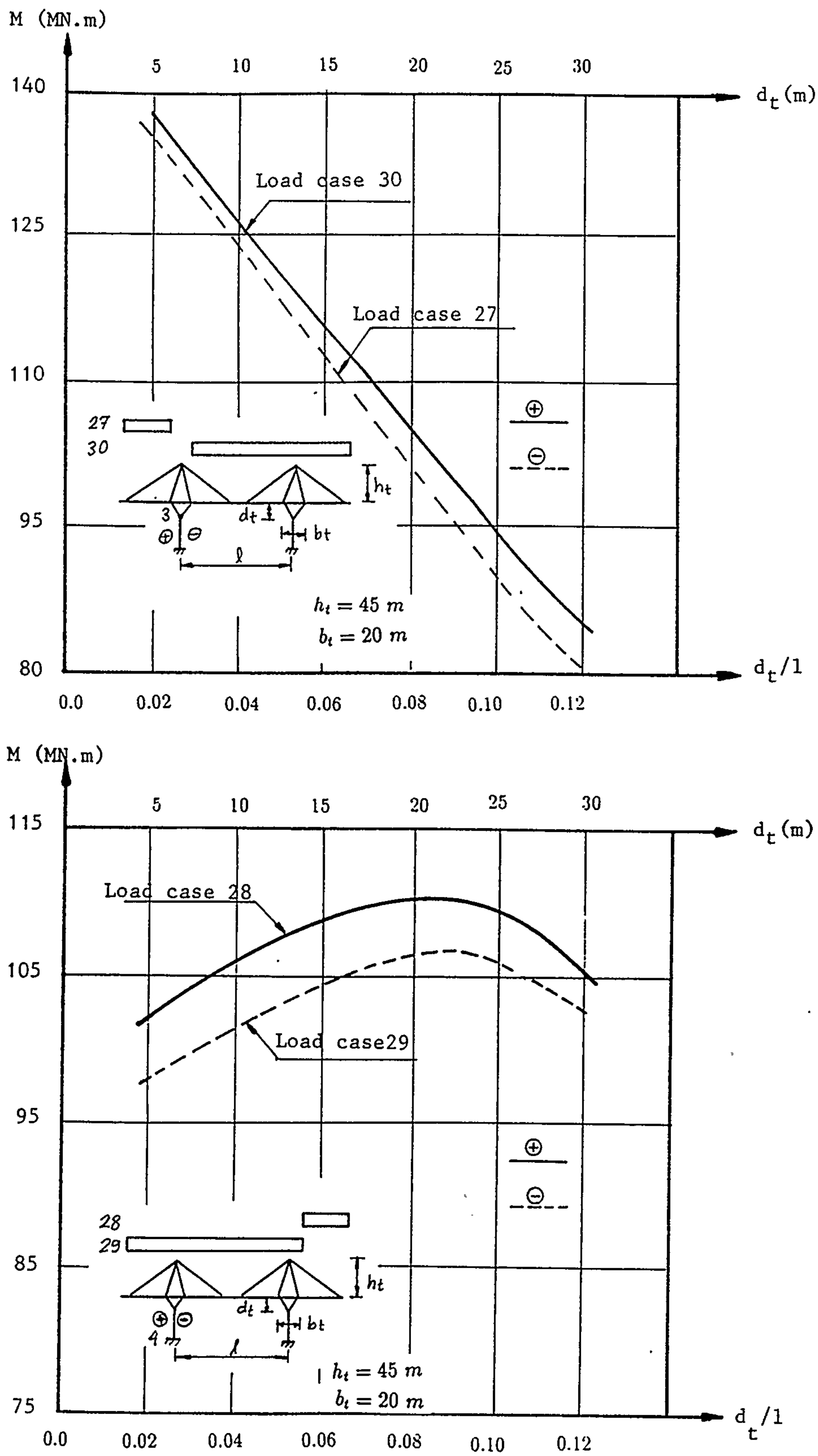

Figure 6.20: Effect of the height of the inclined lower pylon legs (d_t) on the maximum bending moments in the pylon shaft (3: upper point, 4: lower point)

6.3.5 Summary and conclusions

The effects of the pylon dimensions on the maximum deck deflections and maximum bending moments in the pylon shaft have been discussed. Based on the results the following pylon dimensions are recommended for a diamond-shaped pylon:

- Pylon width

  (b_t/l) should lie between 0.06 and 0.08 to decrease the maximum deck deflections (actually 0.08 for the proposed bridge).

- Height of pylon above the deck

  (h_t/l) should lie between 0.18 and 0.24 for reasonable deck deflections and bending moments in the pylon shaft (actually 0.18 for the proposed bridge).

- Height of inclined lower legs of the pylon

  (d_t/l) should be greater than 0.09 to decrease the maximum deck deflections and bending moments in the pylon shaft (actually restricted to 0.084 for the proposed bridge for construction purposes).

It is recommended to use a large deflection analysis in investigating the pylon moments for flexible pylons with a (b_t/l) value of less than 0.016.

6.4 THE DIMENSIONS OF THE CABLES

Since the deck of a cable-stayed bridge can be idealized as a beam supported on springs with a spring coefficient (k) given in Equation 5.7 as $k = EA/L \cdot \sin^2\theta$, an increase in the cable area (A) would increase the stiffness of the spring linearly. High spring stiffnesses simulate a firm soil condition, if the system is compared with the beam-on-elastic foundation model, leading to a decrease in the positive bending moments of the beam-on-elastic foundation or in other words of the deck.

To examine the effectiveness of increasing the cable areas in reducing the maximum bending moments in the deck, the cable areas are increased by up to 80 percent of the values originally required. The results are shown in Figure 6.21. Increasing the cable areas by 80 percent, the maximum positive bending moment in the deck is decreased by only 12 percent from 2432 KN·m to 2164 KN·m. Since the cables are the most expensive structural elements in a cable-stayed bridge, it is certainly not economical to reduce the bending moments in the deck by increasing the cable areas.

6.5 SUMMARY

In this chapter a parametric study is carried out to study the effects of the deck-pylon connection type, the pylon dimensions and the cable areas on the behaviour of multispan cable-stayed bridges. An efficient deck-pylon connection and optimum dimensions for diamond-shaped pylons are recommended as a conclusion of this parametric study.

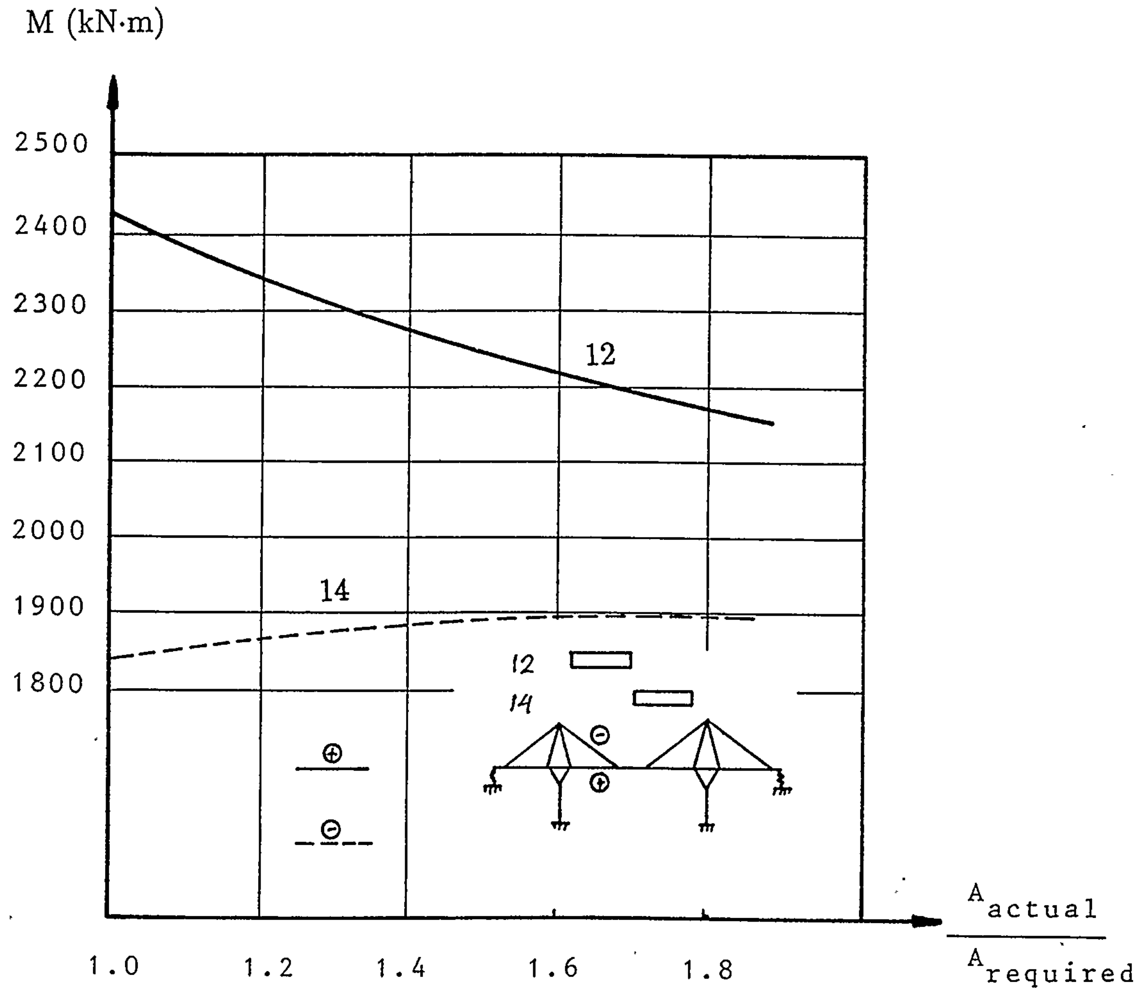

Figure 6.21: Effect of the cable areas on the maximum bending moments in the deck

Chapter 7

THE CONSTRUCTION OF THE BRIDGE

7.1 INTRODUCTION

In this chapter the construction of cable-stayed bridges is discussed. The chapter is divided into four parts. The first part contains a review of the major construction methods for cable-stayed bridges. In the second part a new, economical method suitable for multi-span cable-stayed bridges is described. In the third part of this chapter, the computer model simulating the proposed construction method is introduced. And part four contains the results and conclusions obtained from the used computer model.

7.2 CONSTRUCTION OF CABLE-STAYED BRIDGES

7.2.1 Introduction

Since the method of construction of a bridge is the decisive factor for the success of a contractor's bid, many different methods have been developed over the years to build cable-stayed bridges. Because of high fabrication and erection costs, present trends are to fabricate components as large as possible for simplified construction.

The erection method not only affects the stresses in the structure during construction, but may also have an effect on the final stresses of the completed structure, which is an important factor in chosing which method is to be used.

Other important factors affecting the construction method are (Dilger, 1990):

- Bridge geometry
  - total length
  - span lengths
  - pier height
- Site conditions
  - level terrain
  - sloped or rugged terrain
  - waterway
- Traffic during construction
- Distance from precasting plant
- Availability and cost of formwork system

The methods of erection for cable-stayed bridges are broadly described by three general methods (Podolny, 1986), the staging method, the incremental launching method and the cantilever method. These methods are described next.

7.2.2 The staging method

In this method the entire suspended structure (deck) is erected on temporary piers, followed by the pylon erection and cable connections. Finally, the pylon saddles are jacked to stress the cables to the desired tensile load to obtain the required profile and the temporary piers are removed (see Figure 7.1).

If precast units are used for the suspended deck, these units may reach a length of 105 m, which is the case of the Great Belt Bridge proposal in Denmark. Such heavy units are floated in on barges and lowered into position hydraulically or by submerging the barges. Small precast units are erected by a launching gantry as shown in Figure 7.2.

If cast-in-place concrete is used for the suspended deck, medium spans (35 to 60 m) can be constructed economically with travelling forms which are either supported from below or from above the bridge. An example for supporting the forms from below the bridge superstructure is the so-called sliderule system shown in Figure 7.3. The trussed system shown in Figure 7.4 represents the way of supporting the forms from above the bridge.

The staging method of erection is most often used where there is a low clearance requirement to the underside of the structure and temporary piers will not interfere with any traffic below the bridge. Its advantage is its accuracy in maintaining the required geometry and grade, and its relatively low cost for low clearance. The major disadvantage if long, continuous bridges are to be built with this method, is the numerous temporary piers and their foundations which have to be built.

7.2.3 The incremental launching method

The bridge is constructed behind the abutment in a stationary form in segments which are 10 to 30 m long. The segment under construction is cast against the previously cast segment and connected to it by overlapping longitudinal bars. In case of a steel superstructure the segments are connected by welding or bolts. The

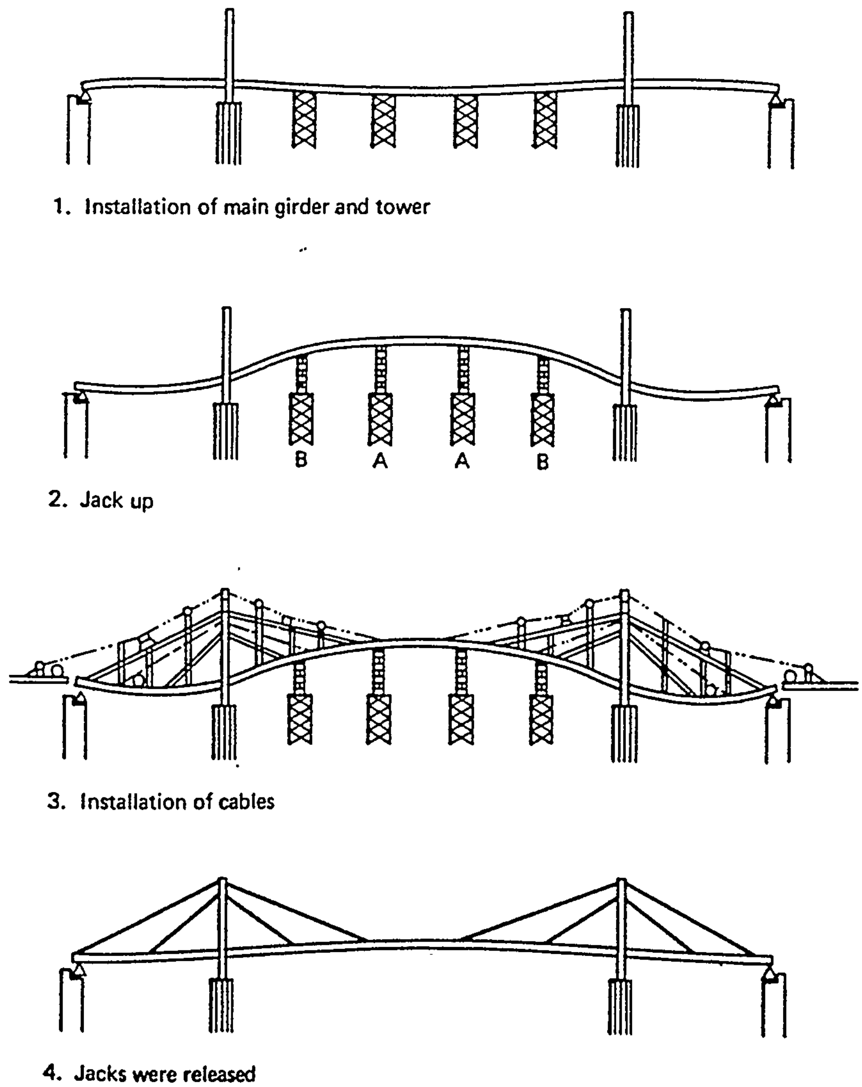

Figure 7.1: Construction procedure using the staging method (Adapted from Kondo et al, 1972)

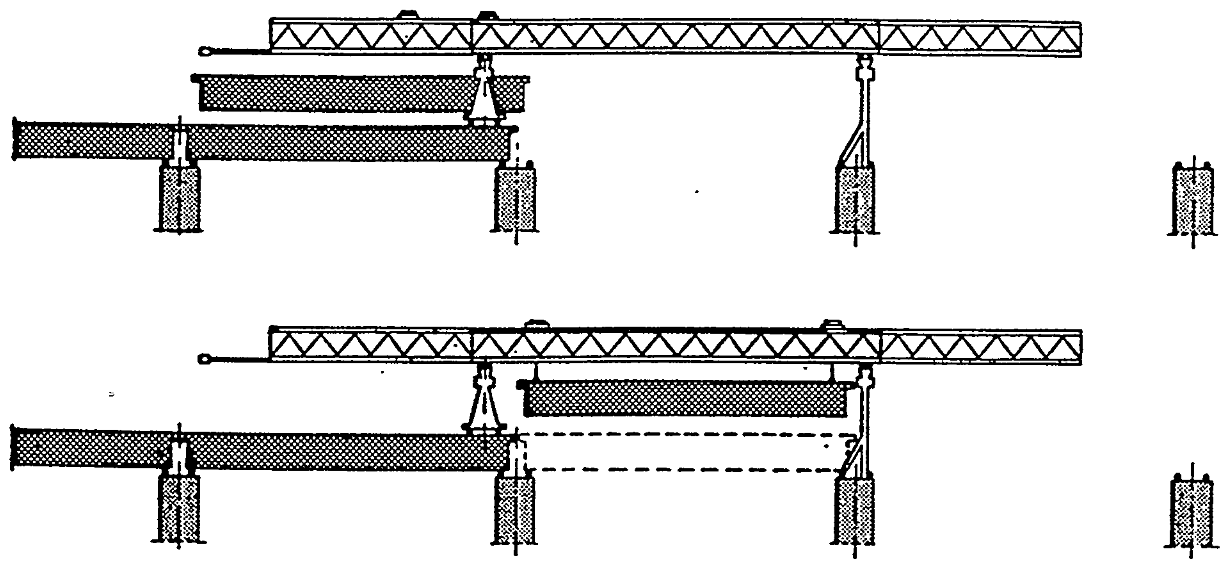

Figure 7.2: Precast units erected by a launching gantry (Dilger, 1990)

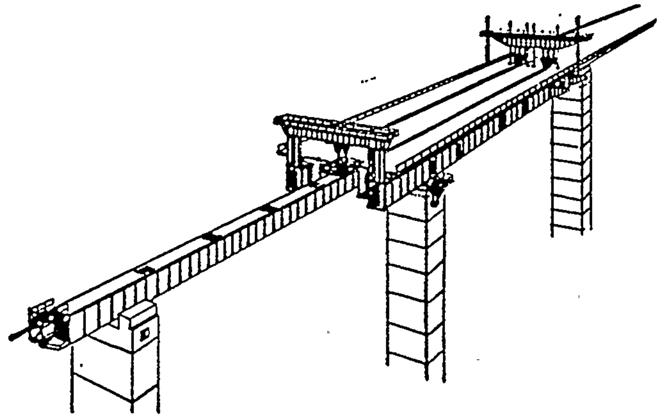

a- Casting position - Span completed

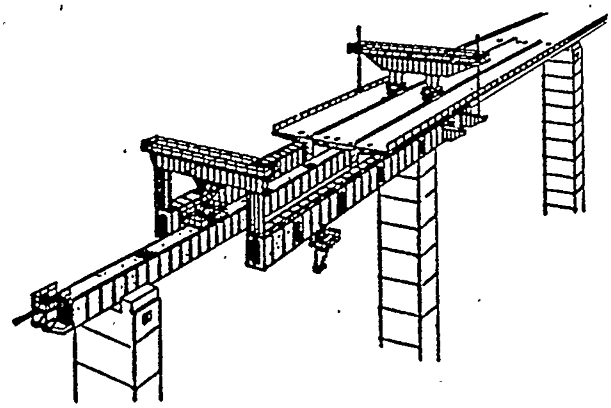

b- Launching of main girders

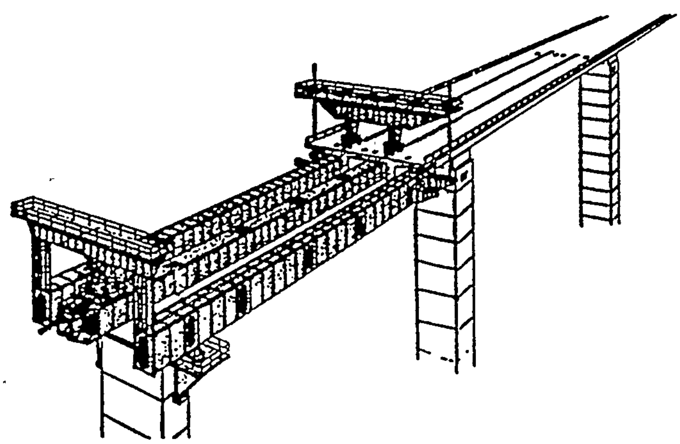

c- Main girders in casting position

Figure 7.3: The sliderule system as an example of supporting the forms from below the superstructure

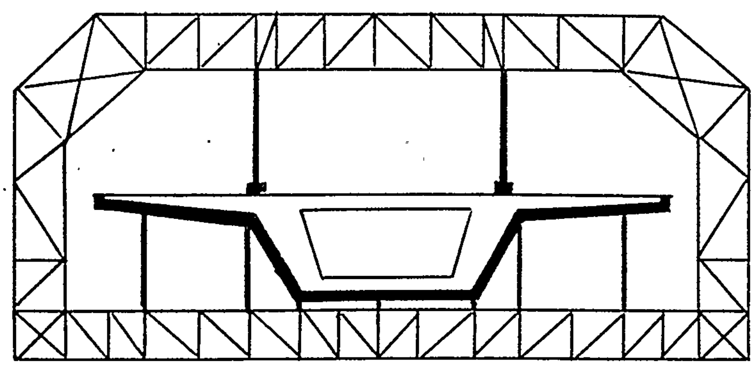

Figure 7.4: Supporting the construction forms from above the bridge

segment is then launched by means of hydraulic jacks together with the already completed portion over the piers on rollers or sliding teflon bearings. A steel nose as shown in Figure 7.5 is used to decrease the cantilever length during launching, but for large spans temporary supports are necessary. Launching may be from one side as shown in Figure 7.6, or from both ends of the bridge.

In order for this method to be applicable, the bridge axis must lie in one plane and if the axis is curved in plan, the curvature must be constant. To overcome this restraint in case of a curved box girder bridge, the box part of the deck may be launched using a constant curvature for its axis, while the deck slab may be cast later following the road alignment.

Spans of up to 140 m and bridges with a total length up to 1200 m (Podolny, 1986) have been built by the incremental launching method. The major advantage of this method is that it combines the advantages of prefabrication, with those of cast-in-situ concrete. The main advantages of prefabrication are:

- The concrete is cast in a protected (ideal) environment
- Good dimensional control during casting
- Repetitive work cycles
- Short transportation distances of the construction materials
- No interference with the traffic below the bridge
- No costly falsework required

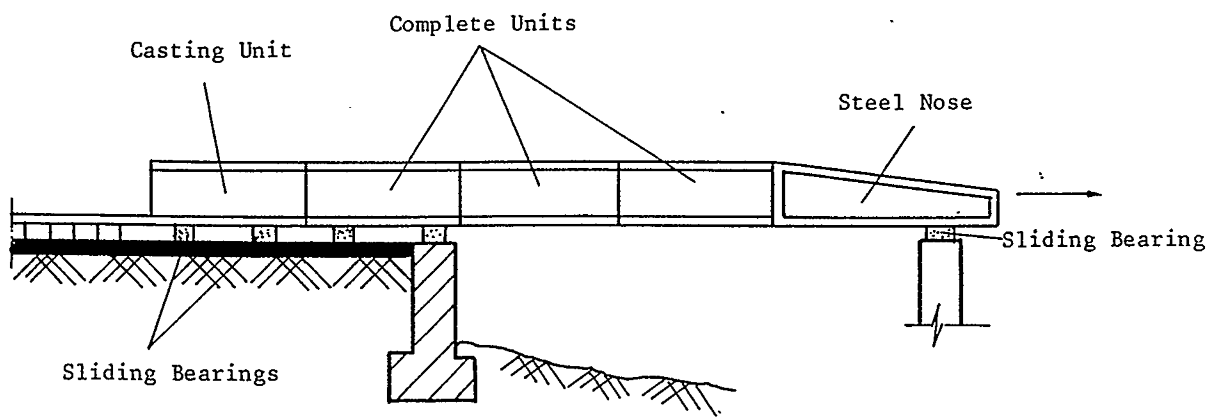

Figure 7.5: Using a steel nose in the incremental launching method

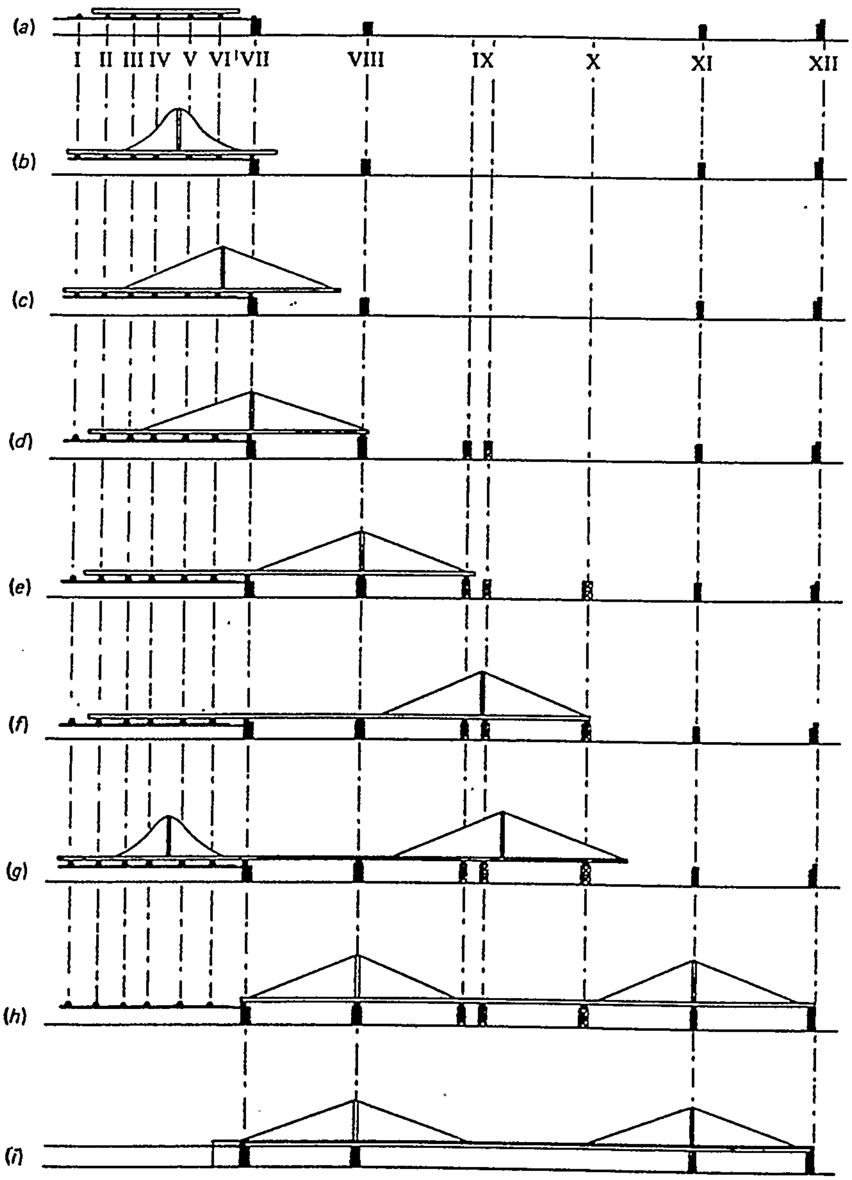

Figure 7.6: The incremental launching method (Adapted from Beyer, 1964)

Where the main advantages of cast-in-place concrete are:

- Monolithic structure without weak joints
- No heavy lifting of the segments is required

7.2.4 The cantilever method

In this construction method, relatively short segments of a cantilever are constructed either at one end or simultaneously at both ends of a balanced cantilever. The forms are supported by an erection crane as shown in Figure 7.7. If the bridge is constructed across a waterway, the erection crane may be supported on a flotation barge. A typical construction sequence of this method is illustrated in Figure 7.8.

The major disadvantage of this method is the slow progress of the construction, namely at about 3 m per week at each end of the cantilever. The construction process can be accelerated if an overhead truss or plate girder is used in supporting the form travellers as shown in Figure 7.9.

7.3 THE PROPOSED CONSTRUCTION METHOD

7.3.1 General description of the construction method

The total length of the proposed bridge is approximately 13 km, with 250 m long spans this means that more than 40 identical spans are required. Due to harsh weather conditions, the construction season is relatively short in the region. So conventional construction methods as previously described are not suitable for such a project. They would take excessively long time to construct such a long bridge (the

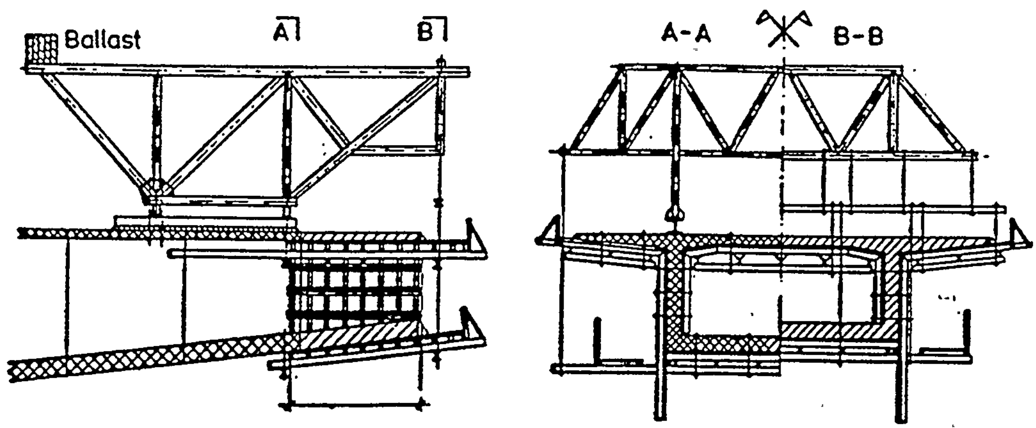

Figure 7.7: Erection crane supporting the forms in the cantilever method (Dilger, 1990)

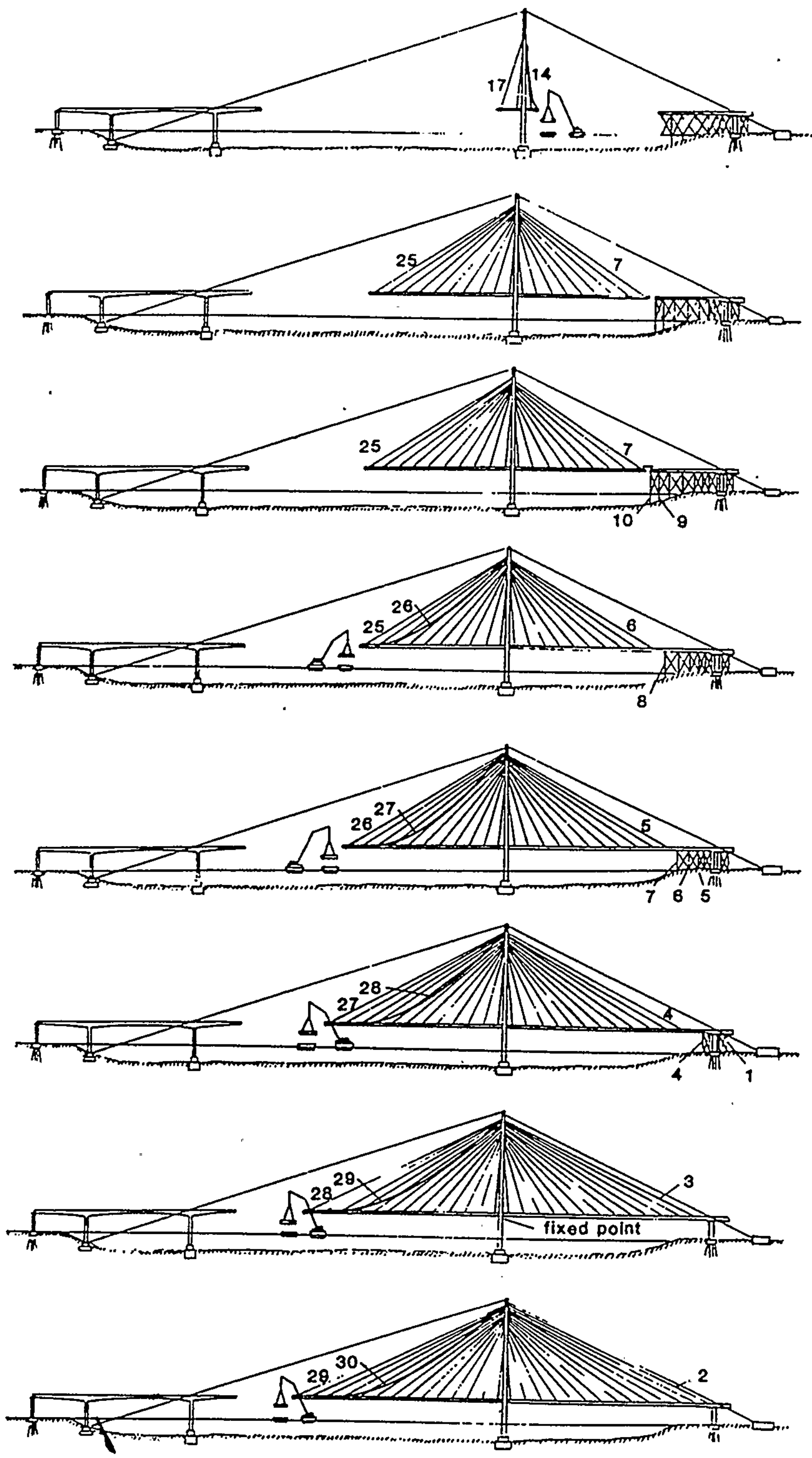

Figure 7.8: Construction procedure of a bridge crossing a waterway using the cantilever method (Adapted from Podolny, 1986)

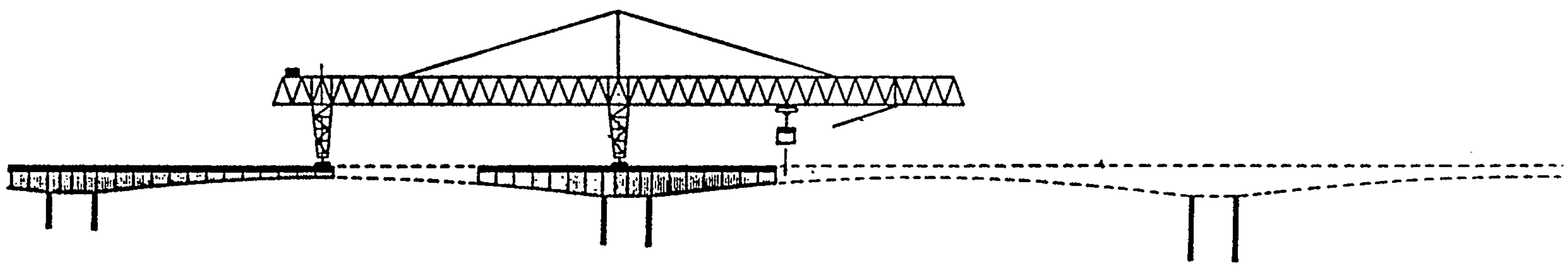

Figure 7.9: Overhead truss used in supporting the form travellers (Dilger, 1990)

cantilever method), or require advanced complicated technology (the incremental launching method).

As a result new techniques had to be developed. The method proposed by Dilger et al (1990 and 1991) is a cast-in-place concrete deck on a steel truss extending over two spans (see Figure 7.10). The truss fits between the space provided below the bridge deck and is launched by means of hydraulic jacks. To support the free ends of the cantilevers during launching, flotation tanks are lowered from the inside of the truss and submerged in the water to produce a constant uplift force of about 2.5 MN. This is approximately the reaction of the truss during launching. The method is considered relatively economical because of the many repetitive cycles. The completing of one cycle, which consists of a 250 m long deck, is estimated at 5 weeks only.

7.3.2 Detailed description of the construction method

Consider stage 1 of Figure 7.10 and assume that the 250 m long span over pier 2 has been completed on the truss. The following steps describe a typical construction cycle:

1. The truss is lowered by about one meter and the flotation tanks are submerged. Each of these tanks produces an uplift force of about 2.5 MN, which represents approximately the end reaction of the truss during launching. This step is shown in Figure 7.10, stage 1.

2. The truss is launched by means of hydraulic jacks (Figure 7.10, stage 2), followed by the withdrawal of the flotation tanks and some additional launching

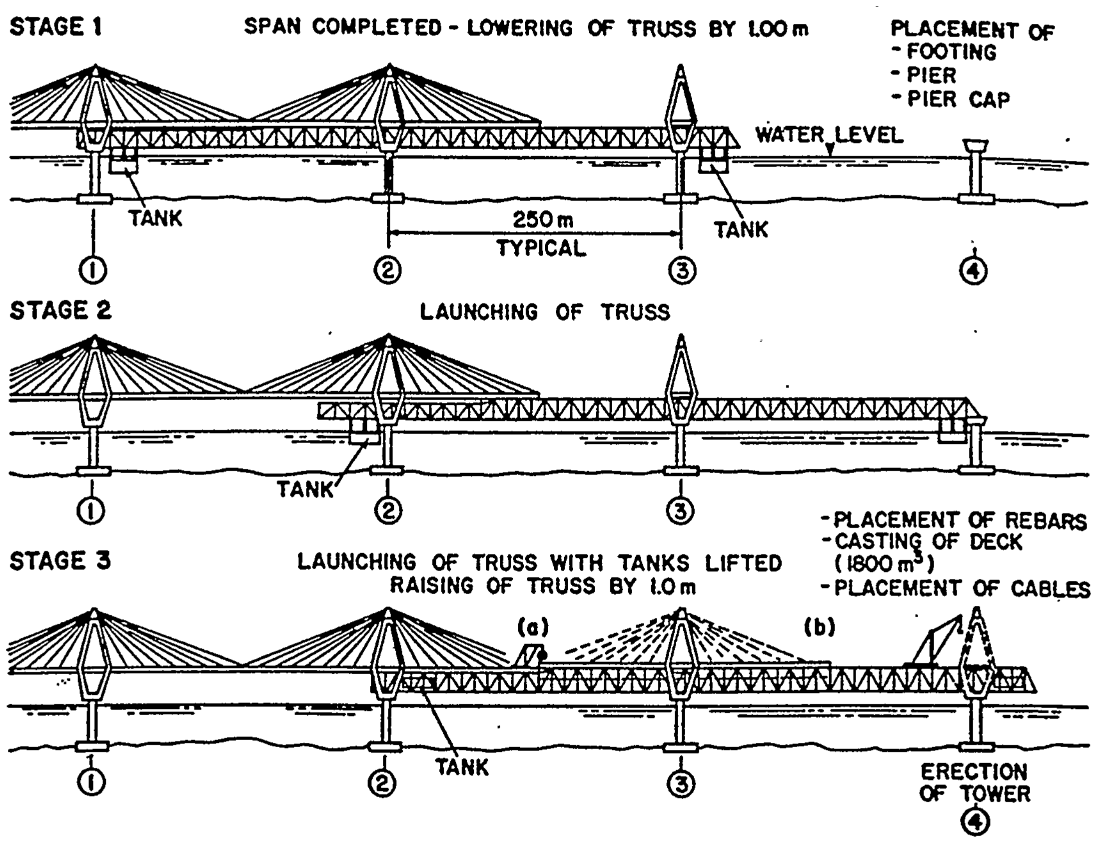

Figure 7.10: Construction stages of the proposed method

to reach a position from which the tanks can be lowered into the water again after the construction of the span is completed (Figure 7.10, stage 3).

3. The truss is lifted till the deck form is 300 to 500 mm above the final position of the deck soffit. When designing the truss, a comparison will be made between lifting it 300 or 500 mm. Note the one meter step in the top chord of the truss at point (a) to accommodate the already finished span.

4. In this elevated deck position, the stay-cables are installed by temporarily anchoring them to the top chord of the truss. The cables near the pylon will be slacked at this time because of the elevated deck position.

5. After placing the rebars and prestressing tendons, the concrete deck ($1800m^3$) is poured in one continuous pour.

6. After the concrete has reached sufficient strength, the temporary anchors are released, thus transferring the cable forces to the concrete deck.

7. The truss is lowered until the deck is freely suspended from the cables. At this stage, all cables have reached their desired forces and the deck level is horizontal. Cable force adjustments can be made if necessary.

8. While the deck is being produced, the precast segments for the new pylon are erected.

7.4 INTERACTION BETWEEN CONSTRUCTION AND DESIGN

7.4.1 Design of the truss

In this section the dimensions of the truss are given, then the load cases occurring during the construction are investigated. Followed by the calculation of the initial cable forces anchored to the truss, and at the end the current forces acting on the flotation tanks are calculated.

7.4.1.1 Dimensions of the truss

The dimensions of the 550 m long launching truss are shown in Figure 7.11. The truss is divided into five regions using symmetry. For each region four cross-section areas are chosen, one for the top chord members, one for the bottom chord members, one for the inclined diagonal members and another for the vertical diagonal members. These areas are listed in Table 7.1.

The total weight of the truss members is about 22,000 kN. The weight of the transversal bracing members and the steel forms is estimated at 11,000 kN, and this weight is distributed proportionally to the cross-section areas of the top chord members as joint loads over the whole truss. So the total weight of the truss is about 33,000 kN including the weight of the formwork of the concrete. These loads cause a maximum truss deflection of 270 mm as shown in Figure 7.12.

A geometric nonlinear analysis, taking the effects of axial forces and large deflections into consideration, is performed in analysing the truss. Thus, the stability of the truss can be studied, should buckling occur.

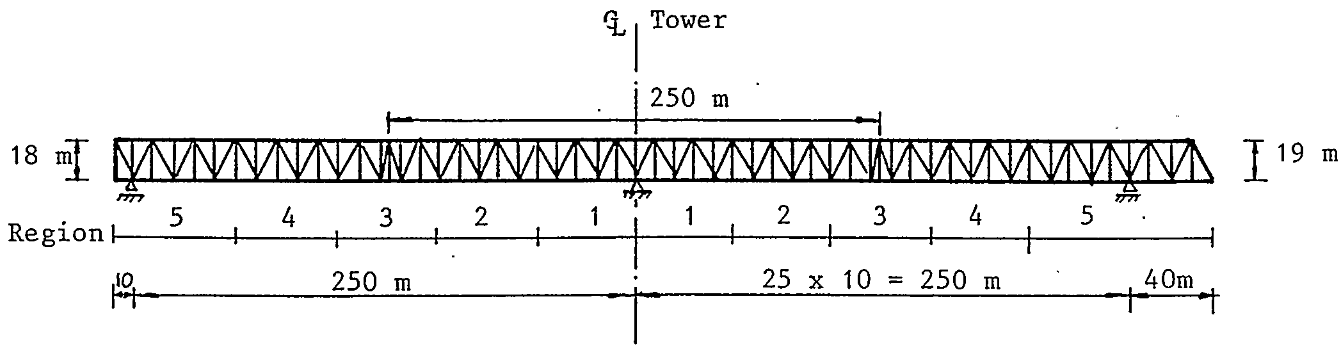

Figure 7.11: Dimensions of the launching truss

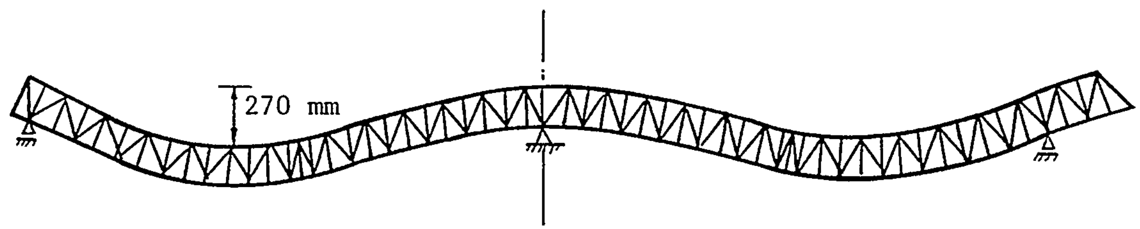

Figure 7.12: Deflection of the truss due to its own weight

Table 7.1: Cross-section areas of the truss members (mm^2)

		Region				
		1	2	3	4	5
Top chord		171,150	62,750	53,800	36,200	20,900
Bottom chord		295,050	79,450	19,950	19,950	13,300
Diagonal	vertical	11,250	10,150	4,750	550	9,000
	inclined	164,000	55,950	13,300	6,500	13,650

7.4.1.2 Load cases

In designing the truss, the following load cases occurring during the construction are investigated:

1. (own weight of the truss)
2. (own weight of the truss) + (temporary cable forces anchored to the truss)
3. (own weight of the truss) + (temporary cable forces anchored to the truss) + (weight of poured concrete)
4. (own weight of the truss) + (weight of hardened concrete deck) + (cable forces anchored to the hardened concrete deck)
5. (own weight of the truss) + (forces acting on the flotation tanks due to water currents during launching of the truss)

These load cases (except load case 5) are not only of major interest for designing the truss, but in order to achieve a level deck for the completed bridge, all the deformations occurring during those load cases have to be considered. At this point it should be noted that time-dependent effects are not considered in this study.

7.4.1.3 Initial cable forces anchored to the elevated truss

The initial strains (prestressing forces) in the cables temporarily anchored to the truss, are based on the unstressed cable lengths L_o established in the previous dead load analysis of the bridge, and the elevated position of the truss according to the following equation for each cable:

$$\varepsilon = \frac{L - L_o}{L_o} \tag{7.1}$$

where:

ε = initial strain in the cable

L = distance between the two ends of the cable i.e. between the top of the pylon and the truss node when connecting the cables to the truss

L_o = strain-free length of the cable

These initial strains (prestressing forces) in the cables decrease by increasing the elevation of the truss for the production of the deck. Two elevated positions, 300 and 500 mm above the final deck level are investigated. The prestressing forces are calculated by multiplying the initial strain ε obtained from Equation 7.1 by the quantity EA, where A is the cross-section area of the cable. The results are listed in Tables 7.2 and 7.3.

7.4.1.4 Current forces on the flotation tanks

During launching, when the truss is supported at its ends on the flotation tanks, these tanks will be subjected to current forces. These forces are a function of the shape and dimensions of the tanks and of the current velocity. The volume of the tank required to provide an uplift force equal to the end reaction of the truss due to its own weight is about 255 m^3. This gives two cylindrical tanks of 4.5 m diameter each and 8 m length at each end of the truss. The drag force on the tank can be calculated using the following equation (Gerhart, 1985):

Table 7.2: Cable forces (kN) during construction stages for elevated truss level +500 mm

No.	Step									D.L.
	1		2	3	4	5	6	7	8	
	Init.	Final								
1	2425	1736	2376	2617	2720	2869	2947	2976	2950	2962
2	2085	1361	2076	2316	2441	2623	2718	2753	2762	2763
3	1580	979	1620	1796	1919	2103	2205	2250	2322	2309
4	1397	800	1476	1624	1780	2012	2143	2201	2351	2346
5	955	470	1085	1178	1341	1587	1726	1787	2005	1996
6	578	221	741	800	1010	1329	1511	1593	1946	1950
7	-	-	346	365	575	908	1099	1183	1632	1623
8	-	-	-	-	-	477	731	846	1517	1534
9	-	-	-	-	-	-	345	472	1314	1275
10	-	-	-	-	-	-	-	192	1331	1355
11	-	-	-	-	-	-	-	-	887	894
12	-	-	-	-	-	-	-	-	890	896
13	-	-	-	-	-	-	-	194	1330	1354
14	-	-	-	-	-	-	347	475	1314	1275
15	-	-	-	-	-	476	733	851	1517	1534
16	-	-	344	360	571	908	1101	1187	1631	1623
17	431	222	739	793	1005	1329	1514	1598	1946	1951
18	817	473	1084	1172	1337	1587	1729	1793	2005	1997
19	1245	804	1475	1618	1775	2012	2147	2209	2352	2346
20	1438	984	1620	1790	1916	2104	2210	2258	2323	2309
21	1923	1368	2077	2309	2437	2625	2723	2758	2755	2763
22	2287	1737	2392	2627	2733	2890	2972	2997	2955	2962

Note:
Step 1 : truss weight
Step 2 : truss weight + deck weight
Step 3 : cables connected to hardened deck
Step 4 to 8: truss lowering steps
D.L. : forces calculated in the dead load analysis of the bridge

Table 7.3: Cable forces (kN) during construction stages for elevated truss level +300 mm

No.	Step 1 Init.	Step 1 Final	Step 2	Step 3	Step 4	Step 5	D.L.
1	2888	1972	2589	2900	2983	2955	2955
2	2624	1643	2334	2646	2747	2759	2763
3	2094	1268	1888	2132	2250	2320	2309
4	2009	1173	1828	2049	2201	2349	2346
5	1576	867	1475	1628	1787	2006	1996
6	1336	662	1265	1383	1593	1946	1950
7	904	402	906	965	1183	1634	1623
8	515	150	523	552	846	1515	1534
9	-	-	151	164	471	1318	1275
10	-	-	-	-	192	1330	1355
11	-	-	-	-	-	886	894
12	-	-	-	-	-	888	896
13	-	-	-	-	194	1330	1354
14	-	-	153	164	475	1318	1275
15	383	153	526	554	851	1516	1534
16	777	406	908	966	1187	1634	1623
17	1188	668	1268	1385	1599	1946	1951
18	1438	874	1479	1630	1793	2006	1997
19	1856	1182	1834	2053	2210	2350	2346
20	1953	1278	1894	2135	2258	2320	2309
21	2461	1657	2343	2649	2753	2756	2763
22	2750	1973	2607	2911	2995	2957	2962

Note:

Step 1 : truss weight

Step 2 : truss weight + deck weight

Step 3 : cables connected to hardened deck

Step 4 to 5: truss lowering steps

D.L. : forces calculated in the dead load analysis of the bridge

$$F_D = C_D \cdot \rho \cdot \frac{V^2}{2} \cdot A_P \tag{7.2}$$

where:

F_D = drag force on immersed body

C_D = coefficient of drag

≈ 0.46 for two cylinders beside each other idealized as an elliptical shape

ρ = fluid density

= 1000 kg/m^3 for water

V = fluid velocity

= 2 m/s in the investigated case

A_P = projected area of immersed body, perpendicular to the flow direction

Equation 7.2 gives a drag force of 33 kN. This drag force, acting on the center of gravity of the tank, produces a torsional moment of about 670 KN·m on the truss.

7.4.2 Computer model used in simulating the construction procedure

The planar model, which is used in the geometric nonlinear analysis, consists of a truss resting on one pylon (hinge support) and having two rollers as end supports (see Figure 7.13). There is no need for using pylons as end supports in the analysis, as in reality, because the end reactions of the truss due to its own weight (about 2.5 MN) are small compared to the intermediate reaction (about 27 MN), so that the vertical displacements of the end supports, if pylons are used instead of rollers, are negligible. The hinged support between truss and pylon is achieved in the analysis by coupling the vertical and horizontal displacements of the two nodes of the hinge connection (see Figure 7.15). Two dimensional truss elements, resisting only axial forces, are used in modeling the truss, whereas the elements used for the pylon, deck and cables are the same as the ones used in the geometric nonlinear dead load analysis of the bridge. However, a new element (interface element) is used for simulating the contact between deck and truss, and for the lowering procedure of the truss. This interface element has two nodes (surfaces), and is capable of resisting a vertical compressive force in case its two nodes (surfaces) are in contact, otherwise its vertical stiffness is removed. In the horizontal direction the two nodes (surfaces) are allowed to slide against each other, if not otherwise specified. These features are used in simulating the contact between deck and truss during the lowering process. The lowering process itself is simulated by the use of an initial gap between the two nodes (surfaces) of the interface elements which are used as the truss supports (see Figure 7.15). The truss is then lowered until this gap is closed. For more information about the used interface element refer to Appendix A.

The analysis of the construction procedure for the case of a 500 mm elevated truss will be described next. The same was also done for a 300 mm elevated truss and the results are compared. For a 500 mm elevation of the truss the construction procedure is divided into 8 steps (these are 5 steps in case of 300 mm elevation of the truss).

- Step 1 (Figure 7.13)

  The truss is elevated so that the steel form supported on the top chord, is 500 mm above the final level of the soffit of the concrete deck and is left to deflect under its own weight. From this deflected shape, which is obtained from a separate dead load analysis, the cables are temporarily anchored to the truss. For this purpose, a computer program is written to convert the results of a previous ANSYS analysis (deflected shape of the truss and final strains in its members), to input data (joint coordinates of the truss and initial strains in its members) for the next analysis. The initial strains (prestressing forces) of the cables temporarily anchored to the truss are calculated from the strain-free length L_o of each cable and the distance L between the end nodes of the cables in this elevated position of the truss using Equation 7.1. The resulting initial cable forces are listed in Table 7.2 (Table 7.3 for the 300 mm elevation). Only the outer 12 cables are stressed as shown in Figure 7.13.

- Step 2 (Figure 7.14)

  The results of step 1, which are the deflected shape of the truss and final strains in the cables and in the truss members, are the input data for step 2, i.e. they are the joint coordinates of the truss and initial strains in the cables and truss members. The concrete weight of the deck, which is poured in this position, is added as joint loads on the truss, resulting in stressing the outer 14 cables. This means that two more cables pick up load as the concrete is placed.

- Step 3 (Figure 7.15)

  Again, the results of step 2 are the input data for step 3. The concrete deck is represented in this stage by a beam element to model the hardened concrete, and the cables are now anchored to the concrete deck. Interface elements are used between the truss nodes and the deck nodes as shown in Figure 7.15. An interface element has the capability of resisting a vertical compressive force in case its two surfaces (nodes) are in contact, thus deck and truss nodes are coincident, or in other words the deck is resting on the truss. In this stage part of the deck weight is supported by the stressed cables, while the other part of the deck weight is supported by the truss through the interface elements. Interface elements without an initial gap, which means that they are capable of resisting vertical compressive forces (reactions), are used in this step to model the roller supports at the truss ends. The hinge support between truss and pylon is achieved by using an interface element between the truss node and the pylon node to restrain the vertical displacement of the truss node, and coupling of the horizontal displacements of the two nodes to restrain the horizontal displacement of the truss node.

- Step 4 (Figure 7.15) - Truss lowered 87 mm

  The results of step 3 are the input data for step 4. In this step 14 cables are stressed. The truss is now lowered to a level at which the next two inner cables (cable 8 and 15) start picking up forces. The lowering process is achieved by the three interface elements representing the supports of the truss. The initial gap, which is chosen between the two surfaces of the elements, is the distance the truss is to be lowered. This means that the truss will undergo a downward motion until the two surfaces of the interface elements representing its supports get into contact.

- Steps 5 to 7 (Figure 7.15) - Truss lowered 235 mm

  The procedure of step 4 is repeated in these steps. In each step the truss is lowered to a level at which the following two inner cables start picking up forces. At the end of step 7 a level is reached, at which all cables will pick up forces in the next step. During those steps the cables get more and more stressed, as a result the part of the deck weight which is supported by the cables is increasing, while the part of the deck weight supported by the truss through the interface elements is decreasing. At the outer cables, which are the most highly stressed ones, the deck becomes supported by cables only, and the interface elements at those cables allow the separation of deck and truss gradually.

- Step 8 (Figure 7.16) - Truss lowered 178 mm

  Again, the results of step 7 are the input data for step 8. The final lowering process of the truss is simulated by using nonlinear force-deflection spring elements (elements 1, 2 and 3 in Figure 7.16). The special behaviour of those spring elements is that the force picked up by them is constant regardless of their shortening (see Figure 7.16). So if the forces (F) for springs 1, 2 and 3 are chosen equal to the reactions of the truss due to its own weight only, then the truss will undergo a downward rigid body motion as long as a part of the deck weight is carried by the truss. This downward motion of the truss results in stressing the cables gradually until the whole deck weight is picked up by the cables, and so no forces are transmitted by the interface elements to the truss. As the springs 1, 2 and 3 are giving the reactions of the truss due to its own weight, which is now the case, stability is reached and the truss stops moving downwards (see Figure 7.17).

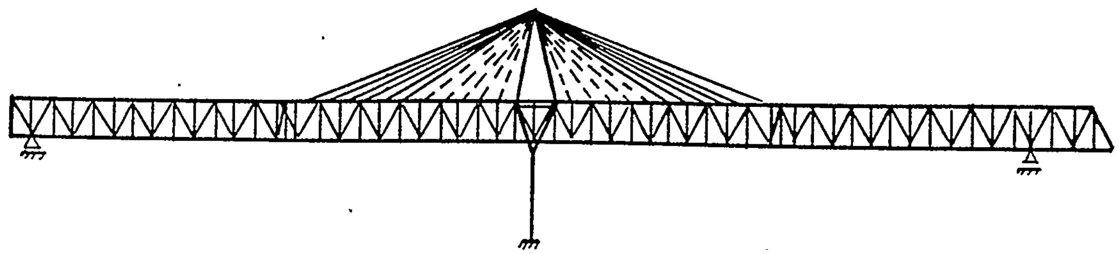

Figure 7.13: Step 1 in the construction procedure (12 stressed cables)

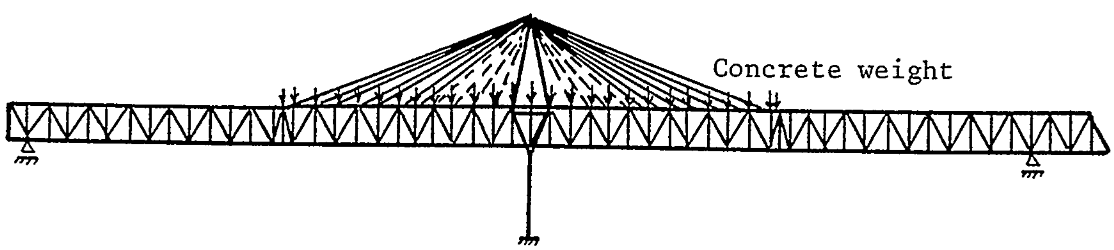

Figure 7.14: Step 2 in the construction procedure (14 stressed cables)

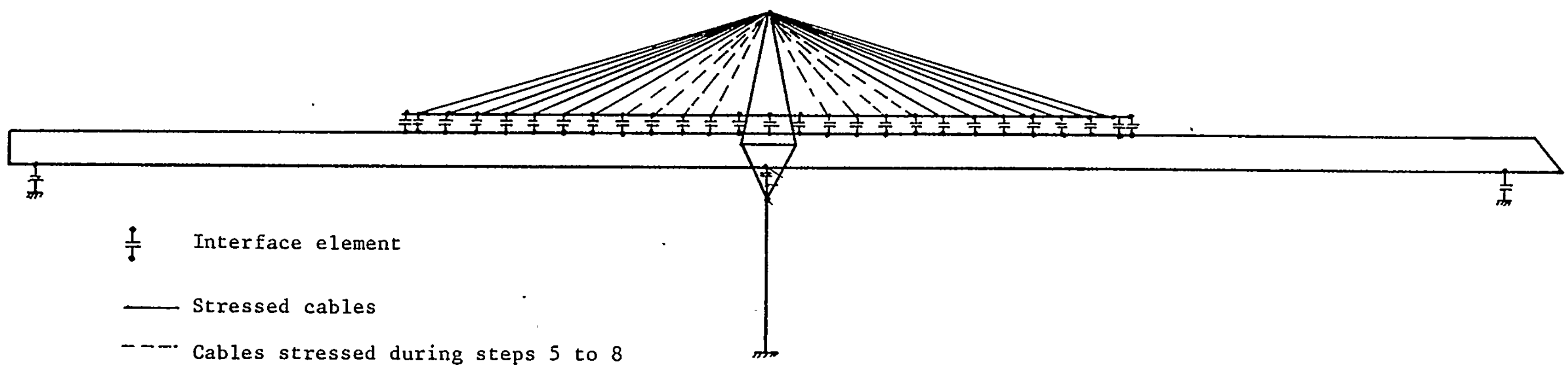

Figure 7.15: Model used in analysing construction steps 3 to 7

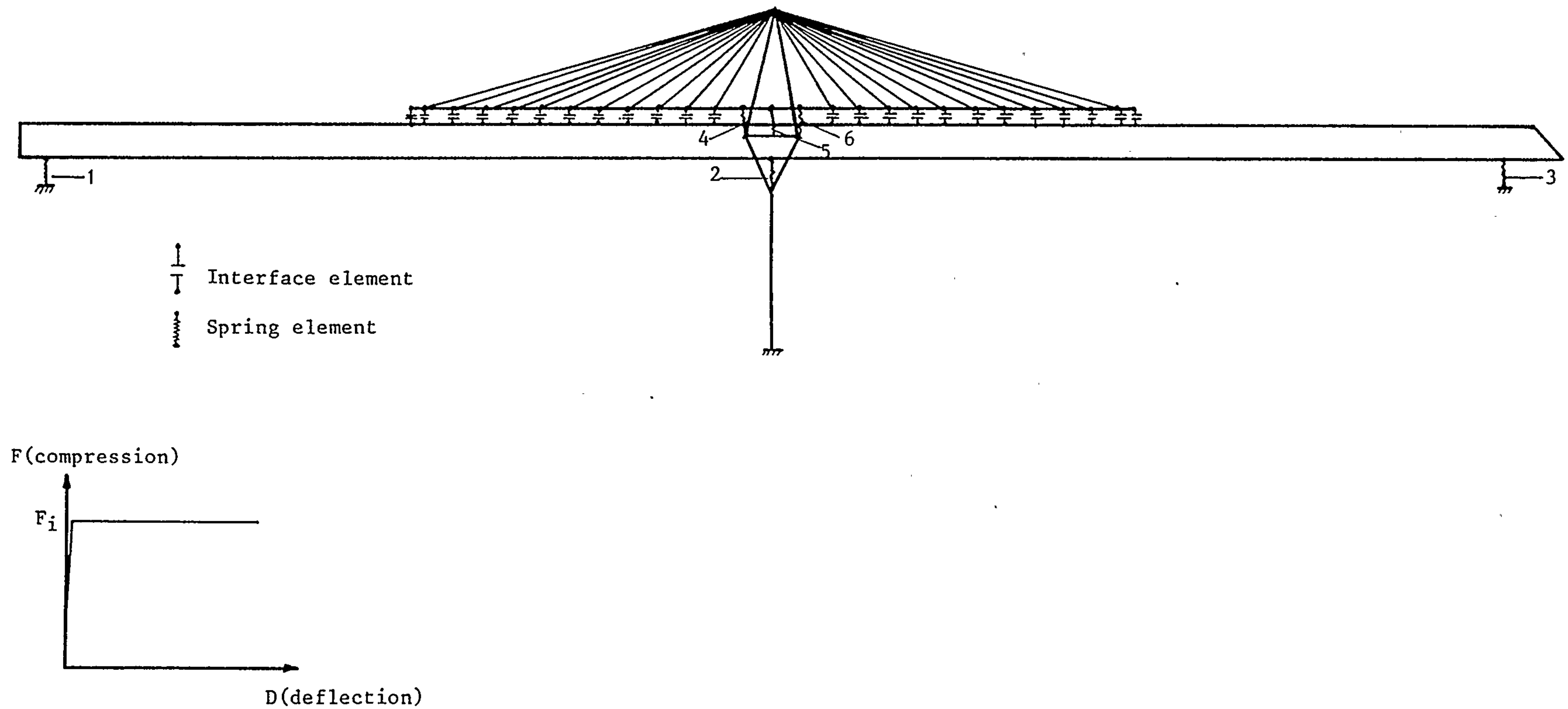

Figure 7.16: Model simulating the final lowering process (step 8)

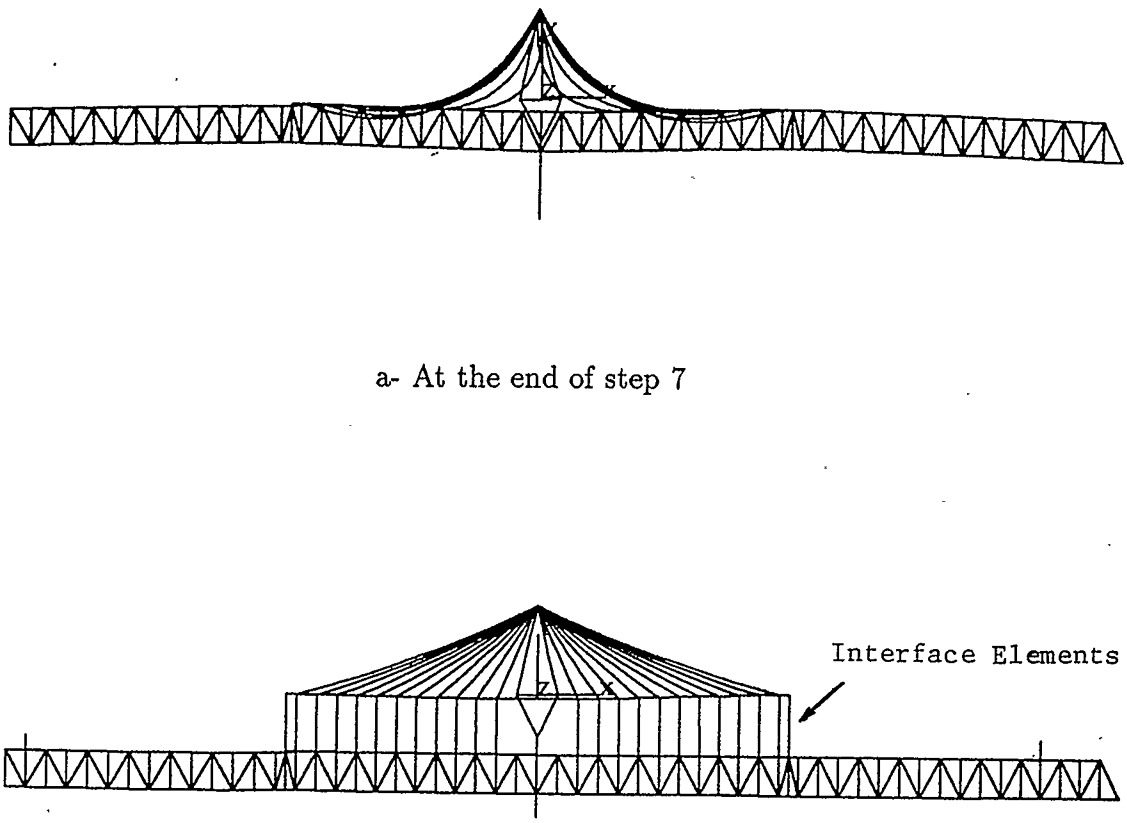

a- At the end of step 7

b- At the end of step 8

Figure 7.17: Lowering process of the launching truss simulated by the computer program ANSYS (distorted scale)

Originally the deck is supported on the tie-beam and on the pylon at three points (two rollers and one hinge). This is simulated during the lowering process by springs 4, 5 and 6 as shown in Figure 7.16. The force (F) in each spring is chosen equal to the reaction between the deck and the pylon (tie-beam) calculated from the previous dead load analysis of the bridge. The springs restrain the vertical displacements of the rollers, in order to achieve the hinge connection the horizontal displacements of the corresponding nodes are coupled.

7.5 RESULTS AND CONCLUSIONS

7.5.1 General

In this section the analysis results of the construction procedure are discussed. Two elevated position for the truss (300 and 500 mm) during pouring of the concrete deck are investigated and compared. The results are divided into five groups:

1. Deflection of the truss
2. Forces in the truss
3. Forces in the stay-cables
4. Deflections of the deck
5. Bending moments and normal forces in the deck

7.5.2 Deflection of the truss

The deflections of the truss during the different construction stages, as shown in Figure 7.18(a) for the 500 mm elevation and Figure 7.18(b) for the 300 mm case, are now discussed.

1. Without any precambering, the truss deflects under its own weight and formwork of the concrete deck a maximum of 270 mm. This gives an acceptable deflection/span ratio of 1/925 (curve 1).

2. The application of the temporary cable forces results in an upward deflection of the truss. In case of a truss elevation of +500 mm, the part of the truss on which the deck will be produced is almost level again (curve 2 in Fig. 7.18(a)).

3. The weight of the poured concrete produces a deflection of 280 mm at the centerline of the span in case of a 500 mm truss elevation. This deflection is reduced to 260 mm in case of a 300 mm truss elevation (curve 3).

4. The transfer of the cable forces from the truss to the hardened deck adds 50 mm to the deflection of the truss in case of a 500 mm truss elevation. This deflection is 70 mm if the truss elevation is 300 mm (curve 4). This results in the same difference of about 330 mm at the centerline of the span between curve 2 (own weight of truss + cables anchored to truss) and curve 4 (after transfer of cable forces to deck) for both investigated deck elevations.

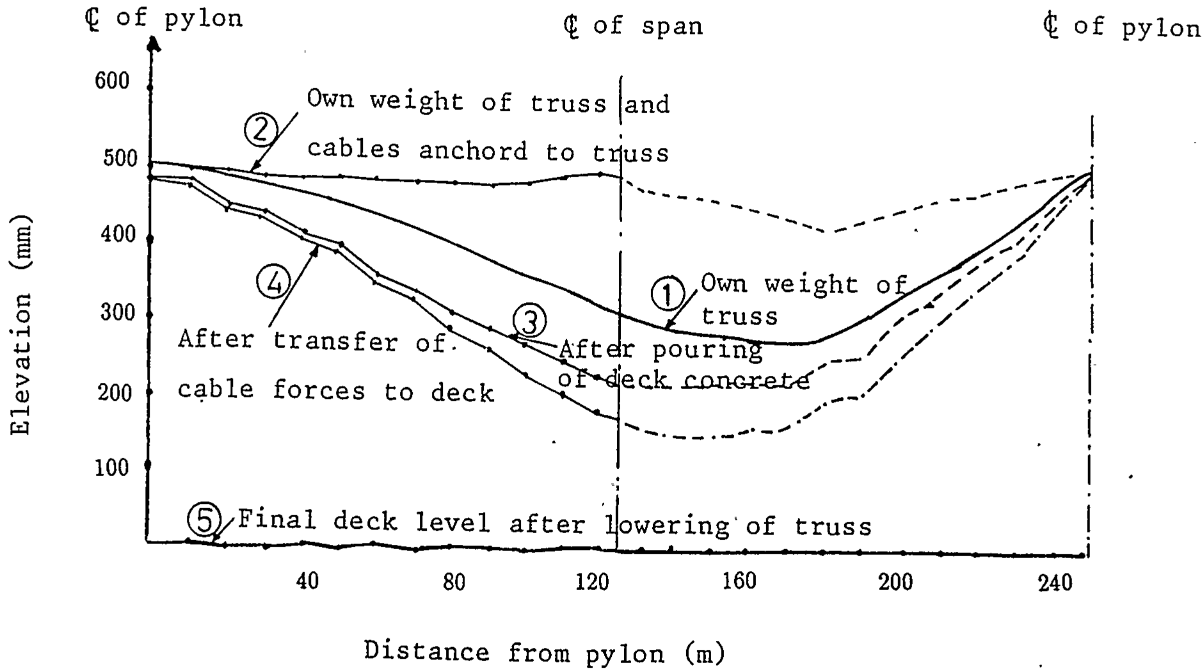

a- Temporary deck elevation +500 mm

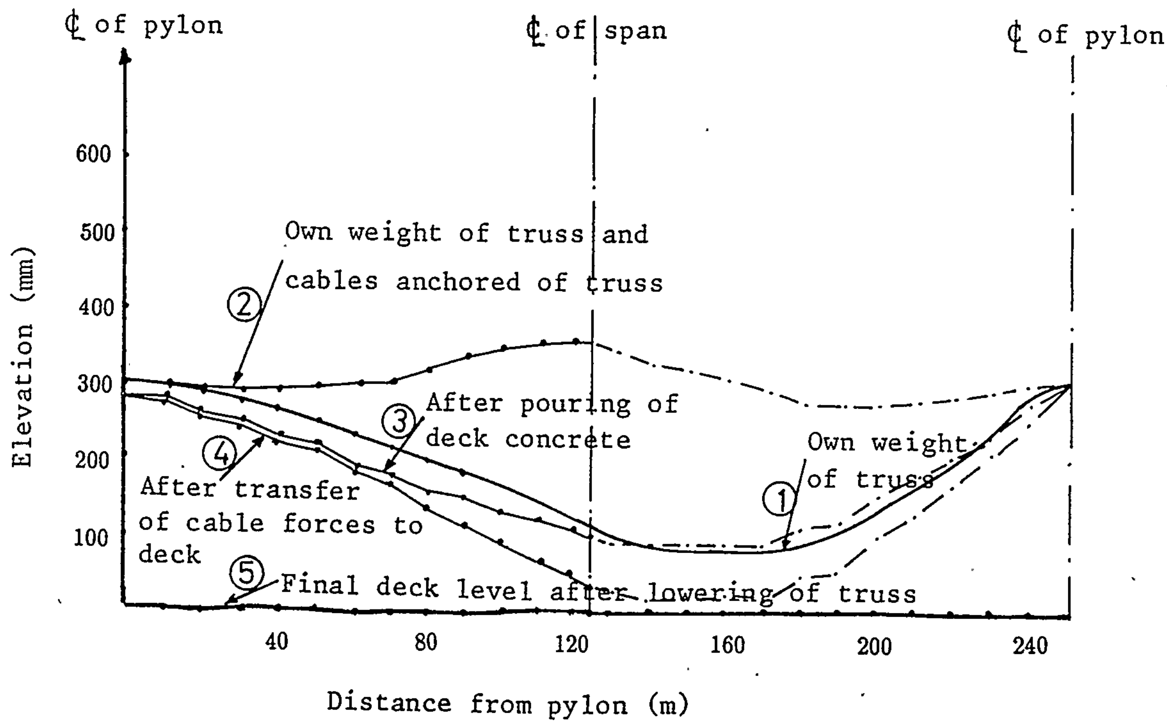

b-Temporary deck elevation +300 mm

Figure 7.18: Deflection of truss and deck during construction

7.5.3 Forces in the truss

The maximum forces in selected truss members in region 1 (over the intermediate support) and region 3 (at the midspan of the truss) during the different construction stages are listed in Table 7.4.

If the truss elevation is +500 mm when producing the deck, the maximum compression force (29.02 MN) occurs in the bottom chord member over the intermediate support after pouring the deck. The maximum tension (33.36 MN) develops in the top chord member over the intermediate support after the cable forces are transferred to the hardened deck. The maximum cable force to be anchored to the truss is 2.43 MN (Table 7.2).

For a truss elevation of +300 mm, the maximum cable force to be anchored to the truss is 2.90 MN (Table 7.3), which corresponds to an increase of 19 percent relative to the +500 mm case. The maximum compression force in the truss is 25.14 MN (16 percent reduction) and the highest tension decreases by 19 percent to 27.16 MN. This means that producing the deck on a low elevated truss will decrease the forces in the truss during the construction of the deck. Chosing how low the truss level may be, depends mainly on the maximum cable force that can be anchored temporarily to the upper chord of the truss.

The drag force (F_D = 33 kN) on the flotation tanks and the corresponding torsional moment on the truss (670 kN·m) are of minor effect, not causing any significant forces in the truss.

Table 7.4: Selected truss forces (MN) during the construction stages for truss elevations of 300 and 500 mm

	Construction Stage	Region 1				Region 3			
		Top	Bott.	Vert.	Incl.	Top	Bott.	Vert.	Incl.
	1-Truss o.w.	16.43	-12.92	-0.42	-7.56	-2.48	2.39	-0.11	-1.00
500 mm	2-Temp. cables + (1)	-2.71	-7.31	-0.41	-5.50	-1.69	-1.26	-0.11	-0.97
	3-Concrete wt. + (2)	27.70	-29.02	-1.42	-16.17	-4.62	2.25	-0.11	-1.46
	4-After cable forces transferred to deck	33.36	-25.89	-1.45	-16.03	-3.32	3.31	-0.11	-1.08
	5-Deck in final position	16.43	-12.92	-0.42	-7.56	-2.48	2.39	-0.11	-1.00
300 mm	6-Temp. cables + (1)	-6.20	-4.29	-0.41	-4.28	-1.44	-2.09	-0.11	-1.09
	7-Concrete wt. + (6)	20.30	-25.14	-1.41	-14.44	-4.23	-1.24	-0.11	-1.37
	8-After cable forces transferred to deck	27.16	-20.68	-1.43	-13.94	-2.79	2.73	-0.11	-1.03
	9-Deck in final position	16.43	-12.92	-0.42	-7.56	-2.48	2.39	-0.11	-1.00

Note: Region 1: over the intermediate support

Region 3: at the midspan of the truss

7.5.4 Forces in the cables

The cable forces during the different construction steps are listed in Tables 7.2 and 7.3. The final cable forces obtained by the used model simulating the lowering process are within 1 percent of those established in the previous dead load analysis of the bridge.

At this point it should be mentioned, that trying to lower the truss in one step using the program ANSYS failed. Initially slacked cables connected to the flexible deck, did not reach a converged solution (the cable elements are nonlinear and need an iterative solution procedure till convergence is achieved). This problem occurred only when initially slacked cables are connected to the flexible deck. It seems that if the truss is lowered in one step, and the initially slacked cables start picking up forces due to their elongation, the flexibility of the deck allows the deck nodes connected to the suddenly stressed cables, to undergo an upward motion resulting in slacking the cables again. This process results in unrealistically small (unconverged) forces in the cables which were initially slacked during the lowering process. To overcome this problem, the truss is lowered in steps. During each step only the stressed cables are included in the computer model.

7.5.5 Deflection of the deck

If the truss is not precambered, then the concrete hardens in the deflected configuration represented by curve 3 in Figure 7.19, which means that there is some initial curvature built into the deck. After lowering the truss, the deck level is almost horizontal as obtained from the previous dead load analysis of the bridge.

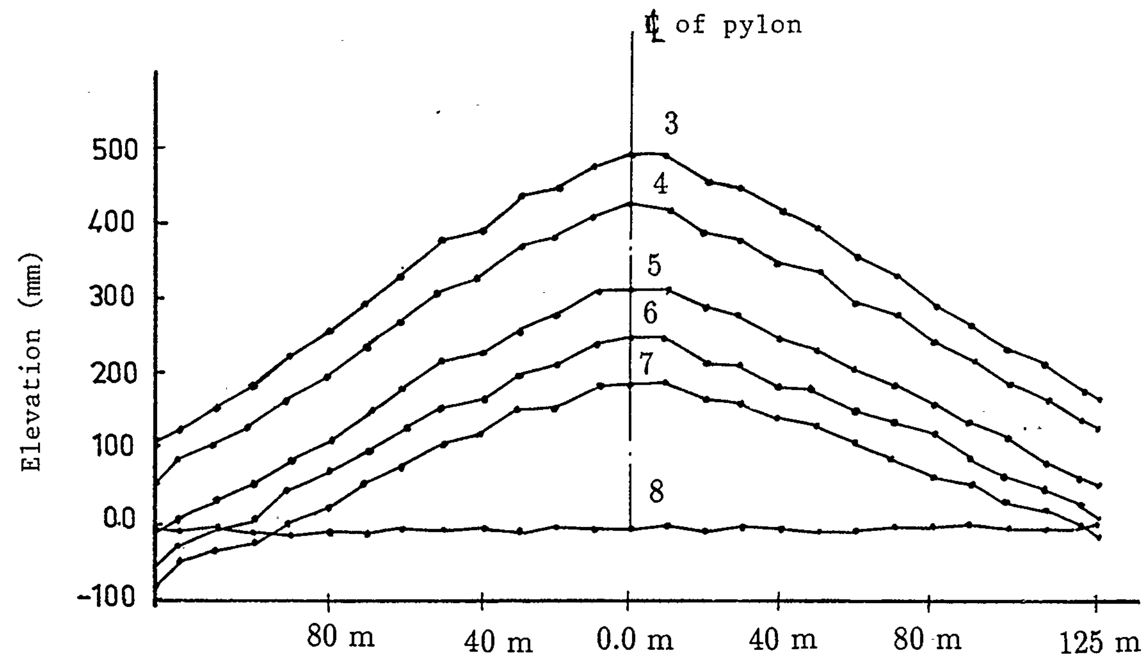

Figure 7.19: Level of hardened deck during construction steps 3 to 8 for a temporary truss elevation of 500 mm

7.5.6 Bending moments and normal forces in the deck

During the lowering process, the bending moments in the deck do not differ in a significant manner from those obtained from the dead load analysis. The final bending moments after the truss is removed are shown in Figure 7.20. The only noticeable difference between the dead load analysis and the analysis of the construction procedure, is the negative moment in the deck under the two cables next to the pylon (see Figure 7.20). The reason may be the springs connecting the deck with the pylon in the last lowering step (step 8). The constant forces, which are equal to the reactions between deck and pylon of the dead load analysis, develop suddenly in those springs during the lowering process. They create a positive moment at the nodes connected to the two cables next to the pylon. So the negative bending moment at these points are reduced.

If a force-deflection relationship is chosen, so that the forces in those springs are developing gradually, this difference between the two bending moments is reduced. But the forces picked up by the cables connected to the considered points (next to the pylon) are much greater than those obtained from the dead load analysis. A gradually increasing reaction, instead of reaching its required value suddenly as shown in Figure 7.16, allows more deck weight to be supported by the two cables next to the pylon instead of supporting this weight by the pylon through the deck-pylon connections. So the cables forces increase and the forces in the springs decrease.

As the final cable forces obtained from the used model are almost identical to those obtained from the dead load analysis, the normal forces in the deck are the same in both analyses.

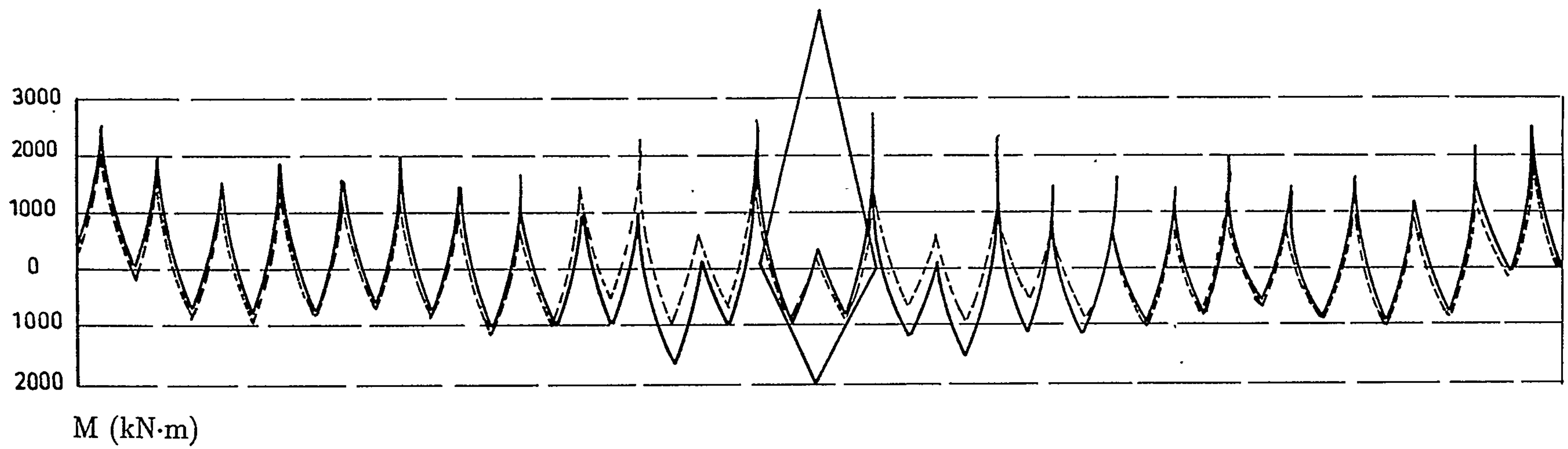

-------- Bending moments obtained from the dead load analysis

———— Final bending moments obtained from the construction analysis after the truss is removed

Figure 7.20: Bending moments in the deck after the truss is removed

7.6 SUMMARY

An economical method for the construction of multi-span cable-stayed bridges is introduced. In the proposed method, the deck is poured in one stage on an elevated truss, and then lowered to its final position. In general, decreasing the elevation of the truss decreases the forces in the truss during the construction stages, but increases the cable forces to be anchored temporarily to the top chord of the truss. These forces are determining the practical elevation of the truss.

A computer model is used in simulating the lowering process of the truss in steps, including only stressed cables. Interface elements are used to model the resting of the deck on the truss and allowing their separation during the lowering process.

After the truss is lowered, the deck is almost horizontal and the cable forces are identical to those calculated in the dead load analysis of the bridge. Since the deck is flexible, the final moments are not much affected by the lowering process.

Chapter 8

SUMMARY AND CONCLUSIONS

8.1 INTRODUCTION

This chapter gives an overall summary of the study. The most important results and conclusions are outlined. At the end, recommendations for further research are presented.

8.2 SUMMARY

The main objective of this study is to present an efficient structural system and a fast construction method for continuous cable-stayed bridges. To achieve this objective the thesis was divided into four parts.

- *Part 1:* Highway live loads (Chapter 2)

  The highway live loads for long continuous bridges according to the Canadian, American and European codes are compared.

- *Part 2:* Literature review (Chapters 3 and 4)

  In this part of the study the different structural systems for multispan cable-stayed bridges are reviewed. Different pylon configurations, cable arrangements and deck types are compared. The basic concepts in the analysis of cable-stayed bridges are discussed, and the sources and solution techniques of the geometric nonlinear behaviour of cable-stayed bridges are presented.

- *Part 3:* Analysis and parametric study (Chapters 5 and 6)

  In this part the proposed bridge is analysed for the dead load, highway live loads and for temperature. The results of a conventional linear and a geometrical nonlinear analysis are compared. To study the effects of the deck-pylon connection types on the bridge behaviour, five different deck-pylon connections are investigated. Since the longitudinal stability of the chosen system is achieved by stiff diamond-shaped pylons, the effect of the pylon dimensions are investigated in a parametric study. In addition the effect of the cable areas on the maximum bending moments in the deck is examined.

- *Part 4:* The construction method (Chapter 7)

  An economical and fast construction method for long multispan cable-stayed bridges is discussed. The method is a cast-in-place deck poured on a launching steel truss at an elevated position and then lowered into its final position. The different steps of this method are simulated and analysed by using the computer program ANSYS.

8.3 CONCLUSIONS

The major conclusions of the present study are:

1. While the Canadian and American Codes give about the same highway live load intensity, the European Code specifies in general a much higher value. For the proposed bridge, loading two lanes and for a 250 m long loaded span, the Canadian and American Codes give a live load intensity of 23.8 kN/m, while the European Code gives 40 kN/m for heavy traffic. This is almost

70 percent higher. With the increasing traffic volume and truck capacities in North America the highway live loads for long continuous bridges should perhaps be reviewed.

2. Designing the cables for a high stress, and keeping the differential deflections of the deck as low as possible by adjusting the initial strains in the cables in the dead load analysis, leads to a more or less linear behaviour of the structure, thus justifying the use of a simple linear analysis instead of a more complicated geometric nonlinear analysis for the dead load.

3. The maximum moment envelope in the deck under live loads has three distinct zones, where the maximum positive and negative moments appear. These zones are at the end of the side span, in the vicinity of the pylons, and at the centre of the main span. Comparing the bending moment envelopes of the linear and geometric nonlinear analyses, a maximum difference of 25 percent in the regions of relatively high bending moments is observed. This percentage increases to 100 percent in regions of low (insignificant) bending moments. These results indicate the significance of a geometric nonlinear analysis for the live loads.

4. Regarding the temperature analysis, the maximum difference in the deck bending moments between the linear and geometric nonlinear analyses in the regions of relatively high bending moments is about 8 percent. This difference increases to 22 percent in regions of relatively low bending moments. This means that the geometric nonlinearity affects the analysis results in case of a temperature analysis to a lesser degree than it does in a highway live load analysis.

5. The statical system recommended for multispan cable-stayed bridges consists of a slender solid concrete deck suspended by closely spaced cables. The deck is acting primarily as a compression member and the bending moments are relatively low. The longitudinal stability of the system is achieved by using stiff diamond-shaped pylons.

6. The optimum dimensions for the pylon in such a system related to the main span (l) are:

   - (b_t/l) should lie between 0.06 and 0.08
     where (b_t) is the pylon width or the distance between the inclined pylon legs at the deck level
   - (h_t/l) should lie between 0.18 and 0.24
     where (h_t) is the height of the pylon above the deck
   - (d_t/l) should be greater tha 0.09
     where (d_t) is the height of the inclined legs below the deck level

7. The optimum deck-pylon connection system consists of a 500 m long continuous deck resting on two pylons, and the deck-pylon connection consists of two rollers and one hinge to prevent a horizontal movement of the deck against the pylons. The continuity of the bridge is provided by expansion joints capable of transferring only shear forces at both ends of the 500 m long deck.

8. Trying to decrease the maximum bending moments in the deck by increasing the areas of the cables is not economical. An increase in the cable areas by 80 percent decreases the maximum bending moment in the deck by only 12 percent.

9. The proposed construction method is an efficient and fast way to construct multiple span cable-stayed bridges. Because of the flexibility of the slender solid concrete slab, the deformations of the steel truss supporting the cast-in-place concrete deck during the different construction stages do not have a significant effect on the final stresses in the deck.

8.4 RECOMMENDATION FOR FURTHER RESEARCH

1. This study is limited to a static analysis, research is needed to investigate the dynamic response of continuous cable-stayed bridges.

2. In addition to the geometrical nonlinearities considered in this study, the effect of the material nonlinearity should be included.

3. The importance of time-dependent effects such as creep and shrinkage on multi-span cable-stayed bridges should be examined.

References

1. ACI- ASCE Committee on Loads and Forces on Bridges, (1981), "Recommended Design Loads For Bridges", Journal of the Structural Division, ASCE, Vol. 107, No. ST7, July, pp. 1161-1213.

2. ANSYS, (1989), "Engineering Analysis System User's Manual, Vol. 1, 2 and Theoretical Manual", Revision 4.4, Swanson Analysis Systems Inc., Houston, Pennsylvania.

3. Bathe, K.J., (1982), "Finite Element Procedures in Engineering Analysis", Prentice-Hall, Englewood Cliffs, New Jersy.

4. Beyer, E. and Ernst, H.J., (1964), "Brücke Jülicher Strasse in Düsseldorf", Der Bauingenieur, Vol. 39, No. 12, December.

5. CAN3-S6-M88, (1988), "Design of Highway Bridges", Canadian Standard Association.

6. CEB-FIP, (1984), Comité Euro-International du Béton and Fédération Interntional de la Précontrainte, "Recommendations on practical design of reinforced and prestressed concrete structures based on the CEB-FIP Model Code (MC 78)", Thomas Telford Limited, London.

7. Cook, R.D., (1989), "Concepts and Applications of Finite Element Analysis", Third Edition, John Wiley & Sons, New York, Chapter 14.

8. Dilger, W.H., (1990), "Prestressed Concrete Bridges and other P/C Structures", Lecture Notes, Department of Civil Engineering, University of Calgary.

9. Dilger, W.H., Tadros, G.S. and Calder, D., (1990), "Construction of Multispan Cable-Stayed Bridges", Proceedings of the Second Symposium on Strait Crossings, Trondheim, Norway, pp. 339-346.

10. Dilger, W.H., Tadros, G.S. and Sherif, A.G., (1991), "Interaction between design and construction of a proposed multispan cable-stayed bridge", IABSE Symposium, Leningrad.

11. Ernst, H.J., (1965), "Der E-Modul von Seilen unter Berücksichtigung des Durchhanges", Der Bauingenieur, Vol. 40, No. 2, February, pp. 52-55..

12. Feige, A., (1966), "The Evolution of German Cable-Stayed Bridges - An Overall Survey", Acier-Stahl-Steel (English Version), No. 12, reprinted AISC Journal, July 1967.

13. Francis, A.J., (1965), "Single Cable Subjected to Loads", Civil Engineering Transactions, Institution of Engineers, Australia, Vol. CÉ7, pp. 173-180.

14. Gerhart, P.M. and Gross, R.J., (1985), "Fundamentals of Fluid Mechanics", Addison-Wesly.

15. Ghali, A. and Neville, A.M., (1989), "Structural Analysis, A Unified Classical and Matrix Approach", Chapman and Hall, London.

16. Gimsing, N.J., (1976), "Multispan Stayed Girder Bridges", Journal of the Structural Division, ASCE, Vol. 102, No. St10, October, pp. 1989-2003.

17. Gimsing, N.J., (1983), "Cable Supported Bridges Concept and Design", Jonn Wiley & Sons, 400 pp.

18. Ivy, R.J., Lin, T.Y., Michell, S., Raab, N.C., Richey, V.J., and Scheffey, C.F., (1954), "Live Loading for Long-Span Highway Bridges", ASCE Transactions, Vol. 119, Paper No. 2708.

19. Kondo, K., Komatsu, S., Inone, H. and Matsukawa, A., (1972), "Design and Construction of Toyosato-Ohhasi Bridge", Der Stahlbau, No. 6, June.

20. Leonhardt, F. and Zellner, W., (1980), "Cable-Stayed Bridges", IABSE Periodica, S 13/80, Zürich, February, pp. 21-47.

21. Leonhardt, F., (1987), "Cable-Stayed Bridges With Prestressed Concrete", PCI Journal, September-October, pp. 52-80.

22. Odenhausen, H., (1965), "Statical Principles of the Application of Steel Wire Ropes in Structural Engineering", Acier-Stahl-Steel (English Version), No. 2, February.

23. Podolny, W.Jr., (1971), "Static Analysis of Cable-Stayed Bridges", Ph.D. Thesis, University of Pittsburgh.

24. Podolny, W.Jr. and Scalzi, J.B., (1986), "Construction and Design of Cable-Stayed Bridges", John Wiley & Sons, New York.

25. Przemieniecki, J.S., (1968), "Theory of Matrix Structural Analysis", McGraw-Hill, London.

26. PWC, (1988), "Northumberland Strait Crossing Project", Public Works Canada, Proposal Call, March 15.

27. Seely, F.B. and Ensign, N.E., (1948), "Analytical Mechanics for Engineers", Wiley, New York, pp. 104-111.

28. Seif, S., (1986), "Nonlinear Analysis and Ultimate Strength of Prestreesed Concrete Cable-Stayed Bridges", Ph.D. Thesis, Department of Civil Engineering, University of Calgary, May.

29. Troitsky, M.S., (1977), "Cable-Stayed Bridges, Theory and Design", Crosby Lockwood Staples, London.

30. Tung, D.H.H. and Kudder, R.J., (1968), "Analysis of Cables as Equivalent Two-Force Members, Engineering Journal, American Institute of Steel Construction, January, pp. 12-19.

31. Walther, R., Houriet, B., Isler, W. and Moia, P., (1988), "Cable-Stayed Bridges", Thomas Telford, London.

Appendix A

Element Types

In this Appendix the different element types used in the analysis are presented. The elements described are:

1. The two-dimensional elastic beam element
2. The two-dimensional elastic tapered beam element
3. The two-dimensional elastic truss element
4. The cable element
5. The nonlinear force-deflection spring element
6. The interface element

The description of the elements (as far as applicable) includes:

- General description of the element
- The theory of the element
- The element stiffness matrix
- The effect of axial forces ($P - \delta$ effect)
- Verification

A.1 The two-dimensional elastic beam element

A.1.1 General description

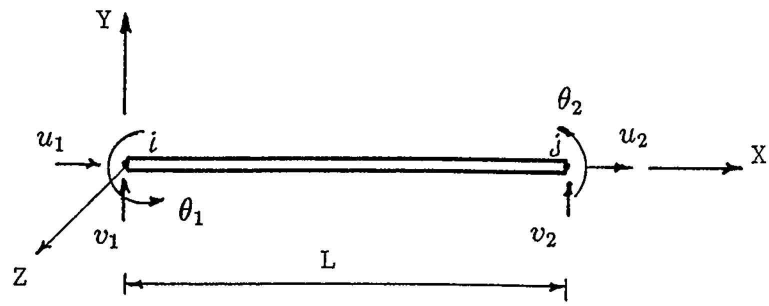

Figure A.1: Two-dimensional elastic beam element

The two-dimensional beam element is a uniaxial element with tension-compression, and bending capabilities. The element has three degrees of freedom at each node (see Figure A.1). These are translations in the nodal x and y directions (u and v) and rotation θ_z about the nodal z-axis.

A.1.2 Theory

The displacement functions are a first order polynomial in the element axial direction and a cubic polynomial in bending. These functions have the following form:

$$u = C_1 + C_2 \cdot x$$

$$v = C_3 + C_4 \cdot x + C_5 \cdot x^2 + C_6 \cdot x^3$$

where $C_1, C_2 \ldots C_6$ are constants, and the rotation θ_z is given by dv/dx.

A.1.3 Element stiffness matrix

The element stiffness matrix in the element coordinates if shear deformations are taken into account is:

$$
[k] = \begin{bmatrix}
\frac{EA}{L} & & & & & \\
0 & \frac{12EI}{L^3\cdot(1+\phi)} & & & & \\
0 & \frac{6EI}{L^2\cdot(1+\phi)} & \frac{EI\cdot(4+\phi)}{L\cdot(1+\phi)} & & & \\
-\frac{EA}{L} & 0 & 0 & \frac{EA}{L} & & \\
0 & -\frac{12EI}{L^3\cdot(1+\phi)} & -\frac{6EI}{L^2\cdot(1+\phi)} & 0 & \frac{12EI}{L^3\cdot(1+\phi)} & \\
0 & \frac{6EI}{L^2\cdot(1+\phi)} & \frac{EI\cdot(2-\phi)}{L\cdot(1+\phi)} & 0 & -\frac{6EI}{L^2\cdot(1+\phi)} & \frac{EI\cdot(4+\phi)}{L\cdot(1+\phi)}
\end{bmatrix} \tag{A.1}
$$

where:

A = cross-section area

E = modulus of elasticity

L = element length

I = moment of inertia

ϕ $= \dfrac{12EI}{GA_rL^2}$

G = shear modulus $= \dfrac{E}{2\cdot(1+\nu)}$

ν = Poisson's ratio

A_r = effective area in resisting shear deformations (reduced area)

A.1.4 Effect of axial forces

The computer program ANSYS uses the Przemieniecki approach, in which the effect of axial forces is taken by adding a stress stiffening matrix $[k_s]$ to the conventional matrix $[k]$ of the element. The stress stiffening matrix for the elastic beam element (as given before in Chapter 4) is:

$$[k_s] = \begin{bmatrix} 0 & & & & & \\ 0 & \frac{6P}{5L} & & & & \\ 0 & \frac{P}{10} & \frac{2PL}{15} & & & \\ 0 & 0 & 0 & 0 & & \\ 0 & -\frac{6P}{5L} & -\frac{P}{15} & 0 & \frac{6P}{5L} & \\ 0 & \frac{P}{10} & -\frac{PL}{30} & 0 & -\frac{P}{10} & \frac{2PL}{15} \end{bmatrix} \tag{A.2}$$

where:

P = axial force acting on the beam

A.1.5 Verification of the axial force effect

The computer program ANSYS is using the Przemieniecki approach, and not the general method, when considering the effect of axial forces. Therefore, an example is calculated by hand using the general method (Ghali and Neville, 1989), and the results are compared with the results obtained by the computer program ANSYS. The example is a propped cantilever as shown in Figure A.2 subjected to a uniform distributed load and an axial force P acting one time as a compression force, and another time as a tension force.

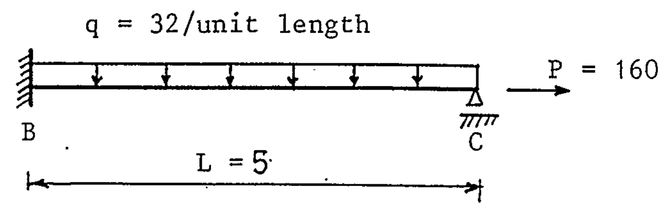

Figure A.2: Example of a propped cantilever subjected to an axial force P

The results of both methods are shown in Table A.1. It is obvious that increasing the number of elements used in the computer model, or in other words decreasing the lengths of the individual elements, leads to the decrease of the quantity $\overline{u} = L\sqrt{P/EI}$. But for low values of $\overline{u}$ both methods give identical results as discused before in Chapter 4, and as can be seen by comparing the results in Table A.1.

Table A.1: Fixed end moment for a propped cantilever subjected to an axial force

Axial Force	Exact	ANSYS					
		1 Element		2 Elements		3 Elements	
		M_{ANSYS}	$\frac{M_{ANSYS}}{M_{EXACT}}$	M_{ANSYS}	$\frac{M_{ANSYS}}{M_{EXACT}}$	M_{ANSYS}	$\frac{M_{ANSYS}}{M_{EXACT}}$
Tens.	88.716	94.380	1.064	89.123	1.005	88.760	1.001
Comp.	116.392	107.300	0.922	115.925	0.996	116.381	1.000

A.2 The two-dimensional tapered elastic beam element

A.2.1 General description

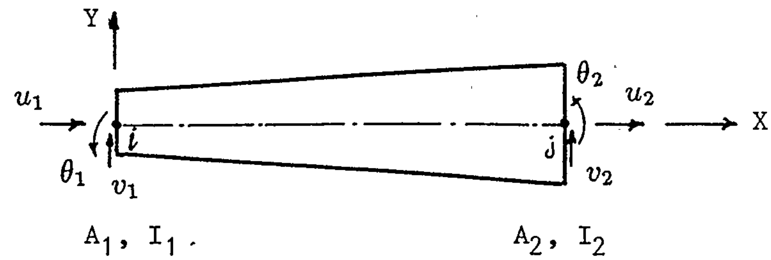

Figure A.3: Two-dimensional tapered elastic beam element

This element is a conventional elastic beam element except it allows a different unsymmetrical geometry at each end, as shown in Figure A.3.

A.2.2 Theory

The displacement functions for this element are the same for the conventional elastic beam element. For the purpose of the stiffness matrix calculation, the average area A_v is taken as:

$$A_{av} = \frac{A_1 + \sqrt{A_1 \cdot A_2} + A_2}{3}$$

And the average moment of inertia I_{av} is taken as:

$$I_{av} = \frac{I_1 + \sqrt[4]{I_1^3 \cdot I_2} + \sqrt{I_1 \cdot I_2} + \sqrt[4]{I_1 \cdot I_2^3} + I_2}{5}$$

Where the 1 and 2 subscripts refer to the end 1 and 2 of the element. It should be mentioned that if A_2/A_1 or I_2/I_1 is between 0.2 and 5, which is the case in the analysed bridge, the values above are close to the values calculated for an average cross-section between end 1 and end 2.

A.2.3 Element stiffness matrix

The element stiffness matrix is the same as for the conventional beam element, the cross-section area and moment of inertia used are those calculated using the previous expressions.

A.3 The two-dimensional truss element

A.3.1 General description

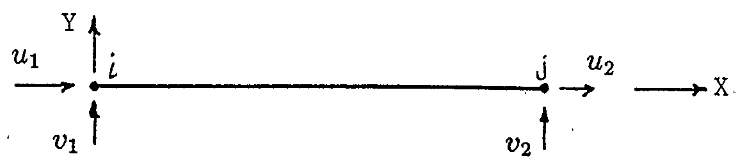

Figure A.4: Two-dimensional truss element

This element is a uniaxial tension-compression element with two degrees of freedom at each node (see Figure A.4). These are translations in the nodal x and y directions (u and v). No bending of the element is considered.

A.3.2 Theory

The displacement function for the truss element is assumed to be linear as follows:

$$u = c_1 + c_2 \cdot x$$

where the element x-axis is oriented along the length of the element from node i towards j. This displacement function implies a uniform stress in the element.

A.3.3 Element stiffness matrix

The element stiffness matrix in the local element coordinates is:

$$[k] = \frac{EA}{L} \cdot \begin{bmatrix} 1 & & & \\ 0 & 0 & & \\ -1 & 0 & 1 & \\ 0 & 0 & 0 & 0 \end{bmatrix} \tag{A.3}$$

where:

A = cross-section area

E = modulus of elasticity

L = element length

A.3.4 Effect of axial forces

The element stress stiffening matrix is:

$$[k_s] = \frac{P}{L} \cdot \begin{bmatrix} 0 & & & \\ 0 & 1 & & \\ 0 & 0 & 0 & \\ 0 & -1 & 0 & 1 \end{bmatrix} \tag{A.4}$$

where:

P = axial force

L = element length

A.4 The cable element

A.4.1 General description

This element is a truss element having the unique feature of resisting uniaxial tension only. The stiffness is removed if the element goes into compression, simulating a slacked cable condition. As the truss element, the cable element has two degrees of freedom at each node, translations in the nodal x and y directions (u and v).

A.4.2 Theory

The displacement function for this element is assumed to be linear for positive forces (tension). The function is of the form:

$$u = c_1 + c_2 \cdot x$$

Where the element x-axis is oriented along the the length of the element from node i to node j. The stiffness of the element is removed if a negative relative displacement between node i and node j occurs.

The element is nonlinear and requires an iterative solution. The solution procedure is as follows:

The element condition at the beginning of the first iteration is determined from the initial strain input:

$$\varepsilon = \frac{L - L_o}{L}$$

where:

L = element length defined by the location of its nodes

L_o = unstressed (unstrained) length of the cable

If this value is less than zero, the element stiffness is taken as zero for this iteration. If at the end of the iteration the element is in tension ($L > L_o$), the element stiffness is included in the next iteration. The effect of axial forces on the stiffness matrix should always be included to provide numerical stability.

A.4.3 Element stiffness matrix

The element stiffness matrix in the local element coordinates is:

$$[k] = \frac{EA}{L} \cdot \begin{bmatrix} c & & & \\ 0 & 0 & & \\ -c & 0 & c & \\ 0 & 0 & 0 & 0 \end{bmatrix} \tag{A.5}$$

where:

c = 1.0 if previous iteration resulted in a tensile stress

c = 0.0 if previous iteration resulted in a compressive stress

A.4.4 Effect of axial forces

The stress stiffness matrix, which should always be included to provide numerical stability, is:

$$[k] = \frac{P}{L} \cdot \begin{bmatrix} 0 & & & \\ 0 & c & & \\ 0 & 0 & 0 & \\ 0 & -c & 0 & c \end{bmatrix} \tag{A.6}$$

where: c = 1.0 if previous iteration resulted in a tensile stress

c = 0.0 if previous iteration resulted in a compressive stress

A.4.5 Verification

The sag of a cable hanging between two hinged supports (see Figure A.5) is calculated for the parabola configuration and for the catenary configuration and compared with the results obtained by the ANSYS analysis in Table A.2.

From the comparison it can be shown, that the difference between the catenary and the parabola configurations are almost negligible for small sag/span ratios. The results obtained by the computer program ANSYS are almost identical to the results of the catenary configuration.

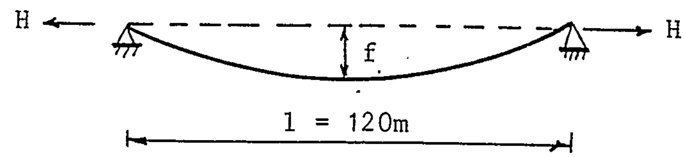

Figure A.5: Example of a hanging cable

γ = material density = 77 kN/m^3

A = cross-section area = 0.0042 m^2

w_p = weight of cable per unit length measured along the horizontal chord

$= \gamma \cdot A = 0.323$ kN/m (for parabolic configuration)

w_c = weight of cable per unit length measured along the cable center-line.

$= w_p \cdot l/l_c$ (for catenary configuration)

l = horizontal projected length of the cable (120 m)

L_c = length of the catenary

$$= 2 \cdot \frac{H}{w_c} \cdot \sinh\left(\frac{lw_c}{2H}\right)$$

H = horizontal reaction at the hinged support

$$f_c = \text{catenary sag} = \frac{H}{w_c} \cdot \left(\cosh\frac{lw_c}{2H} - 1\right)$$

$$f_p = \text{parabola sag} = \frac{w_p \cdot l^2}{8H}$$

Table A.2: Comparison between the sags of different cable configurations

H (KN)	f_{ANSYS} (m)	$f_{parabola}$ (m)	$\frac{f_{ANSYS}}{f_{parabola}}$	$f_{catenary}$ (m)	$\frac{f_{ANSYS}}{f_{catenary}}$
397	1.46608	1.46454	1.0010	1.46424	1.0010
79	7.33677	7.36329	0.9964	7.32583	1.0015
35	16.09183	16.42011	0.9800	15.98471	1.0067

A.5 The nonlinear force-deflection spring element

A.5.1 General description

This is a unidirectional element with a nonlinear generalized force-deflection relationship explicitly defined by the user (see Figure A.6). The used element has one degree of freedom at each node, which is a translation in the nodal x-direction (u).

A.5.2 Theory

The element is nonlinear and requires an iterative solution. During the stiffness pass of a given iteration, the element will use the results of the previous iteration to determine which segment of the force-deflection curve is active and calculate the slope k^{tg}, which will be used in the calculation of the stiffness matrix. The deflections of the current iteration are examined to see whether a different segment of the force-deflection curve should now be active. If so, the solution is not converged.

A.5.3 Element stiffness matrix

The element stiffness matrix in the element local coordinates is:

$$[k] = k^{tg} \cdot \begin{bmatrix} 1 & -1 \\ -1 & 1 \end{bmatrix} \tag{A.7}$$

where:

k^{tg} = slope of the active force-deflection segment from the previous iteration

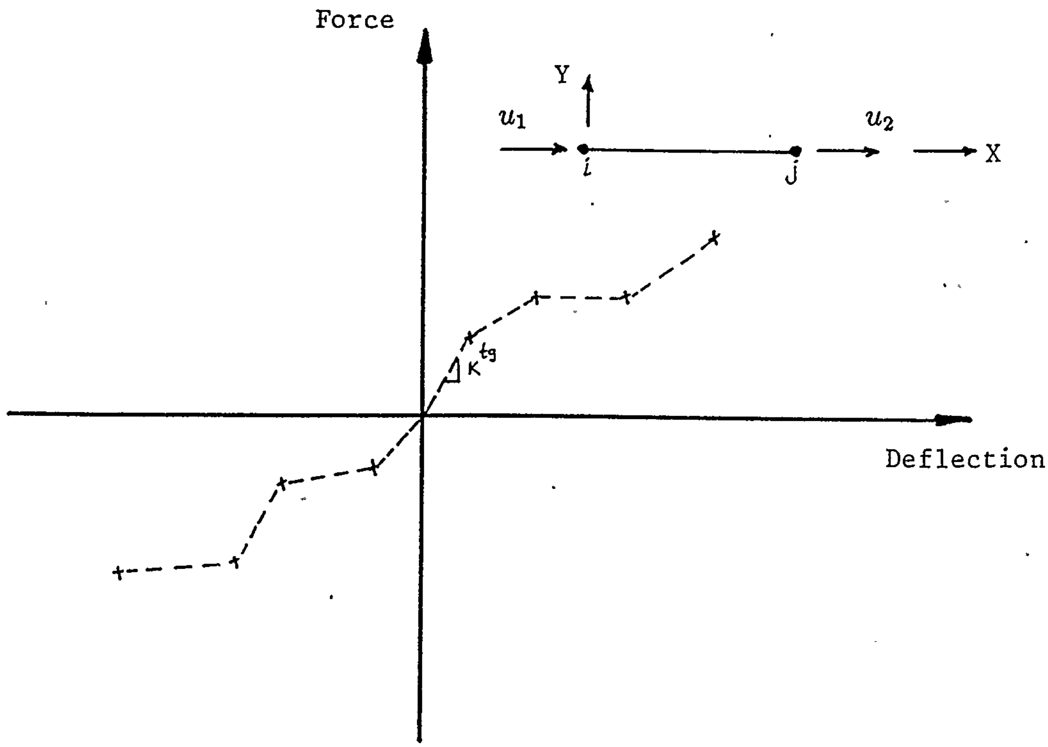

Figure A.6: Example for a defined force-deflection curve for a nonlinear spring element

A.6 The interface element

A.6.1 General description

This element represents two surfaces which may maintain or break physical contact and may slide relative to each other (see Figure A.7).

The used element is capable of supporting only compression in the direction normal to the surfaces, and has two degrees of freedom at each node, translations in the nodal x and y directions (u and v). The element may be given an initial gap, the specified normal stiffness is active when this gap is closed.

A.6.2 Theory

The element is nonlinear and requires an iterative solution. The element condition at the beginning of the first iteration is determined from the initial gap. If the interface is open, no stiffness is associated with this element for this iteration. If the interface is closed, k_n (the normal stiffness) is used in the gap resistance.

A.6.3 Element stiffness matrix

If the two nodes i and j of the element are coincident (the two surfaces are in contact), then the element stiffness matrix in the local element coordinates is:

$$[k] = \begin{bmatrix} 0 & & & \\ 0 & k_n & & \\ 0 & 0 & 0 & \\ 0 & -k_n & 0 & k_n \end{bmatrix} \tag{A.8}$$

where: k_n = stiffness of the interface element normal to its surfaces

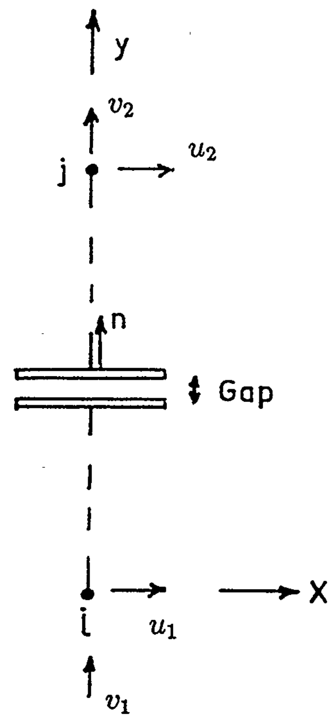

Figure A.7: The interface element